Vadose zone response to pumping in unconfined aquifers

by

Melissa Irene Bunn

A thesis
presented to the University of Waterloo
in fulfillment of the
thesis requirement for the degree of
Doctor of Philosophy
in
Earth Sciences

Waterloo, Ontario, Canada, 2011

Author's Declaration

I hereby declare that I am the sole author of this thesis. This is a true copy of the thesis, including any required final revisions, as accepted by my examiners.

I understand that my thesis may be made electronically available to the public.

Abstract

The interaction between drainage from the variably saturated zone above the water table, and the response of an unconfined aquifer to pumping has been the source of debate for many decades. While various field tests (Nwankwor et al., 1992 and Moench et al., 2001) have supported the concept that variably saturated flow processes delay drainage above a falling water table, Neuman (1972, 1974, 1975), has asserted that the impact is minimal, delay in response of the water table is due to elastic storage effects, and instantaneous yield above the water table is a reasonable assumption in unconfined aquifer analysis. This assumption results in exceedingly low estimates of specific yield in comparison to other analysis techniques (Neuman, 1987). A 7-day pumping test by Bevan et al. (2005) in the unconfined aquifer at Canadian Forces Base Borden has highlighted the complexity in drainage from above the water table during pumping, as the tension saturated zone was found to increase in thickness as a function of both proximity to the pumping well, and elapsed pumping time. This extended thickness persisted for the 7-day pumping duration. Analytical analysis of the test by Endres et al. (2007) resulted in significant underestimates of specific yield in comparison to laboratory values for most solutions. Narasimham (2007) suggested that the use of numerical simulators which include variably saturated flow may provide the most accurate representation of the test results. An attempt to replicate test results using a numerical simulation of variably saturated flow by Moench (2008) could not provide a complete physical mechanism for the extension observed by Bevan et al. (2005). This study provides a detailed investigation on the effect of heterogeneity, hysteresis, and entrapped air on drainage during unconfined pumping tests using numerical simulations, field experiments, and laboratory observations. The results of the Bevan et al. (2005) pumping test are used as a standard for comparison.

Three variably-saturated groundwater flow numerical codes were evaluated for their ability to replicate the variations in soil moisture content observed during pumping by Bevan et al. (2005). Results of the numerical simulations were also analyzed for their similarity to the peak and subsequent decrease in vertical gradients observed during pumping in the Borden aquifer. While the models generated vertical gradients through the capillary fringe during pumping, these gradients dissipated significantly before 1000 min. of pumping. No gradients in the saturated zone generated by the numerical model would be capable of shifting the pressure head sufficiently to cause an apparent capillary fringe extension following the first few hours of pumping. Significant gradients were persistent throughout the test at locations where saturation was less than 85%. Accounting for the formation of vertical gradients, no simulation was able to replicate the soil moisture distributions observed by Bevan et al. (2005). Based on these results, heterogeneity, hysteresis, and entrapped air were proposed as processes with the potential to significantly affect drainage from above the water table during pumping, as their investigation may provide the physical mechanism for

the observed capillary fringe extension. Compaction of the aquifer material was dismissed as a potential mechanism based on the results of a proctor test.

The effect of heterogeneity on drainage from the Borden aquifer during pumping was investigated numerically using geostatistical methods. A log-normal saturated hydraulic conductivity distribution was used to represent the Borden aquifer. Brooks and Corey parameters were used to describe the pressure-saturation-relative conductivity relationships. The air-entry pressure parameter was scaled to the saturated conductivity using the scaling relationship for Borden sand proposed by Keuper and Frind (1991). The Brooks and Corey lambda parameter was kept constant. A Monte Carlo analysis was performed on the results. While several realizations of the hydraulic conductivity distribution resulted in the formation of perched water during drainage, the ensemble capillary fringe thickness was unchanged from the thickness generated using a homogeneous conceptual aquifer model. No single realization produced a capillary fringe extension in which the magnitude was a function of elapsed pumping time, or distance from the pumping well. Approximation of the effect of air-entry barriers on drainage did not increase the estimated capillary fringe thickness. The presence and location of finer grained layers appeared to have a much greater impact on the thickness of the capillary fringe than the drawdown induced by pumping. Ensemble results for the hydraulic head drawdown provided improved matches to the field observations in comparison to the homogeneous numerical model during intermediate and late times in the pumping test. A mild degree of heterogeneity appears to have sufficient effect on drainage from above the water table during pumping to impact hydraulic drawdown. The effect would be magnified with the greater degree of heterogeneity that is more typical of natural aquifer systems.

A 24-hour pumping test was conducted at CFB Borden to gain a better understanding of the nature of drainage during a pumping test. Due to the wet site conditions prior to the test, the moisture profile during pumping was significantly influenced by hysteresis. The hydraulic head drawdown generated during the test was insufficient to generate any drainage due to the lowering of the top of the saturated zone, and the formation of perched lenses could not occur. Hysteresis in the moisture profile was a controlling factor in this result. Although there was no significant drainage initiated due to the lowering of the top of the saturated zone, an inflection point was still apparent in the time-drawdown curve for the four monitoring wells observed. Vertical gradients measured throughout the saturated zone, including the capillary fringe, remained low throughout the duration of pumping, and no significant increase was apparent in the transition from saturated to tension-saturated conditions. Hysteresis has the potential to increase the delay in drainage as the water table falls during pumping.

A laboratory tank apparatus was used to determine the effect of entrapped air, grain size distribution, and horizontal gradient on drainage in a primarily horizontal flow regime. The tank was packed on three separate occasions, once with a coarse well sorted silica sand, and twice with sand from the Borden aquifer.

For each packing, the tank was drained twice, using two different horizontal gradient magnitudes. Results show that horizontal gradient magnitude has no impact on soil moisture distributions during drainage. Air-entry pressure was elevated in comparison to gravity drainage derived pressure head – saturation curves. This elevation was not transient, nor dependant on gradient or grain size distribution. The increase in air-entry pressure does not appear to be due to insufficient equilibration time between water level drops or flow redistribution around the TDR Rods.

Results of this study support a conceptual model of unconfined aquifer response in which drainage from above the water table is a complex and time dependant process. Individually, heterogeneity and hysteresis have been shown to cause a time delay between the lowering of the water table and the subsequent drainage of the tension saturated zone during intermediate to late pumping times. The magnitude and duration of this delay varies by process and is a function of the degree of heterogeneity, moisture conditions in the aquifer prior to pumping, and the drawdown rate of the water table. While no individual process tested could produce the capillary fringe extension observed by Bevan et al. (2005), the investigation of each has led to an improved conceptual understanding of the response to pumping in unconfined aquifers. Due to the complex interaction of these processes it is unlikely that pumping test results, even those which include moisture content observations, could be used to accurately predict unsaturated flow parameters. Storage parameter (i.e. specific yield) estimates made using analytical solutions may not be appropriate unless delayed drainage from above the water table is properly accounted for.

Acknowledgements

I would like to thank my supervisors Drs. Anthony Endres and Jon Paul Jones for providing me with such a challenging topic to spend 5 years exploring. Thank you to JP for getting me interested in variably saturated flow back in Porous Media, and thank you to Tony for always pushing me forward in the science, and keeping me caffeinated at Tim Horton's.

I would like to thank my committee members Drs. David Rudolph, Robert Gillham, and Neil Thomson for imparting their wisdom and guidance through each step of this work. Special thanks to Dave for providing guidance for my pumping test in the field and the subsequent publication.

A big thank you to my friend and office mate Colby Steelman. Colby provided a friendly ear to bounce ideas off of, and was always a big help in the field. I will miss our talks.

Thanks to Steve Berg for answering endless questions and constantly lending supplies. Thanks to Cameron McNaughton and John Mosquera for keeping the mood light in the field. Cameron Toy, and Jon Rigg were helpful in the early trials and errors with my tank work. To Steve Frey, Joanna Neimi, Jeff Melchin, Greg Friday, Ed Cey, Bob Ingleton, Paul Johnson, and Dr. Gary Parkin for their help and advice on all of the field methods I used in this work.

My parents Mike and Lori Bunn have been long supporters of my curiosity and desire to learn. I thank them for providing so much support through a lifetime of learning. Thanks to my little sister Lindsay for keeping me both humble and well dressed. Also thank you to my extended family, uncles, aunts, cousins, and in-laws for your encouragement.

A special thank you to my husband Nick Bishop, without you I would never have made it. Thank you for being a great teammate in all aspects of life, for supporting what I was doing without question, and for and hanging out in the emergency room with me more times than anyone should have to.

Dedication

In memory of my grandparents Burt and Pat McIsaac and Betty Bunn

Table of Contents

List of Figures

List of Tables

Chapter 1
Introduction

1.1 Background

Pumping tests are an integral tool for quantitative hydrogeologists. Simple tests can be completed with a minimum of a single pumping well and pressure transducer. However, pumping tests are typically more complex. It is not uncommon to conduct a pumping test on a time scale of several months, using many automated water level logging systems in observation wells separated by kilometers. The results of these complex pumping tests can generate aquifer properties over large scales, indicate the interaction between aquifer systems, and determine the potential impact of pumping on surface water bodies and environmentally sensitive areas such as wetlands. Pumping test results can be used to extrapolate the long term response of an aquifer for water supply purposes, or help to define the design of contaminated site remediation systems. Clearly pumping tests are a valued component of the characterization of any groundwater system.

Following the introduction of an analytical solution for transient pumping of confined aquifers by Theis (1935), separate solutions for pumping in unconfined systems were developed. Early tests in unconfined aquifers, such as the test completed at Grand Island Nebraska by Wenzel (1936), were found to display significantly different time-drawdown curves in comparison to confined aquifer tests. Figure 1.1 shows idealized time-drawdown curves for both an unconfined and confined aquifer. The curve for the confined aquifer shows a fairly consistent progression, wherein drawdown rates are high early in the test, and decrease to negligible amounts as a steady state condition is reached. The unconfined aquifer response is markedly different as three distinct phases are distinguishable. The first phase is similar to the confined aquifer with a high rate of drawdown. The second phase, during the intermediate portion of the pumping test, is represented by a decreased rate of drawdown. The final phase is represented by an increase in the rate of drawdown prior to the final reduction in drawdown rates as the system reaches steady state. Clearly a more complex conceptual model was required to account for these changes. It is noted here that in this thesis, drawdown refers to hydraulic head drawdown. In discussion of other types of drawdown (i.e., water table, saturation surface) the variable in question will be referenced.

Conceptual models of the unconfined pumping response can be broken into two broad categories: those that assume the entire drainable volume is released instantly as the water table drops; and those that assume water held in storage above a falling water table will drain more gradually. These two conceptual models are implemented through analytical solutions for pumping test analysis. The first such solution to account for the characteristic flattening of the time-drawdown curve was developed by Boulton (1954, 1963). This solution accounts for delayed yield using an exponential function and an

empirical time constant. Later solutions by Neuman (1972, 1974, 1975) made an assumption of instantaneous drainage, such that any volume of soil through which the water table passes will instantly yield its drainable volume. It is noted here that the upper boundary for both solutions, the water table, is the zero pressure isobar, not the top of the saturated zone. While both types of solutions are capable of replicating hydraulic head drawdown observations, their predictions of specific yield are significantly different. Many studies (Nwankwor et al., 1984, 1992, Narasimham and Zhu, 1993; Moench et al., 2001; Moench, 2004; and Endres et al., 2007) have shown that an instantaneous drainage type solution will tend to predict a lower specific yield than would be expected based on laboratory values, drained volumes in the field, or numerical simulations which incorporate delayed drainage. Other studies have compared analytical solutions to analog (Stretslova, 1973) and numerical (Krozinski and Dagan, 1975) models to show that the delay in drainage from above the water table is negligible and can be ignored in most field cases. Neuman (1987) has argued that while delayed yield solutions do provide a higher estimate of specific yield, an instantaneous drainage estimate is more representative of what can be achieved in shorter pumping intervals.

With the development of more complex analytical solutions for pumping test analysis, technological advancements in monitoring and pumping equipment have permitted comprehensive data collection during pumping tests in unconfined aquifers. Nwankowr et al. (1992) conducted a 3-day pumping test in an unconfined medium sand aquifer at Canadian Forces Base (CFB) Borden, Ontario. That test included gamma measurements of moisture content, and tensiometric measurements of pressure head above the water table. Observations showed the presence of excess storage in the tension saturated zone during the early period of the pumping test. This transient effect resulted from vertical gradients that formed throughout the saturated zone. The excess storage was found to drain as vertical gradients decreased. The decrease in vertical gradient magnitude was found to coincide with the reduction in drawdown rates observed below the water table (Nwankwor et al., 1992).

Moench et al. (2001) analyzed the drawdown from a highly detailed and discretely monitored pumping test in the coarse glacial outwash sediments at Cape Cod, MA, and found that analytical solutions which incorporated delayed yield provided a significantly better match to drawdown observed below the water table. Numerical experiments conducted by Narasimhan and Zhu (1993) also confirmed that flow in the variably saturated zone above the water table can have significant impact on drawdown in the saturated zone. Researchers who support an instantaneous drainage assumption have maintained doubts over the significance of these effects (Neuman, 1979, Neuman, 1987, and Mao et al, In Press), arguing that the shape of time-drawdown curve for unconfined aquifers is the result of a transition from elastic storage to gravity drainage effects. A more detailed summary of the conceptual

models for pumping in unconfined aquifers and the associated analytical analysis methods is included in Appendix A.

A 7-day pumping test conducted in the unconfined aquifer at CFB Borden by Bevan et al. (2005) again highlighted the complex nature of drainage from above the water table during pumping. The test included moisture content measurements from above the water table, and pressure head measurements below the water table. The moisture profiles collected during the Bevan et al. (2005) test showed that the top of the saturated zone was drawn down at a slower rate than the water table, resulting in an extension of the capillary fringe. This extension persisted to the end of pumping at 7 days. The magnitude of the extension was found to be a function of elapsed pumping time, and radial distance from the pumping well. It is noted here that the first moisture content observations in the Bevan et al. (2005) test were made after approximately 500 min. of pumping, and the extension is not related to the excess storage observed in early time by Nwankwor et al. (1992). Endres et al. (2007) completed an analytical analysis of that test and concluded that no solution could properly account for the flux across the water table observed during pumping.

It has been suggested by Narasimhan (2007) that numerical models which incorporate variably saturated flow above the water table may be more appropriate for the analysis of the Bevan et al. (2005) test. Numerical simulation of the Nwankowr et al. (1992) test was completed by Akindunni and Gillham (1992) using the variably saturated flow code SUNFLOW. Their results showed that numerical simulations can properly predict the effect of vertical gradients on the development of excess storage above the water table during early periods of pumping. Moench (2008) attempted to simulate the late and intermediate time data from the Bevan et al. (2005) test using both semi-numerical analytical models and a sophisticated, variably saturated numerical model. No models tested were able to reproduce the intermediate and late time capillary fringe extension observed by Bevan et al. (2005) using spatially and temporally consistent parameters. Moench (2008) was able to match simulation results to moisture content observations at discrete times by varying a relative conductivity parameter over three discrete time periods. Heterogeneity, entrapped air and hysteresis, and viscoelastic compression of the unconsolidated aquifer material with pumping were proposed by Moench (2008) as the possible causes of the moisture content profiles observed.

The data set collected by Bevan et al. (2005) provides a unique opportunity to investigate the impact of various processes known to affect variably saturated flow on pumping induced drainage, and hydraulic head drawdown in unconfined aquifers. A better understanding of the impact of unsaturated flow processes on pumping may help to provide more reliable estimates of unsaturated parameters from pumping test data. While various researchers have investigated how unsaturated flow is impacted by

heterogeneity (Stevens and Heerman, 1988, McCord et al. 1990, McCord et al., 1991, Ursino et al. 2001, Glass et al., 2005, Ward and Zhang, 2007), hysteresis (Kaluarachchi and Parker, 1987, McCord et al., 1990, McCord et al., 1991, Basile et al., 2003, and Canone et al., 2008), and entrapped air (Faybishenko, 1995, Ronen et al., 1997, Wildenschild et al., 2001, and Berekowitz, 2004), these studies have been conducted either on the lab scale, or under one-dimensional flow in the field due to the difficulties in observing and simulating these processes. Investigation of the effect of these processes on the pumping response of the well characterized Borden aquifer will provide new insight into the sensitivity of pumping results in unconfined aquifers to the complex flow regime that occurs above the water table.

1.2 Objectives

The main objective of this thesis is to provide an increased understanding of impact of various unsaturated flow processes on the response of unconfined aquifers to pumping stress. The goal of this work is to expand the conceptual model of unconfined pumping tests to include how these processes may influence drawdown and drainage during intermediate and late portions of the test. Specific objectives of this study were:

- To reproduce the capillary fringe extension observed by Bevan et al. (2005) using state-of-the-art variable saturated groundwater flow codes
- To evaluate the impact of a mild degree of heterogeneity on the drainage response of the vadose zone to a field scale pumping test
- To monitor the effect of hysteretic behavior on drawdown during pumping in an unconfined aquifer
- To monitor the impact of air entrapment, horizontal gradient magnitude, and grain size distribution on drainage from a sandy soil under horizontal gradients

1.3 Thesis Organization

This thesis has been organized into 6 chapters. Chapters 3 through 5 constitute the main components of this thesis. These chapters were completed as stand-alone manuscripts and contain their own introduction and conclusions. The introduction sections of published chapters have been shortened from their publication form to limit repetition.

Chapter 2 briefly summarizes the data collected by Michael Bevan during a 7-day pumping test which was completed as part of his Master's Thesis (Bevan, 2001). This data set was a primary motivator for this study. Chapter 2 also includes a brief summary of the initial numerical simulations of the Bevan et al. (2005) pumping test. The vertical gradients generated by the numerical models are also analyzed and compared to the field data. A more detailed discussion of these simulations is included as Appendix B.

As the conceptual model introduced in Chapter 2 used only an anisotropic and homogeneous approximation of the hydraulic conductivity heterogeneity of the aquifer, geostatistical methods were used to more fully account for this heterogeneity in Chapter 3. This chapter was written in collaboration with Jon Paul Jones, David Rudolph and Anthony Endres, and was published in the *Journal of Hydrology* (Bunn et al., 2010). The results of the Bevan experiment were used to evaluate model performance and the impact of heterogeneity on simulation results.

The simulations of the hydraulic conductivity heterogeneity highlighted the need for additional field data regarding the response to pumping in simple aquifer systems. Chapter 4 presents the results of a 24-hour field scale pumping test completed in October 2009. The setting of the test provided new insights into the effect of hysteresis on pumping test results. This chapter was written in collaboration with David Rudolph, Anthony Endres, and Jon Paul Jones, and was published in the *Journal of Hydrology* (Bunn et al., 2011).

Chapter 5 presents the results of a laboratory experiment to further investigate drainage under a primarily horizontal gradient. A laboratory scale flow through tank permitted the use of a homogeneous soil structure, and controlled flow conditions. The results of this experiment show the effects of entrapped air, grain size distribution, and horizontal gradient on soil drainage under a predominately horizontal flow field. These effects can be extrapolated to the conceptual model of a field response to pumping. Unique results relating to the magnitude of the air entry pressure were observed.

Chapter 6 summarizes the findings of the individual chapters and applies the findings to the general conceptual model of the link between drainage from above the water table and hydraulic head

drawdown during pumping tests. Potential mechanisms for the capillary fringe extension observed by Bevan et al. (2005) are suggested. This chapter includes recommendations for future study.

1.4 Figures

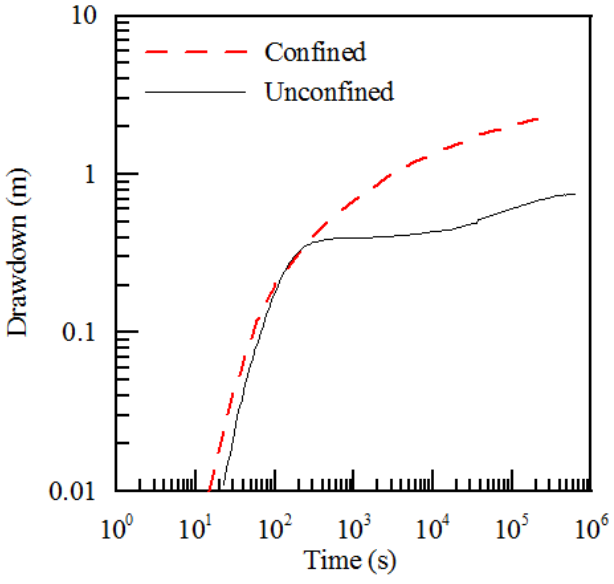

Figure 1.1. Idealized time-drawdown curves for confined and unconfined aquifers

Chapter 2

Research Context

As introduced in Chapter 1, the unique results of the Bevan et al. (2005) test provide an excellent opportunity to evaluate the impact of various variably saturated flow processes on the response to pumping in an unconfined aquifer. This chapter presents the results of an evaluation of three modern groundwater flow codes for their ability to simulate the results of the Bevan et al. (2005) experiment. While all three codes solve Richards' equation for variably saturated flow, each differs in their mathematical implementation of the solution. Testing of three codes permitted the differentiation of effects of the conceptual model from the effects of the mathematical implementation. The formation and dissipation of vertical gradients during the early portion of the test is also analyzed. A more detailed summary of the results of the Bevan et al. (2005) test is also included for reference.

2.1 Test Description

Two pumping tests were conducted in the Borden aquifer as a component of the M.Sc. thesis work of Michael Bevan (Bevan, 2001). The site used for these tests was the same as the site established by Nwankowr et al. (1984) and used by Nwankwor et al. (1992). The Borden aquifer consists of prograding foreshore deposits of glacial Lake Algonquian (Bohla, 1986). The texture of the aquifer varies locally from fine to coarse grained sand with hydraulic conductivities ranging within two orders of magnitude (Sudicky, 1986). While significant heterogeneity is present on the scale of a soil core, the aquifer is typically described as homogeneous at the pumping test scale (MacFarlane et al., 1983). The aquifer is 9 m thick and is underlain by a clayey aquitard.

The first test was designed to investigate the use of ground penetrating radar (GPR) as a method for monitoring the evolution of the drawdown cone during pumping. GPR generates a strong reflection where there is a large change in moisture content, such as the transition between fully and partially saturated conditions at the top of the capillary fringe (Bevan et al., 2001). Volume balance methods were used to determine the drained volume from both the GPR data and the piezometric data. Based on these calculations it was found that the GPR derived volumes underestimated the volume drained based on hydraulic data. In analyzing the drawdown of both the transition zone (neutron data and GPR) and the hydraulic head, it was concluded that the moisture profile was drawn down at a slower rate than the hydraulic head, resulting in excess storage that appeared to be contained within the capillary fringe. This excess storage not only persisted, but continued to grow through the 7 days of the pumping test. It was concluded that additional work was required to determine the cause of this difference (Bevan et al., 2003).

A second test was initiated at the same site in 2001. Prior to pumping, the static water table was 2.75 m below ground surface. During this test, the well was pumped at a rate of 40 ± 1 L/min. for a period of 168 hours, with recovery monitored for 120 hours. Neutron probe moisture content logging was performed in a series of six neutron access tubes using a 0.05 m vertical sampling interval from 1.25 to 3.5 m below ground surface. Neutron moisture profiles were completed at 18 times in all six access tubes during pumping. A total of 11 piezometers were continuously logged, these were grouped in shallow – deep piezometer pairs at 1.5, 3, 5, 10, 15 m radial distance from the pumping well. An additional 14 piezometers were measured periodically by hand (Bevan et al., 2005).

The monitored piezometers responded predictably for the majority of the test. Following a typical unconfined response curve, the hydraulic head-drawdown rates were high early in the test, slowed in the intermediate period, and increased again towards the end of the test. By the fourth day of pumping, hydraulic head drawdown rates decreased, indicating a potential interaction with a recharge boundary; however, this did not impact the main conclusions of the test. The neutron derived moisture profiles generated during pumping deviated significantly from the moisture profiles observed prior to the commencement of the test. Specifically, the moisture profiles showed a tension saturated zone (capillary fringe) that increased in thickness (i.e. extended) due to differential drawdown between the water table and the top of the capillary fringe (Bevan et al., 2005). The capillary fringe extension increased with pumping duration throughout the entire test. The extension was inversely proportional to distance from the pumping well, with less extension occurring at larger distances from the well. Vertical gradients were calculated between the shallow and deep piezometer pairs. The peak magnitude was of similar order to the gradients observed during the Nwankwor et al. (1992) test; gradients decreased gradually following the peak in magnitude. The capillary fringe extension discussed herein is observed only during intermediate and late times and is independent of the vertical gradients formed. The extension and processes which occurred at intermediate and late times discussed herein are considered independent from the excess storage observed by Nwankowr et al. (1992) during the early portions of pumping.

Endres et al. (2007) used the Bevan et al. (2005) data set to evaluate the ability of several analytical models to predict aquifer properties. The Neuman (1972, 1974) instantaneous drainage solutions was compared to two delayed drainage type solutions; the Moench (1995) single exponential solution, and the Moench et al. (2001) solution using three empirical coefficients. While both the Neuman (1974) and Moench (1995) solutions significantly underestimated the laboratory derived specific yield value of 0.3 for Borden sand determined by Nwankwor et al. (1984), the linear combination solution with three α parameters (Moench et al. 2001) generated a reasonable estimate of 0.284. None of the analytical solutions tested were able to accurately replicate the cumulative drainage flux across the water table or

the persistence of undrained vadose zone storage inferred from the neutron probe data. Consequently, Endres et al. (2007) concluded the implicit boundary conditions used to represent drainage in these analytical solutions do not accurately reflect the physical response of the vadose zone to pumping. Narasimhan (2007) has suggested the physical processes leading to the results observed by Bevan et al. (2005) may be more realistically simulated using numerical codes which incorporate variably saturated flow.

2.2 Numerical Simulations

Simulations of the Bevan et al. (2005) pumping test were performed using three different numerical codes; HydroGeoSphere (HGS) (Therrien et al., 2006), Integrated Hydrogeology Model (InHM) (VanderKwaak, 1999), and VS2D (Lappala et al., 1987). All three codes fully account for variably saturated flow in the subsurface. A homogeneous and anisotropic conceptual model was used to describe the Borden aquifer. Material properties were set using literature derived values. Simulations were completed using both Brooks and Corey (1964), and van Genuchten (1980) descriptions of the pressure head – saturation – relative conductivity relationship. As initial results provided a good match to hydraulic head drawdown observed in the field, no further calibration was performed. Properties used to populate the numerical simulations are included in Appendix B. Full details of these simulations can be found in Appendix B. The following section summarizes pertinent components of the study.

All three numerical codes successfully replicated the hydraulic head drawdown measured below the water table, as well as the water table drawdown estimated from the hydraulic data for the Bevan et al. (2005) test. Illustrative results showing the simulated drawdown at 3 m radial distance from the pumping well are shown in Figure 2.1 (hydraulic head drawdown) and Figure 2.2 (water table drawdown). The temporal variations in vadose zone water content inferred from neutron moisture probe data could not be reproduced by any of the numerical simulations. None of the numerical simulations were able to reproduce the observed capillary fringe extension. Figure 2. 3 shows a comparison between the observed moisture profile at the end of pumping, and the moisture profile generated by each of the numerical simulations. As shown in the figure, the models used were unable to replicate the soil moisture distributions observed above the water table during pumping.

Although Bevan et al. (2005) did not include observations of hydraulic head above the water table during pumping; they were able to calculate the vertical gradients between piezometer pairs. Gradients were found to peak after approximately 10 min. of pumping, and slowly decreased through pumping duration (Bevan et al., 2005). These results conform to the conceptual model presented by Nwankwor et al. (1992). The results of the HydroGeoSphere numerical simulation were analyzed for their ability to

predict the formation and dissipation of vertical gradients. The vertical gradients between observation wells simulated by HydroGeoSphere at various stages in the pumping test are shown as solid lines in Figure 2.4. The associated observations made during the Bevan et al. (2005) pumping test are shown as symbols in Figure 2.4. Positive vertical gradients correspond to downwards vertical flow. Gradients at all four radial distances peaked at approximately 10 min., and decreased progressively for the remainder of the simulation. Vertical gradient magnitude was found to increase with proximity to the pumping well. The simulated vertical gradients were similar to those observed by Bevan et al. (2005) in terms of both magnitude and development over time. The numerical simulations slightly over predict the magnitude of the vertical gradients from approximately 5 min. of pumping through to the end of the test. This difference is not considered significant. The vertical gradient magnitudes simulated at 3 m radial distance from the pumping well remained below 0.087 m/m during the neutron observation period, resulting in a potential error in pressure head estimations of 0.03 m. Thus, the intermediate and late time capillary fringe extension observed by Bevan et al. (2005) cannot be attributed to poor estimates of water table positions based on peizometer data.

To test the continuity of vertical gradients across the water table, gradients simulated by HydroGeoSphere throughout the entire aquifer thickness were calculated and the results are shown in Figure 2.5 for radial distances of 1.5 m (a) 3 m (b), 5 m (c) and 15 m (d), at four times during the test. The top of the saturated zone is marked on each profile. Within the saturated zone vertical gradients remain below 0.1 m/m throughout the entire pumping duration. The time to the peak in vertical gradient magnitudes in the tension saturated zone is a function of distance from the pumping well, but is approximately 10 min. All vertical gradients in the saturated zone decrease significantly within 1000 min. of pumping. These results are in agreement with the numerical modeling completed by Akindunni et al. (1992)

As the pumping well was partially penetrating, vertical gradients below the water table increase in the region near the well screen. The effects of the partially penetrating well are most apparent at locations within 3 m radial distance of the pumping well, and decrease significantly with radial distance from the well. Vertical gradients are also high above the saturated zone. Above the water table vertical gradient magnitudes in zones at less than 85% saturation increase throughout the entire duration of pumping, and begin to approach a unit gradient within 1000 min. pumping duration. Gradients of this magnitude would have significant implications on the relationship between pressure head and elevation during pumping, and may affect the transition portion of the pressure head – moisture content profiles presented by Bevan et al. (2005). However, given the low vertical gradient magnitudes in the saturated zone after 1000 min., the capillary fringe extension observed by Bevan et al. (2005) cannot be attributed to vertical gradients.

Similar numerical simulations of the Bevan et al. (2005) pumping test were performed by Moench (2008) using a numerical groundwater flow model. The simulations conducted in that study yielded similar estimates of capillary fringe thickness, and no extension was generated using a homogeneous anisotropic conceptual model. An improved fit to the observed soil moisture distributions was achieved using the Assouline (2001) model for the saturation - relative hydraulic conductivity relationship. The Assouline model included an additional parameter in comparison to the Brooks and Corey or van Genuchten type models used herein. By varying this parameter with pumping duration, Moench (2008) was able to match the observed soil moisture distribution at three discrete times. However, this method was unable to replicate the moisture distribution over the entire duration of the test, or within portions of the aquifer at lower moisture content. Moench (2008) suggested some potential mechanisms for the observations made during the Bevan et al. (2005) test; it is these and other mechanisms which were investigated in detail in this study.

2.3 Processes with the potential to influence drainage during pumping tests

The failure of all tested numerical simulations to produce a consistent match to the intermediate and late times soil moisture data collected by Bevan et al. (2005) suggests the influence of some process or processes are not properly accounted for in the codes. This study will focus on the potential impact of compaction of the aquifer, heterogeneity, hysteresis, and entrapped air on the response of an unconfined aquifer to pumping. A better understanding of these processes may improve the conceptual model of unconfined aquifer response, help to explain the results of the Bevan et al. (2005) test and improve methods used to estimate unsaturated parameters from pumping test data as attempted by Moench (2003). A brief introduction of each process is included herein.

Compaction

The numerical simulations of Moench (2008) made use of a decoupled relative permeability relationship using the Assouline (2001) function, which incorporates an additional parameter (η) to account for variations in soil structure and texture. Calibration of a numerical model to the hydraulic head drawdown and moisture content results of Bevan et al. (2005) resulted in an increase in the parameter η as the duration of pumping was increased. One of the implications of this finding is that the unconsolidated glacial fluvial sand deposits that form the Borden aquifer underwent compression due to pumping stress (Moench, 2008). With increased hydraulic head drawdown, the stress on the aquifer material is increased such that compaction of the material is drawdown dependent. The effect of changes in bulk density on water retention and relative conductivity can be incorporated using the models outlined in Assouline (2006a, 2006b). Relative hydraulic conductivity curves for unconsolidated sand over a bulk density change of 4% show minor compactive effects (Assouline, 2006b), with the water retention model predicting a 2×10^{-5} m decrease in maximum pore radius with

compaction (Assouline, 2006b). This decrease in pore radius would result in an increase in capillary fringe thickness by a factor of 1.2, significantly less than that observed in the field by Bevan et al. (2005). To estimate a possible range of bulk density changes for the Borden aquifer material, a standard proctor test was performed where the soil was compacted into a mold at various moisture contents under a standard force of 594 kN/m^2 (Sawangsuriya et al., 2008). The compactive pressure applied in a proctor test would be equivalent to a change in pressure head of approximately 60 m, a value significantly greater than the change in pressure expected during a pumping test. The results show a potential range in bulk density from 1.68 kg/m^3 to 1.92 kg/m^3, a change of 12%. Given the similarity of the Borden sand to the unconsolidated sand used in Assouline (2006a, 2006b), it seems unlikely for compaction during pumping to have had a significant effect on the observed soil moisture profile. Further, the head change developed during pumping is far less than what would be expected to cause significant changes in bulk density, making it unexpected for compaction of an aquifer to play a significant role in water retention during pumping from a surficial sandy aquifer. Compaction was not given further consideration in this study.

Soil Heterogeneity

The Borden aquifer is generally considered to be homogeneous on the scale of a pumping test. While the presence of finer grained sand lenses within the medium grained sand has been well documented (Sudicky, 1986), the impact of these lenses during a pumping test are not well understood. Small scale vertical variations in soil moisture content observed by Bevan et al. (2005) were attributed to this minor degree of heterogeneity. In a heterogeneous porous medium, the variation in pressure-saturation relationship for each soil type will act to increase the heterogeneity in the system and increase the complexity of the flow path as the material drains. Stephens and Heermann (1988) introduced the concept of saturation dependent anisotropy to describe the increasing heterogeneity of horizontally layered sands during drainage. This concept has been further developed by field studies (McCord et al., 1990, McCord et al., 1991, Glass et al., 2005, Ward and Zhang, 2007, Zhang et al., 2007), and laboratory investigations (Ursino et al., 2001). Laboratory studies by Silliman et al. (2002), Dunn and Silliman (2003), and Dunn et al. (2004) have shown the control of heterogeneity on flow through the capillary fringe, and the potential for air-entry barriers to restrict the drainage from course materials. Heterogeneity in the Borden aquifer certainly has the potential to impact drainage from the vadose during pumping. Heterogeneity is likely more significant in other natural aquifer systems, and the impact on pumping in the Borden aquifer would serve as a limiting case. This process is investigated in detail in Chapter 3.

Hysteresis

In a natural aquifer system, the gradual seasonal rise and fall of the water table will generate hysteresis in the moisture profile observed in the field. At the Borden aquifer, the water table has been observed to vary by as much as 1.5 m per year (Conant, 1991). It has been noted that hysteresis will significantly increase the heterogeneity of soil typically classified as homogeneous (Kalaurrachchi and Parker, 1987, McCord et al., 1990, and McCord et al., 1991). In unsaturated parameter estimation performed on intact cores, both Basile et al. (2003) and Canone et al. (2008) found accounting for hysteresis was essential. Various methods have been proposed to account for the effect of hysteresis and entrapped air on vadose zone flow simulations. Gillham et al. (1979) proposed and tested a numerical solution against a 1-D column experiment. Lenhard et al. (1991) conducted a similar experiment using the hysteresis description of Lenhard and Parker (1987) and Parker and Lenhard (1987). Both columns were packed with sandy soil; and, in both cases, it was found that a numerical description of hysteresis was necessary to reproduce the observed moisture content distribution. It is noted, however, that profiles generated using standard laboratory methods on fully saturated soil serve as the limiting curves for field profiles (Basile et al., 2003). On the field scale, numerical simulations of dune sand conducted by McCord et al. (1991) indicate that heterogeneity should have a greater influence on moisture content distributions than hysteresis. Early work by Bouwer (1979) indicated that hysteresis may play a role in the delayed drainage observed during pumping in unconfined aquifers. This delay in drainage would only be expected to persist until the drainage air-entry pressure for the soil was reached, and would be unlikely to impact the Bevan et al. (2005) pumping test. The impact of hysteresis on pumping test results will be explored in the discussion of the field data in Chapter 4.

Entrapped Air

Entrapment of air is a component of the hysteresis that occurs as a soil is drained and subsequently rewetted. Gillham et al. (1979) observed air entrappment of 8% under zero tension conditions following a single drainage-rewetting cycle in a laboratory column of Borden sand. Berekowitz et al. (2004) noted the prevalence of an entrapped air phase in the shallow region below the water table, and introduced the term “partially saturated fringe” to represent the zone of entrapped air that sits both below and above the water table. Entrapped air has been observed to significantly impact hydraulic conductivity during percolation experiments in columns (Fabishyenko, 1995). Sakaguchi et al. (2005) used column experiments to show that the hydraulic conductivity of soils at air-entry pressure is greatly reduced in comparison to the unsaturated hydraulic conductivity derived from the pressure-saturation curve. Clearly entrapped air has the potential to significantly impact hydraulic conductivities above the water table, and may act to reduce the downward drainage during pumping. As the Bevan et al. (2005) test was conducted during a seasonal low in water table elevation, entrapped air is not expected to have an

impact on the results of that test. However, the impact of entrapped air on drainage in a horizontal flow regime is briefly investigated in Chapter 5.

2.8 Figures and Tables

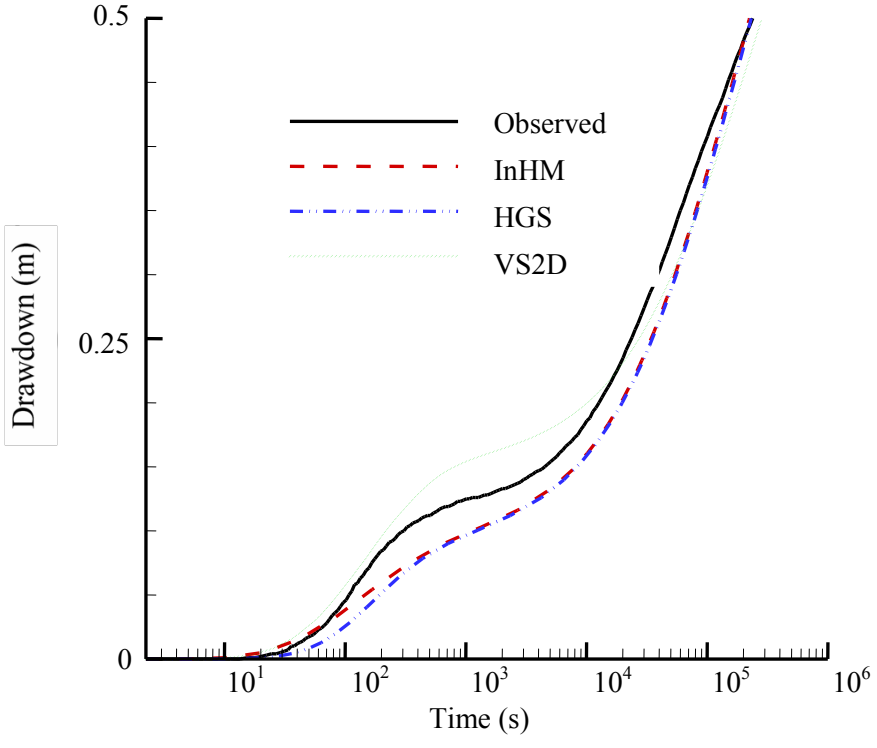

Figure 2.1. A semi-log comparison between computed results and field observations of the hydraulic head drawdown in the shallow well at 3 m radial distance using the van Genuchten constitutive relationship.

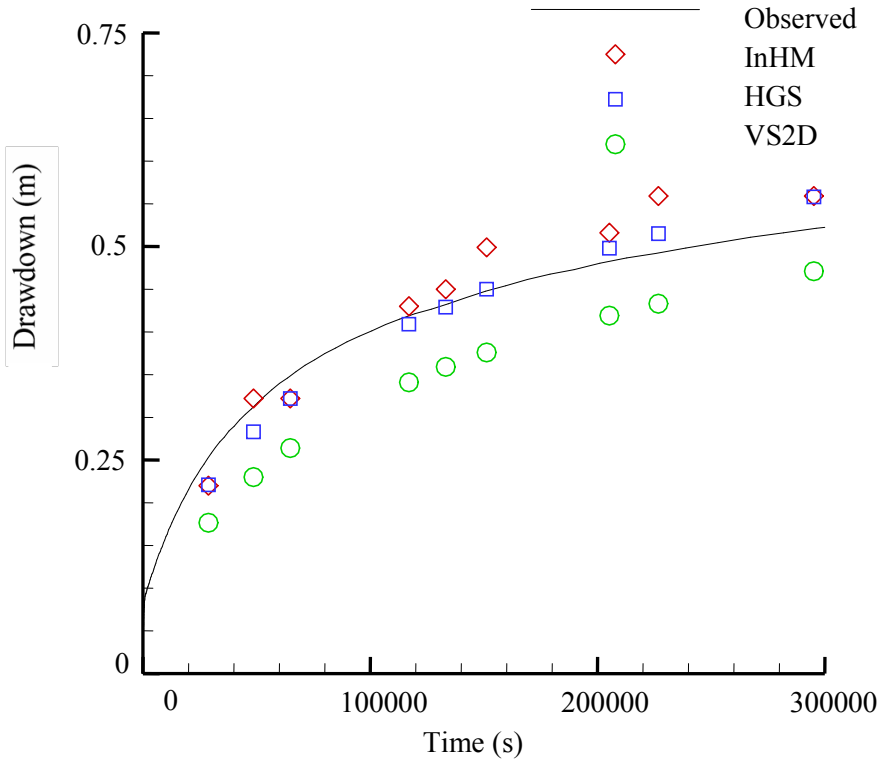

Figure 2.2. A comparison between computed results and field estimate of the water table drawdown at 3 m radial distance using the van Genuchten constitutive relationship. (Radial distances: a. 3 meters; b. 5 meters; c. 15 meters)

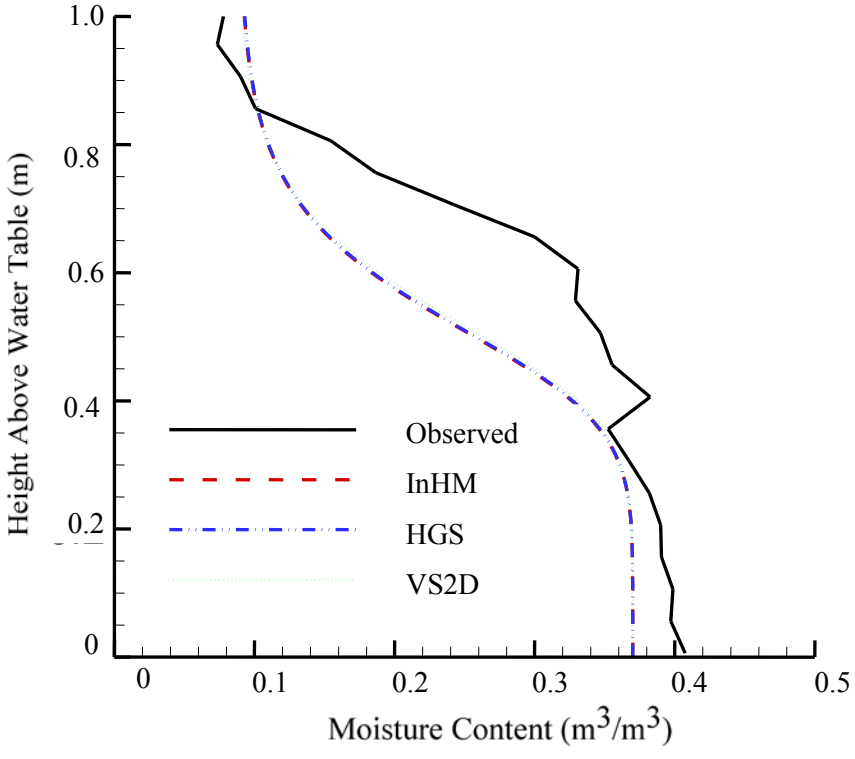

Figure 2.3. End of pumping moisture content profiles at 3 m radial distance observed and computed using the van Genuchten constitutive relationship.

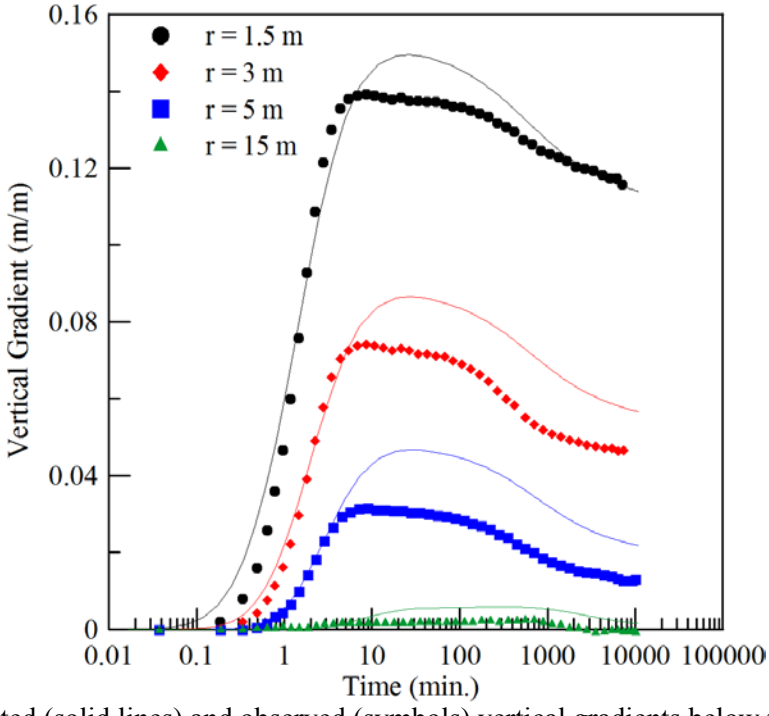

Figure 2.4. Simulated (solid lines) and observed (symbols) vertical gradients below the water table during the Bevan et al. (2005) pumping test.

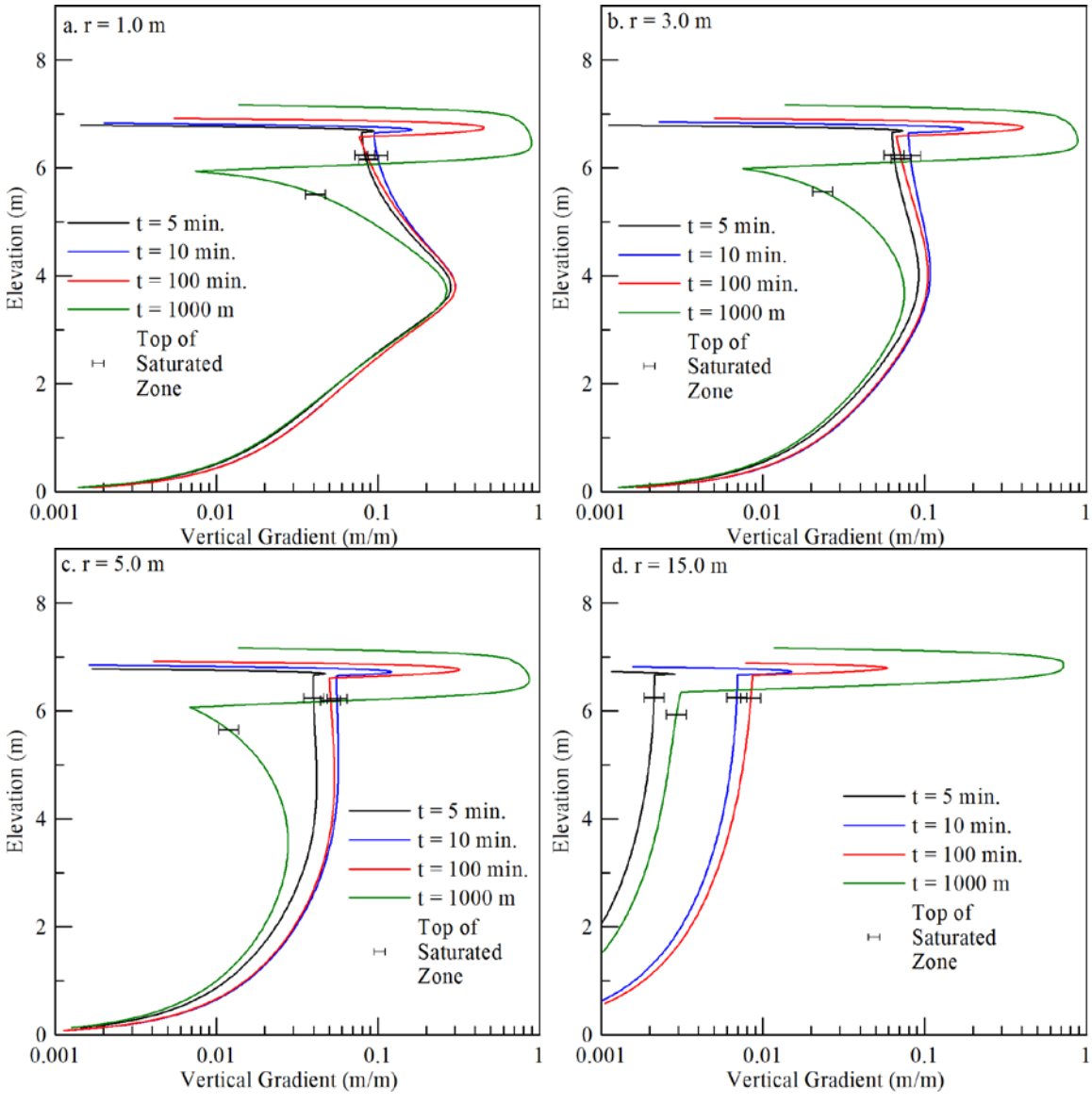

Figure 2.5. Simulated vertical gradients through entire aquifer thickness using HydroGeoSphere, Elevation is measured from base of aquifer. (Radial Distance: a. 1.5 m, b. 3 m, c. 5 m, d. 15 m)

Chapter 3

Effects of Hydraulic Conductivity Heterogeneity on Vadose Zone Response to Pumping in an Unconfined Aquifer

3.1 Introduction

Hydraulic conductivity heterogeneity has been proposed as a potential mechanism for the capillary fringe extension observed in the field by Bevan et al. (2005). Although the Borden aquifer is only mildly heterogeneous, the effects of heterogeneity in the unsaturated zone are magnified. Theoretical analysis (Yeh et al., 1985a, Yeh et al., 1985b, Yeh et al., 1985c, Mantoglou and Gelhar, 1987, Green and Freyberg, 1995, Li and Yeh, 1998, Jacobs and Gelhar, 2005) and experimental observations (Stephens and Heermann, 1988, Yeh and Harvey, 1990. Silliman et al., 2002, Wildenschild and Jensen, 1999, Glass et al., 2005) have shown that heterogeneity can have a controlling effect on the variation in moisture content and pressure head above the water table under a natural gradient. A numerical simulation of this heterogeneity was designed to determine whether the inclusion of small scale heterogeneities in pumping test modeling could provide a better approximation of the moisture content distributions observed by Bevan et al., (2005) in the Borden aquifer. The inclusion of heterogeneity in the numerical model will result in a reduction of the uncertainty in our numerical description of the vadose zone at the Borden aquifer, furthering our understanding of the mechanisms at play during pumping induced drainage in unconfined aquifers.

The Borden aquifer has been well characterized through numerous field studies, and the heterogeneity in saturated hydraulic conductivity at the site is well documented. MacFarlane et al. (1983) noted the variation of grain size from medium sand to fine sand and silt on the core scale, but asserted the aquifer is homogeneous on the scale of a pumping test. As part of a natural gradient experiment, Sudicky (1986) performed permeameter measurements on 1279 samples from this aquifer resulting in a lognormal conductivity distribution with a mean of 7×10^{-5} m/s and a variance of 0.38. The results of the natural gradient experiment in the Borden aquifer show the effects of the elongated bedding which impedes flow in the vertical direction (Freyberg, 1986, and MacKay et al., 1986). A mild degree of anisotropy has been typically used to represent this stratified and cross-bedded aquifer (see Akindunni and Gillham, 1992, Endres et al., 2007, Moench, 2008).

In this study the Borden aquifer was viewed as heterogeneous and geostatistically characterized using the results of Sudicky (1986). A homogeneous model assuming a mild degree of hydraulic conductivity anisotropy is used for comparison. The effect of heterogeneity on the pumping test was determined using a Monte Carlo analysis.

3.2 Numerical Simulations

All numerical simulations were completed using the three-dimensional control-volume finite-element code HydroGeoSphere (HGS) (Therrien et al., 2006). Borehole and well bore storage are not accounted for in the simulations presented; however, these factors are expected to have a limited effect on the results presented owing to the duration of the test and the distance from the observation points to the well. Numerical simulations of the pumping test were implemented using a 400 m x 400 m x 9 m finite element grid. The horizontal discretization varied from 10 m elements near the outer boundaries to 0.01 m elements in the regions surrounding the observation wells, the pumping well, and the neutron access tubes. The vertical grid spacing was divided into 2 regions. From the ground surface to 1.75 m BGS (i.e., within the zone of residual saturation), a vertical element spacing of 0.25 m was used. The second region was composed of 0.05 m vertical element spacings and extended from 1.75 meters BGS to the aquitard. Finer vertical discretization schemes were also tested (i.e 0.01 m), but resulted in substantially greater computational effort and no appreciable changes in the modeling results. Hence, the results presented were generated using the coarser 0.05 m mesh.

A no flow boundary condition was applied at the bottom of the domain, simulating the clayey-silt aquitard underlying the Borden aquifer. The lateral boundaries of the finite element flow domain were located 200 m from the pumping well. Two different simulations were conducted to verify that the nature of the lateral boundary conditions (i.e., a constant head boundary versus a no flow boundary) had little or no influence on the flow solution in the vicinity of the pumping and observation wells. The difference in the hydraulic head results generated using the different lateral boundary condition types was insignificant (drawdown at the lateral boundaries was less than 0.05m); results presented were generated with constant head boundaries. The pumping well boundary is represented by a one-dimensional line element. Horizontal 1-D flow to the well is described following Therrien and Sudicky (2000). Storage both from the compressibility of the water and from the drop of the water level in the well are accounted for (Therrien et al., 2006). When the water table is drawn into the well screen, flux into the well from elements at negative pressure heads is limited by setting the conductivity of the well screen adjacent to those nodes at less than that of the aquifer material (Therrien et al., 2006)

3.2.1 Homogeneous Approximation

Historically, the Borden aquifer has been treated as homogeneous and mildly anisotropic for numerical and analytical studies. In comparison to most other natural aquifers, this assumption is viewed as a reasonable approximation for pumping test simulations in the saturated zone. A homogeneous numerical model was calibrated to the hydraulic head drawdown observations made by Bevan et al. (2005) at the 3, 5, and 15 m shallow-deep piezometer pairs as a basis for comparison to the heterogeneous simulations. Hydraulic conductivity values and specific storage for the aquifer were

calibrated using PEST (Watermark Numerical Computing, 2004). The calibration was carried out to 3.5 days of pumping to avoid the influence of the potential recharge boundary interaction.

Unsaturated parameters were not calibrated concurrently to the hydraulic data. The Brooks - Corey relationship was fitted to the laboratory drainage curve generated for Borden sand by Nwankwor (1984), and these parameters were fixed to describe both the pressure-saturation and saturation-hydraulic conductivity relationships used in the calibration. Attempts made by Moench (2008) to calibrate the Brooks and Corey (1964) parameters to the Borden test hydraulic head data resulted in insensitivity of the air entry parameter, and a pore-size distribution parameter that did not match the observed static moisture profile. Our initial calibration experiments had similar results. Although calibration of the unsaturated parameters may improve simulation results, the lack of pressure head data above the water table in the Bevan et al., (2005) data set prevents further calibration efforts. Residual and saturated water contents were fixed at the values given in Akindunni and Gillham (1992). Calibrated parameters, fixed parameters, initial values, root mean squared error, and initial sources are presented in Table 3.1 . Calibration was performed using data from all 11 monitoring wells simultaneously. The hydraulic head drawdown results produced by the calibrated model for the 3.5 day period are presented in Figure 3.1 (a-c) for the three shallow-deep piezometer pair locations. It can be seen that the hydraulic heads predicted by the homogeneous model provide good approximations to the field observations. This goodness of fit was observed for all of the 11 monitoring wells observed by Bevan et al. (2005).

The modeled moisture profiles for the 3 m neutron access tube generated by HGS prior to pumping, and at 3.5 days are given in Figure 3.2. Prior to pumping, the simulated moisture profile is an approximation of the field observations inferred from the neutron data. The slight variability in the field curve is a result of the mild degree of heterogeneity present in the Borden aquifer. Throughout the duration of the pumping test, the results of the numerical model differ significantly from the field observations. This difference is most apparent near saturation in the moisture profiles presented in Figure 3.2(a). Specifically, the elevation above the water table at which the profile begins to desaturate in the model predictions is consistently lower than the field observations. While the numerical model predicts a capillary fringe of constant thickness, the field results indicate the capillary fringe extends in comparison to its static thickness.

The capillary fringe extensions inferred from the field data are compared with the homogeneous model predictions in Figure 3.3 for the three locations with shallow-deep piezometer pairs. It can be seen that while the extension inferred from the field observations increases with time and proximity to the pumping well, the homogeneous model predicts little to no extension. It should be noted that small

negative extension values (i.e., compressions of the capillary fringe compared to its static thickness) in the model predictions appear to be a model artifact due to the 0.05 m vertical discretization. Although the numerical simulation of a homogeneous aquifer provided an excellent replication of hydraulic heads below the water table, it was unable to replicate the moisture distribution above the water table during pumping.

3.2.2 Numerical Approximation of Aquifer Heterogeneity

The mild degree of anisotropy used in the above homogeneous simulation was able to approximate the effects of heterogeneity on the hydraulic head drawdown below the water table. However, this degree of heterogeneity has the potential to influence moisture content distributions within the vadose zone. Hence, we have used a heterogeneous conceptual model to examine the influence of the Borden aquifer heterogeneity on the moisture content distribution observed during pumping.

Hydraulic conductivity fields were generated using the random field generator FGEN, based on the inverse Fourier transform method presented by Robin et al. (1993). Following the results of the Sudicky (1986) analysis, a Gaussian log-permeability correlation was used with vertical and horizontal correlation lengths set to 0.15 m and 3.0 m respectively. The mean saturated hydraulic conductivity was set to 5.8×10^{-5} m/s to coincide with the value used for the homogeneous approximation. Variance of ln(K) was set at 0.25 after Woodbury and Sudicky (1991). Element-scale anisotropy was not used in the heterogeneous simulation as the large-scale anisotropy present in the homogeneous approximation is a means of accounting for the macroscopic heterogeneity of the system. The heterogeneous simulation is implicitly anisotropic on the macroscopic scale through the use of differing correlation scales in vertical and horizontal directions.

Brooks - Corey parameters were scaled to hydraulic conductivity following the variation on the Leverett (1941) scaling method outlined by Kueper and Frind (1991). The Leverett (1941) equation was altered to:

$$P_{Dd} = \frac{P_D}{\sigma}\left(\frac{k}{\phi}\right)^{\tau} \tag{3.1}$$

where P_D is the displacement pressure of the unit, σ is the interfacial tension of air and water, k is the permeability of the unit of interest, P_{Dd} is the dimensionless displacement pressure and τ is an empirical scaling exponent. Following the analysis of seven samples of Borden sand, P_{Dd} and τ were found to be 0.00558 and 0.65, respectively (Kueper and Frind, 1991). The Brooks - Corey parameter β was assigned a constant value of 2.48 (Kueper and Frind, 1991). Representative Brooks - Corey curves for the range of hydraulic conductivity in the heterogeneous approximations are given in Figure 3.4. As

the conductivity is decreased, the air-entry pressure increases to approximately 1m, while the slope of the moisture profile through the transition zone steepens. Residual and full saturation values were held constant.

A Monte Carlo analysis was used to investigate the impact of heterogeneity on the pumping test observations. The variance of each field generated by FGEN differs slightly from the target value of 0.25. A series of random fields were generated until the cumulative mean variance in hydraulic conductivity became stationary. While a total of 75 realizations were used in this study, the variance converges much more rapidly. The cumulative variance converges to within 0.84% of its final value within 26 realizations. A vertical cross-section through the pumping well of the conductivity field for a single realization is shown in Figure 3.5. The horizontal axes have been truncated to show the field in the vicinity of the pumping well and observation locations; in addition, a 5x vertical exaggeration has been added. The conductivity field clearly exhibits the nature of the bedding structure in the Borden aquifer, with thin layers that are more continuous in the horizontal direction.

The ensemble mean of the results from 75 realizations of the hydraulic conductivity field was compared to the hydraulic head drawdown and moisture profiles predicted from the homogeneous aquifer model, and to the field observations. As adaptive time-stepping is used in HGS, the ensemble mean hydraulic head drawdown curve was generated as a composite of each realization in the Monte Carlo analysis at 50 output times. The results for the three shallow-deep piezometer pair locations are presented in Figure 3. 6(a-c). Figure 3. 7 (a-c) shows only the ensemble results generated by the heterogeneous field, including the standard deviation of the ensemble. The variability of the ensemble results increases with duration of pumping, and proximity to the pumping well. Although the ensemble mean tends to over predict the hydraulic head drawdown at later times in the test, the resulting maximum error of 0.1 m is considered to be small. Both the homogeneous and the ensemble mean results for the hydraulic head drawdown approximate the field observations quite well. However, it is noted that at all of the shallow-deep piezometer pairs the ensemble mean provided a closer fit to the observed hydraulic head drawdowns than the homogeneous numerical model at early and intermediate times. This result implies that a homogeneous and slightly anisotropic approximation of aquifer heterogeneity may not fully capture the effect of the heterogeneity on hydraulic head drawdown, even for aquifers with a mild degree of heterogeneity.

Water table drawdown was predicted from field data using the method presented in Bevan et al. (2005). This method assumed that for radial distances greater than 3 m the magnitude of the vertical gradient was relatively constant above the lower piezometer. Based on this assumption, water table drawdown Δh^{wt} was estimated from piezometer data using:

$$\Delta h^{wt} = (\Delta h^{u} - m d^{u})/(1-m) \tag{3.2}$$

where Δh^{u} is the drawdown in the upper piezometer d^{u} is the separation between the static water table and the upper well screen. The vertical gradient m given by:

$$m = (\Delta h^{b} - \Delta h^{u})/(\Delta l) \tag{3.3}$$

where Δh^{b} is the drawdown in the lower piezometers, and Δl is the separation between the screens of the two piezometers. Water table drawdown was derived from the numerical simulations by tracking the zero pressure isobar. Results are shown in Figure 3.8(a-c). At early times, both the homogeneous model and the ensemble mean provide a good match to the field predictions. At later times (after 100,000 s), the homogeneous simulation provides a better fit to the field prediction as the ensemble mean of the heterogeneous simulations over predicts the drawdown. This discrepancy increases with time and proximity to the pumping well. These results suggest that our method for the estimation of water table drawdown from the field data provides a conservative estimate of the capillary fringe extension.

The moisture profiles generated by the heterogeneous realizations were extremely discontinuous with areas of high water content present within the transition zone in 90% of the realizations. Figure 3.9 shows moisture profiles generated by single heterogeneous simulations representative of both a capillary fringe extension (a-b) and a compression (c-d). As pumping continued perched zones would form and subsequently drain following the pressure saturation relationship of the individual zone. These perches zones were much more prevalent in the dryer portions of the transition zone than in the wetter region near the capillary fringe. The magnitude and frequency of these discontinuities did not appear to be a function of proximity to the pumping well. It is also noted that none of the heterogeneous realizations showed the downward translation of the transition zone as observed in the field.

For this study, the top of the capillary fringe was determined using the first instance of desaturation above the water table. As the Brooks-Corey pressure-saturation relationship was used each profile analyzed displayed a distinct initial desaturation point. The ensemble mean predictions of the capillary fringe extension obtained from the Monte Carlo simulation, including the standard deviations and the extremes of the individual realization values are presented in 3.10(a-c). It is noted here that several realizations included a static capillary fringe as thick as 0.6 m, which proceeded to collapse with pumping. Due to this effect, several of the minimum values included in 3.10(a-c) show a compression of the capillary fringe (negative values of extension) relative to its static thickness. The ensemble mean

capillary fringe extension generated by the heterogeneous simulation is on the order of the vertical discretization of the mesh, and is not significantly different from the homogeneous approximation, as shown in Figure 3.10(a-c). A total of 52 realizations resulted in a capillary fringe extension greater than the mesh discretization of 0.05 m. Within the pumping period analyzed in this study the maximum extension observed was 0.56 m. This extension was observed at the 3m observation location after 3.5 days. The extensions generated by the heterogeneous numerical simulation were significant, with at least one realization generating an extension greater than 0.1 m for every location and observation time. The magnitude of the maximum extension observed in the Monte Carlo simulation was found to grow with time. This was consistent across all observation locations; however, no single realization resulted in a consistent increase in capillary fringe extension throughout the duration of pumping.

The capillary fringe thickness observed in each realization appears to be a function of the distribution of heterogeneity, its dependence on pumping duration or distance from the pumping well is not evident from our results. As the duration of pumping is increased, there appears to be a slight increase in the variance of the capillary fringe extension, as seen in Figure 3.10. This increase in variance is likely related to the increase in drawdown with time. As drawdown is increased, the volume of soil above the water table is also increased, incorporating greater variability of soil properties into the soil moisture profiles. Figure 3.11 is a contour map of capillary fringe extension after 3.5 days of pumping for a single heterogeneous realization. The axes have been truncated to highlight the zone near the pumping well. The top of the capillary fringe has been defined for this figure as the lowest elevation at which 95% saturation exists. Although there is a slight radial dependence in the contours due to the radial nature of the drawdown cone, the contours clearly illustrate the random nature of the capillary fringe extension. Results from each realization show random patterns, while the Monte Carlo ensemble would show a zero contour plot indicating no change in thickness over the field site. The neutron probe data indicates a more regular variation in thickness, decreasing with distance away from the pumping well, and increasing with the duration of pumping. Although the neutron probe data only covers a single cross section of the pumping test drawdown cone, these results are supported by the ground penetrating radar (GPR) data presented in Bevan et al. (2003). Figure 6 in Bevan et al. (2003) shows the drawdown of the GPR reflection generated by the transition zone. This GPR reflection is the result of a sharp change in moisture content, typically associated with the top of the capillary fringe. The depth to the transition zone reflection varies in a quasi-radial fashion. This behavior implies a capillary fringe thickness that decreases with radial distance from the pumping well. The inability of the heterogeneous simulations to produce this radial variation represents a major discrepancy between the simulated and observed results.

3.2.2.1 Influence of Variance on the Moisture Content Distribution

The Borden aquifer is an ideal location for hydraulic field studies as the level of heterogeneity is quite mild when compared to other aquifers. While the ensemble mean capillary fringe thicknesses generated by the Monte Carlo analysis are not significantly different from that of the homogeneous approximation, inspection of the individual realizations reveals a distinctly different moisture content distribution from the homogeneous approximation. Hence, it is of interest to test the sensitivity of the moisture content distributions computed to the variance of the random field used for the model, as the variance of the Borden aquifer is quite low in comparison to most other unconsolidated aquifers. Variance values more typical of those used to model heterogeneous aquifers are in the range of 0.5 – 8 (Salandin and Fiorotto, 1998, Trefry et al., 2003, Janković et al., 2006, Frippiate and Holeyman, 2008).

Four additional realizations of the hydraulic conductivity field were generated with variance values of 0.02, 0.06, 1, and 4 to investigate the sensitivity of the moisture content distribution to variance in hydraulic conductivity. As a full Monte Carlo analysis was not performed, these results are not a complete representation of the effect of variance on the simulation results. Therefore, they will be used simply to infer the potential impact of variance. The mean hydraulic conductivity and unsaturated scaling parameters were the same as those used in our Monte Carlo analysis. The range of hydraulic conductivity was much larger as variance was increased, therefore the Keuper and Frind (1991) scaling method was altered such that calculated displacement pressure values greater than 1 m were fixed at 1 m while values less than 0.05 m were fixed at 0.05 m.

In the realizations where the variance was increased, the discontinuity in the moisture profile became much more prominent. The profiles generated by the two realizations with higher variance contained multiple perched water zones; the prevalence and magnitude of these discontinuities appear to increase with variance. In the two realizations with decreased variance, the prevalence of perched water was reduced; however, even the realization with the lowest variance contained a major discontinuity. Capillary fringe thickness was determined for each simulation both prior to and during pumping. The results of the simulations completed with increased variance show much larger magnitude (but negative in value) capillary fringe extensions (compressions). The realizations with reduced variance resulted in capillary fringe extensions on the order of the changes generated by the Monte Carlo simulation. The simulation completed with a variance of 0.06 was the only simulation completed in this study to display time dependence of the capillary fringe thickness at each of the observation locations. It is not expected that this result would be replicated by a Monte Carlo simulation using a variance of 0.06.

The hydraulic head results were slightly influenced by the change in variance, with the higher variance realizations under predicting hydraulic head drawdown by as much as 0.25 m. Given that the observations presented are based on single realizations of the hydraulic conductivity field they are not indicative of the full behavior of the system being simulated. However, we believe that the trend towards increasing variability in capillary fringe thickness with increasing field variance is likely to be replicated in an ensemble result. It is interesting to note that the lower values of variance used in these simulations would be representative of aquifers that would normally be described as homogeneous. The existence of perched zones in those low variance simulations indicate that the homogeneous approximation of alluvial aquifers is likely to misrepresent the actual moisture content distribution, and under predict the influence of heterogeneity in the unsaturated zone.

3.3 Discussion

The Borden aquifer used in this study is a relatively simple natural system. The aquifer has been studied in great detail, such that the geology and geometry are well understood. Though the numerical model used in this study includes a very detailed representation of unsaturated flow processes it does not reproduce the moisture content observations of Bevan et al. (2005). The results of this study indicate that even in very well characterized systems such as the Borden aquifer, ample uncertainty exists, which prevents proper prediction of the pumping response above the water table by numerical simulation.

Fifty-two of the heterogeneous realizations resulted in a capillary fringe extension; however, none of the realizations displayed any relationship between the capillary fringe thickness and duration of pumping, or proximity to the pumping well, as was observed in the field. Although the ensemble mean capillary fringe extension generated by the Monte Carlo simulation was not significantly different from the extension generated by a homogeneous approximation of the aquifer, the addition of heterogeneity did have some impact on the numerical results. The soil moisture profiles produced by the heterogeneous simulations are more discontinuous than the homogeneous simulation, with zones of perched water existing above the capillary fringe. This phenomenon was observed in more than 90% of the realizations, and persisted for the duration of the simulations. The presence of these perched zones in the numerical results indicates that there is the potential for heterogeneity to cause water to be stored above the water table beyond the extent expected in a homogeneous simulation. However, if these perched zones were the cause of the observed capillary extension we would expect to see much more variability in the observed moisture profiles. The neutron data presented by Bevan et al. (2005) does not provide any evidence of perched zones.

There are several factors which may have contributed to the discrepancies between the heterogeneous modeling results and the field observations. These factors include the method used to assign the unsaturated zone parameters; the type of data collected in the field, the presence of vertical gradients above the water table, the potential for air-entry barriers and the cumulative influence of other extension mechanisms discussed in Chapter 2.

3.3.1 Heterogeneous Fields and Unsaturated Parameter Assignment

It has been hypothesized that vadose zone heterogeneity exhibits increased variance in capillary pressure with increasing mean capillary pressure, which in turn increases the anisotropy of a soil (Yeh et al., 1985). The numerical work of Kueper and Frind (1991) highlights this effect in a two-phase system as a NAPL source emplaced below the water table exhibits significant lateral spreading. Numerical analysis of field data by McCord et al. (1991) predicted as much as an order of magnitude increase in anisotropy and a significant decrease in vertical flow with decreasing saturation. Using the same approach as outlined in Kueper and Frind (1991) to define the unsaturated parameters for Borden sand, the variance of the capillary fringe thickness was found to increase with time; however, the ensemble mean capillary fringe thickness did not increase with pumping duration or proximity to the pumping well as was observed in the field. The simulations demonstrated the effect of increased anisotropy as thin lenses of increased water content formed and vertical flow was impeded due to the heterogeneity.

The inability of the ensemble result to replicate the capillary fringe extension may be influenced by the scaling relationship used to generate the unsaturated zone parameters. The work of Jacobs and Gelhar (2005) suggests that the simple scaling relationship used by Kueper and Frind (1991) may not be sufficient to capture all aspects of the heterogeneity in the vadose zone. Their analysis of the seven samples of Borden sand used in the Kueper and Frind (1991) study shows a significant degree of variation in the pore size distribution parameter m (a van Genucthen function was used). Perturbation techniques were used to generate stochastic fields for both the air-entry and pore size distribution parameters. In comparison to Leverette (1941) scaling, the perturbation techniques show a one to two order of magnitude increase in anisotropy ratio when effective saturation is greater than 0.7. Ferrante and Yeh (1999) simulated variably saturated flow in one-dimension by generating a stochastic field for the Gardner (1958) parameter α. In their analysis, the unsaturated parameter was uncorrelated to conductivity. The proper method for assigning unsaturated zone parameters in stochastic simulations is not well understood; however, the scaling method used in this paper may not fully represent field conditions. The relationship between hydraulic conductivity, air entry pressure, and pore size distributions is complex, and stochastic methods may require more rigorous parameters determination, such as that done by Jacobs and Gelhar (2005). Geostatistical variability of the pore size distribution

factor would have an influence on the relative permeability values and could have a significant impact on fluid flow above the water table.

3.3.2 Sampling Effects of the Neutron Probe

The smoothness of the soil moisture profiles measured in the field in comparison to the more variable profiles generated by the heterogeneous realizations may be partly attributable to the nature of the sampling volume of the neutron moisture probe. The effective sampling volume of this instrument is dependent on the source-detector separation (7.6 cm), and varied with moisture content. Although neutron moisture measurements were taken at very discrete intervals (0.05 m), these measurements are a complex average of the moisture values within the sampling volume.

To examine this effect we have applied a 0.40 m uniform averaging window to the moisture profiles generated by several heterogeneous realizations. The 0.40 m window (representing a 0.2 m radius of influence) is an over estimate of the sampling size of the neutron probe, the actual volume sampled in the field is expected to be smaller. Further, the uniform averaging should significantly overweigh the contribution of a distant point in the sampling volume as the response function of the probe decreases with distance from the source detector unit.

Application of this uniform averaging window did smooth out the sharp contrasts in the modeled profiles; however, the presence of the discontinuities was still quite apparent within the transition zone. These averaged profiles are in contrast to the neutron probe data collected by Bevan et al. (2005), which show no indication of discontinuities within the transition zone. Averaged profiles with a shorter uniform averaging window (smaller sampling volumes) provide more obvious evidence of the perched zones.

In addition Bevan et al. (2005) noted that the neutron probe data collected prior to pumping is a close approximation of the static moisture profile obtained gravimetrically at the Borden site by Nwankwor et al. (1992). Further, Mickle (2005) showed that the neutron moisture profile obtained in a large test cell packed with Borden sand provided a very good match to the profile predicted from the laboratory capillary pressure-saturation data from Nwankwor (1982). These results clearly indicate that the tool has sufficient resolution to replicate the shape of the moisture profile. We can conclude that if the pumping test were to produce perched zones on the scale of those produced by the numerical model they would be apparent in the field data. It is unlikely that a series of perched zones above the water table would be interpreted as an extended capillary fringe in the neutron data.

3.3.3 Vertical Gradients above the Water Table

In this analysis and in previous numerical analyses of the Borden test (Moench, 2008) capillary fringe thickness is defined using height above the water table, opposed to pressure head. This implies equilibrium conditions, such that vertical gradients are negligible. This definition of capillary fringe thickness is necessary due to the lack of pressure head data in the Bevan et al. (2005) data set. Upward vertical gradients (downward flow) would be expected to cause an apparent capillary fringe extension; however, the magnitude of the vertical gradient required to produce the capillary fringe thickness observed during the Borden test is quite high. Figure 3.12 shows the effects of different vertical gradients on the pressure head profile representing the possible range of gradient values in the capillary fringe during the Borden test. These gradients include those observed in the field by Nwankwor et al. (1992), those generated by the numerical simulation, and the gradient that would be required to generate a 0.25 m extension. The vertical gradient required for the maximum observed capillary fringe extension inferred from the Bevan et al. (2005) data is significantly higher than the gradients observed by Nwankwor et al. (1992) or predicted by the numerical results discussed in Chapter 2. These results suggest the influence of vertical gradients on the observed capillary fringe extension is minimal; however, field observations of the gradients developed above the water table during pumping would be a useful tool for further examination of the mechanism for the capillary fringe extension.

3.3.4 Air-Entry Barrier Effects

Air-entry barriers were first noted by Silliman et al. (2002). The term is used to describe a drainage condition that occurs when a coarse material is completely surrounded by a finer material with a higher air-entry pressure. During drainage the coarse material will reach air-entry pressure before the fine material, yet it will be unable to drain as the fully saturated fine material prevents air from flowing into the coarse material. As HydroGeoSphere is a single phase model, it will not simulate air entry barrier effects, such that any layer will drain at its air-entry pressure, regardless of the presence of a connected pathway for air. While it is not expected that air-phase flow limitation would have such a significant impact in a three-dimensional system, the potential for air entry effects remains.

Simulation of the heterogeneity of the Borden aquifer may be possible using multiphase flow simulators; however, it is not within the scope of this work. To approximate the potential for air entry barriers to impact the capillary fringe thickness estimation, the results of the heterogeneous simulation in HydroGeoSphere were re-analyzed such that the top of the capillary fringe was defined as the highest elevation at which the soil remained saturated. This method is simply an approximation of air-entry effects, and assumes no horizontal pathways for air phase flow. The results of the reanalysis were not significantly different from the original analysis discussed above. Significant effects were only apparent in a few realizations in which fully saturated zones formed above the capillary fringe. In all

realizations where this occurred, the perched zone drained prior to the end of pumping, resulting in a collapse of the capillary fringe thickness. While these results suggest that air-entry barriers have a minimal effect on results, the complexities of multi-phase flow warrant further investigation.

3.3.4 Hysteresis and Entrapped Air

Entrapped air and hysteresis are potentially important factors in vadose zone flow at the Borden site. The water table is known to fluctuate by approximately 1.5 m per year (Conant, 1991), being high in the spring and fall, and low in the summer months. Hysteresis in the pressure-saturation relationship due to drainage and subsequent rewetting of a soil profile has been observed both in the laboratory (Gillham et al., 1979), and in the field (Basile et al., 2003, and Green et al., 2005). Gillham et al. (1979) observed as much as 8% entrapped air at 0.0 m pressure head after one resaturation cycle in dune sand. Hysteresis is expected to reduce the height of the capillary fringe, in subsequent rewetting cycles however the impact of the air entrapped during rewetting is expected the reduce the relative hydraulic conductivity of the system, which may reduce vertical drainage rates, temporarily increasing the amount of water stored above the water table.

3.5 Conclusions

Numerical experiments completed in this study were intended to determine whether the mild degree of heterogeneity present in the Borden aquifer could be a viable physical mechanism for the moisture content distributions observed during by Bevan et al. (2005). Numerical simulations with a homogeneous aquifer model, using Richards' equation and a rigorous description of unsaturated flow successfully replicated the hydraulic head data measured below the water table. However, the observed temporal variations in the vadose zone moisture content distribution inferred from neutron moisture probe measurements could not be reproduced by the numerical simulations. Specifically, the field data shows that the moisture profile experiences slower drawdown than the water table, resulting in an extended capillary fringe. This extension is significant close to the well (0.35 m at 3 m from the pumping well) and decreases with distance (0.05 m at 15 m from the pumping well). The homogeneous numerical simulations were not able to reproduce the observed capillary fringe extension, nor the dependence of the capillary fringe thickness on pumping duration and proximity to the pumping well.

The numerical simulation of the Bevan pumping test was modified to account for the effects of heterogeneity by using the variations in hydraulic conductivity determined for the site by Sudicky (1986). Conductivity fields were generated based on geostatistical parameters, and unsaturated parameters were scaled to conductivity using the relationship outlined in Kueper and Frind (1991). A Monte Carlo analysis involving 75 realizations was completed. The ensemble mean hydraulic head

drawdowns produced an improved match to the field observations in comparison to the homogeneous simulation results. The ensemble mean capillary fringe extension more closely approximated the numerical results of the homogeneous approximation than the field observations. Several realizations resulted in an extended capillary fringe, or the presence of perched water; however, this excess water was not dependent on pumping duration or distance from the pumping well, as observed in the field. The only time dependence shown by the numerical simulation was a slight increase in variance of the capillary fringe thickness.

The conceptualization of the Borden aquifer as mildly heterogeneous does not provide an accurate numerical representation of the moisture content distributions observed during pumping. The formation of perched water saturated layers predicted in a large portion of the realizations is on a scale that would allow detection by the neutron probe. The neutron probe data provided by Bevan et al. (2005) does not provide evidence of these perched water layers. The heterogeneous description of the system may be further improved by allowing variation in the Brooks and Corey (1964) pore size distribution parameter β, and by allowing the air-entry pressure to vary independently from hydraulic conductivity.

It remains to be determined whether the failure to reproduce the field observations are the result of the necessary assumptions made in the numerical simulation of the field experiment, or other additional uncertainties. Subsequent field work is planned which will include discrete observation of moisture content and pressure heads above the water table. This field work will be used to guide future numerical investigations. The results of this study are a step towards an improved understanding of the level of complexity required to properly simulate moisture content distributions in response to pumping stresses. Even in a relatively simple system such as the Borden aquifer where heterogeneity is relatively mild, the effects in the vadose zone are significant. Perched water layers can occur even at very low levels of hydraulic conductivity variability. The use of the Borden test data to determine those mechanisms and data sources necessary to replicate moisture content is essential. Technological advancements continue to improve our ability to both monitor and simulate flow fields within the vadose zone. As it becomes more feasible to collect detailed observations of unsaturated flow it is essential that numerical simulation methods are updated to reflect our improved understanding of the field data. This will improve our ability to predict both the vadose zone response during pumping, and in a more general sense improve our understanding of the flow processes occurring above unconfined aquifers.

3.6 Figures and Tables

Table 3.1. Parameters used to populate the homogeneous numerical model

Parameter	Initial Value	Calibrated Value	RMSE	Source for Initial Value
K_x (m/s)	6.18×10^{-5}	5.85×10^{-5}	0.047	Endres et al. (2007)
K_y (m/s)	6.18×10^{-5}	5.85×10^{-5}	0.047	Endres et al. (2007)
K_z (m/s)	3.10×10^{-5}	2.54×10^{-5}	0.031	Endres et al. (2007)
S_s (m^{-1})	3.25×10^{-4}	4.50×10^{-4}	0.042	Akindunni and Gillham (1992)
α (m^{-1})	2.68	Fixed		Nwankowr (1982)
β(-)	2.48	Fixed		Akindunni and Gillham (1992)
θ_S (-)	0.37	Fixed		Akindunni and Gillham (1992)
θ_r (-)	0.07	Fixed		Akindunni and Gillham (1992)

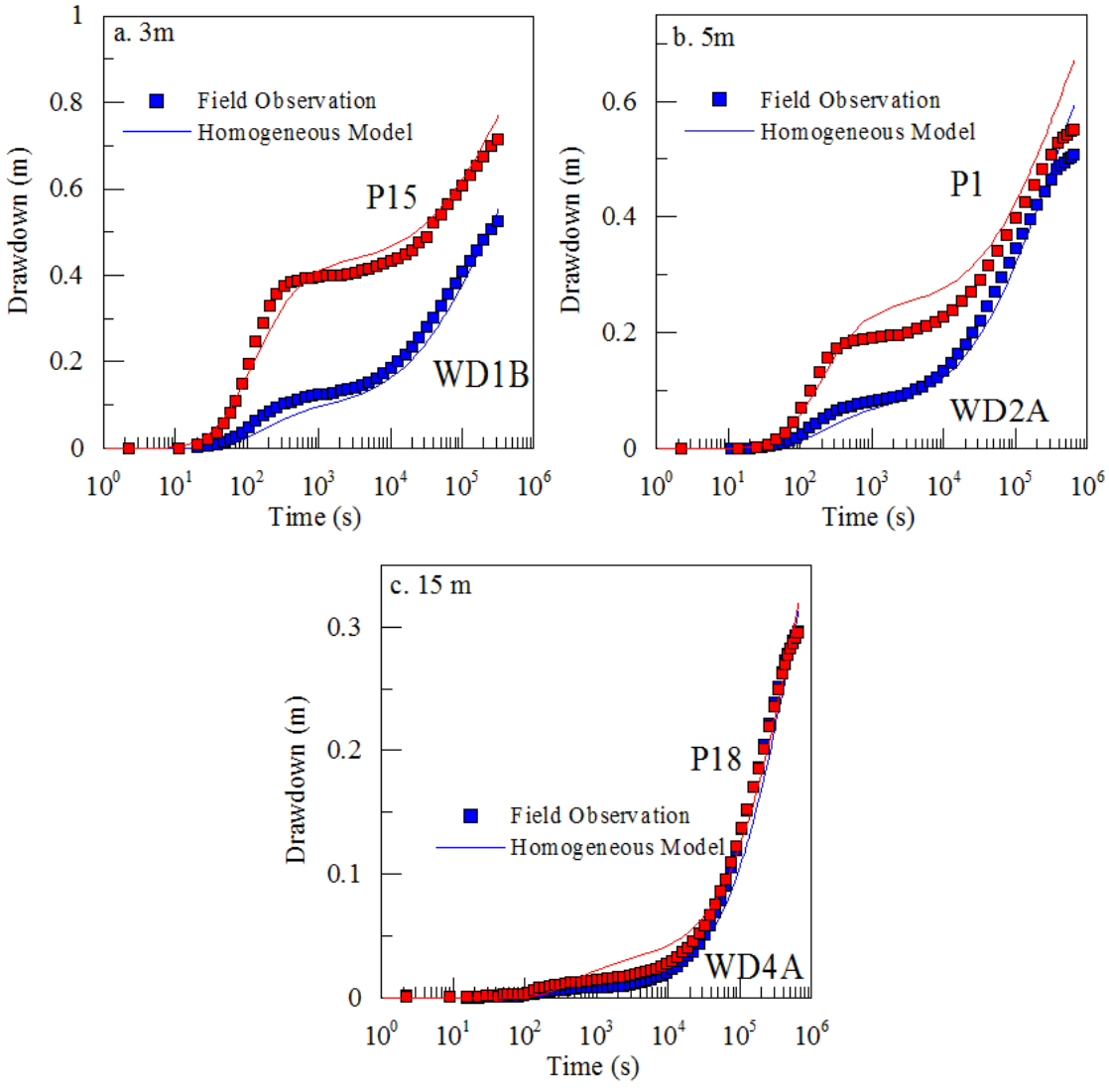

Figure 3.1 (a-c). A semi-log comparison between simulated results using a calibrated homogeneous aquifer model and field observations of the hydraulic head drawdown in shallow-deep piezometer pairs. P-series wells are deep, and WD-series wells are shallow. (Radial distance: a. 3 m, b. 5 m, c. 15 m)

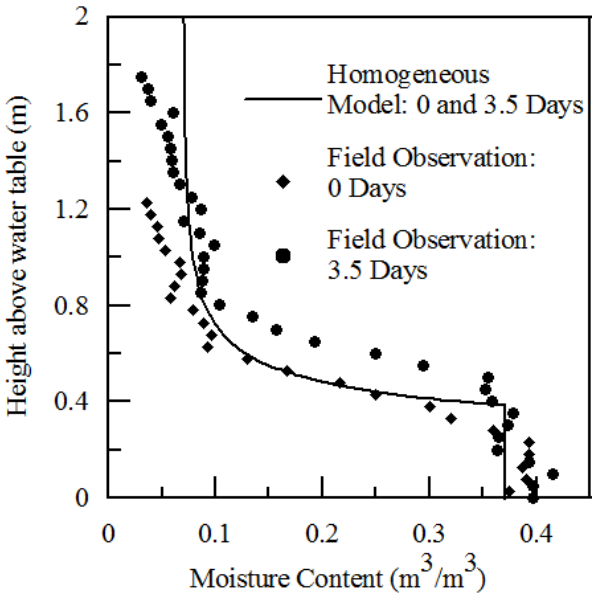

Figure 3.2. Moisture content profiles inferred from neutron probe data, and simulated in HGS using a homogeneous aquifer model.

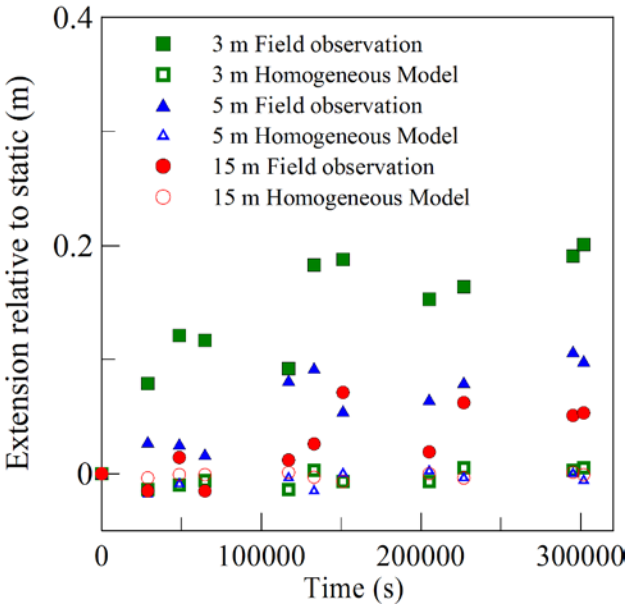

Figure 3.3. A comparison of the capillary fringe extension relative to static thickness inferred from field data and predicted using a homogeneous aquifer model.

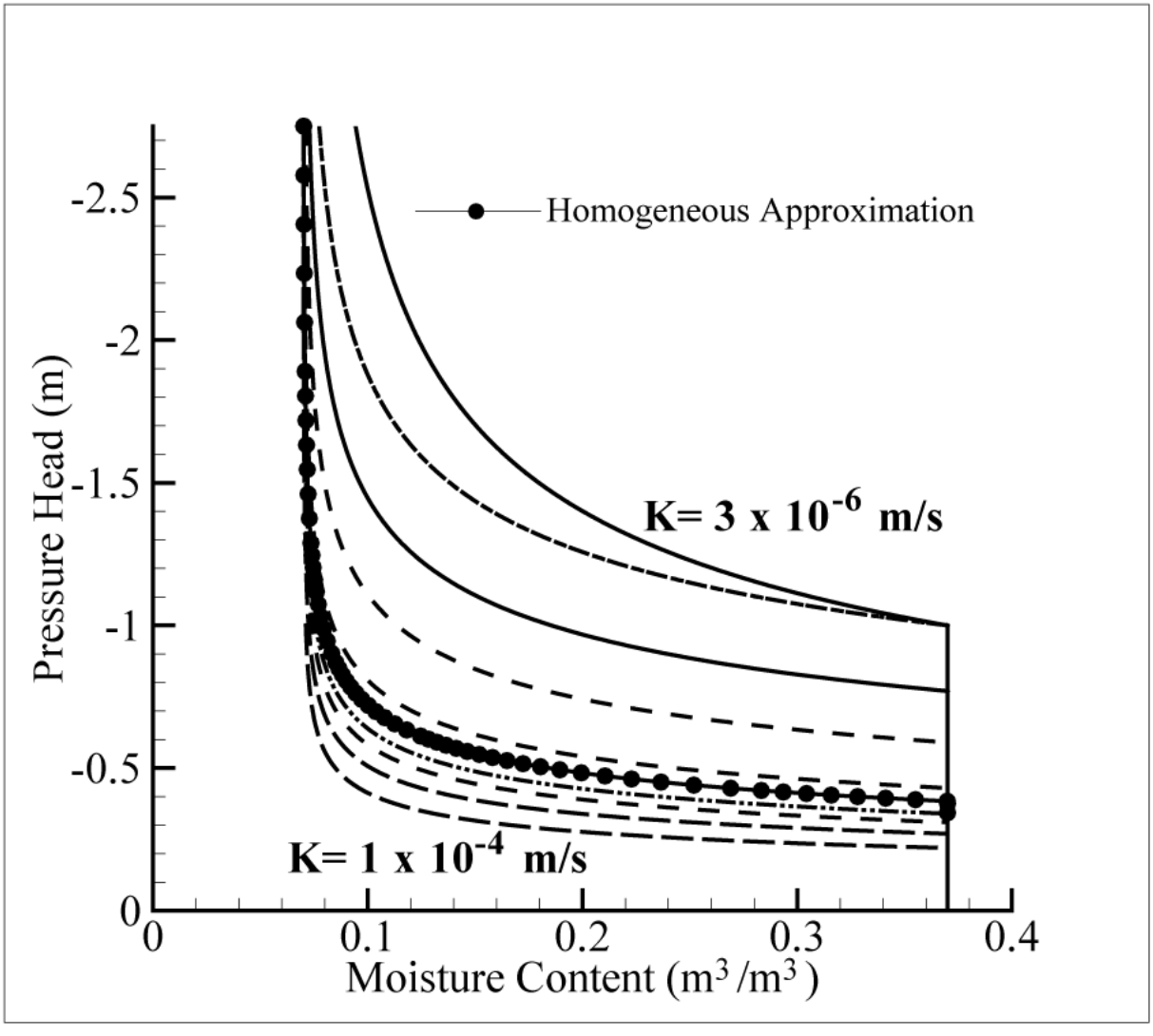

Figure 3.4. Representative Brooks and Corey (1964) moisture retention curves generated for the heterogeneous field using the Kueper and Frind (1991) scaling relationship.

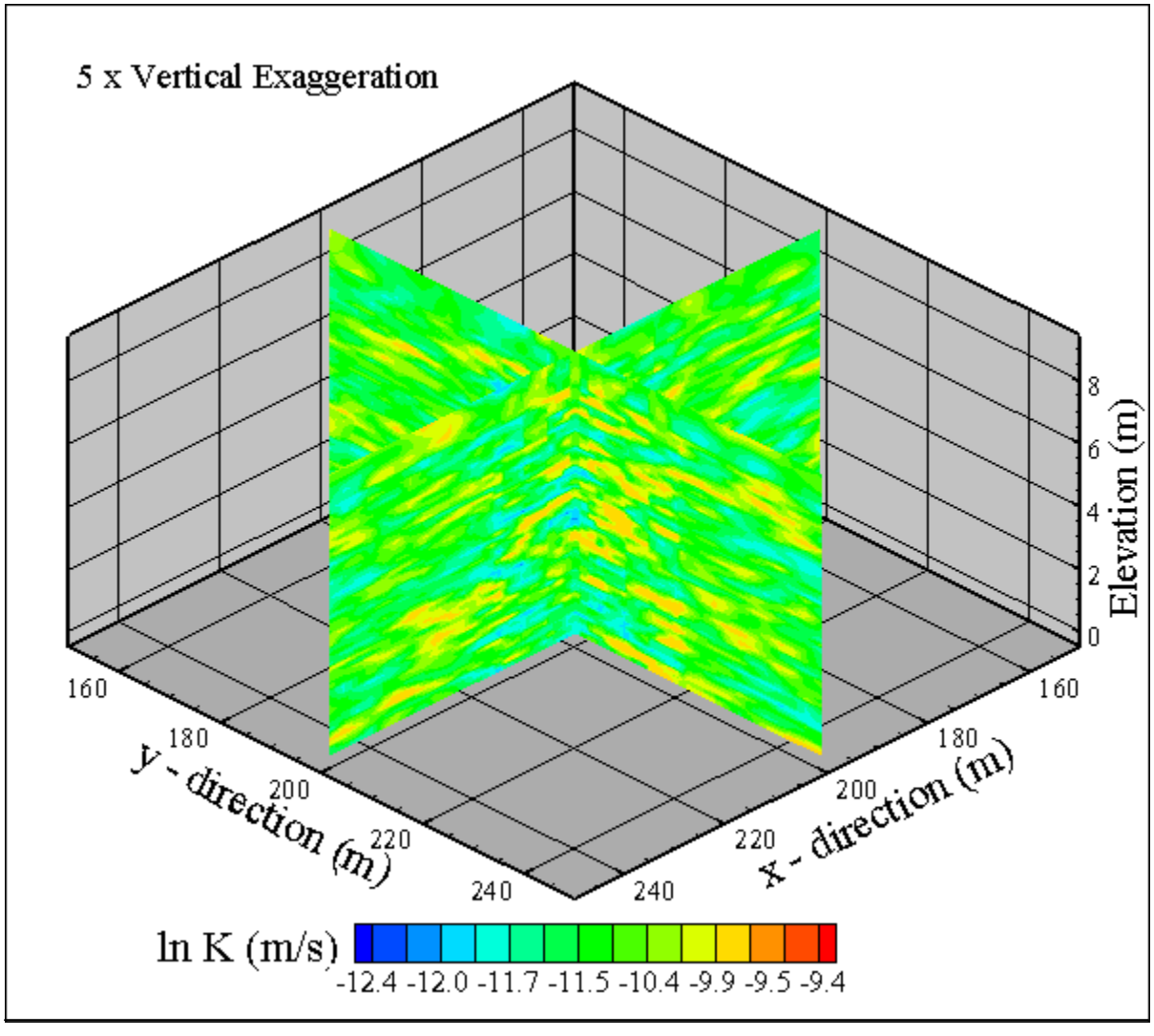

Figure 3.5. Vertical cross-section through a single realization of the heterogeneous hydraulic conductivity field used to represent the Borden aquifer. A 5x vertical exaggeration has been applied.

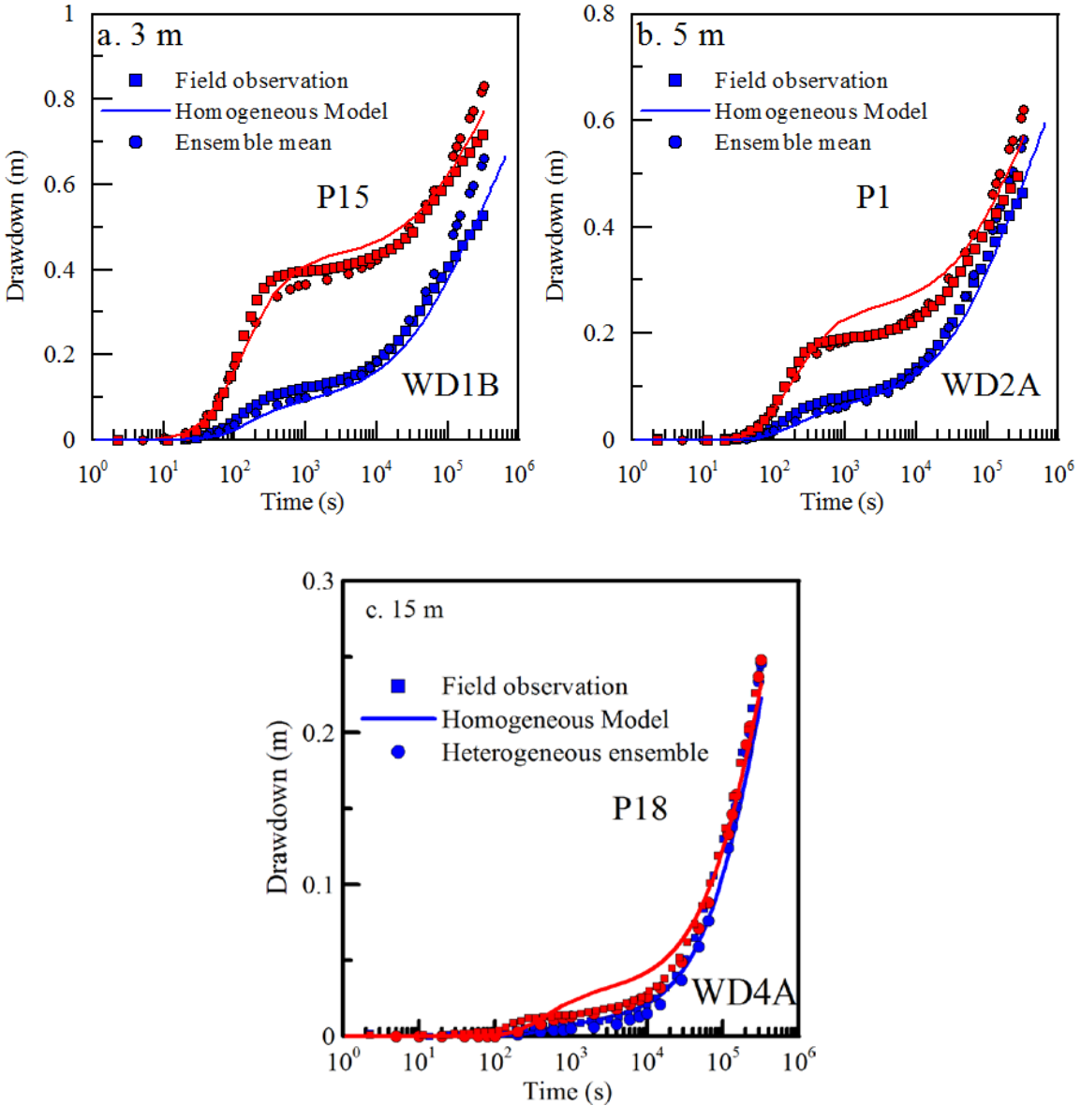

Figure 3.6 (a-c). A semi-log comparison of the hydraulic head drawdown during pumping between results inferred from field data, simulated results using a homogeneous approximation, and ensemble results from a Monte Carlo simulation of hydraulic conductivity heterogeneity for the shallow-deep piezometer pairs. Deep well are the P-series wells, shallow wells are the WD-series wells. (Radial distance: a. 3 m, b. 5 m, c. 15 m)

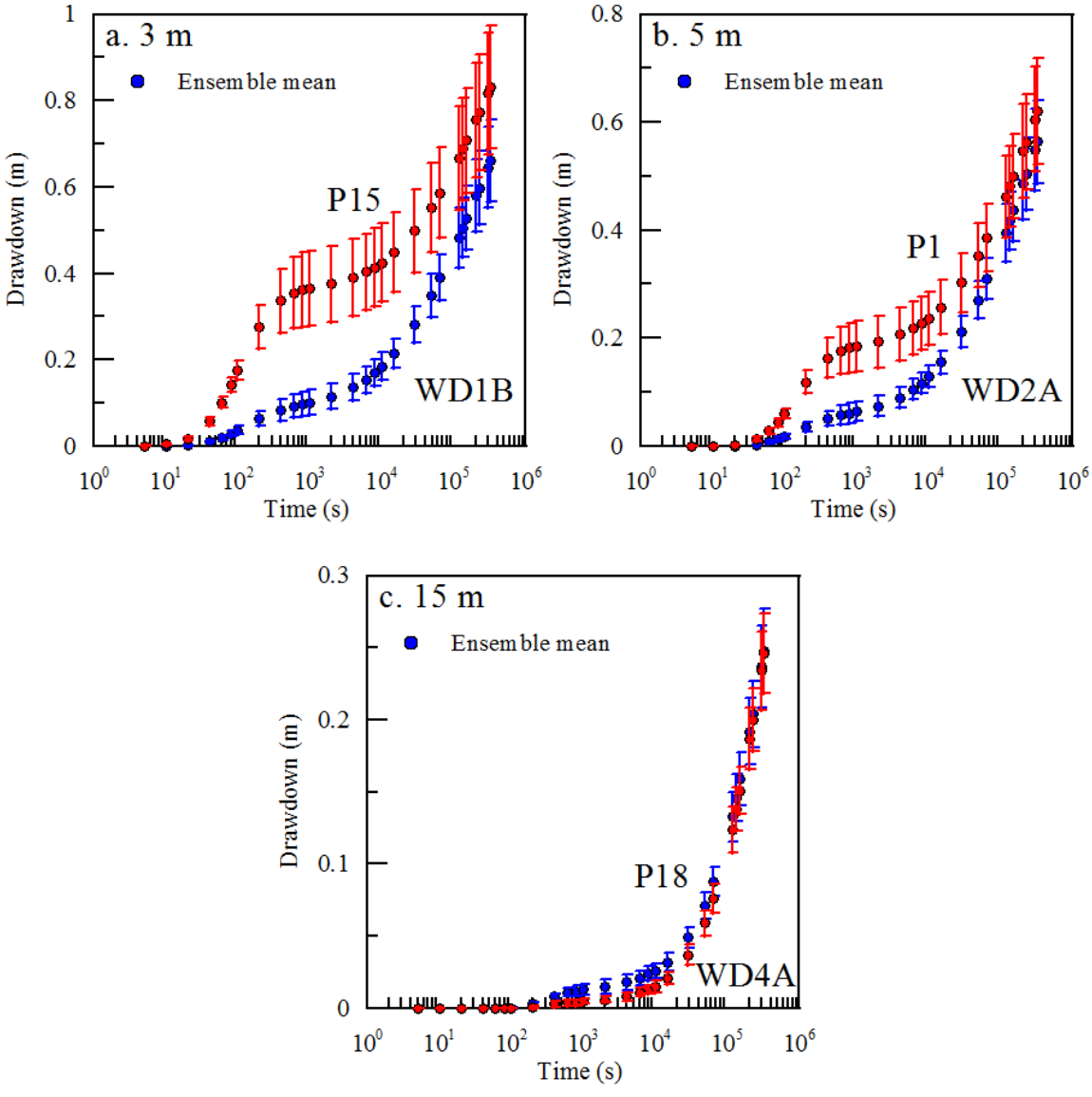

Figure 3.7 (a-c). Hydraulic head drawdown ensemble results from a Monte Carlo simulation of hydraulic conductivity heterogeneity for the shallow-deep piezometer pairs. Deep wells are the P-series wells, shallow wells values are the WD-series wells. Error bars represent one standard deviation from the mean. (Radial distance: a. 3 m, b. 5 m, c. 15 m)

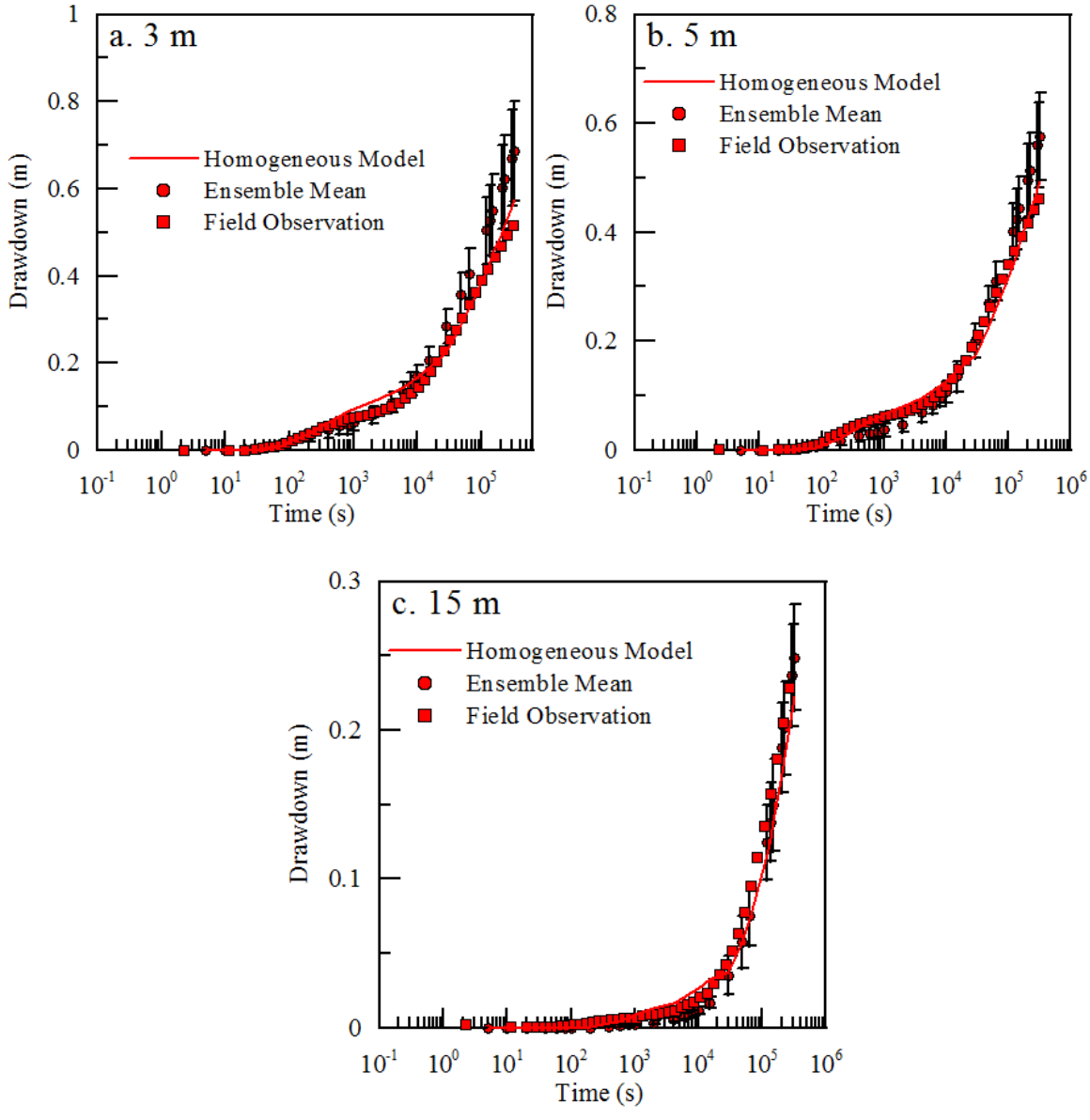

Figure 3.8 (a-c). A semi-log comparison of the water table drawdown during pumping between results inferred from field data, simulated results using a homogeneous approximation, and ensemble results from a Monte Carlo simulation of hydraulic conductivity heterogeneity. Error bars represent one standard deviation from the mean for the ensemble results (Radial distance: a. 3 m, b. 5 m, c. 15 m).Figure 12(a-d).

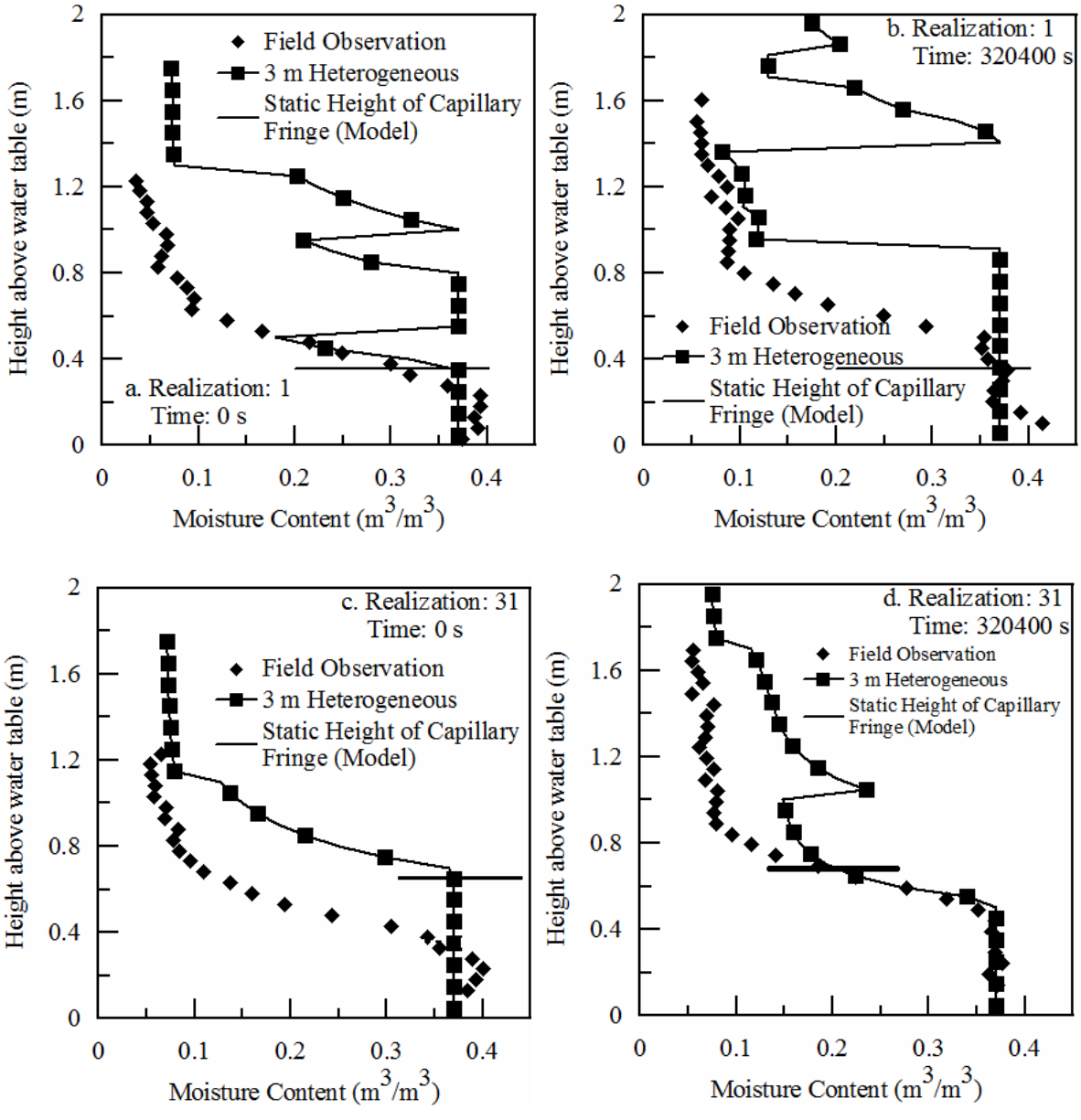

Figure 3.9 (a-d). Moisture content profiles from single realizations representing an extension (Realization 1: a. 0s, b. 320400s), and a compression (Realization 31: c. 0s, d. 320400s) of the capillary fringe.

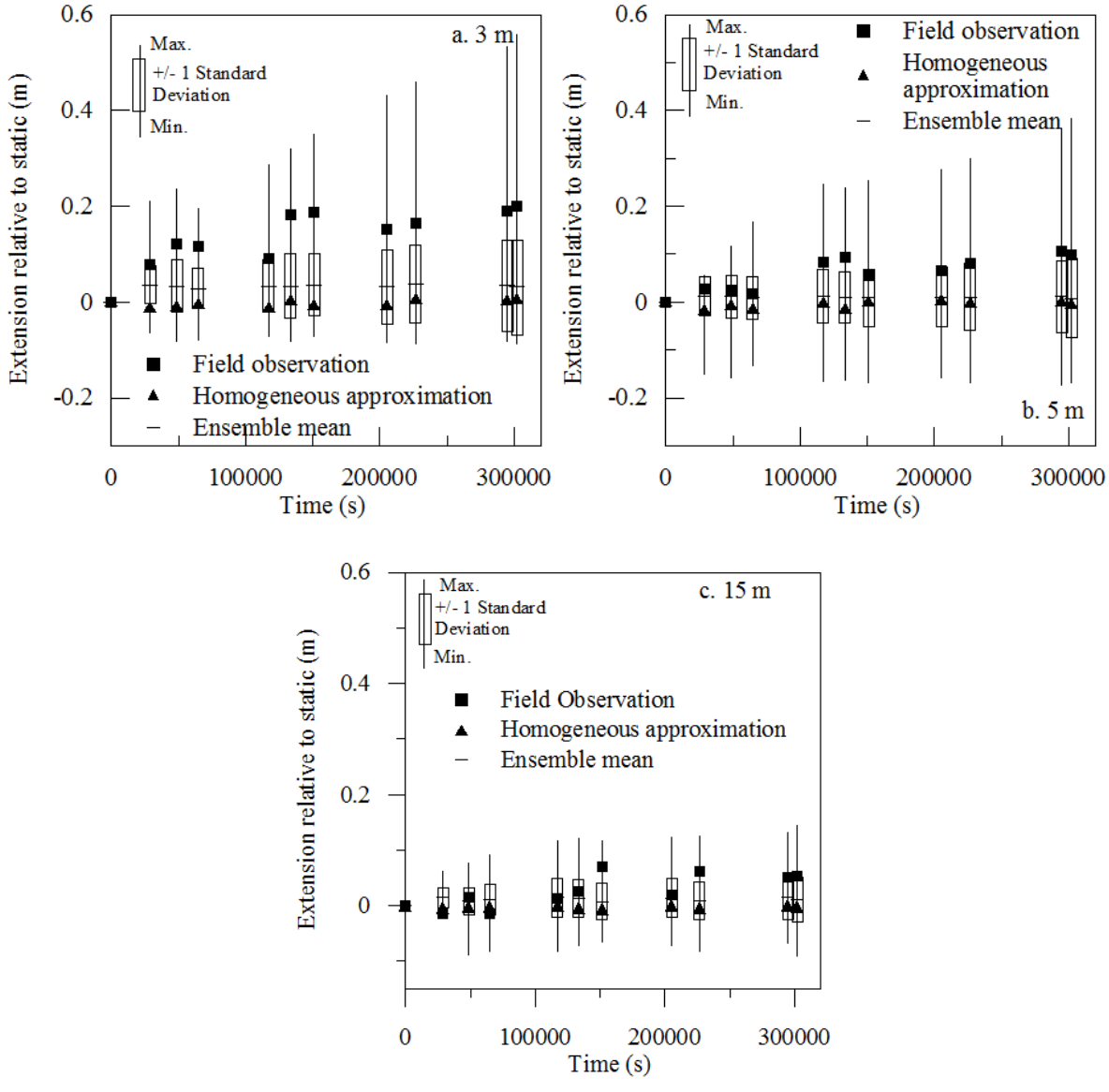

Figure 3.10 (a-c). Comparison of capillary fringe extension relative to static thickness inferred from field data, with the predictions of the homogeneous aquifer model and the Monte Carlo simulation of the heterogeneous aquifer (Radial distances: a. 3 meters; b. 5 meters; c. 15 meters).

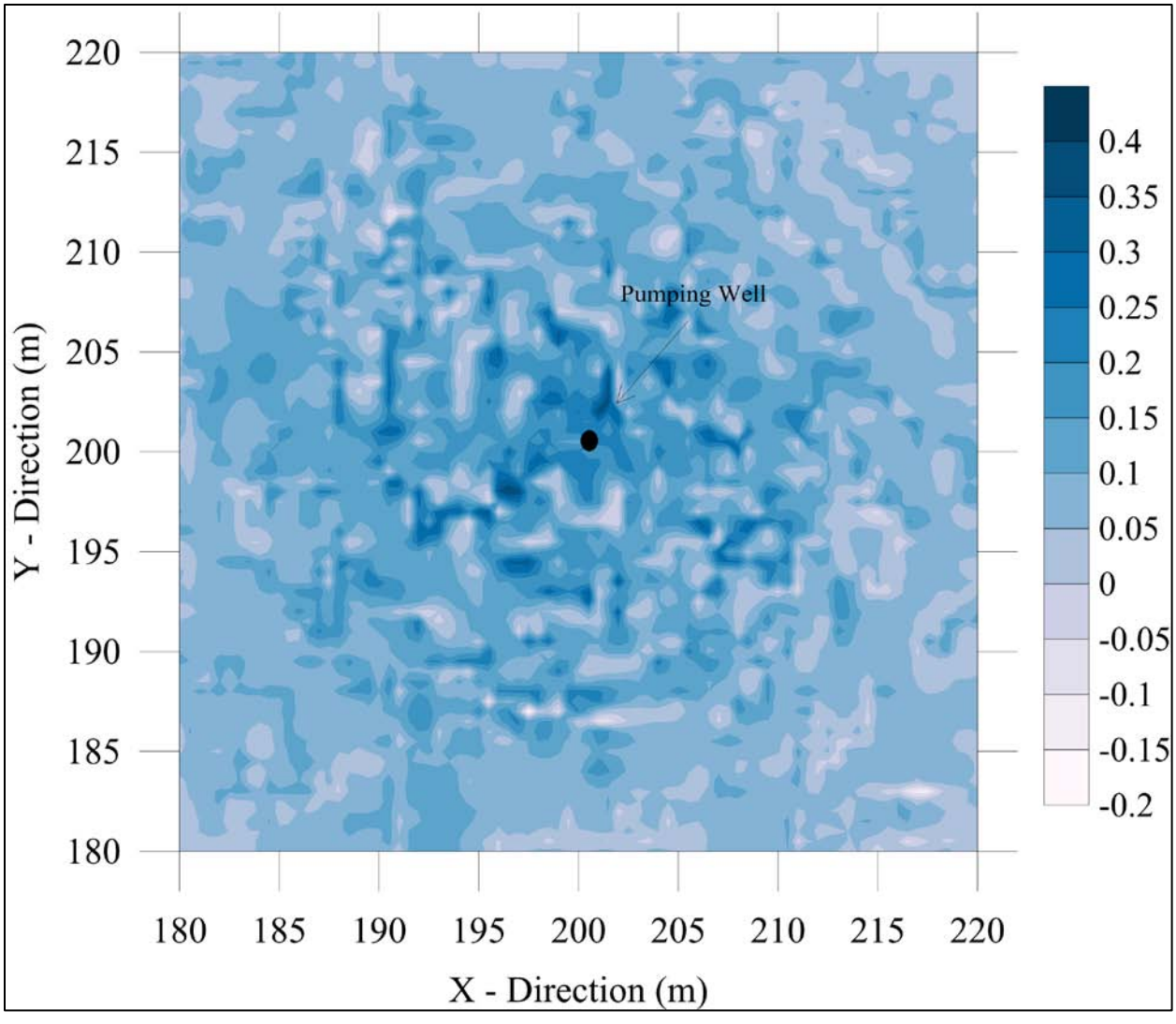

Figure 3.11. Capillary fringe extension contours generated by a single heterogeneous realization after 3.5 days of pumping. Axes have been truncated to highlight zone surrounding the pumping well. The pumping well is shown at (200,200).

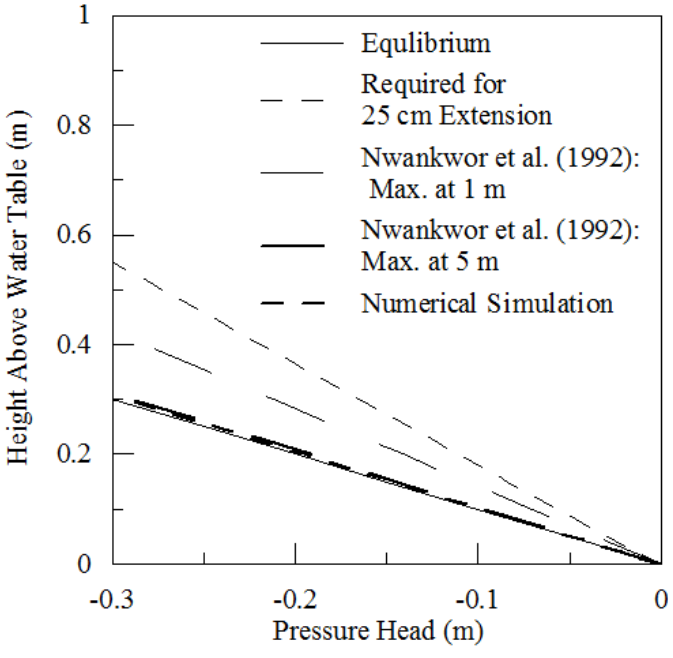

Figure 3.12. Pressure head profile through the capillary fringe for a variety of vertical gradients. Apparent capillary fringe thickness for each profile is represented by the y-intercept.

Chapter 4

Field observation of the response to pumping and recovery in the shallow water table region of an unconfined aquifer

4.1 Introduction

A 24-hour pumping test was conducted in the shallow water table portion of an unconfined aquifer located at Canadian Forces Base Borden near Alliston, Ontario, Canada. This test was designed to monitor the dynamic nature of the vertical gradients that form within the zone of tension saturation above the water table during pumping and recovery, and to monitor the formation of perched zones as indicated by the heterogeneous modeling results presented in Chapter 3. The conditions prior to the test were wet and the moisture profile prior to pumping fell on an imbibition type curve. These conditions provided an opportunity to observe the impact of hysteresis on pumping test results.

4.2 Site Description

The previous pumping tests conducted at CFB Borden (Nwankowr et al., 1992, Bevan et al., 2005) were conducted on a local high where the aquifer is 9 m thick and the water table typically sits 2-3 m below ground surface (BGS). The current study was conducted approximately 200 m to the southeast of the former test site in a topographical low that resulted from historical aggregate extraction. This site is within the same aquifer unit; however, the upper portions have been removed such that the water table sits within 1 m of the ground surface. The water level in the Borden aquifer varies by approximately 1.5 m per year (Conant, 1991), and the water table at this location can sit above ground surface for a portion of the year. The water table was approximately 0.63 m below ground surface (BGS) prior to this pumping test in October 2009.

The pumping well and observation wells were pre-existing at the site. Full details of their installation and use can be found in Doughty (2006). The pumping well was constructed of 0.05 m ID schedule 40 PVC and was screened from 3.5 to 4.5 m BGS. Shallow – deep observation well couplets were used to monitor the pumping induced hydraulic head drawdown below the water table. A total of five couplets were used, located at 2 m, 4 m, 6 m, 9 m, and 11 m from the pumping well (Figure 4.1a). These wells were constructed of 0.025 m schedule 40 PVC with a 0.15 m long screen. The screen of the shallow wells was centered at approximately 2.5 m BGS, while the deep screen was centered at approximately 4.0 m BGS (Figure 4.1b.).

In addition to the previously installed wells, new tensiometers, neutron moisture access tubes and TDR rods were installed for this pumping test. Neutron access tubes were constructed of 0.05 m ID

schedule 40 PVC. A total of two tubes were installed by hand auger adjacent to the 2 m and the 4 m observation well couplets. Three T5 pressure-transducer tensiometers (UMS, Munich, Germany) were installed at each of the 2 m and 4 m well couplet locations. The T5 tensiometers consist of a 0.06 m long porous cup with a 0.024 m diameter. As water fills only the porous cup of the T5 tensiometer, temperature effects are minimized. Tensiometers were installed by hand auger, and set in place using slurry comprised of augered material. At each site the shallow, intermediate and deep tensiometers were placed at approximately 0.30, 0.60 and 0.95 m below ground surface, respectively (Figure 4.1b.). A total of 10 TDR rods were used in this study. The rods consisted of two 0.15 m stainless steel prongs housed in resin following the construction details outlined in Or et al. (2004). A small pit was hand dug adjacent to the 2 m well couplet, and the rods were installed horizontally every 0.08 m from 0.08 to 0.8 m BGS (Figure 4.1b.). The pit was then backfilled with excavated material.

4.3 Field Methods

The pumping test was run at a constant pumping rate of 10 ± 1 l/min. for a 24 hour period. The pumping rate was verified hourly by recording the volume change on a calibrated flow meter that was connected in line with the pump discharge. For the duration of the test, pumped water was discharged to an adjacent holding tank. Subsequent to the pumping test, the recovery of the aquifer was monitored for a period of 4 hours. Although the intent was to monitor the aquifer until fully recovered, a rain event occurred which dramatically elevated the position of the water table, limiting our ability to observe the pumping induced recovery. The effect of the rainfall on the TDR derived pressure-saturation profiles is discussed in more detail in the following sections.

During the test, the hydraulic head in the 2m and 4 m well couplets was measured using Solinst Levelogger Gold data loggers which are accurate to 0.003 m. The Leveloggers were programmed to record data at 0.25 min. intervals at the start of the test and were gradually increased to 60 min. for the final 660 min. of the test. The recovery portion of the test was logged following the same measurement interval pattern as drawdown. The remaining monitoring well couplets were measured by hand using an acoustic sounder accurate to 0.005 m. These measurements were taken every 5 min. early in the test; but as the drawdown slowed, the measurement interval was progressively increased to 60 min. The hydraulic head drawdown at the tensiometers was measured by hand using an Infield7 data readout device (UMS, Munich, Germany), which gives a pressure reading to the nearest 0.01 m. Readings were taken at 5 to 60 min. intervals and were timed to coincide with the collection of the neutron moisture profiles.

Neutron moisture profiles were collected using a 503DR Hydroprobe from Campbell Pacific Nuclear Corporation. The neutron source for this instrument is 50 mCi Am-Be, with a source-detector

spacing of 0.076 m. A 4 s count rate was used, with each reading given as an apparent 16 s count. Based on the statistics of the neutron count rate, the average uncertainty in each count recorded (apparent 16s count) is expected to be ± 367. The profiles consisted of 15 readings spaced at 0.05 m vertical intervals from approximately 0.3 to 1.0 m BGS. A single profile took approximately 5 min. to complete, including time to move to the next location. During the initial stages of pumping profiles were collected constantly, with the interval time increasing to 60 min. after the first 3 hours of pumping, as drawdown slowed significantly.

TDR readings were taken manually using a Tektronix 1502C Metallic Cable Tester. Prior to installation the length of each rod was calibrated with deionized water. Following the background reading, no TDR was collected until the recovery portion of the test. The proximity of the pumping well to the TDR rods led to a large degree of electromagnetic noise which far exceeded the TDR response to moisture content changes. Transient monitoring within the TDR network began immediately after the pump was turned off. Readings were taken at 20 min. intervals, immediately prior to the neutron profiles.

4.4 Pumping Test Results

4.4.1. Hydraulic Head and Gradient Results

Hydraulic head drawdowns for the 2m and 4 m well couplets are plotted in a log-log format in Figure 4.2. The remaining well couplets are not shown as these locations were monitored by hand, making curve inflections difficult to detect due to less frequent monitoring. Both locations display a difference in drawdown between the shallow and deep piezometers, with greater drawdown at the deep monitoring locations. This difference decreases with time, but does so more quickly and more significantly at the 4 m location in comparison the 2 m location. At the 2 m and 4 m locations, it is apparent the second stage of the time-drawdown curve was reached during the early portion of this test (within the first 5 min.). Towards the end of the pumping test drawdown rates at all piezometers appear to increase, suggesting that the third stage of the drawdown curve may have begun. This is consistent with previous tests in the same aquifer (Bevan et al., 2005, Nwankwor et al., 1992). This test was terminated before pseudo-steady-state conditions had been achieved. The observation of the pseudo-steady-state phase of pumping was not necessary for this experiment, as the transient nature of the vertical gradients was of primary interest. Hydraulic head drawdown observations at the tensiometer locations are shown in Figure 4.3. The shallow well drawdown data are included as a reference in each figure. It is noted here that while the shallowest tensiometers were installed near the top of the capillary fringe, the neutron probe data from the same elevation does not indicate significant dewatering through the duration of the pumping test. It appears that the porous medium around all tensiometers remained at or near saturation for the duration of pumping. Within the first 15 min. of

pumping the drawdown at the tensiometers was consistently smaller than the drawdown observed at the shallow well. This trend indicates the formation of downward vertical flow across the water table. The difference in drawdown remained small and was not indicative of the formation of large vertical gradients. Following the first 15 min. of pumping, the drawdown at the tensiometers became more consistent with the shallow piezometer, indicating a reduction in the vertical gradients as pumping continued. The similarity between drawdown below the water table, and within the capillary fringe supports the assumption that gradient development and hydraulic head response remained fairly uniform throughout the saturated zone, both above and below the water table.

Vertical gradients below the water table were calculated using the well couplet drawdown data at the 2 m and 4 m locations and the results are given in Figure 4.4. A positive vertical gradient indicates downward flow. There is a clear trend of higher vertical gradients at shorter radial distances from the pumping well. Vertical gradients were found to increase sharply for the first 2 minutes of pumping after which they were found to decrease monotonically for the remaining duration of pumping. The reduction in vertical gradient at the 4 m location is more significant than that at the 2 m location. Vertical gradients below the water table were low, owing to the vertical location of the screens in relation to the pumping well screen.

Vertical gradients were calculated across the water table between the shallow well and the shallow and intermediate tensiometers. Results are shown in Figure 4.5(a-b). The intermediate and shallow tensiometers remained within the capillary fringe (i.e. the zone of tension saturation) for the duration of pumping as indicted by the soil moisture data collected from the neutron probe. The uncertainty in the vertical gradient calculations as a result of the hydraulic head uncertainties are 0.005 m/m for the interval between the shallow tensiometer and the well, and 0.006 m/m for the interval between the intermediate tensiometer and the well. The vertical gradients calculated display some noise, making trends over time difficult to precisely characterize; however, several important observations can be made. The average vertical gradients in the interval to the shallow tensiometers are lower than those in the interval to the intermediate tensiometers, or those observed below the water table. This difference provides evidence of a general trend of decreasing vertical gradient magnitudes with elevation through the tension saturated zone. It is clear that there is no significant increase in vertical gradient magnitudes in the transition across the water table. In fact, the lower vertical gradients observed between the shallow tensiometer and the piezometer suggests that vertical gradient magnitudes may slightly decrease with elevation in the tension saturated zone. These results support a conceptual model in which vertical gradients are the same or slightly lower in the tension saturated zone in comparison to those below the water table at depths closer to the well screen following the first minutes of pumping.

Pressure heads determined from the tensiometers are only accurate to ± 0.01 m. Based on the vertical separation of the tensiometers the uncertainty in the calculation of vertical gradients above the water table is approximately 0.05 m/m. Vertical gradients calculated between the shallow-intermediate, and intermediate-deep tensiometer pairs fluctuate within the range of uncertainty. Although the exact magnitude of vertical gradients within the capillary fringe cannot be determined from the data collected, the data suggests that the vertical gradients above the water table, in the tension saturated zone, remained very low following the first minute of pumping, and no positive gradients of significant magnitude were present following the first minutes of the test.

The hydraulic head data collected during the pumping portion of this test implies that gradients are low throughout the saturated zone both above and below the water table. These vertical gradients tend to be more persistent at greater radial proximity to the pumping well. Questions have been raised regarding the potential for downward vertical flow through the capillary fringe to result in a perceived capillary fringe extension. The extension of the capillary fringe during pumping, as observed by Bevan et al. (2005), was determined by taking the elevation above the water table as a proxy for capillary pressure. As discussed in Bunn et al. (2010), in the presence of significant downward vertical drainage, capillary pressures would be displaced upwards from their equivalent elevation above the water table. An overestimation of capillary fringe thickness may result if this phenomenon were not adequately accounted for. None of the hydraulic head measurements, from either above or below the water table indicate the formation of large gradients within the tension saturated zone. Rather, these results are consistent with the conceptual model of low vertical gradient magnitudes that peak early in the test and subsequently decrease as observed by Nwankwor et al. (1992) and used by Bevan et al. (2005), Moench (2008), and Bunn et al. (2010).

4.4.2 Saturation Results

Background saturation profiles collected prior to the commencement of pumping are given in Figure 4.6. These profiles are plotted as saturation versus pressure head, where pressure head values were interpolated from the tensiometer data. Profiles collected with the neutron probe at the 2 m and 4 m access tubes are shown along with the TDR profile (at 2 m) and the laboratory drainage and imbibition values determined using a repacked soil sample from the site. This pressure-saturation profile shows the top of the tension saturated zone at approximately -0.25 m pressure head. This curve is in good agreement with the laboratory derived imbibition curve for the site. Neutron probe count rates were converted to saturation values using the standard count procedure and calibration constants given in Doughty (2006). This calibration method accounts for the impact of PVC tubing on observed the count rate. Background neutron saturations are in good agreement with the average TDR derived saturation. The TDR derived saturation is more variable due to small scale variations in soil texture. This minor

variability is smoothed out in the neutron derived profile. All background data from the site plot near the laboratory derived imbibition curve, likely due to rain events which preceded the test. Previous pumping tests conducted in the Borden aquifer (Nwankowr et al., 1992, Bevan et al., 2005) began with moisture profiles which plotted on the laboratory derived drainage curve, resulting in a thicker initial capillary fringe.

TDR saturation profiles were not collected during pumping due to electromagnetic interference with the pumping well. Neutron derived saturations collected during pumping are shown as a function of depth in Figure 4.7(a-b) for the 2 m and 4 m locations. A total of 15 neutron profiles were collected at each location during pumping; these figures show 5 representative profiles for each location that illustrate the nature of the observed response. Tensiometer locations are included for reference. Error bars indicate the average uncertainty in background saturation values (0.04) based on the count rate error. Profiles collected at both locations are moderately variable due to the small scale heterogeneities present at the site. Changes in saturation throughout pumping are minimal, and for the most part can be accounted for by the natural variability of the collection method. Small decreases in saturation near the top of the profile indicate the potential for very slight dewatering at shallower depths.

The saturation data in Figure 4.7 has been plotted versus tensiometer derived pressure head in Figure 4.8 (a-b). Once again individual profiles show moderate variability due to small scale heterogeneities present at the site. As pumping progressed the saturation profile shifted upwards towards more negative pressure head values, however, at each location only the two most shallow observation points reached pressure heads lower than -0.46 m (the air-entry pressure determined in the laboratory), and no significant dewatering was evident in the profile. Based on the neutron derived saturations and the hydraulic head observed at the tensiometers, it is clear that the pumping induced drawdown had not reached levels significant enough to cause drainage. It is of significance that while the saturation data does not provide evidence of any dewatering within the capillary fringe, the drawdown curves observed below the water table still display a typical unconfined response, normally attributed to drainage contributions from the capillary fringe.

4.5 Recovery Results

4.5.1 Hydraulic Head and Gradient Results

Heavy rains began at 300 min. into the recovery test which quickly brought the hydraulic heads to 0.15 m above the background values at all locations. Following the rain, which lasted for approximately 200 min., hydraulic heads began to fall. By the end of the monitoring period, which corresponds to 1100 min. following the end of the rain event, hydraulic heads remained above the pre-pumping values.

Given the strong influence of this rain event on the hydraulic head observations, the remaining discussion of the recovery portion of the test will be focused on the initial 300 min. of recovery.

As with the pumping data, the hydraulic head drawdowns for the logged observation well couplets are given in log-log format in Figure 4.9(a-b). At both the 2 m and 4 m locations, the hydraulic heads recover to within 0.05 m of the background values (approximately 75% recovery) within the first 300 min. of recovery. The hydraulic head recovery follows a similar pattern to the pumping induced drawdown, with an initially high rate of recovery that peaks early, and subsequently decreases with recovery duration. The hydraulic head recovered at a rate of 0.03 m/min. at the 2 m (deep well) location during the initial 3 min. of recovery. Pumping induced drawdown occurred at the same rate during the initial 3 min. of pumping at the same location. From 3 min. of recovery until the rain event at 300 min., recovery occurred at a significantly lower rate of 2×10^{-4} m/min. During the 3 min. to 300 min. pumping duration interval, drawdown of hydraulic head occurred at a similar rate of 3×10^{-4} m/min. In contrast to the pumping results, the deep wells recovered in a similar manner to the shallow wells, indicating a reduction of the vertical gradients.

Hydraulic head data observed during recovery at the tensiometer locations are shown in log-linear format on Figure 4.10(a-b). The shallow well recovery data is included as a reference in each figure. It is noted again that the deep tensiometer remained below the water table throughout pumping and recovery. As with the pumping data, the recovery of the pressure heads in the tension saturated zone exhibit the same response as the shallow well at both the 2 m and 4 m locations. The degrees of recovery were similar both below the water table and within the tension saturated zone. Due to the manual collection method, data is sparse within the first 10 min. of recovery; however, the general trend is distinguishable. As with the hydraulic heads below the water table, the hydraulic heads observed at the tensiometers recover at a rate that is one order of magnitude higher in the initial 10 min. of recovery compared to the rate observed during the subsequent 240 min. The average recovery rate for all tensiometers is 3×10^{-2} m/min. during the first 10 min. of recovery, and 2×10^{-4} m/min. for the following 240 min.

Vertical gradients were calculated both below and across the water table following the methods given in the preceding section. The results are given in Figure 4.11 for the well couplets and Figure 4.12(a-b) for the well-tensiometer pairs; a positive vertical gradient indicates downward flow. From the well couplet data, there appears to be a 0.25 min. lag between when the pump is turned off and when the gradients begin to decrease. This is likely evidence of well bore storage. Within the first minute of recovery, the vertical gradients between the monitoring wells at both locations became negative indicating the development of upward flow. The magnitudes of the vertical gradients below the water

table were significantly lower for the recovery portion of the test in comparison to the drawdown portion.

The vertical gradients calculated across the water table followed a similar trend to those observed at the well couplets, where a fast development of upward flow was observed early in recovery (Figure 4.12(a-b)). With continued recovery the vertical gradients between the well and the tensiometers gradually shifted towards low magnitude, positive gradients, indicating downward flow. It is again noted that due to the uncertainty in the tensiometer measurements gradient calculations may be in error by as much as 0.006 m/m for the intermediate tensiometers, and 0.005 m/m for the shallow tensiometers. The presence of very low positive gradients during this time period may be indicative of a period of negligible vertical flow.

Vertical gradients observed within the tensiometer network during recovery are consistent with those observed during pumping in that the values fluctuate within the uncertainty in the calculation for the duration of recovery. Given the low magnitude of the values observed, and the possible range in observations it is reasonable to conclude that vertical gradients across the water table, and through the tension saturated zone were very low during the recovery portion of the test, lower than those observed during pumping. Although there is some indication of minor downward flow during recovery, it is potentially the result of the tensiometer resolution.

Vertical gradients throughout the saturated zone are very low during recovery, lower than those observed during drawdown, and vertical gradients are much less significant than those observed during pumping. This observation holds both above and below the water table. Thus, the results of this test support a conceptual model in which the vertical gradients do not undergo a significant change in the transition from saturated to tension saturated conditions, and where vertical flow is significantly diminished during recovery.

4.5.2 Saturation results

Neutron and TDR derived saturations collected during recovery are shown as a function of depth in Figure 4.13(a-c). Error bars indicate the average uncertainty in background neutron derived saturation based on the count rate error. A total of 8 neutron profiles were collected at each location during recovery; 5 representative profiles are shown. A total of 9 TDR profiles were collected during the course of recovery of which 4 representative profiles are shown. The profiles collected at approximately 1300 min. were collected following the rainfall event. The neutron results show that changes in saturation throughout the depth profile are very minor, indicating that very little change in saturation occurred within the tension saturated zone during the pumping or recovery phases of this test. The TDR data is consistent with the neutron derived saturations, as only minor increases in

saturation are observed throughout the depth monitored by neutron probe. As with the background profiles, the TDR derived moisture profile shows slightly more variation with depth as a result of local scale heterogeneities. The three shallowest TDR locations show a trend of increasing saturation through recovery, providing evidence that drainage occurred above the tension saturated zone during pumping.

Neutron derived pressure-saturation profiles are shown in Figure 4.14(a-b). Profiles collected prior to pumping are included for comparison. Pressure head values used in the profiles were interpolated from the tensiometer data. The final profile, taken following the rain event, shows the similarity between the background profile and the rain influenced profile. This similarity highlights the initially wet condition of this pumping test. In general, the pressure-saturation profiles display a shift in the profile towards less negative pressure head values, with little change in saturation levels throughout recovery.

TDR derived pressure-saturation profiles are shown in Figure 4.15. The background profile, and the laboratory derived drainage and imbibitions curves are included for reference. The profile collected at 1311 min. was collected following the rainfall event. It has been included to illustrate the agreement of the natural state of the field saturation profile during the wet season with the laboratory derived imbibition curve. Clearly, the saturation profiles collected during recovery show a significant difference from those collected prior to pumping and following the rainfall event. These field profiles appear to follow a scanning loop between the main imbibition and drainage curves observed in the laboratory, with the background curve falling close to the main imbibition branch of the laboratory curve. The saturation profile collected at the start of recovery approaches the laboratory derived drainage curve, while following the rainfall event the profile approaches the laboratory derived imbibition curve. These field profiles display the effect of hysteresis on the saturation profiles in the Borden aquifer. The implications of this observation are discussed in the following section.

4.6 Discussion

The pumping test conducted for this study differs from previous tests in the Borden aquifer (Nwankwor et al., 1992, and Bevan et al., 2005) in that the top of the tension saturated zone was not drawn down due to the low pumping rate and background moisture profile conditions. As a result of these circumstances drainage was limited to the unsaturated zone and a unique relationship between drainage and saturated zone drawdown was observed. Although certain aspects of the test are unique, observations such as the vertical gradient development can be expected to apply to a more general conceptual model for unconfined pumping tests. An important component of the conceptual model for unconfined pumping tests used by Bevan et al. (2005) is the assumption that vertical gradients are low and uniform throughout the entire saturated zone. This component permits the estimation of water table position

using well couplet data in the absence of tensiometric data. These aspects of the conceptual model can be evaluated using the results obtained during the current test.

Water table position during pumping was determined using the Bevan et al. (2005) well couplet method described in Chapter 3. The drawdown of the water table (the zero pressure isobar) was also determined using linear interpolation between tensiometer measurements (the deep tensiometers remained just below the water table for the duration of the test). The water table drawdowns at the 2 m and 4 m locations are shown in log-linear format in Figure 4.16 (a-b). The calculated water table drawdown using the Bevan et al. (2005) method provides a good approximation of the actual water table drawdown measured with the tensiometers at all times during pumping. At the 2 m location there is a slight under prediction of the water table drawdown using the well couplet data, likely due to the increasing complexity of the flow field and increasing prominence of the vertical flow component with greater proximity to the pumping well.

The recovery of the water table at the 2 m and 4 m locations are shown in log-linear format in Figure 4.17(a-b). The hydraulic head profiles remained linear through recovery; therefore, the water table position was determined using the methods applied during drawdown. The water table predictions made using the well couplets are improved in comparison to the drawdown test. This improvement was expected as the flow field is reduced in complexity during recovery, with vertical flow being reduced significantly in comparison to the pumping portion of the test. As with the hydraulic head, the water table recovers very rapidly in the first few minutes following the end of pumping. The rate of water table recovery slowed as the duration of the recovery increased. Given these results, the water table interpolation method provides a conservative approximation of the actual water table drawdown and recovery.

The presence of low and uniform vertical gradients throughout the entire saturated zone during this test can be confirmed using observations from within the capillary fringe and the shallow zone below the water table. Vertical gradients below the water table were found to increase rapidly at the onset of pumping, a result of the partially penetrating well screen. The peak magnitude in vertical gradient below the water table was reached at 2 min. at both the 2 m and 4 m observation locations, with the magnitudes being 0.023 and 0.01 m/m respectively. The vertical gradients observed above the water table do not exceed the uncertainty in the measurement of approximately 0.05 m/m. Given the similarity between the vertical gradients above and below the water table, a conceptual model in which the vertical gradient magnitudes are similar throughout the saturated zone seems appropriate.

It is important to note here that the tensiometers used in this test remain in soil that is at or near saturation for the duration of pumping. The previous conclusions regarding the magnitude of the

vertical gradients are applicable only within the tension saturated zone. The nature of the vertical gradients above the tension saturated zone can be investigated using a simple homogeneous numerical model of drawdown in the Borden aquifer. Full details of the simulation can be found in Section 3.1 of Bunn et al. (2010). Results of the vertical gradient profiles, and saturation profiles are shown in Figure 4.18. Although large gradients develop, these are found only above the saturated zone where mass flux continuity requires large gradients to overcome the reduction in hydraulic conductivity. This result is supported by the observations of Nwankwor (1985), who was able to detect high gradients above the zone of tension saturation, while gradients remained low through the saturated zone. The model results also show vertical gradients that decrease in magnitude with increasing elevation through the tension saturated zone. These results are consistent with the general trend of the vertical gradients observed across the water table shown in Figure 4.5. Given these results, it is clear that there is no evidence to support any significant change in vertical gradient magnitude throughout the saturated zone, either above or below the water table, during unconfined pumping tests. The model results show that vertical gradient magnitudes within the saturated zone are highest near the top of the well screen, and decrease with increasing elevation until the top of the tension saturated zone. The agreement between the model trends and those observed in the field supports the ability of the numerical simulations to predict the hydraulic head distributions within the tension saturated zone during pumping with an acceptable level of accuracy.

The influence of hysteresis on the soil moisture profile was observed during both pumping and recovery. The proximity of the water table to the ground surface prevented the collection of a full soil moisture profile during pumping; however, this proximity facilitated the collection of TDR data during recovery which was sufficient to more closely examine the influence of hysteresis on the moisture profile. The saturation profiles inferred from the TDR data are shown in Figure 4.15. Prior to pumping the moisture profile closely approximated the laboratory derived imbibition curve, at the beginning of recovery the moisture profile fell between the main laboratory drainage and imbibition curves, while prior to the rainfall the profile again appeared closer to the laboratory imbibition curve. Thus, while a hydraulic head drawdown of 0.13 m occurred at the top of the tension saturated zone, there was minimal vertical movement of this saturation interface. In comparison of the results of this test to the moisture content recovery observations made by Bevan et al. (2005), the Bevan test took place when the water table was in the process of seasonal lowering such that the background saturation profile was very similar to the main drainage curve observed in the laboratory. As pumping progressed, the width of the tension saturated zone of the saturation profile extended well beyond any values observed in the laboratory. When pumping ceased and recovery began, the shape of the moisture profile changed rapidly, such that within the first 200 min. of recovery, the saturation profile was similar to that observed during imbibition in the laboratory.

To further examine the influence of hysteresis on the recovery of the moisture profile following pumping it is useful to consider the evolution of the capillary fringe thickness. The top of the capillary fringe is defined as the first point at which a significant and continuous drop in saturation occurs. For the data collected in the current study the thickness is taken as the absolute value of the pressure head at the top of the tension saturated zone. For the Bevan test, used in comparison, the thickness was taken as the difference in elevation between the top of the saturated zone (inferred from neutron derived moisture content) and the water table (inferred from shallow deep piezometer pairs). The changes in thickness are plotted in Figure 4.19, with the background thickness prior to pumping included as a reference. Due to the extension observed during the pumping portion of the Bevan test, the temporary compression that occurred during recovery resulted in a tension saturated thickness that was 0.15 m less than the background thickness. In the current test, the background thickness was much closer to that observed during the imbibition portion of the laboratory curve. The change in thickness during recovery resulted in a final thickness that more closely approximated the background observations. It is noted here that while the first TDR profile collected during recovery results in a capillary fringe thickness that is slightly thicker than the background thickness observed, it is still less than the capillary fringe thickness determined during drainage in the laboratory using a sample from the site. Based on these profiles and the preceding discussion, it appears that hysteresis was a dominant process controlling the shape of the saturation profiles observed during the current test.

Data collected during this test also provides significant observations which may highlight a unique response to pumping. A typical unconfined time-drawdown curve displays a high rate of drawdown that reduces during the middle portion of the test. The drawdown rates typically increase again prior to reducing significantly as steady state is reached. The cause of the shape of the time-drawdown curve is typically attributed to vertical drainage as a result of the lowering of the top of the saturated zone. More recent studies (Nwankwor et al., 1992, Narasimhan and Zhu, 1993, and Endres et al., 2007) support the notion that flow in the unsaturated zone plays a significant role. During this test, a reduced rate of draw down was achieved after approximately 2 min. in the saturated zone (see Figure 4.2). Further analysis of the derivatives of the time drawdown curve also result in a typical unconfined response, with a peak at approximately 1 min, followed by a period near zero, before rising again at approximately 11 min. However, due to the low pumping rate used, and the imbibing condition of the moisture profile prior to pumping, no drainage was produced by the lowering of the top of the saturated zone. These observations suggest that flow contributions from other sources, including the potential for lateral flow through the unsaturated zone, may have had a significant impact on the hydraulic head drawdown in the saturated zone during this test.

4.7 Conclusions

A constant rate, 24-hour pumping test was conducted in the shallow water table portion of the Borden aquifer. The test was conducted at a different location in comparison to earlier tests at CFB Borden, which necessitated the use of a lower pumping rate. This test was also conducted with a background moisture condition that appeared to have undergone imbibition, such that the pumping induced drawdown did not initiate a lowering of the top of the capillary fringe. Although the proximity of the water table to the surface during the test limited the collection of a full saturation profile using a neutron probe, it facilitated the installation of TDR rods and tensiometers which provided a large amount of data pertinent to an increased understanding of the transient nature of the vertical gradients within the saturated zone and the development of drainage in unconfined pumping tests.

Tensiometer data collected resembles the time-drawdown curves produced by the shallow well. Vertical gradients measured by the tensiometers were low, below 0.05 m/m. The vertical gradients measured across the water table using the shallow well and the intermediate and shallow tensiometers are also quite low, with the magnitudes in the deeper interval being on the order of those below the water table, and the magnitudes in the shallow interval being somewhat less. The TDR data collected during the recovery potion of the test verifies that the only significant drainage to occur during the test was limited to the transition zone above the capillary fringe. No drainage occurred from the tension saturated zone during pumping.

The field data presented in this paper provides an additional step towards the understanding of the flow processes involved during pumping of an unconfined aquifer. The results show that the vertical gradients through the capillary fringe are as low if not lower than those observed below the water table, closer to the well screen. Numerical modeling supports this observation. Previous studies of the unconfined response to pumping in the Borden aquifer have investigated the possible impact of soil texture (Moench, 2008), and heterogeneity (Bunn et al., 2010) on observed thickness of the capillary fringe. All of these works have relied on assumptions of low and uniform vertical gradients, and minimal hysteretic effects to confirm the presence of an extended capillary fringe. The tensiometer observations support the assumption that vertical gradients remain low, and are of similar magnitude throughout the entire saturated zone. Given the uniform magnitude of the vertical gradients, the method used to predict the position of the water table using well data appears to be valid, particularly in the later portions of a pumping test. As the magnitudes of the vertical gradients are similar both above and below the water table it is unlikely that an apparent capillary fringe extension would result from such gradients. The TDR data collected during recovery shows the impact of hysteresis on the development of the saturation profile in response to pumping and recovery.

This test provides additional insights into the response of unconfined aquifers to pumping not previously observed. Although the drawdown induced during this test was insufficient to generate drainage from the tension saturated zone given the initial condition of the moisture profile, the second phase of the unconfined aquifer drawdown response was observed. This observation provides evidence that during this test the three-part time-drawdown curve was not the result of vertical drainage from a lowering of the saturated - unsaturated interface. This result warrants further investigation into the source of drainage to the saturated zone that permitted the observed reduction in drawdown rates.

4.8 Figures and Tables

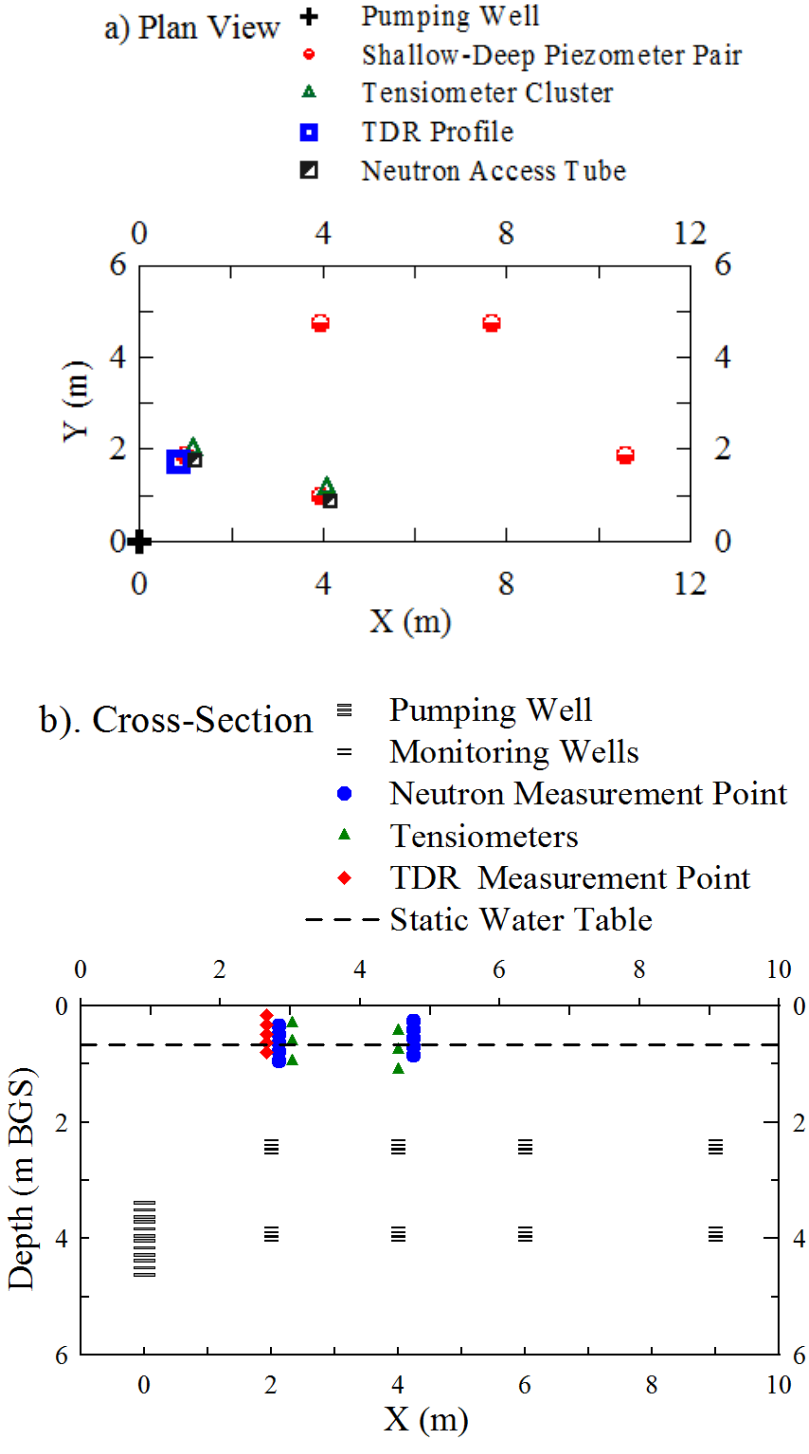

Figure 4.1 (a-b). Map of the Borden aquifer showing the instrumentation used in the pumping test. (a. Plan view, b. Cross-section)

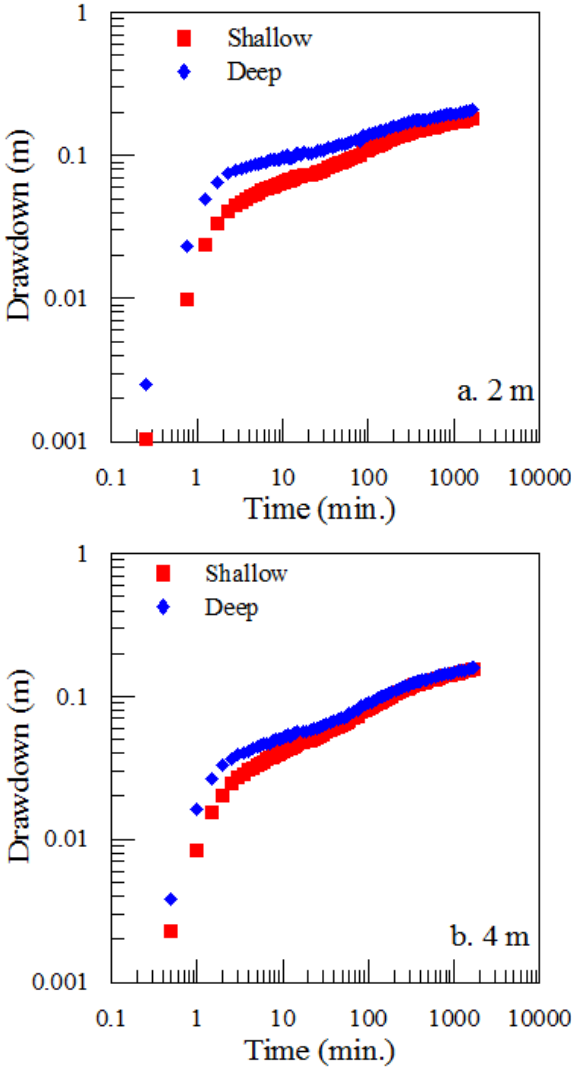

Figure 4.2. Log-Log plots of hydraulic head versus time for shallow deep well couplets during pumping. (Radial distance: a. 2 m, b. 4 m).

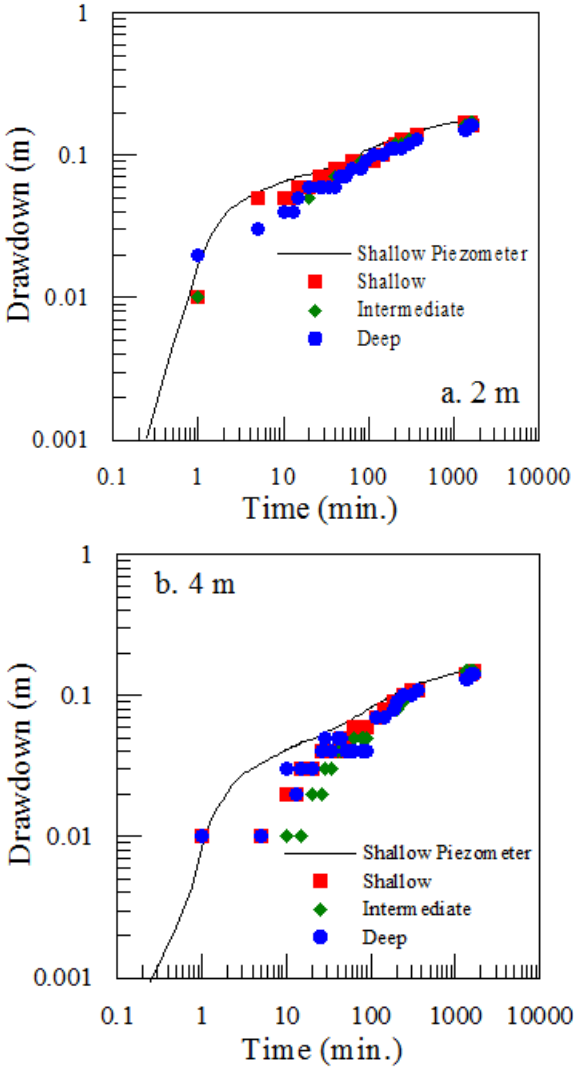

Figure 4.3. Log-Log Plots of hydraulic head versus time for tensiometers during pumping. (Radial distance: a. 2 m, b. 4 m).

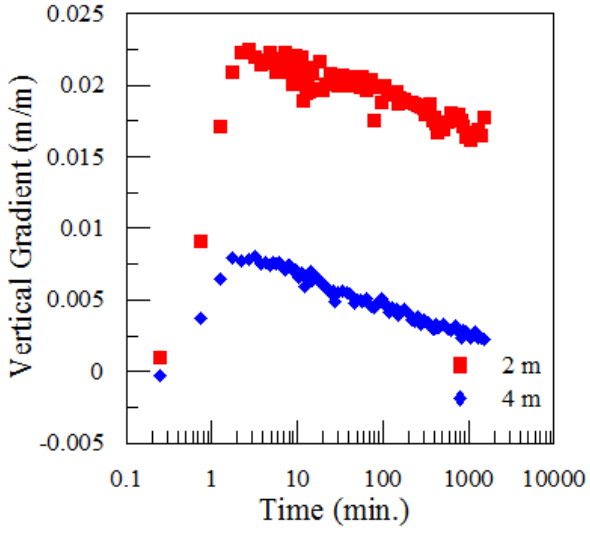

Figure 4.4. Vertical gradients calculated using well couplets during pumping; positive values represent downward flow.

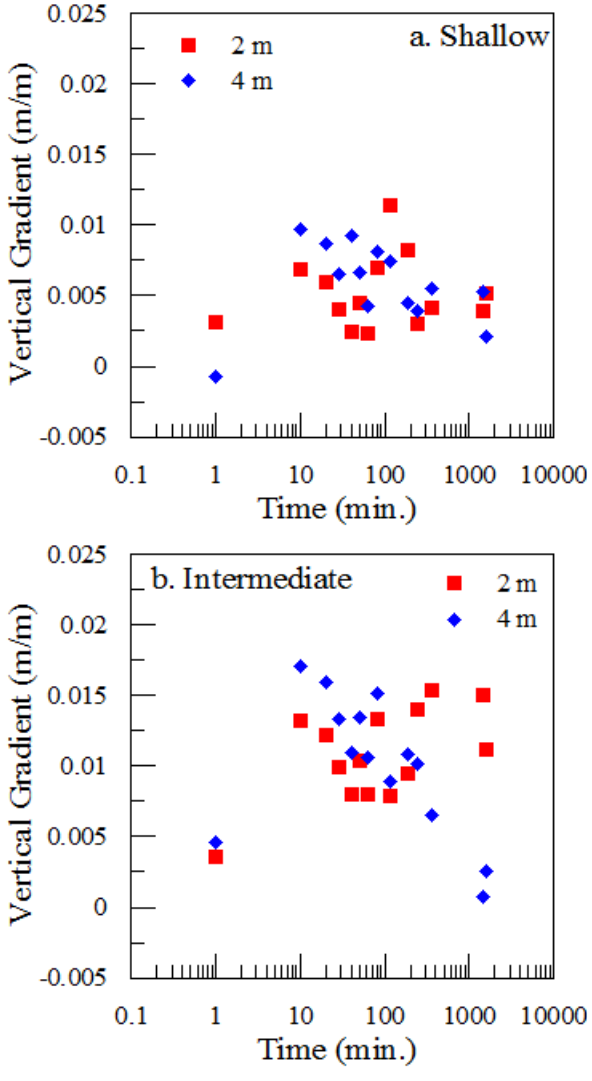

Figure 4.5 (a-b). Vertical gradients calculated across the water table during pumping. Positive values represent downward flow. (Tensiometer Location: a. Shallow, b. Intermediate)

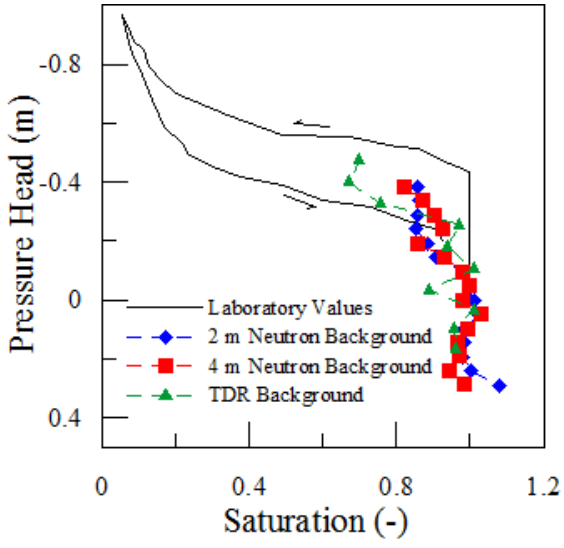

Figure 4.6. Static pressure head – saturation profiles collected prior to pumping.

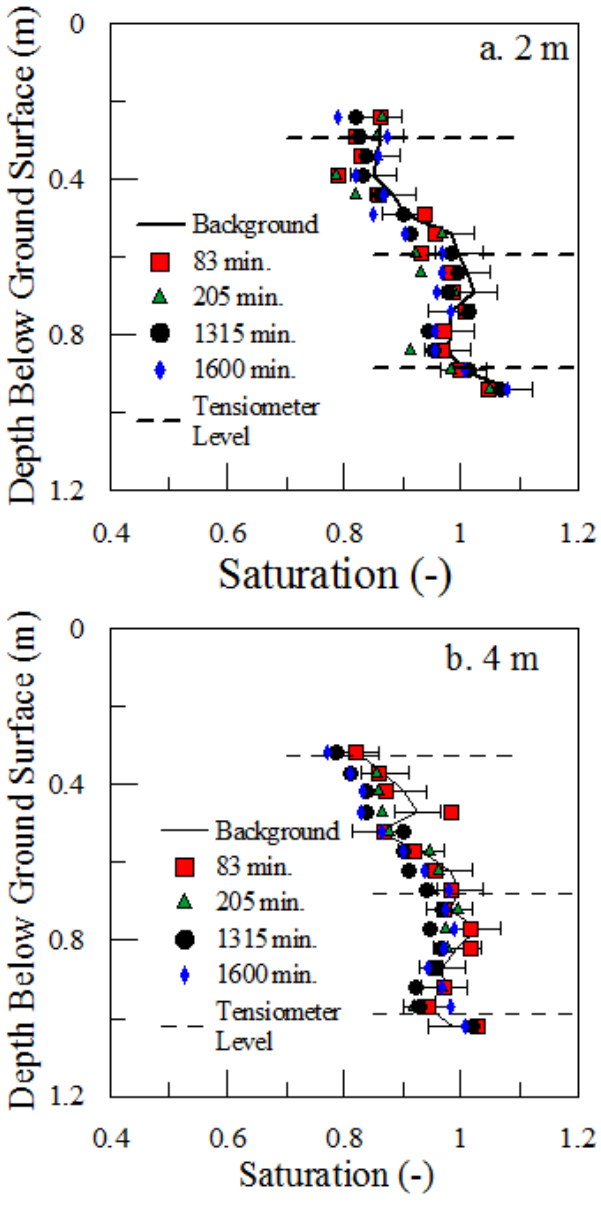

Figure 4.7 (a-b). Depth – saturation profiles collected during pumping. Error bars indicate saturation uncertainty based on neutron count rate (Radial distance: a. 2 m, b. 4 m)

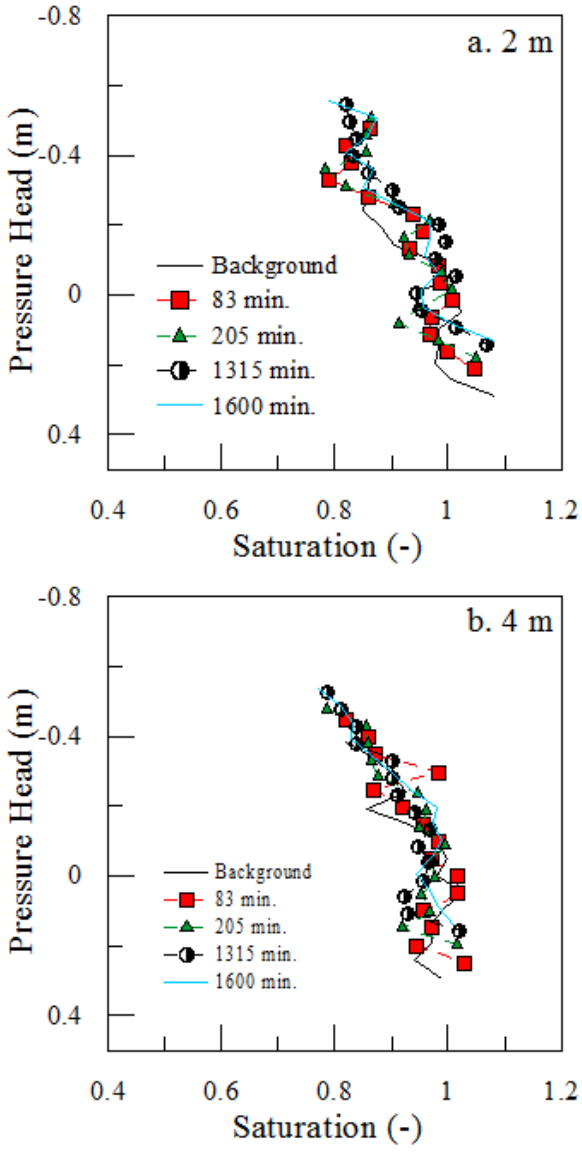

Figure 4.8 (a-b). Pressure head – saturation profiles collected by neutron probe during pumping (Radial distance: a. 2 m, b. 4 m)

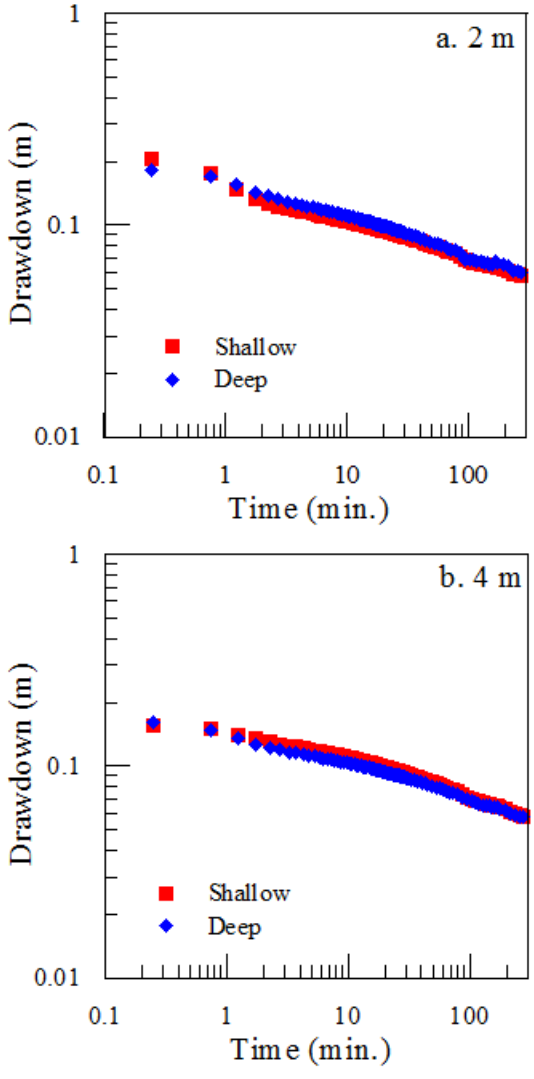

Figure 4.9 (a-b). Log-Log plots of hydraulic head versus time for shallow deep well couplets during recovery. (Radial distance: a. 2 m, b. 4m).

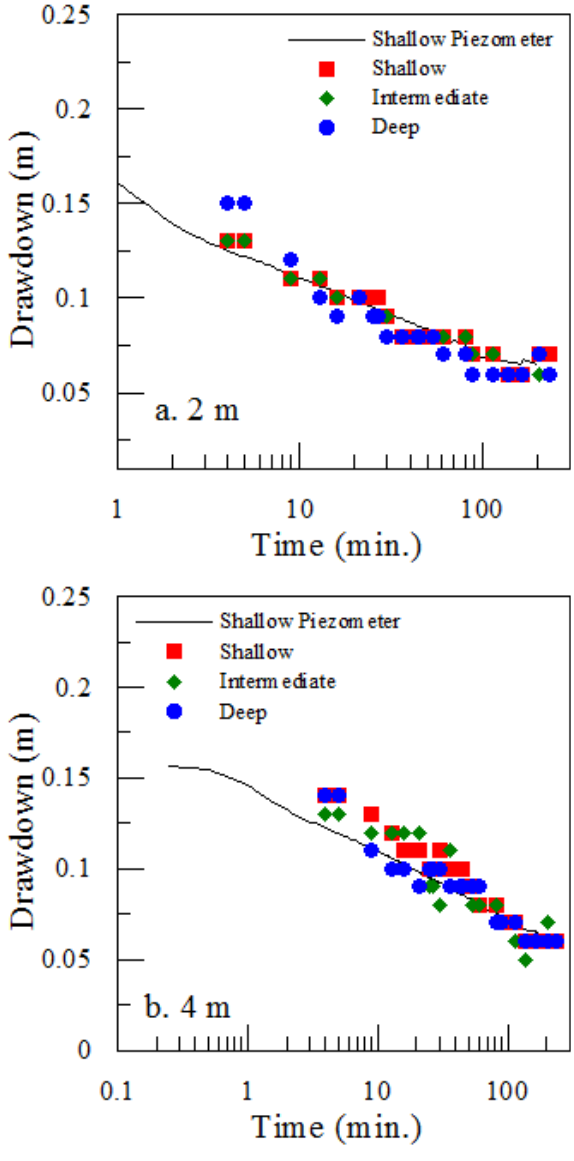

Figure 4.10 (a-b). Log-Linear plots of hydraulic head versus time for tensiometers during recovery. (Radial distance: a. 2 m, b. 4 m).

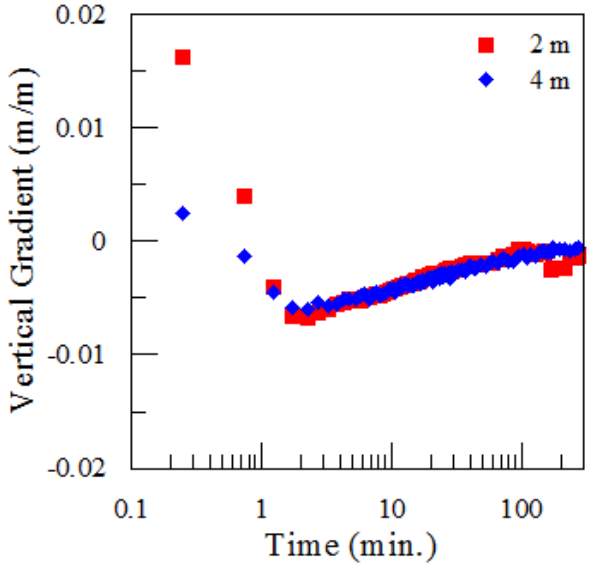

Figure 4.11. Vertical gradients calculated using well couplets during recovery. Positive values represent downward flow.

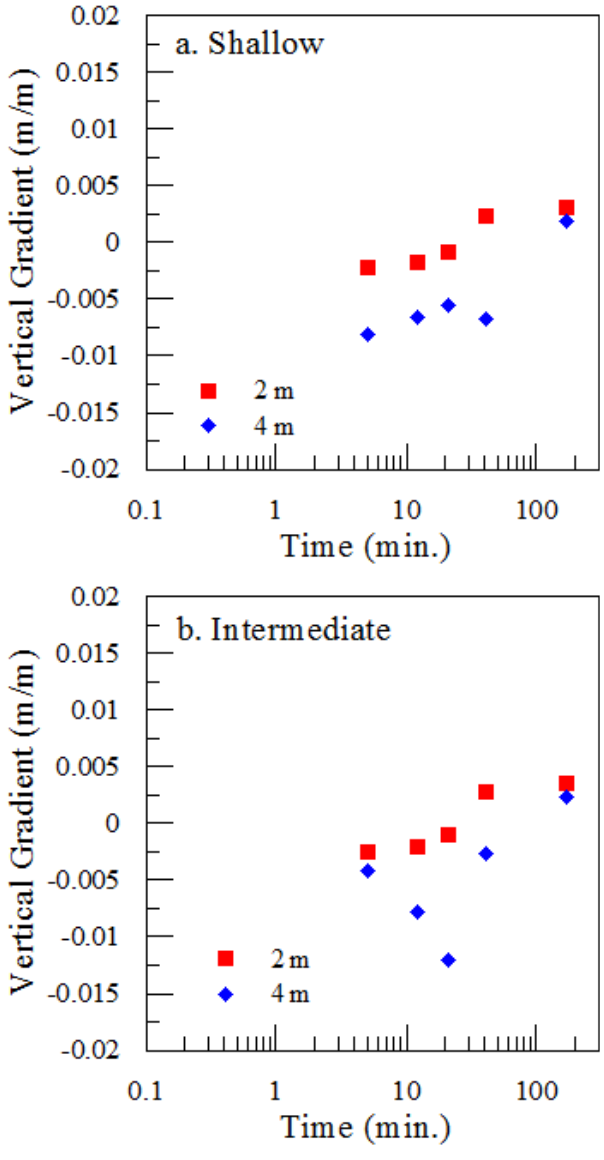

Figure 4.12 (a-b). Vertical gradients calculated across the water table during recovery. Positive values represent downward flow. (Tensiometer Location: a. Shallow, b. Intermediate)

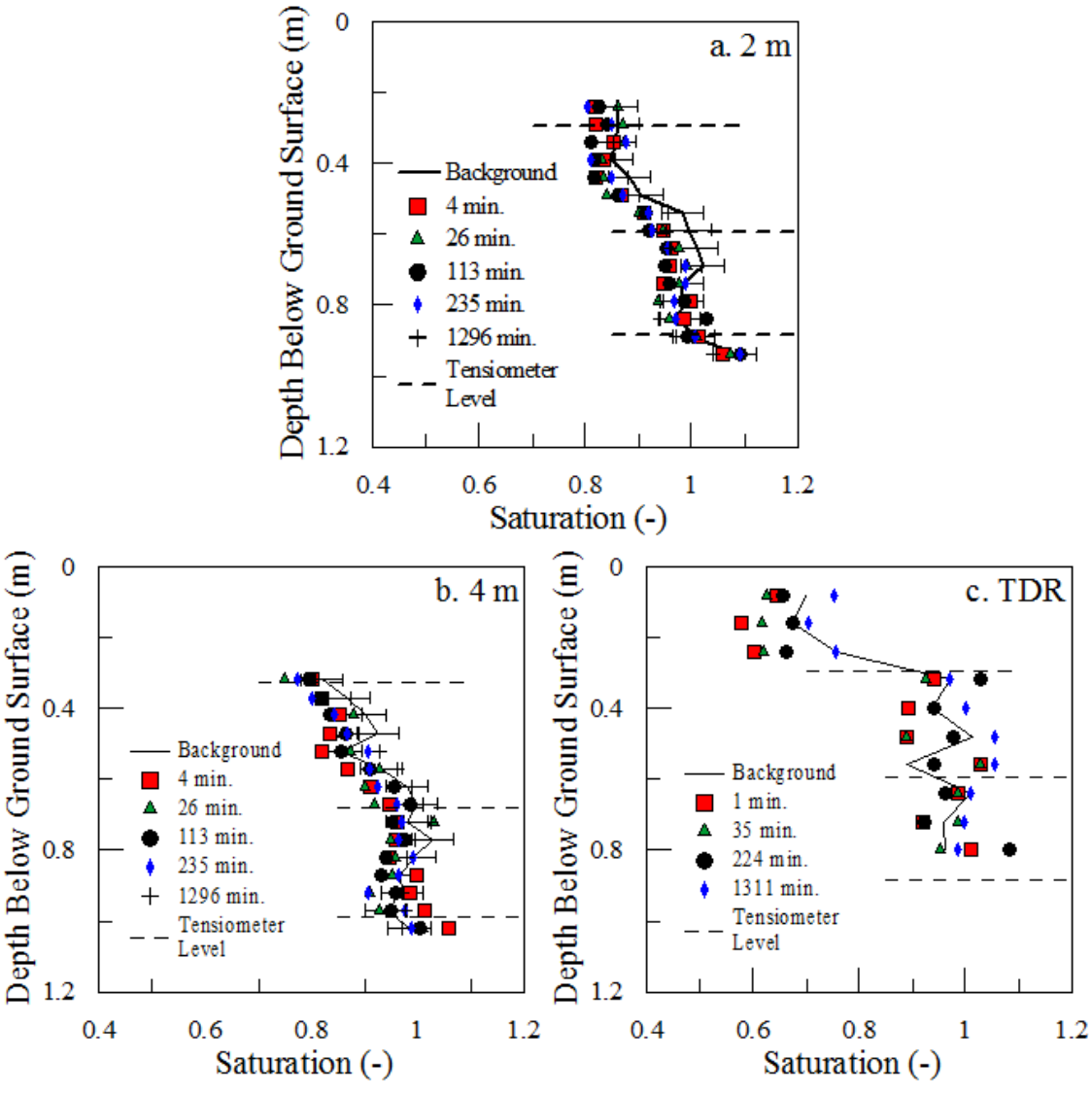

Figure 4.13 (a-c). Depth – saturation profiles collected during recovery. Error bars indicate neutron derived saturation uncertainty based on neutron count rate. (a. 2 m Neutron, b. 4 m Neutron, c. 2m TDR)

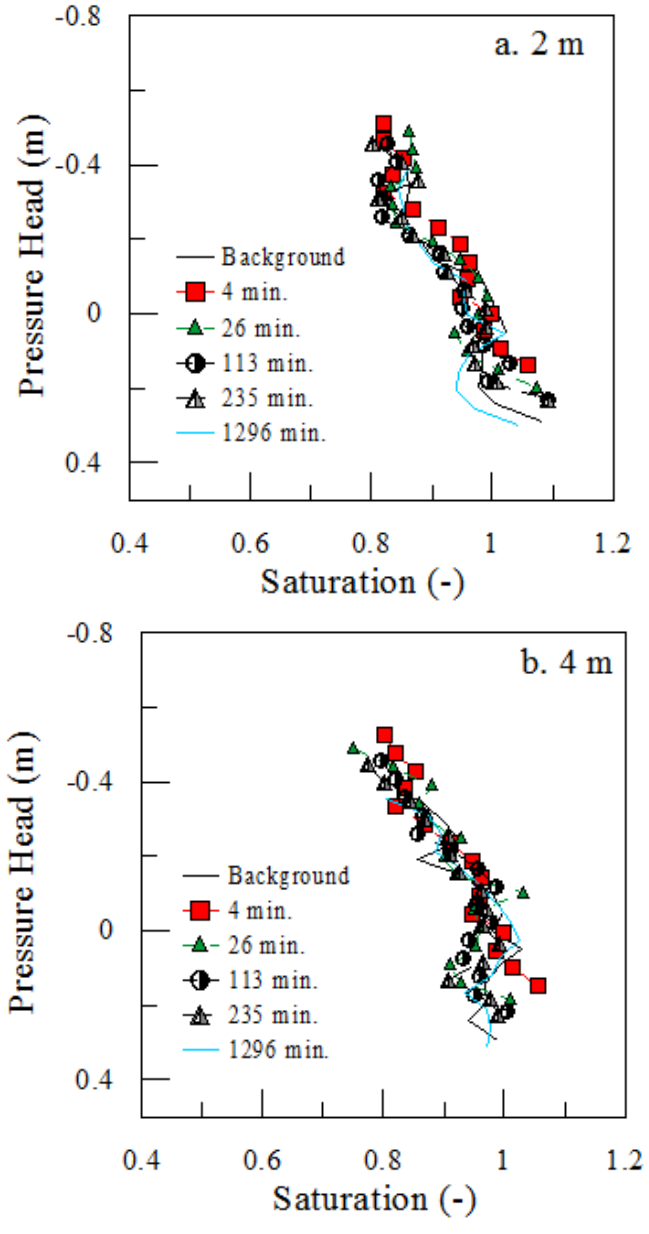

Figure 4.14. Pressure head – saturation profiles collected by neutron probe during recovery (Radial distance: a. 2 m, b. 4 m)

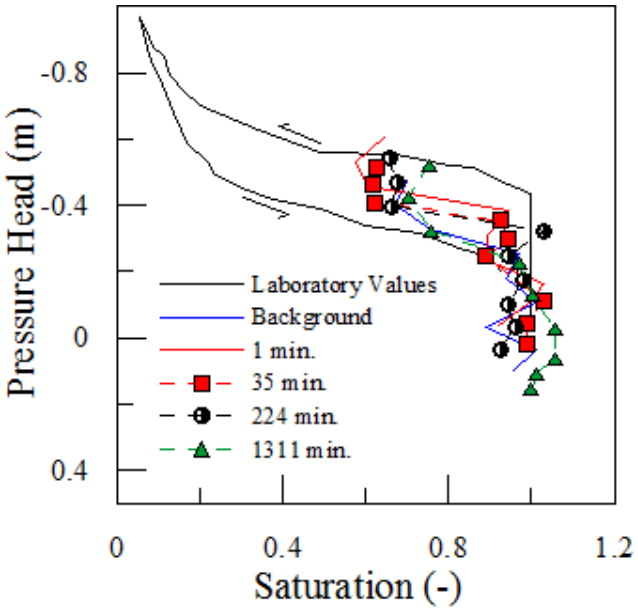

Figure 4.15. Pressure head – saturation profiles by TDR during recovery

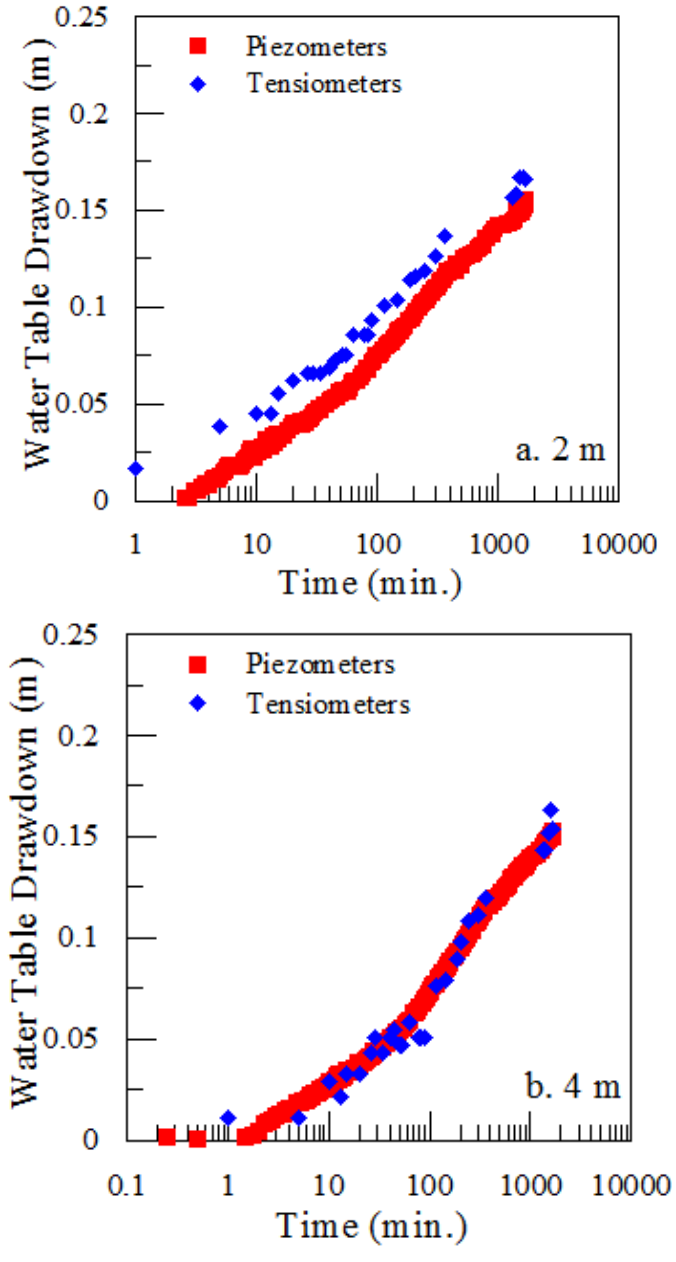

Figure 4.16. Water table drawdown during pumping calculated using well couplet drawdown, and interpolated using tensiometer measurements (Radial Distance: a. 2 m, b. 4 m).

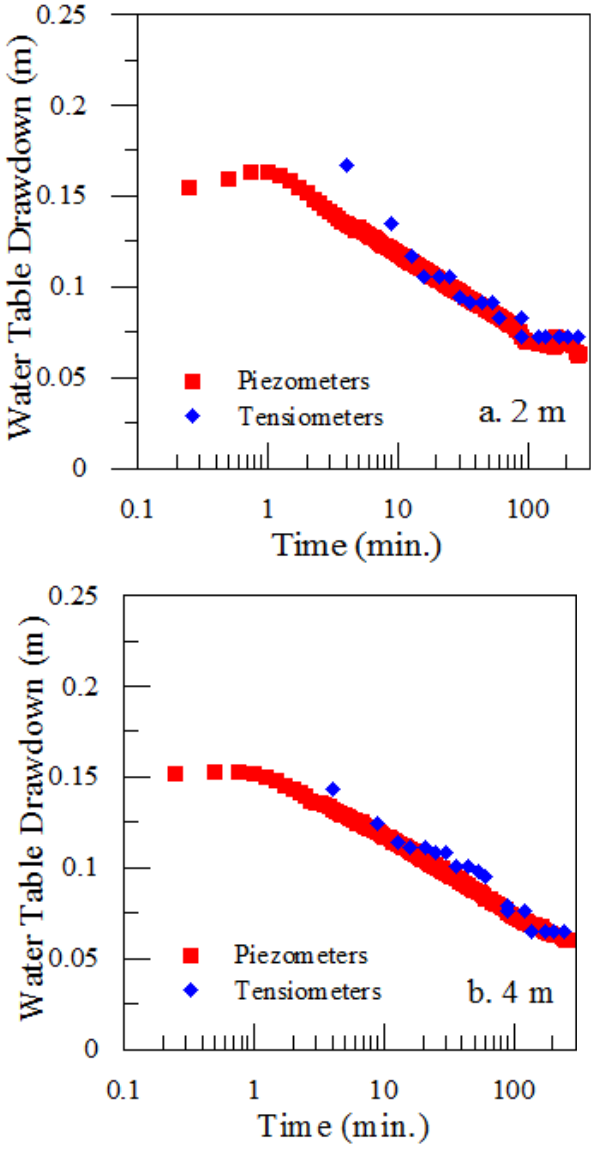

Figure 4.17. Water table drawdown during recovery calculated using well couplet drawdown, and interpolated using tensiometer measurements (Radial Distance: a. 2 m, b. 4 m).

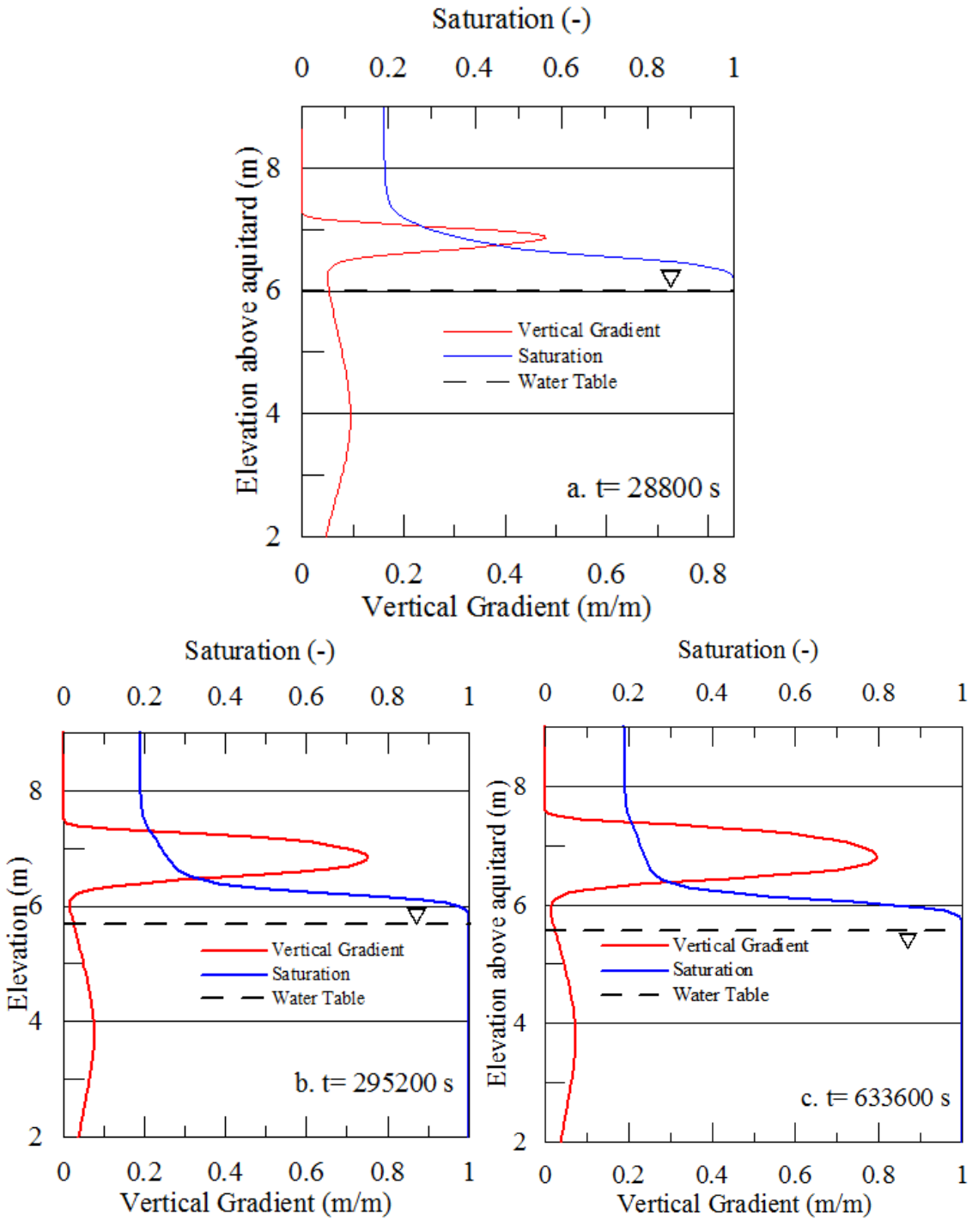

Figure 4.18. Vertical profiles of vertical gradient and saturation values generated by a numerical simulation of the Bevan et al. (2005) pumping test.

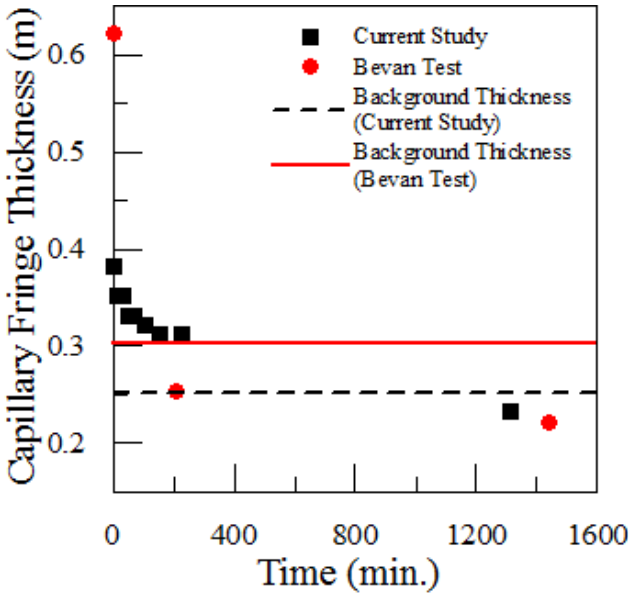

Figure 4.19.Capillary fringe thicknesses during recovery calculated using TDR data from this study, and determined using the neutron probe data from Bevan et al. (2005).

Chapter 5

Tank Scale Investigations of Horizontal Flow Dynamics through the Capillary Fringe

5.1 Introduction

Horizontal flow through the capillary fringe was originally recognized by Wyckoff et al. (1932), and Luthin and Day (1955) early in the development of hydrogeology. However, for many years vertical drainage was considered the only significant component of flow within the capillary fringe, and horizontal flow was ignored. In some natural aquifers this is an appropriate approximation for saturated flow analysis as the thickness of the capillary fringe can be many orders less than the total thickness of the aquifer.

More recent work has begun to highlight the failure of the vertical drainage simplification to capture the important flow processes occurring in the capillary fringe. Work by Silliman et al. (2002) in laboratory scale tanks showed that flow into the capillary fringe from the region below the water table can be a significant process that may affect transport, mixing, and microbial activities. Related work by Dunn and Silliman (2003) and Dunn et al. (2004) has shown that the capillary fringe is an important component of flow and transport both horizontally and vertically. Berkowitz et al. (2004) noted that field and laboratory experiments in the capillary fringe have shown that the flow regime above the water table is complex and highly sensitive to the presence and distribution of heterogeneities including entrapped air. It was suggested that in place of the term capillary fringe, the term partially saturated fringe be used to describe the flow region both below and above the water table where a connected water phase dominates the flow in the presence of entrapped air (Berkowitz et al., 2004). These studies have focused more on flow paths, and transport conditions under a set water level. Other laboratory scale studies have focused on the impact of unsaturated flow on seepage faces. Experiments by Wyckoff (1932), Luthin and Day (1955), and Simpson et al. (2003) have helped to better characterize the flow rates and distributions at seepages face under variable water table heights. The results of these experiments highlight the importance of horizontal flow through the capillary fringe. Recently, Berg and Gillham (2010) used a specially designed velocity probe to measure horizontal flow velocities in the capillary fringe. Their results showed that horizontal flow in the capillary fringe is similar in magnitude to flow in the saturated zone below the water table.

While previous studies of the capillary fringe on the laboratory scale have provided a great deal of insight into the dynamics of flow in the capillary fringe, few experiments exist in which the response of moisture content and pressure head is monitored under falling water table conditions. In light of the observations made by Bevan et al. (2005) of a capillary fringe that grew in thickness during the duration of a pumping test, further investigation into these dynamics under the conditions of a falling water table

are warranted. This study presents the results of several laboratory scale experiments of drainage under dominantly horizontal flow conditions. Moisture content and pressure head distributions were collected during steady state conditions following step drops in water level in a flow through tank. Experiments were completed in a well sorted coarse sand and a poorly sorted medium sand. Drainage was conducted under two different horizontal gradients, and the amount of entrapped air was varied by shortening the equilibration time between drainage cycles. The objective of this experiment was to determine the effect of horizontal gradient magnitude, and grain size distribution on moisture content distributions during drainage under a primarily horizontal flow regime.

5.2 Materials

All experiments were conducted in 0.62 m long rectangular plexiglass box with an internal cross-section of 0.26 m by 0.3 m. The tank was designed by Berg (2007) using porous metal end plates such that vertical flow at the tank inlet and outlet would be avoided. Flow through the tank was established using 10 μm porous steel plates with dimensions of 0.24 by 0.28 m installed at each end of the tank. Each plate was mounted to hollowed plexiglass sheets forming a sealed reservoir. The air-entry pressure of the porous plate was -0.65 m, which permitted the plate and reservoir to remain water filled, while the water level was lowered to 0.65 m below the top of the tank. Access tubing was installed in each reservoir which allowed the pressure in the plate to be controlled by drip point at the outlet, and by a constant head overflow at the inlet. Figure 5.1 shows a schematic of the reservoirs used in the tank.

A monitoring network was installed to measure vertical distributions of soil moisture and pressure head within the tank. At 0.3 m from the inflow plate four UMS T5 tensiometers were installed horizontally through ports in the side wall of the tank. The tensiometers were placed with a 0.07 m vertical spacing and the 0.005 m porous tips were situated in the centre of the tank. A total of 14 TDR probes were also installed horizontally through the side walls of the tank. The probes were organized in two vertical rows, one at 0.19 m from the inlet plate, and one at 0.19 m from the outlet plate. Probes were placed with a 0.03 m vertical separation within each row from 0.03m to 0.27 m below the top of the tank such that the length of the probe was perpendicular to flow through the tank. The probes were constructed of two stainless steel rods with an approximate length of 0.16 m, and diameter of 0.003 m. In accordance with the 1:10 ratio recommended by Knight (1992), the rods were separated by 0.03 m. A schematic of the tank and the instrumentation is shown in Figure 5.2. TDR measurements were taken using a Tectronix 1502C Cable tester. Rods were calibrated following installation in the tank using deionized water.

Experiments were run using two distinct sands. A commercially available silica sand, F35 grade (U.S., Ottawa, Illinois) which was coarse and well sorted. The light colour and coarse structure of the sand made it ideal for the visual monitoring of dye tracers. The second sand was a poorly sorted fine to medium grained sand collected from the CFB Borden field site. The Borden sand was run through a 0.001 m sieve prior to use to ensure the removal of any large pieces of organic material. Figures 5.3 and 5.4 show the pressure-saturation curves generated for the Ottawa and Borden sands using standard steady-state gravity drainage methods (referred to as gravity drainage data in this study). These curves were generated using the hanging column of water technique. Changes in pressure were initiated after steady-state head conditions were reached (from 15 min. to several hours). The Ottawa sand shows an air-entry pressure of approximately -0.10 m, significantly lower than the -0.42 m air-entry pressure for Borden sand. The pressure-saturation curves also give evidence of the sorting difference between sands, as the well sorted Ottawa sand shows a much sharper decrease in saturation through the transition zone in comparison to the Borden sand. All sands were mixed prior to testing to ensure homogeneity.

5.3 Experimental Methods

At the beginning of each test, prior to packing the tank, the end plates were saturated by immersing the reservoir assembly horizontally in a water filled basin and applying a vacuum to the access tube for a period of 24 hours to ensure removal of any entrapped air. Plates were then installed in the tank, and the water level in the tank was raised to 0.04 m from the tank bottom. The tank was filled with sand under saturated conditions to avoid air entrapment. Wetted sand was placed in 0.03 m lifts in the tank. Between lifts the sand was mixed, lightly tapped, and leveled. The water level in the tank was then raised by 0.04 m prior to addition of the subsequent lift. Tests have been numbered 1 to 3. Test 1 was completed using the Ottawa sand (F35) packed to a dry bulk density of approximately 1.85 g/cm^3, while Tests 2 and 3 were completed using Borden sand packed at 1.70 g/cm^3 and 1.73 g/cm^3 respectively. Following the emplacement of the final lift the tank was left to equilibrate for a period of approximately 48 hours.

All experiments were started by setting a fixed gradient across the tank to initiate flow. The difference in elevation between inlet and outlet remained fixed for the duration of the test to ensure that the gradient remained constant. For each step change in water level in the tank, pressure heads, TDR readings, and outflow rates were measured. All observations were collected after both the outflow rate, and the pressure heads had reached steady state (no observable changes over a period of 1 to 4 hours). This condition occurred within 4 hours of all drops; however, measurements were taken after significantly longer intervals. During Test 3, a set period of 8 hours was given between measurements based on the results of some initial numerical modeling. The water level was dropped in 0.02 m

increments for Tests 1 and 2. For Test 3, the water level was dropped in 0.05 m increments. All drainage cycles were terminated immediately following visual detection of air bubbles in the reservoir, indicating air-entry into the plate. For several drainage cycles, the outlet plate drained overnight due to bubbling, and the final measurements shown are those taken prior to the final drop in water levels. Test 1 consisted of two drainage cycles to compare the effect of flow rates. The first drainage cycle in test 1 began from fully saturated conditions. Due to kinking of the inlet tubing during the initial drainage for test 2, only the second, high gradient, drainage cycle will be discussed. Between drainage cycles water level in the tank was raised gradually, and the tank was allowed to equilibrate for 48 hours. Although this process eliminated any impact of packing differences between cycles, entrapped air was introduced in the shallow portions of the tank. For test 3, three drainage cycles were completed. The first two drainage cycles were completed under the same horizontal gradient. Water level in the tank was raised rapidly, and left to equilibrate for only 8 hours between cycles to observe hysteretic effects. The third cycle was completed under a lower gradient, and 48 hours was allowed to elapse before drainage was initiated. Table 5.1 presents a summary of tests completed, while Figure 5.5 shows a time series of the mean water level in the tank for each test. For the purpose of this study, the mean water level is defined as the water level at the mid-way point between inlet and outlet, measured as distance below the top of the tank. The high gradient drainage cycle was completed first for all tests.

In addition to the drainage experiments, a dye tracer experiment was conducted using Ottawa sand following the drainage experiments in test 1. The mean water level in the tank was placed at 0.23 m below the top of the tank, and the gradient was set at 0.2 m/m. Flow was allowed to equilibrate for a period of 48 hours. Following equilibration, several 3.5 mL slugs of food dye were placed at various points in the sand near the front face of the tank using a syringe. The food dye was diluted to eliminate any density effects. Slugs were placed below, above and within the capillary fringe, both distant from and proximal to the outlet plate. Position and orientation of the slugs was visually monitored to investigate the flow regime in the tank.

5.4 Results

5.4.1 Test 1 (Ottawa Sand)

A composite plot of all pressure head - saturation profiles collected during test 1 is shown as Figure 5.6. Points collected in the drier region of the curves are in good agreement with the pressure head - moisture content profile generated using a steady state gravity drainage method. In the wetter region of the curve, the air-entry pressure appears to be elevated in comparison to the gravity drainage curve. To illustrate the spatial variation in moisture content and pressure head through the progression of the test Figure 5.7 plots the pressure head - saturation profiles for each TDR probe location. TDR locations are labeled A to G, with probe A located closest to the top of the tank. All pressure head observations were

made at the centre of the tank. Pressure head – saturation profiles using TDR data were generated using linear interpolation between the tensiometers, and the inlet and outlet boundary pressure heads. This method is considered appropriate as all measurements were made while pressure heads and flow rates were at steady-state. Results for the high gradient (0.08 m/m) cycle are shown in Figures 5.7 (a-b), while Figure 5.7 (c-d) shows the results for the low gradient (0.03 m/m) cycle. For both cycles, the air-entry pressure is reached at approximately -0.2 m. This value represents an increase of 0.1 m over the gravity drainage value. During the high gradient experiment, as locations began to dry, pressure-saturation measurements more closely approximated the gravity drainage curve. Saturation values through the transition zone were slightly elevated near the outlet plate. For the lower gradient cycle moisture contents were slightly elevated through the transition zone. There was no difference in observations between the outlet and inlet end of the tank. Entrapped air was not observed in any of the moisture content values for the duration of the test, likely due to the coarse structure and uniform pore size distribution of the material.

Following the second drainage cycle in test 1, the water level in the tank was raised such that the water level at the mid-point of the tank sat 0.23m below the top of the tank. The gradient across the tank was set at 0.2 m/m and the flow was allowed to equilibrate for a period of 48 hours. Dye was injected at various elevations in the tank close to the front face. Dye slugs were visually monitored, and dye velocities were estimated by measuring the position of the front of the dye pulse in time. A summary of the dye injection locations and slug velocities is given in Table 5.2.

Dye slugs injected both below the water table and within the fully saturated capillary fringe displayed similar flow trajectories and velocities. Instrumentation present in the tank resulted in slight disturbances in the flow direction. Figure 5.8 shows the location of two dye slugs in saturated material (one below and one above the water table) during interaction with tank instrumentation. The lower slug (below the water table) was retarded slightly by the TDR probe. Afterwards, the upper portion of the slug began to migrate upwards (towards the capillary fringe) slightly. This effect was fairly minimal. Slugs in the saturated zone retained the same horizontal flow path for their entire flow path, including the approach to the outlet plate. To better examine the effect of the outlet plate on the flow through the tank, an additional dye slug was injected 0.08 m from the outlet tank at an elevation that represented the mid-point of the tension saturated zone. The path of this slug was slightly impacted by density differences with the water; however, as shown in Figure 5.9, the porous plate was found to have little effect on the outflow from the tank in the saturated zone. Flow remained horizontal as it approached the tank outlet whether below the water table or within the capillary fringe.

Dye injected in the partially saturated zone above the capillary fringe displayed distinctly different flow patterns. Figure 5.10 shows the flow path of a dye pulse injected above the water table, in a zone

where moisture content was approximately 0.3 (85% saturated). The velocity of this pulse was only slightly slower than the velocity below the water table, suggesting that this region is dominated by connected pathways for water flow. The presence of the disconnected air phase in this zone appeared to increase the tortuosity of the system, elongating the slug. The effect of the outlet plate in this region differs from the fully saturated region. A dye slug injected 0.08 m from the outlet plate in the zone of 85% saturation was found to undergo vertical flow as it approached the outlet plate. This trajectory is shown in Figure 5.11. The slug appeared to exit the tank at an elevation approximately 0.03 m lower than the injection point. This behavior was not the result of density effects. It appears as though flow out of the tank only occurs in zones of higher saturation, above 95%. This result was not expected given the high air-entry of the porous metal plate. This vertical flow component does not appear to extend more than 0.1 m into the tank from the outlet; however, this effect and its associated vertical gradients may account for some of the difference observed between inlet and outlet moisture content profiles.

5.4.2 Test 2 (Borden Sand)

A composite plot of all pressure head - saturation profiles collected during test 2 is shown as Figure 5.12. It is apparent that there is an elevation in air-entry pressure. For all drainage observations made below TDR location A, the air-entry point occurred at a pressure heads greater than -0.55 m, significantly higher than the -0.42 m air-entry pressure observed for the gravity drainage experiment. Entrapped air is present at higher elevations in the tank. Due to the higher soil moisture retention of the Borden sand in comparison to the Ottawa sand, relatively few points were observed in the transition zone prior to desaturation of the reservoirs and termination of the experiment. Thus, the nature of the moisture profile through the transition zone cannot be determined.

Figure 5.13 (a-b) shows the pressure head – saturation observations made for individual tensiometer locations during the high gradient (0.17 m/m) drainage cycle. Points not impacted by entrapped air remain close to saturation for the duration of the test. By analyzing the outlet row observations it appears that the air-entry pressure is slightly below -0.60 m. Observations made at TDR location A are slightly impacted by entrapped air. Desaturation at probe A was gradual, and began at pressure heads below -0.4 m. Measurements made through the transition zone at TDR location A appear to follow a scanning curve and provide reasonable agreement with the gravity drainage values.

5.4.3 Test 3 (Borden Sand)

A composite plot of all pressure head - saturation profiles collected during test 3 is shown in Figure 5.14. The second drainage cycle completed at a gradient of 0.17 m/m is considered an example of the effects of hysteresis on drainage from the tank, as the equilibrium time between cycles was short. Results from all drainage cycles show an elevation in air-entry pressure.

Figure 5.15 (a-f) includes pressure - saturation profiles by TDR probe location for each cycle. The higher gradient (0.17 m/m) cycles were completed first and results are shown in Figure 5.15 (a-b) for the primary high gradient drainage cycle. For primary drainage, the saturation profiles at TDR point A are in good agreement with the gravity drainage derived curve. All other TDR locations show a slightly elevated air-entry pressure. Profiles collected at the outlet row show a more elevated air-entry pressure and higher moisture contents in the wetter portions of the transition zone in comparison to the inlet row. These effects are likely the result of the vertical gradients at the outlet plate noted in the dye tracer experiments. No locations displayed evidence of entrapped air in this drainage cycle.

Figure 5.15 (c-d) shows the results for the second high gradient (hysteretic) drainage cycle. Observations made at location A showed approximately 12% entrapped air at both inlet and outlet rows. Observation made at TDR locations B - D showed approximately 4% entrapped air at both inlet and outlet rows. Pressure head – saturation values observed at location A appear to follow a scanning curve and fall on the gravity drainage derived curve at higher pressures. Drawdown during this experiment was not significant enough to initiate drainage at locations B through G, indicating an increase in air entry pressure to at least -0.46 m.

Results from the third drainage cycle, run at a lower gradient, are shown in Figure 5.15 (e-f). Profiles collected at TDR observation locations B through G show an air-entry pressure of approximately -0.52 m, 0.07 m greater than the gravity derived curve. There was no significant difference between inlet and outlet moisture distributions for this cycle. Entrapped air was detected at TDR probe location A. The pressure head – saturation profile for that location showed a very gradual drainage pattern with an air-entry pressure of approximately -0.43 m. The moisture profile appears to follow a scanning curve, and values begin to approximate the gravity drainage curve in the transition zone. The saturation profile generated during this drainage cycle was similar to the profile generated during the higher gradient cycles.

5.6 Discussion

The results of the three drainage tests presented above vary in terms of the amount of entrapped air, the gradient applied, the soil type, and the wetting history. A summary of the most pertinent observations is given in Table 5.3. Although the elevation in air-entry pressure prevented the observation of drainage at many of the TDR locations several important observations can be highlighted. These include the effect of grain size distribution, horizontal gradient magnitude, and degree of air entrapment. The elevation in air entry pressure and the possible causes are also discussed.

The coarse, well-sorted Ottawa sand was not significantly impacted by entrapped air following imbibition. TDR probes detected entrapped air in the poorly sorted Borden sand following slight

dewatering. It appears that poorly sorted material, which is heterogeneous on the pore scale, has a much greater potential to entrap air during re-wetting. This result was expected as imbibition into a heterogeneous pore system will tend to fill smaller pores first, trapping air in the large pore bodies. With a uniform pore size distribution the potential for air entrapment is diminished. This phenomenon was initially recognized in pore scale modeling studies by Lowry and Miller (1995). Saturation profiles for both sands showed an increased air-entry pressure, and outlet plate effects. It appears that the only significant impact of pore scale heterogeneity on drainage and imbibition is the degree of air-entrapment.

Drainage in each cycle was completed under two different horizontal gradient magnitudes. The lower gradient was set based on laboratory apparatus configuration. The higher gradient was set based on a compromise between the need to generate a high gradient, and the ability to initiate drainage in the sand prior to air entry in the outlet plate. Saturation profiles for the Ottawa sand showed no impact of horizontal gradient magnitude. Drainage observations made at location A approximated the laboratory derived drainage curve for both drainage cycles, while observations at all other TDR locations showed an increase in air-entry pressure, and agreement with the gravity drainage values through the transition zone. This drainage pattern was the same for both drainage cycles completed in the Ottawa sand. Saturation profiles during drainage are not impacted by horizontal gradient magnitude. All soils showed a slight difference between moisture profiles observed at the inlet and outlet TDR profiles when higher gradients are applied. This variation indicates that vertical gradients in the region of the outlet plates impacted the pressure head estimations made for the TDR outlet row. It is assumed that flow rates were sufficiently low during the low gradient experiment that significant vertical gradients did not develop.

Although attempts were made to limit entrapped air in all but one of the drainage tests, minor amounts remained present following lengthy equilibration periods. The quantity of entrapped air was a function of elevation, such that greater amounts of entrapped air were present near the top of the tank, and more entrapped air was present at the outlet end of the tank, where larger pressure drops were present. This result confirms the assumption that in a homogeneous aquifer system entrapped air would be most prevalent in the shallow regions of an aquifer, and reduce with depth in the system. Observations made at location A which were impacted by entrapped air show a reduction in air-entry pressure, and drainage follows a scanning loop to reach the gravity drainage derived soil moisture curve. Observations made during the hysteretic drainage cycle show entrapped air at greater depths in the tank. These results suggest that the presence of horizontal gradients does not alter the way in which entrapped air impacts drainage in comparison to drainage under vertical flow conditions only. Observations made at other locations impacted by entrapped air do not show evidence of drainage.

Entrapped air affected not only moisture content distributions during drainage, but also the flow rates through the tank. Outflow rates during the high gradient components of test 3 were compared for the observation points representing a water level at 0.1 m above the bottom of the tank. At that level, the entire tank remained within the saturated zone. During the first drainage cycle, the tank was completely saturated, and the outflow rate for the tank was 7.8 mL/min. During the second drainage cycle, entrapped air was present at TDR locations A through B, and the outflow rate was 5.2 mL/min. This difference represents a 33% drop in outflow as a result of entrapped air in the system. A theoretical difference in flow rate was calculated using the relative hydraulic conductivities calculated using the Brooks and Corey parameters for Borden sand. The tank was divided into 7 horizontal layers corresponding to each TDR location. Each layer was assigned a relative hydraulic conductivity related to the average saturation at both TDR locations for the given layer. The effective horizontal conductivity was determined using the weighted arithmetic mean for the system. This method resulted in a potential decrease in outflow rate of 16%. These rates are comparable, suggesting that entrapped air effects on horizontal flow rates in homogeneous systems can be predicted with some accuracy using parameters derived in vertical gravity drainage experiments. Further investigation is necessary to determine the degree to which the porous plates may affect outflow rates, and the cause of the discrepancy.

Packing procedures were consistent for each drainage cycle completed in an attempt to eliminate any influence in comparison of the tests within the same material. However, the resulting bulk density of the sand used in test 3 was approximately 2% higher than the bulk density of the sand used for test 2. Although this difference resulted in saturated moisture contents that were approximately 5% less for test 3, it did not appear to significantly affect the shape of the soil moisture curves for the experiments. For both packing bulk densities similar air-entry pressures were observed, with the increase in air-entry pressure slightly greater in test 2. It is clear that this small change in bulk density has little effect on drainage for the sand. These results are similar to the observations made by Assouline (2006b) using unconsolidated sand, and confirm the conclusions made in Chapter 2, that compaction during pumping would have little to no effect on the water retention of Borden sand.

Vertical flow in the tank during steady-state conditions was apparent during the dye tracer experiments. During steady-state flow conditions, dye slugs injected in the drier (less than 85% saturated) region of the tank flowed vertically in their approach to the outlet plate. These slugs only entered the outlet tank from regions in which saturation was greater than 95%. Although these effects may delay drainage from the tank, with the potential to cause an increase in air-entry pressure, the evidence of this effect is minor. During the higher gradient experiments, there was a slight shift to more negative pressure heads for all saturation values at the outlet in comparison to the inlet for the all tests.

This difference appears to be less than 0.03 m for all high gradient drainage cycles. If vertical flow at the outlet plate were to significantly impede drainage from the tank, it would be expected that this build-up of excess water would lead to increased pressures detectable in the tensiometer network in the tank. As no pressure build-up was observed and the pressure shift is minimal, the outlet boundary effects do not appear to have a significant impact on drainage from the tank.

While observations made at TDR location A follow a predictable pressure-saturation relationship for each sand and each horizontal gradient tested, observations from TDR locations at greater depths in the tank show an elevation in air-entry pressure in comparison to gravity drainage derived values. As an initial investigation of these results, the impacts of drawdown rate and flow disruption due to the instrumentation in the tank were considered. While all measurements discussed previously were taken at steady-state (evaluated based on flow rate and pressure head changes), there is the potential that some measurements were made during transient flow conditions, impacting results. The dye tracer test provided some evidence of flow disruption around the TDR rods. Horizontal flow around instrumentation in the tank may increase saturation in the region above the instrumentation. Two additional drainage experiments were conducted to evaluate these effects.

Following a 48 hours equilibration period, flow was established through the tank with a gradient of 0.17 m/m. Mean water level in the tank was initially 0.1 m below the top of the tank. After a set of background measurements, the water level in the tank was lowered such that the mean water level in the tank was approximately 0.6 m below the top of the tank. Transient changes in saturation and pressure head were monitored to evaluate the impact of drawdown rate on drainage from the tank. Following a 72 hour observation period, the tank was re-saturated and left to equilibrate for a 48 hour period prior to the second experiment. For the second drainage experiment, the constant head overflow was disconnected from the tank such that both plates were connected to drip points. Drip points for both plates were set at 0.1 m below the top of the tank, and observations were taken following the cessation of outflow from the tank. Following the collection of background observations the drip points were lowered to an elevation of -0.65 m below the top of the tank. Outflow rates, pressure heads, and TDR measurements were taken throughout the drainage experiment to determine the impact of horizontal flow on experimental results. The experiment was considered to be at steady state when outflow from the tank stopped.

The results from single step drop under a horizontal gradient are shown in Figure 5.16 (a-b), for each TDR location monitored. Pressure heads at each monitoring point were calculated based on the vertical gradients observed at the tensiometers. Transient horizontal gradients could not be monitored, and were assumed to be equal to the applied gradient for all times during the test. Pressure heads

reached steady state within 4 hours. Moisture contents at points initially below saturation (due to entrapped air upon rewetting) drained as expected, following a scanning curve to reach the gravity drainage curve. Observations made at TDR locations B and C were also found to dewater, and are in reasonable agreement with the gravity drainage curve. Drainage was not observed for Borden sand at TDR locations B and C prior to this drainage cycle. Observations made at TDR locations D through G show an elevated air-entry pressure. The water levels and gradient in the tank were maintained for a period of 72 hours following the initial drop. During this period, no observations with elevated saturations were found to drain. This result confirms the assumption that overly short observation intervals were not the cause of the increase in air-entry pressure observed during the previous experiments.

Pressure head – saturation observations made during the no horizontal gradient experiment are shown in Figure 5.17 (a-b) for the inlet and outlet rows respectively. Observations made at locations A through C show the presence of entrapped air. These locations drain following a scanning curve, and are in reasonable agreement with the gravity drainage derived curve. Observations made at the remaining locations show an elevation in air-entry pressure. Results are similar to the single step drainage experiment. It appears that flow around the TDR rods due to horizontal flow does not play role in the excess moisture retention during drainage. A large single step drop in water level appears to more readily initiate drainage from the tank. This effect may be related to air phase flow effects, and warrants further investigation.

5.7 Conclusions

This study presents the results of drainage tests completed under a primarily horizontal flow regime in a laboratory scale tank; the main observations were made under steady-state conditions. Pressure head – saturation profiles observed during drainage were not dependant on the magnitude of the horizontal gradient applied. Entrapped air did not impact drainage from the Ottawa sand, due to its well sorted grain size distribution. The impact of entrapped air was more significant during drainage from the poorly sorted, medium sand collected from CFB Borden. Entrapped air acted to reduce the air-entry pressure for the moisture profile, and generated scanning curves that sat below the main drainage curve generated using gravity drainage methods. Pore scale heterogeneity appears to impact only the degree of air-entrapment. Small changes in bulk density due to packing differences did not affect the shape of the saturation profile. Observations made at TDR location A (the top most TDR location) were in agreement with the gravity drainage derived curve for all drainage cycles in both sands. All other TDR observations showed an increase in air-entry pressure during multi-step lowering of the water table. Subsequent tests in which the water level in the tank was lowered in a single step eliminated the observation of increased air-entry pressure at TDR locations B and C. Horizontal flow around tank

instrumentation and transient effects are unlikely to have caused the observed increases in air-entry pressure. The impact of drawdown rate on the presence of an elevated air-entry pressure warrants a more detailed investigation.

5.8 Tables and Figures

Table 5. 1: Test Summaries

Test Number	High Gradient Value	Low Gradient Value	Drop Criteria	Time between drainage Experiments
1	0.08	0.03	Outflow and pressure reached steady state	48 Hours
2	0.17	0.02	Outflow and pressure breached steady state	48 Hours
3	0.17	0.03	8 Hours between drops	8 and 48 Hours

Table 5. 2: Summary of Dye Tracer Experiments

Location	Velocity (m/s) (Front of Pulse)
Directly Above the Capillary Fringe	7.5×10^{-6} [a]
Lower Half of Capillary Fringe	9.0×10^{-6}
Directly Below the Water Table	8.5×10^{-6}

[a] Note: there was significant elongation of the pulse

Table 5. 3: Summary of Experimental Results

Test 1	Air-Entry of approximately -0.2 m for both cycles (-0.10 for gravity drainage) Observations made at TDR locations A followed curve that agreed with the gravity drainage curve. Extension collapses through transition zone Effect of vertical gradients at outlet visible for higher gradient experiment Gradient magnitude has no effect on saturation profile
Test 2	Air-Entry of over -0.55 m (-0.43 for gravity drainage) Outlet row shows a slight extension in moisture profile in comparison to inlet for higher gradient experiment, likely a plate effect. Observations made at TDR locations A followed a scanning curve that agreed with the gravity drainage curve.
Test 3	Air-Entry of -0.52 m for the low gradient and high gradients drainage cycles. Observations made at TDR locations A followed a scanning curve that agreed with the gravity drainage curve. Outlet effects observed for high gradient experiments

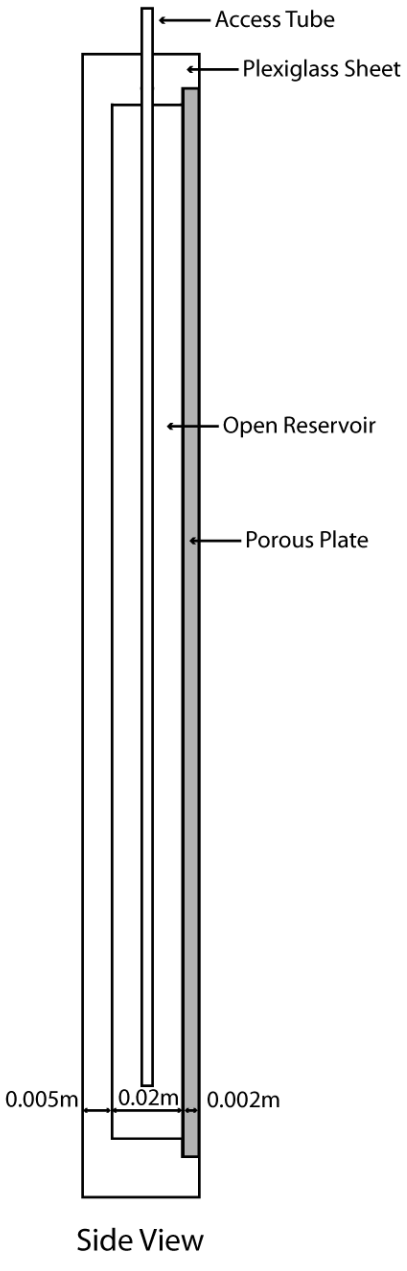

Figure 5.1. Side view of tank reservoir

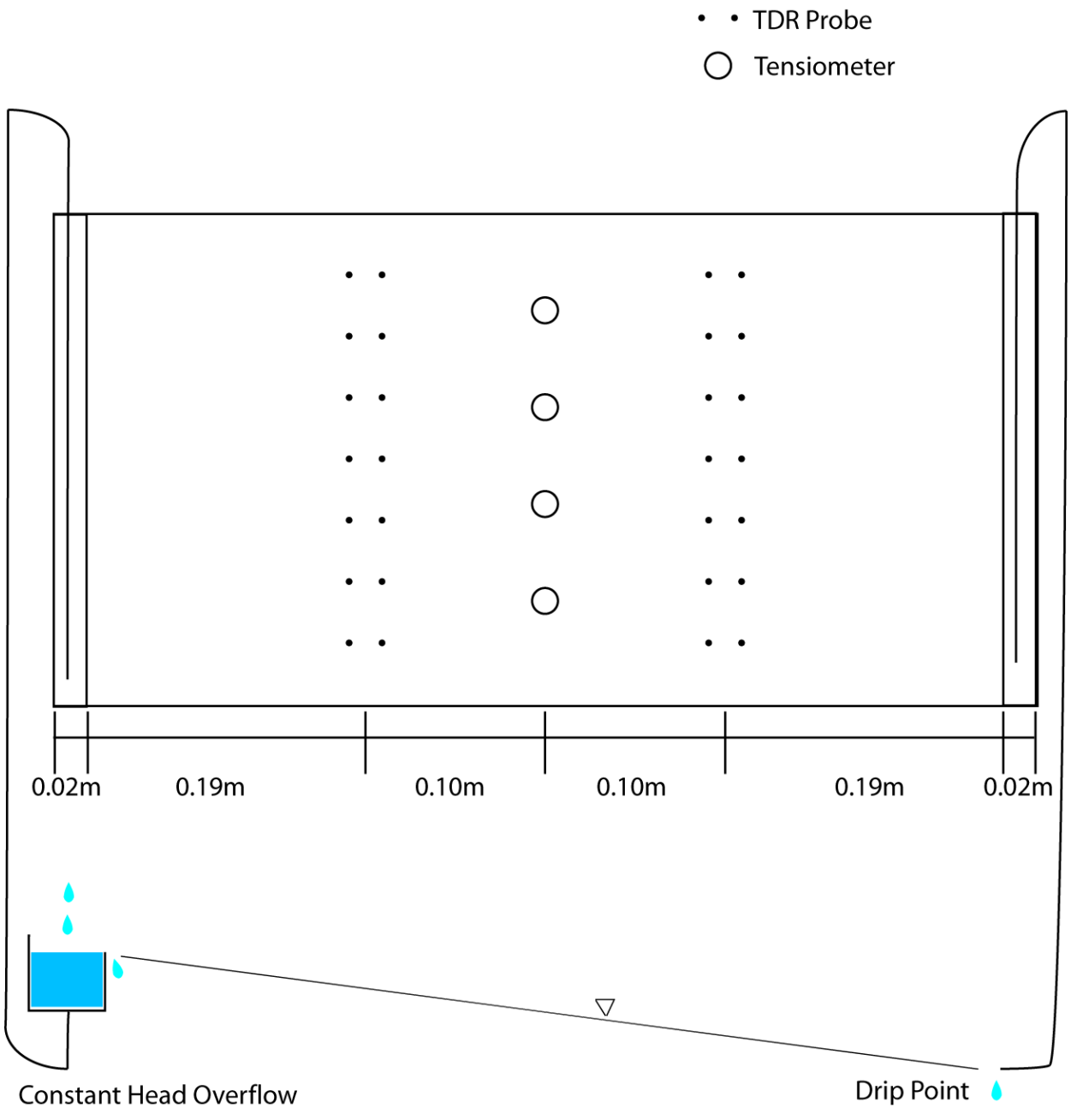

Figure 5.2. Schematic of tank instrumentation

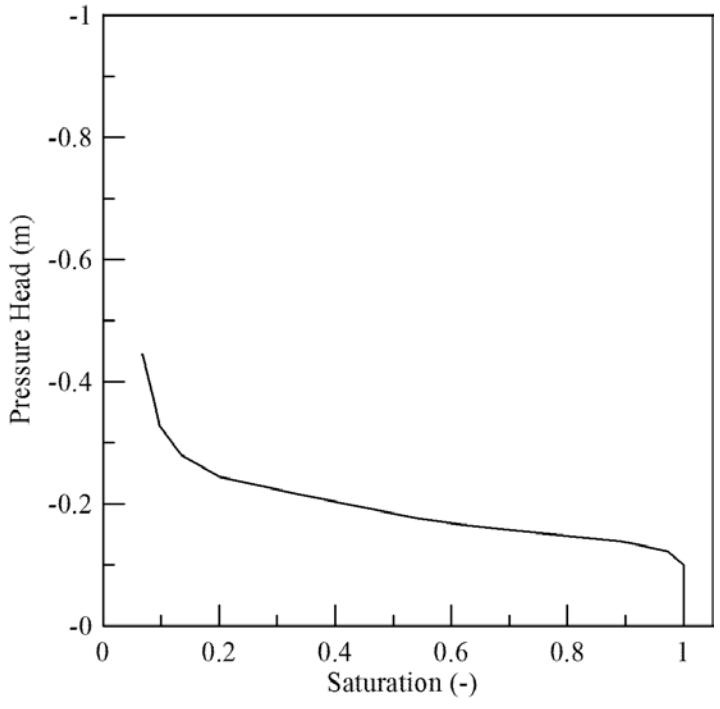

Figure 5.3. Pressure Head - Saturation Relationship for Ottawa Sand (F35)

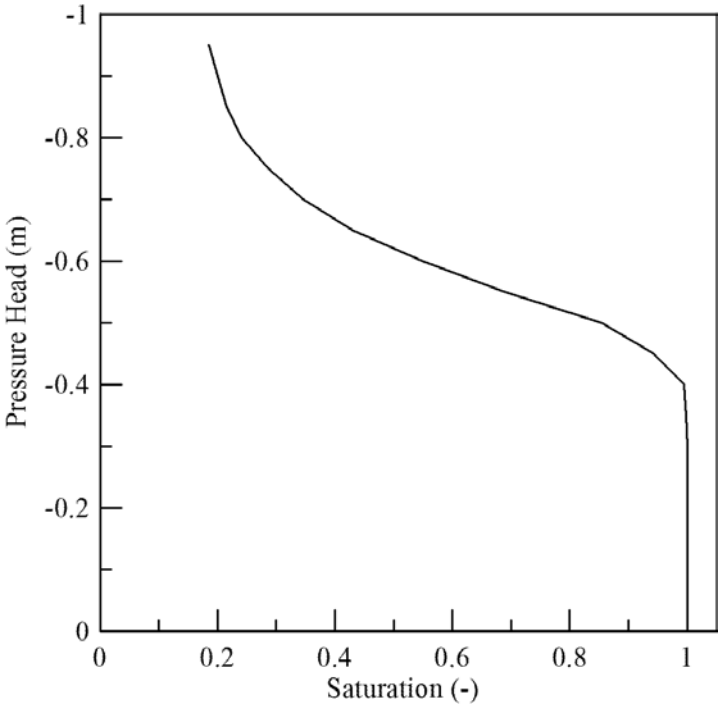

Figure 5.4. Pressure Head – Saturation Relationship for Borden Sand

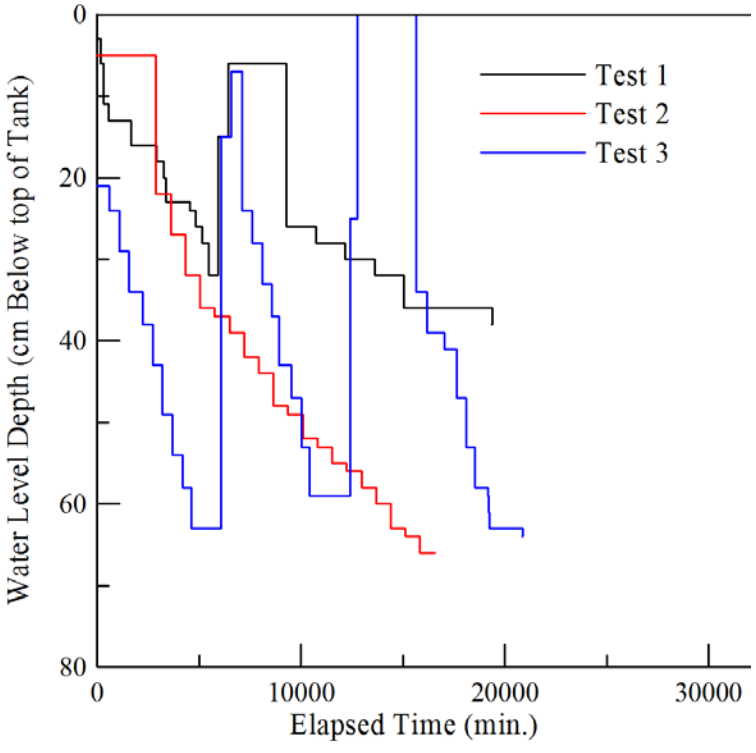

Figure 5.5. Tank Mean Water level during experimental cycles

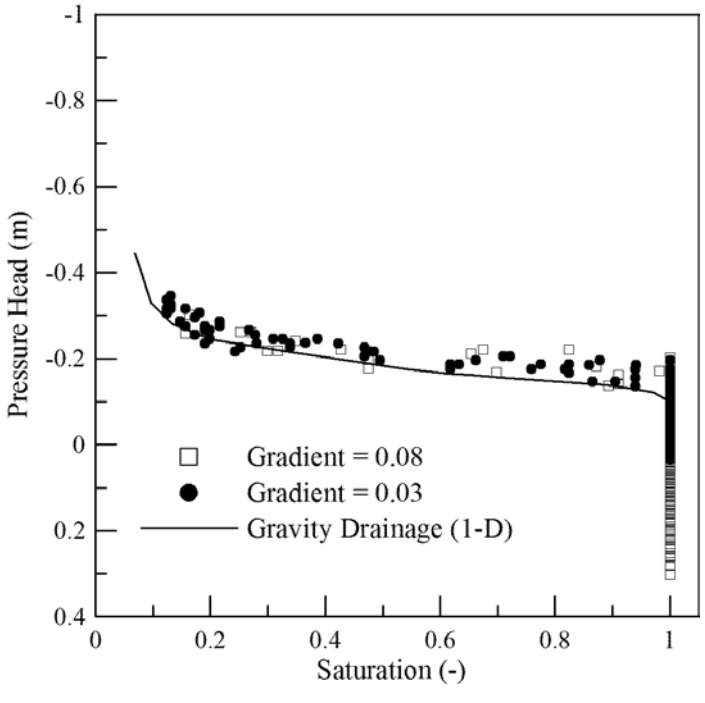

Figure 5.6. Composite plot of all Pressure head – Saturation profiles for Test 1

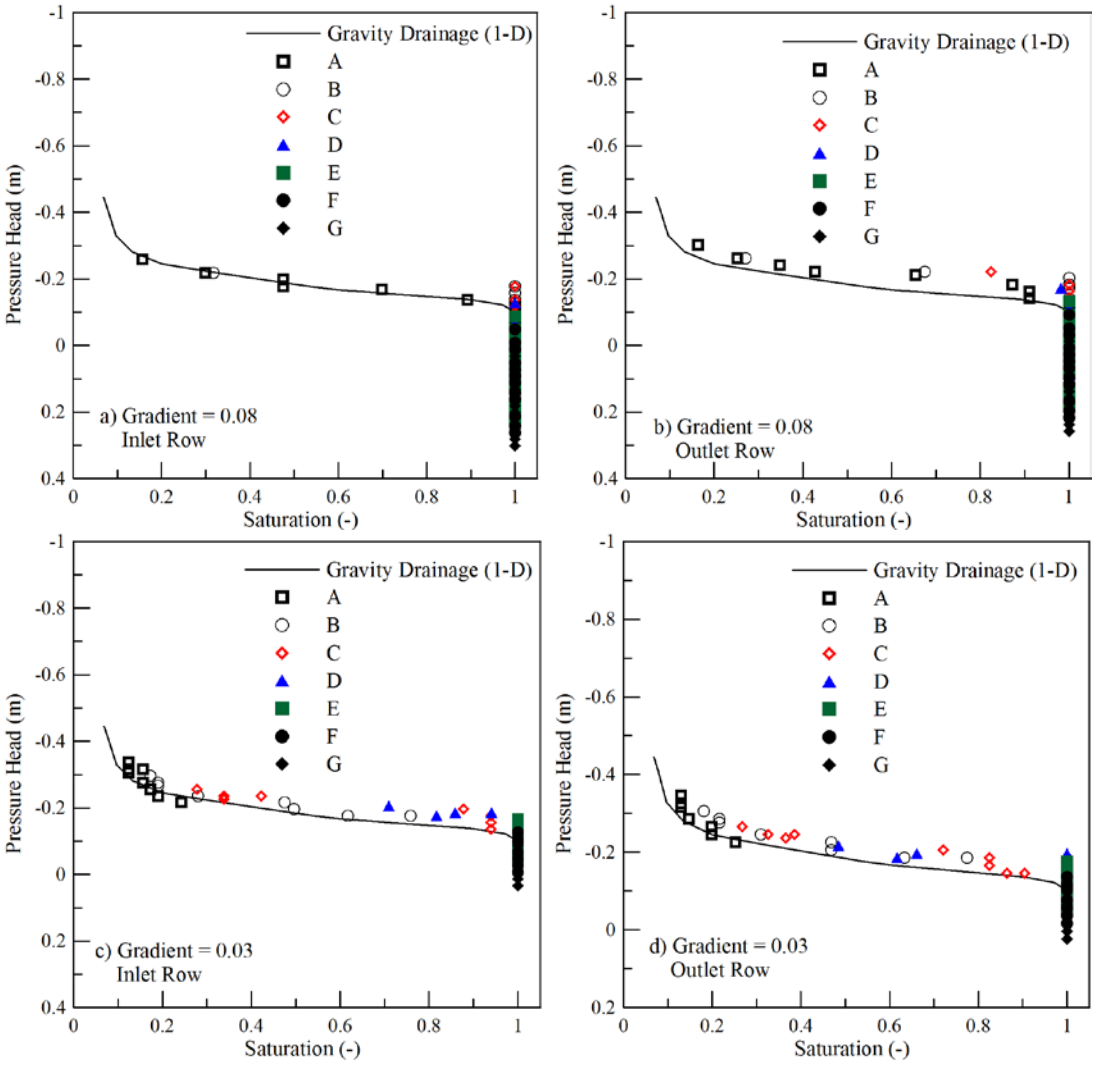

Figure 5.7. Pressure Head – Saturation profiles by locations for Test 1 (a. Inlet Row (high), b. Outlet Row (high), c. Inlet Row (low), d. Outlet Row (low))

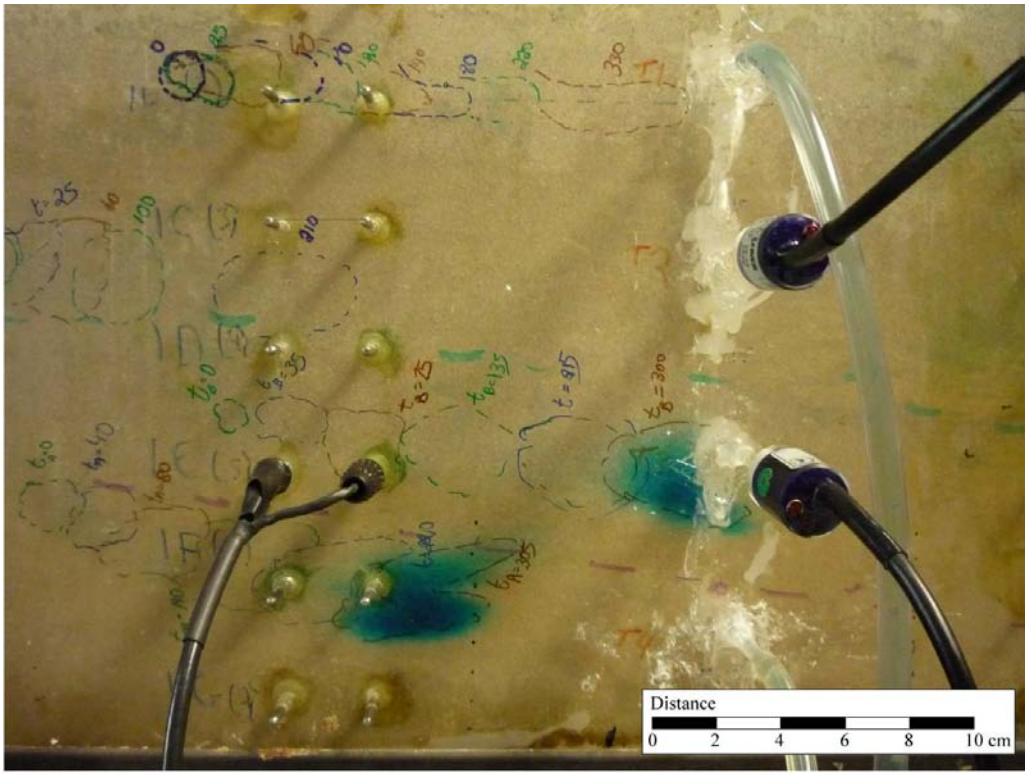

Figure 5.8. Saturated zone dye pulse locations.

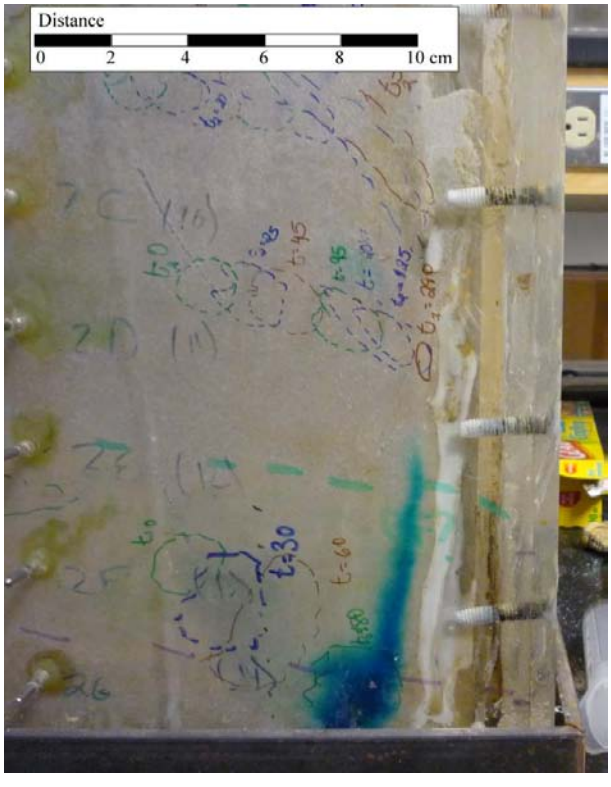

Figure 5.9. Saturated dye pulse flow near tank outlet.

Figure 5.10. Partially saturated dye pulse flow path.

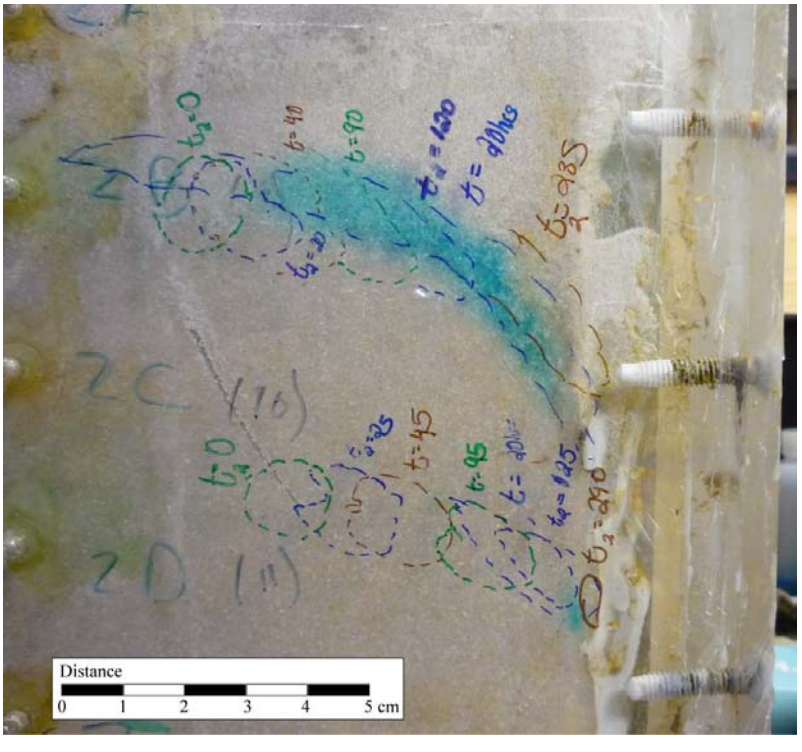

Figure 5.11. Partially saturated flow path towards tank outlet.

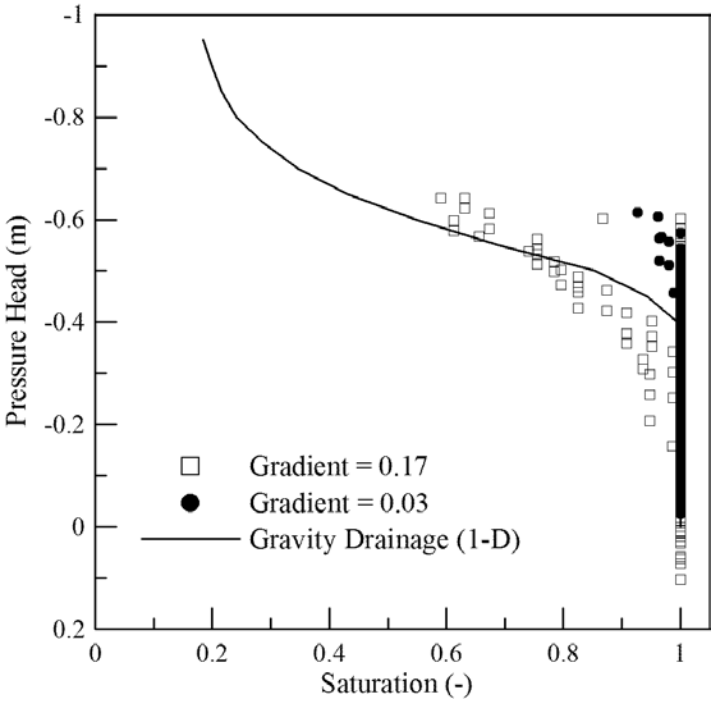

Figure 5.12. Composite plot of all Pressure head – Moisture Content profiles for Test 2

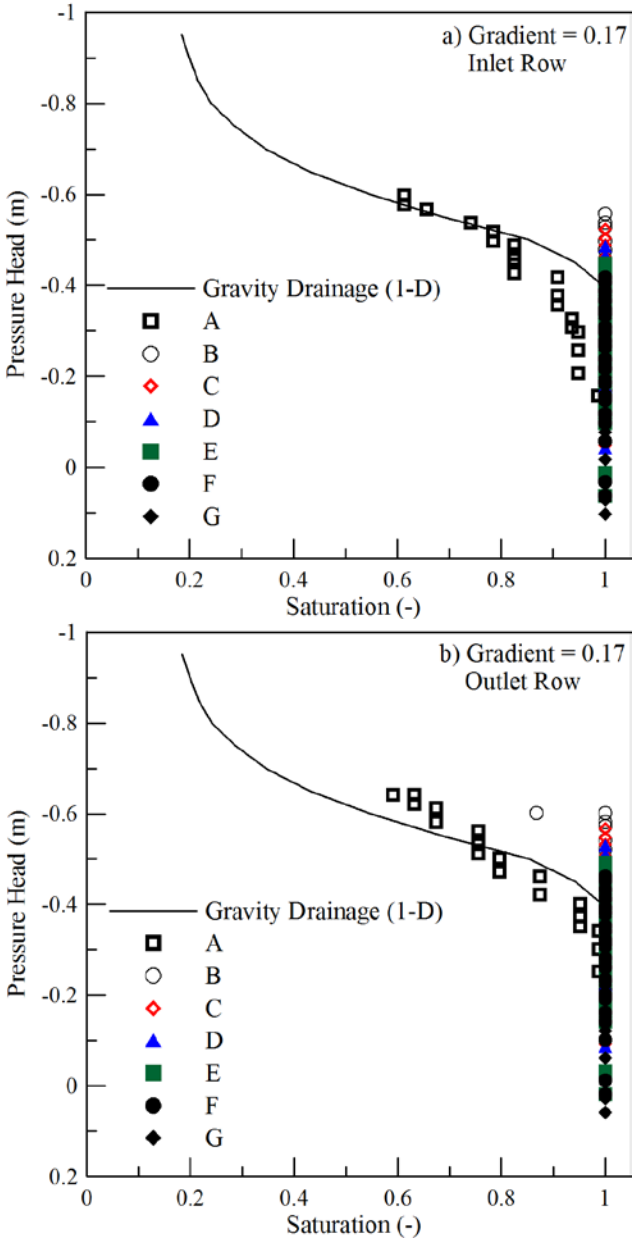

Figure 5.13. Pressure Head – Saturation profiles by locations for Test 2(a. Inlet Row (high), b. Outlet Row (high))

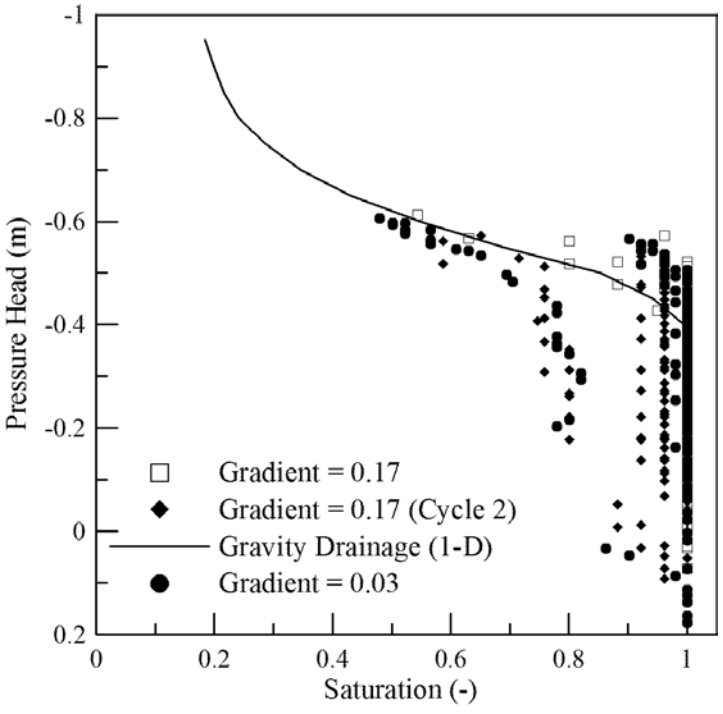

Figure 5.14. Composite plot of all Pressure head – Moisture Content profiles for Test 3

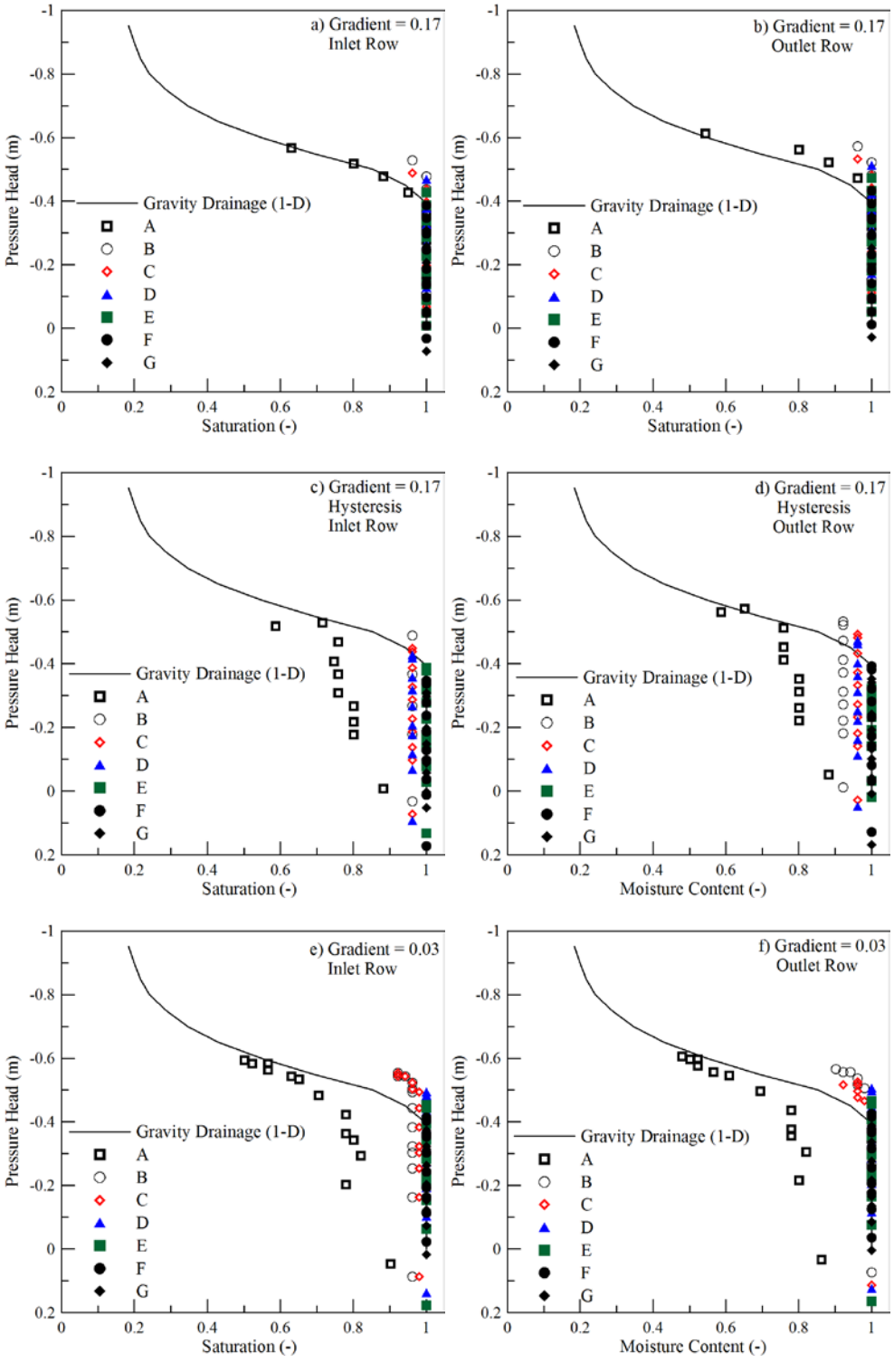

Figure 5.15. Pressure Head – Saturation profiles by locations for Test 3 (a. Inlet Row (high), b. Outlet Row (high), c. Inlet Row (high, hysteretic, d. Outlet Row (high, hysteretic), e. Inlet Row (low), f. Outlet Row (low),)

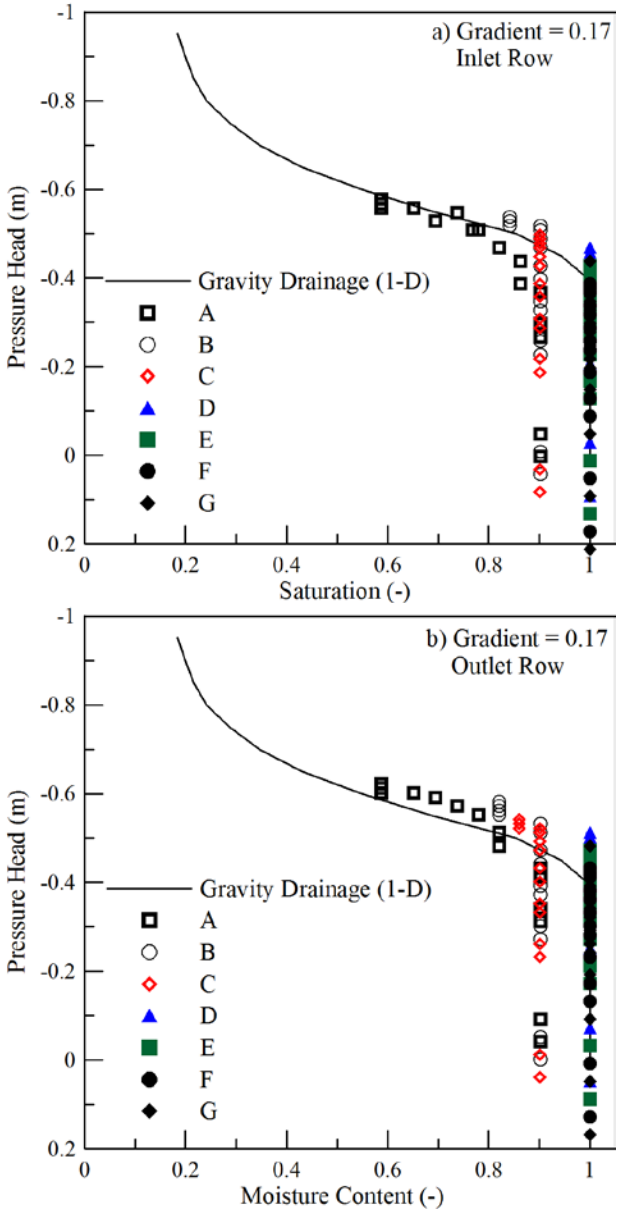

Figure 5.16. Pressure Head – Saturation profiles by locations for transient drainage under horizontal flow (a. Inlet Row, b. Outlet Row)

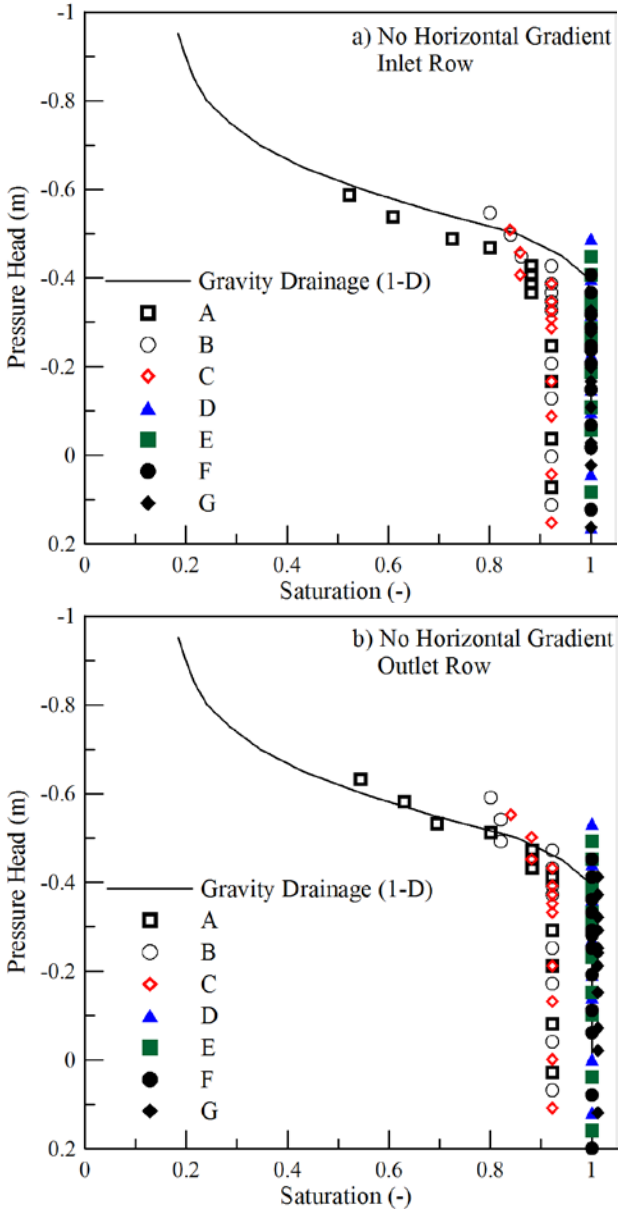

Figure 5.17. Pressure Head – Saturation profiles by locations for transient vertical drainage (a. Inlet Row, b. Outlet Row)

Chapter 6

Summary and Recommendations

6.1 Summary of Accomplishments

The main goal of this research work was to provide an increased understanding of the impact of various factors (including variably saturated flow, heterogeneity, and hysteresis) on drainage induced by pumping tests in unconfined aquifers. This investigation was motivated by the results of the test completed by Bevan et al. (2005). To accomplish the goal, several numerical models incorporating variably saturated flow were first tested for their ability to match the pumping test observations of Bevan et al. (2005). The effect of a mild degree of heterogeneity on pumping tests results was then evaluated using a stochastic numerical simulation technique. A 24-hour pumping test completed at CFB Borden provided additional evidence regarding the impact of hysteresis on pumping test results during a wet season. A flow-through tank was used to investigate the nature of drainage under a predominately horizontal flow regime, taking into account the effects of grain size distribution and horizontal gradient magnitude. Effects of entrapped air and hysteresis were also observed. Results from each study were compared to the moisture content observations made by Bevan et al. (2005). No single process investigated herein appears to have caused the persistent capillary fringe extension observed during that test. It is clear that a complex relationship exists between the effects of these processes, drainage from above the water table, and the cumulative impact on hydraulic head drawdown during pumping.

Specific contributions of this study are described below.

- Variably saturated groundwater flow representations used in a suite of modern numerical codes are able to properly represent the formation of vertical gradients during early times in unconfined pumping tests, and the hydraulic head drawdown typical of unconfined pumping tests. The late time capillary fringe extension observed by Bevan et al. (2005) could not be predicted by any variably saturated numerical simulation.

- Chapter 3 presented the first fully three-dimensional numerical representation of the impact of a mild degree of aquifer heterogeneity on unconfined pumping response. Based on the results of that study it appears that a mild degree of hydraulic conductivity heterogeneity can result in the formation of perched lenses of high moisture, reducing the degree of drainage during pumping. The development of these lenses occurred as a function of the heterogeneity distribution, and they tended to collapse with time. The

amount of drawdown at a given location was less influential to the development of lenses. The ensemble impact on capillary fringe thickness during pumping was minimal.

- A mild degree of heterogeneity can impact hydraulic head drawdown in the intermediate and late phase of an unconfined pumping test. Monte Carlo simulation results showed a reduction in drawdown at intermediate times. This result provided a closer match to the field observations of Bevan et al. (2005) in comparison to a homogeneous approximation of the system. Any horizontally layered heterogeneity in an aquifer system will cause a time delay in drainage above a falling water table, reducing drawdown rates at intermediate and late times as perched water drains.

- The results of the field test discussed in Chapter 4 are the first to show the impact of hysteresis in soil moisture on drainage during pumping in unconfined aquifers at the field scale. Hysteretic effects resulted in a lack of drawdown of the top of the saturated zone during pumping; yet, an inflection point remained present in the time-drawdown curve. This inflection point was coincident with the peak in vertical gradients observed. Without prior knowledge of the occurrence of hysteresis during pumping, test results may be improperly interpreted.

- Vertical gradients within the capillary fringe observed during the field experiment were of similar magnitude to those below the water table. Vertical gradients peaked during early times in pumping tests, and the peak occurs at the same time as the inflection point in the time-drawdown curve. Vertical gradients within the capillary fringe remain low following the peak in vertical gradient magnitudes.

- In homogeneous sands, horizontal gradient magnitude does not impact the water retention curve generated during drainage in the presence of horizontal flow.

- Pore scale heterogeneity related to the grain size distribution of a soil will impact the degree of air-entrapment during imbibition under primarily horizontal flow. Well sorted sands will not be significantly impacted by entrapped air.

- In predominately horizontal flow regimes in homogeneous systems the presence of entrapped air will act to reduce the thickness of the tension saturated zone. This effect is similar to what would be expected in a vertical flow regime.

- Variably saturated flow dynamics resulting from heterogeneity and hysteresis both impact the time-drawdown curve at intermediate and late periods during pumping. Calibration of

unsaturated parameters to drawdown without prior knowledge of these processes will likely produce unrepresentative results.

- All processes investigated during this study result in drainage from above the water table that is non-instantaneous. This result suggests that delayed yield type analytical solutions are a more accurate representation of the physical processes occurring at the field scale during pumping tests in comparison to instantaneous yield type solutions.

- While no single process investigated was able to account for the capillary fringe extension observed by Bevan et al. (2005) it is clear from the results of this research that drainage from above the water table during pumping is a complex process, and an extension of the capillary fringe is the result of a combination of these processes. Both entrapped air and hysteresis will act to increase the effective heterogeneity in the system, impeding vertical drainage in the horizontally stratified Borden aquifer.

6.2 Implications for the Conceptual Model of the Unconfined Response to Pumping

This research has provided evidence of the relationship between flow processes above the water table and the hydraulic head drawdown observed below the water table during pumping tests. Pumping tests in unconfined aquifers are used to determine field scale values for saturated hydraulic conductivity, specific storage and specific yield. Based on the results of this study it appears that saturated hydraulic conductivity and specific storage of an unconfined aquifer can be reliably estimated using the early portion of the time drawdown curve. As this study was not able to provide a conceptual model of the vadose zone response to pumping observed by Bevan et al. (2005) it appears that the most appropriate method for determining the specific yield of an aquifer may be through laboratory determinations of drainable porosity. The use of this method of specific yield determination would reduce the pumping time required for tests in unconfined aquifers as only early time data would be required to derive specific storage and saturated hydraulic conductivity. This section will provide a summary of the impact of hydraulic conductivity heterogeneity and hysteresis on drainage and drawdown. The impact of air entrapment will be briefly discussed. The potential implications of these findings on pumping test analysis will be addressed.

The Borden aquifer, used as a benchmark in this study, has a very minor degree of hydraulic conductivity heterogeneity in comparison to most natural aquifer systems; yet numerical simulation results show that even minor heterogeneity can impact pumping test results. Heterogeneity in hydraulic conductivity forms barriers to downward drainage during pumping. While these barriers do not persist indefinitely, they do impede drainage above a falling water table. The formation of barriers to drainage

is not widespread in sandy aquifers, such as Borden, and tends to impact drier regions of the aquifer much more significantly, such that only small volumes of water are impeded in drainage. The impact of heterogeneity on drawdown is most significant through the intermediate and late stages of pumping, as water slowly drains through or around these barriers, reducing drawdown in comparison to a homogeneous and anisotropic conceptual model. Specific yield will be underestimated if late time drawdown values are influenced by continued drainage from perched lenses. Analytical solutions using non-instantaneous yield assumptions are likely better suited to pumping tests in which even a mild degree of heterogeneity is present.

Hysteresis is a process that is likely to occur in most pumping tests in the field. The test run by Bevan et al. (2005) may be an exception, given the gradual seasonal drawdown in the aquifer prior to the test. During wetter periods, or following other pumping activities, transition of the moisture profile from imbibition to drainage conditions will affect the amount and timing of drainage from above the water table. Field results show that the elevation of the top of the saturated zone will remain static until the drainage air-entry pressure is reached. This delay in drainage from the tension saturated zone does not appear to be significant enough to eliminate the inflection point in the time drawdown curve. However, if pumping rates are low, intermediate and late phases of pumping may be reached prior to significant drawdown of the top of the capillary fringe (as observed in Chapter 4). This effect changed the shape of the time drawdown curve, causing drawdown rates to remain slightly elevated through the intermediate phase of the test. In low drawdown pumping tests, hysteresis will significantly impact the shape of the time- drawdown curve following the inflection point. While drawdown observed during the test run as a component of this research did not reach the air-entry pressure, it is expected that in most pumping tests this would occur prior to the inflection point for observation points proximal to the well. At observation locations at greater radial distances from the pumping well, hysteresis may impact intermediate and late time date, and should be considered in analysis at those locations. Overall, it is likely that hysteresis will impact drainage during pumping, and should be considered when analyzing hydraulic head data from tests which have followed previous pumping activity or are completed during wet conditions.

Entrapped air is likely to play a role in drainage processes in any natural aquifer system. In a homogeneous sand tank that was allowed to equilibrate for 2 days, a small amount of entrapped air was found to significantly affect the shape of the drainage moisture profile. The effect will always result in lower water contents than would be expected based on a fully saturated drainage curve. In a more heterogeneous natural system, such as the Borden aquifer, air entrapped in coarser lenses may act to impede downward flow of water. While the heterogeneous conceptual model did not account for entrapped air, it did show that while low conductivity lenses may impede downward flow, they do not

eliminate it, and perched water will drain as pumping progresses. Cleary this process would not be able to generate a persistent extension of the tension saturated zone as observed by Bevan et al. (2005). The presence of entrapped air, and the associated enhancement of heterogeneity, promotes a conceptual model of pumping response in which slow drainage from above the water table may contribute to recharge to the saturated zone for long periods during pumping in unconfined aquifers.

While no single process tested herein was capable of accounting for the capillary fringe extension observed by Bevan et al. (2005), the investigation of each process has provided valuable insight into the physical processes effecting drainage from the vadose zone during pumping. It is clear that drainage from above the water table during pumping is a complex and time delayed process. While vertical gradients, hysteresis, entrapped air and heterogeneity all act at different times during pumping, and vary in their magnitude of impact on drainage and drawdown, they are all processes which slow the drainage from above a falling water table. While the early portion of the time drawdown curve for unconfined aquifers is accounted for by the vertical gradient effect introduced in the Nwankwor et al. (1992) conceptual model and simulated by Akindunni et al. (1992), the influence of variably saturated flow processes on the intermediate and late portions of the time-drawdown curve warrant further consideration. These effects have the potential to alter the estimates of specific yield generated by analytical analysis of the response curve. Clearly the assertion made by Neuman (1988) that specific yield is a constant that is adequately represented by the low values predicted by analytical analysis, is not physically representative of the true dynamics of the system. Specific yield in the context of a pumping test is a transient parameter. The volume of water released will drain gradually over time as a function of drawdown rate, heterogeneity, and saturation history. The conceptual model of aquifer drainage presented by Neuman (1975) is accurate in its mathematical representation of the theory presented, but the assumption of instantaneous yield does not represent field conditions during pumping. The impact of this model on estimates of saturated flow parameters is negligible; however it is clear that this physical model is not suitable for estimation of specific yield in most natural aquifer systems.

6.3 Recommendations for Future Work

This research has provided some new insights into the processes affecting drainage from above the water table during pumping tests in unconfined aquifers. However, a conceptual model capable of accounting for the extension observed by Bevan et al. (2005) has not been found. Several components of this study warrant further investigation, these components include:

1. Determination of the occurrence and persistence of perched zones

While the field test presented in Chapter 4 was originally intended to include the verification of the formation of perched zones indicated by the heterogeneous modeling in Chapter 3, this was not achieved. Due to the hysteresis of the moisture profile, drawdown was insufficient for the formation of perched water, and minimal drainage was observed at the TDR profile. Formation of perched zones has been observed during infiltration experiments in unsaturated portions of the Borden aquifer (Personal Discussion with David L. Rudolph), but it is of interest to determine whether the lenses will form during drainage from saturated portions of the aquifer, and if the lenses are more or less prevalent than predicted by the heterogeneous model. As a component of this work, it would be of interest to install additional tensiometers in lower moisture content regions of the aquifer to monitor for the presence of the large vertical gradient magnitudes that were predicted by the numerical simulations discussed in Chapter 2.

2. Investigation of relative flux contributions to the well

The potential for horizontal flux through the capillary fringe to be greater than the vertical flux to below the water table and into the well screen may provide a component of the capillary fringe extension observed by Bevan et al. (2005). It is expected that any mounding at the well would result in an associated increase in pressures, and that any variably saturated numerical model would exhibit the effect. However, the processes near the well become highly non-linear, and are more difficult to observe and simulate. A more focused field and numerical investigation of these effects within 2 m radius of the pumping well would be of interest.

An additional component of the flux to the well was introduced during the field experiment discussed in Chapter 4. While an inflection point was observed in the time-drawdown curve, no drainage associated with a falling water table was initiated due to hysteresis. Obviously there is some contribution of flux to the well occurring that cannot be accounted for by vertical drainage from within the saturated zone monitored. This component could be accounted for by elastic storage effects or horizontal flow. The monitoring network was not sufficiently extensive to determine horizontal fluxes to the well, but a test in which a reasonable estimate of the bounds of the horizontal flux contribution may help to determine the source of this additional recharge to the well.

3. Additional heterogeneous simulations

The heterogeneous simulation presented in Chapter 3 was sophisticated, and did form a physically realistic conceptual model of the Borden aquifer; however, the simulation remained incomplete. The scaling relationship presented by Keuper and Frind (1991) allowed only the air-entry pressure to vary, such that all saturation relative permeability relationships took the same form. Additionally, while there is a reasonable physical rationale to link air-entry to saturated conductivity, it is a simplification of

more complex pore connection relationships. The perturbation method suggested by Jacobs and Gelhar (2005) may help to increase the effective saturation dependant anisotropy of the system, and may provide improved agreement with the results of Bevan et al. (2005)

While the results of this study clearly show that no single process tested could result in a significant capillary extension (that is both persistent in time, and drawdown dependant), no interaction of these processes was investigated. Entrapped air can increase the effective heterogeneity of a system, as can hysteresis. Air phase flow can also act to limit drainage in heterogeneous environments due to the formation of air-entry barriers. The numerical simulation of a heterogeneous conceptual model using a multiphase flow code would provide the most accurate simulation of pumping in the Borden aquifer.

4. Prediction of effects for other natural aquifer systems

The Borden aquifer is relatively homogeneous on the scale of a pumping test. Most natural aquifer systems, including those used for benchmark tests such as the Cape Cod aquifer, are considerably more heterogeneous. Given that that inclusion of heterogeneity in pumping test simulations of the Borden aquifer had some effect on the time drawdown curve, impact on other systems may help to better understand the physical basis for some of the assumptions made in analytical analysis of these tests. Analysis of the Cape Cod pumping test for unsaturated parameter estimation by Moench (2003) yielded estimates more representative of fine grained materials. Numerical simulation of the Cape Cod test using a heterogeneous conceptual model may help to determine to what extent perched water impacted parameter estimates.

5. Tank Experiments

Tank experiments were terminated prior to a complete investigation of the impact of entrapped air and gradient magnitudes on drainage, due to the observed increase in air-entry pressure. While some of the results can be extrapolated to field scale tests, it has not yet been determined how the effects would be altered in a horizontally layered heterogeneous medium. Although it may be difficult to replicate the effects of field scale heterogeneity in the lab, horizontally elongated sand layers may provide an analog for the system, and help to better understand the most important aspects of the drainage process. Given that moisture content and vertical gradients will be a function of the distribution of heterogeneities, the monitoring network for any heterogeneous testing should be expanded significantly. Also, as there is greater potential for air phase mobility to impact drainage in a heterogeneous system, monitoring of the air phase pressures would be beneficial.

6. Recovery Analysis

The pumping test conducted as a component of this study, as well as the test conducted by Bevan et al. (2005) included monitoring of the recovery of the aquifer following pumping. While it has been suggested by Neuman (1975) that recovery of hydraulic head in unconfined aquifers should follow the inverse path of the drawdown process, the assumption has not been verified. The recovery data from these tests has not yet been analyzed, yet it would be a useful step in verification of the methods used to incorporate recovery data into aquifer response analysis.

7. Quantification of the timing and magnitude of the effects of variably saturated flow processes

Each of the process investigated in this study was found to delay drainage above a falling water table during pumping. The magnitude and the timing of that delay is a function of factors such as the degree of heterogeneity, drawdown rate, and moisture conditions in the aquifer prior to pumping. Quantification of both the magnitude and duration of the impact of these processes in response to a variety of aquifer conditions would help to better determine the appropriate conceptual model to use during pumping test analysis. Recently Mao et al. (In Press) used a numerical simulation to estimate changes in storage at various locations in an aquifer to quantify the relative magnitude and duration of contributions from elastic storage and gravity drainage during pumping. A similar analysis including heterogeneity, hysteresis and entrapped air would help to more accurately characterize the response to pumping in unconfined aquifers.

8. Application of study results to natural drainage phenomenon

The processes considered in this study have the potential to impact many natural processes. An extended capillary fringe would provide a thicker saturated zone through which to transmit water, increase hydraulic head response to rainfall in shallow water table conditions, and reduce the volume derived from drainage. It is of interest to determine which natural systems are most likely to be impacted by these conditions.

References

Akindunni, F.F., 1987. Effect of the capillary fringe on unconfined aquifer response to pumping: Numerical simulations, Ph.D. thesis, Univ. of Waterloo, Waterloo, Ontario, Canada.

Akindunni F.F., and R.W. Gillham, 1992. Unsaturated and Saturated flow in response to pumping of an unconfined aquifer: Numerical investigation of delayed drainage. Ground Water 30, 873-884.

Assouline, S., 2001. A model of soil relative hydraulic conductivity based on water retention characteristics. Water Resources Research. 37, 265-27.

Assouline, S., 2006a. Modeling the relationship between soil bulk density and the water retention curve. Vadose Zone Journal 5, 554-563.

Assouline, S., 2006b. Modeling the relationship between soil bulk density and the hydraulic conductivity function. Vadose Zone Journal 5, 697-705.

Barbour, S.L., 1998. Nineteenth Canadian geotechnical colloquium: The soil-water characteristic curve: a historical perspective. Canadian Geotechnical Journal, 35, 873-894.

Basile, A., Ciollaro, G., and A Coppola, 2003. Hysteresis in soil water characteristics as a key to interpreting comparisons of laboratory and field measured hydraulic properties. Water Resources Research, 39, 1355.

Batu, V. 1998. Aquifer Hydraulics: A comprehensive guide to hydrologic data analysis. John Wiley & Sons Inc., New York.

Berg, S.J. 2007. A device for measuring groundwater velocity in the capillary fringe. M.Sc. Thesis, University of Waterloo, Waterloo, Ontario, Canada.

Berg, S.J., and R.W. Gillham. 2010. Studies of Water Velocity in the Capillary Fringe: The Point Velocity Probe. Ground Water, 48(1), 59–67.

Berkowitz, B., S.E. Silliman, and A.M. Dunn, 2004. Impact of the capillary fringe on local flow, chemical migration, and microbiology. Vadose Zone, 3(2), 534–548.

Bevan, M.J., 2001. A detailed study of water content variation during pumping and recovery in an unconfined aquifer. M.Sc. Thesis, University of Waterloo, Waterloo, Ontario, Canada.

Bevan, M.J., Endres, A.L., Rudolph, D.L., and G. Parkin, 2003. The non-invasive characterization of pumping-induced dewatering using ground penetrating radar. Journal of Hydrology, 281, 55-69.

Bevan, M.J., Endres, A.L., Rudolph, D.L., and G. Parkin, 2005. A field-scale study of pumping-induced drainage and recovery in an unconfined aquifer. Journal of Hydrology, 315, 52-70.

Bohla, J., 1986. A sedimentological investigation of a progadational foreshore sequence: CFB Borden. M.Sc. Thesis, University of Waterloo, Waterloo, Ontario, Canada.

Boulton, N.S., 1954. Unsteady radial flow to a pumped well allowing for delayed yield from storage. International Association of Scientific Hydrology Publication, Rome, 37, 472-477.

Boulton, N.S., 1963. Analysis of data from non-equilibrium pumping tests allowing for delayed yield from storage. Proceedings of the Institute of Civil Engineers, 26, 469-482.

Bouwer, H., Rice, R.C., 1978. Delayed aquifer yield as a phenomenon of delayed air entry. Water Resources Research, 4(6), 1068-1074.

Bouwer, H., 1979. Soil Water Hysteresis as a Cause of Delayed Yield from Unconfined Aquifers. Water Resources Research, 15(4), 965-966.

Brooks, R.H., and A. T. Corey, 1964. Hydraulic Properties of Porous Media. Hydrology Paper, Colorado State University, Fort Collins, CO.

Bunn, M.I., Jones, J.P., Endres, A.L., and D. L. Rudolph, 2010. Effects of hydraulic conductivity heterogeneity on vadose zone response to pumping in an unconfined aquifer. Journal of Hydrology, 387, 90-104.

Bunn, M.I., Jones, J.P., Endres, A.L., and D. L. Rudolph, 2011. Field observation of the response to pumping and recovery in the shallow water table region of an unconfined aquifer. Journal of Hydrology (In Review).

Burdine, N.T. 1953. Relative permeability calculation from pore size distribution data. Transactions of the American Institute of Mining Engineering, 198, 71-78.

Canone, D., Ferraris, S., Sander, G., and R. Haverkamp. 2008. Intrepretation of water retention field measurements in relation to hysteresis phenomena. Water Resources Research 44, doi:10.1029/2008WR007068

Conant, B., 1991. Field studies of vertical well-screen placement: effect on recovery of stratified contaminants from an unconfined aquifer. M.Sc. Thesis, University of Waterloo, Waterloo, Ontario, Canada.

Dagan, G. 1967. Linearized solutions of free-surface groundwater flow with uniform recharge. Journal of Geophysical Research, 72(4), 1183-1193.

Doughty, C., 2006. NAPL recovery using CO_2-supersaturated water injection: distribution of the CO_2 gas phase. M.Sc. Thesis, University of Waterloo, Waterloo, Ontario, Canada.

Dunn, A.M., and S.E. Silliman, 2003. Air and water entrapment in the vicinity of the water table: A laboratory study on heterogeneous sands. Ground Water, 41, 729–734.

Dunn, A.M., Silliman, S.E., Dhamwichukorn, S., and C.F. Kulpa, 2004. Demonstration of microbial transport into the capillary fringe via advection from below the water table. Journal of Hydrology 306, 50-58.

Endres, A.L., Jones, J.P., and E.A. Bertrand, 2007. Pumping-induced vadose zone drainage and storage in an unconfined aquifer: A comparison of analytical model predictions and field measurements. Journal Hydrology, 335, 207-218.

Endres, A.L., Jones, J.P., and E.A. Bertrand, 2007b. Reply to comments provided by T.N. Narasimhan on “Pumping-induced vadose zone drainage and storage in an unconfined aquifer: A comparison of analytical model predictions and field measurements”. Journal Hydrology, 335, 221-222.

Fabyishenko, B.A. 1995. Hydraulic behavior of quasi-saturated soils in the presence of entrapped air: Laboratory experiments. Water Resources Research, 31(10), 2421-2435.

Freyberg, D.L., 1986. A natural gradient experiment on solute transport in a sand aquifer, 2, Spatial moments and the advection and dispersion of non-reactive tracers. Water Resources Research, 22, 2031-2046.

Ferrante, M., and T.-C.J. Yeh, 1999. Head and flux variability in unsaturated soils under transient flow conditions. Water Resources Research, 35, 1471-1479.

Frippiat, C.C., and A.E. Holeyman, 2008. A comparative review of up scaling methods for solute transport in heterogeneous porous media. Journal of Hydrology. 362, 150-176.

Gardner, W.R., 1958. Some steady state solution of the unsaturated moisture flow equation with application to evaporation from a water table. Soil Science, 85, 228-232.

Gillham, R. W., Klute, A., and D.F. Heermann, 1979. Measurement and numerical simulation of hysteretic flow in a heterogeneous porous medium, Soil Science Society of America Journal, 43, 1061-1067.

Glass, R.J., Brainard, J.R., and T.-C.J. Yeh, 2005. Infiltration in Unsaturated layered fluvial deposits at Rio Bravo: Macroscopic Anisotropy and Heterogeneous Transport. Vadose Zone Journal, 4, 22-31.

Green, T.R., Freyberg, D.L., 1995. State-dependent anisotropy: Comparisons of quasi analytical solutions with stochastic results for steady gravity drainage. Water Resources Research, 31, 2201-2212.

Green, C.T., Stonestrom, D.A., Bekins, B. A., Akstin, K.C., and M. S. Schulz, 2005. Percolation and transport in a sandy soil under a natural hydraulic gradient. Water Resources Research, 41, W10414.

Jacobs, B., and L. W. Gelhar, 2005. Effective properties of two-phase flow in heterogeneous aquifers. Water Resources Research, 41.

Janković, I., Fiori, A., and G. Dagan, 2006. Modelling flow and transport in highly heterogeneous three-dimensional aquifers: Ergodicity, Gaussianity, and anomalous behavior -1. Conceptual issues and numerical simulations. Water Resources Research, 42, W06D12.

Kaluarachchi, J. J., and J. C. Parker, 1987, Effects of hysteresis with air entrapment on water flow in the unsaturated zone, Water Resources Research, 23, 1967-1976.

Knight, J.H. 1992. Sensitivity of time domain reflectometry measurements to lateral variations in soil water content. Water Resources Research, 29(9), 2345-2352

Kueper, B.H., and E.O Frind, 1991. Two-phase flow in heterogeneous porous media: 2. Model application. Water Resources Research , 27, 1059-1071.

Krosynski, U.I., and G. Dagan, 1975. Well pumping in unconfined aquifers: The influence of the unsaturated zone, Water Resources Research, 11(3), 479-490.

Lappala, E.G., R. W. Healy, and E.P. Weeks, 1987. Documentation of computer program VS2D to solve the equations of fluid flow in variably saturated porous media, US Geological Survey Water-Resources Investigations Report, 83-4099.

Lenhard, R. J., and J. C. Parker, 1987. A model for hysteretic constitutive relation governing multiphase flow, 2, Permeability-saturation relations. Water Resources Research. 23, 2197-2206.

Lenhard, R.J., Parker, J.C., and J. J. Kaluarachchi, 1991. Comparing Simulated and Experimental Hysteretic Two-Phase Transient Fluid Flow Phenomena. Water Resources Research, 27, 2113-2124.

Leverett, M.C., 1941. Capillary behavior in porous solids. Transactions of the American Institute of Minerals and Metallurgical Petroleum Engineering, 142, 152-169.

Li, B., and T.-C.J. Yeh. 1988. Sensitivity and moment analysis of head in variable saturated regimes. Advances in Water Resources, 21, 477-485.

Lowry, M.I., and C.T. Miller. 1995. Pore scale modeling of nonwetting-phase residual in porous media. Water Resources Research, 31(3), 455-473.

Luthin, J.N., and P.R. Day. 1955. Lateral flow above a sloping water table. Soil Science Society of America Journal, *19*, 406–410.

Mathias, S. A., and A. P. Butler. 2006. Linearized Richards' equation approach to pumping test analysis in compressible aquifers. Water Resources Research, 42, doi:10.1029/2005WR004680.

MacFarlane, D.M., Cherry, J. A., Gilham, R.W., and E.A. Sudicky, 1983. Migration of contaminants at a landfill: A case study, 1, Groundwater flow and plume delineation. Journal of Hydrology, 63, 1-29.

MacKay, D.M., Freyberg, D.L., Roberts, P. V., and J.A. Cherry. 1986. A natural gradient experiment on solute transport in a sand aquifer : Approach and overview of plume movement. Water Resources Research, 22(13), 2017-2029.

Mantoglou, A., and L.W. Gelhar, 1987. Stochastic modeling of large-scale transient unsaturated flow. Water Resources Research, 23, 37-46.

Mao, D., Wan, L., and T-C. J. Yeh, 2010. Transition of water release mechanism during unconfined aquifer pumping test. Water Resources Research, In Press

McCord, J.T., Stephens, D.B., and J.L. Wilson, 1990. Toward validating state-dependent macroscopic anisotropy in unsaturated porous media: Field experiments and modeling considerations. Journal Contaminant Hydrology, 7, 145-175.

McCord, J.T., Stephens, D.B., and J.L. Wilson, 1991. Hysteresis and State-dependent anisotropy in modeling unsaturated hillslope hydrologic processes. Water Resources Research, 27(12), 3257-3260

Mickle, R.J., 2005. A coupled hydrogeological-petrophysical analysis of geophysical variation in the vadose zone, M.Sc. Thesis, University of Waterloo, Waterloo, Ontario, Canada.

Moench, A.F., 1995. Combining the Neuman and Bolton models for flow to a well in an unconfined aquifer, Ground Water, 33, 378-384.

Moench, A.F., 2003. Estimation of hectare scale soil moisture characteristics from aquifer-test data. Journal of Hydrology, 281, 82 -95.

Moench, A.F., 2008. Analytical and numerical analysis of an unconfined aquifer test considering unsaturated zone characteristics. Water Resources Research, 44, W06409.

Moench, A.F., S.P. Garabedian, and D. R. LeBlanc, 2001. Estimation of hydraulic parameters from an unconfined aquifer test conducted in a glacial outwash deposit, Cape Cod, Massachusetts. US Geological Survey Professional Paper, 1629.

Mualem, Y. 1976. A new model predicting the hydraulic conductivity of unsaturated porous media. Water Resources Research, 12, 513-522.

Narasimhan, T.N., and M. Zhu, 1993. Transient flow of water to a well in an unconfined aquifer: applicability of some conceptual models. Water Resources Research, 29, 179-191.

Narasimhan, T.N., 2007. Comment on "Pumping-induced vadose zone drainage and storage in an unconfined aquifer: A comparison of analytical model predictions and field measurements", Journal Hydrology, 335, 219-220.

Neuman, S.P., 1972. Theory of flow in unconfined aquifers considering delayed response of the water table, Water Resources Research, 8, 1031-1045.

Neuman, S.P., 1974. Effect of partial penetration on flow in unconfined aquifers considering delayed gravity response, Water Resources Research, 10(12), 303-312.

Neuman, S.P., 1975. Analysis of Pumping test data from Anisotropic Unconfined Aquifers Considering Delayed Gravity Response. Water Resources Research, 11(2), 329-342.

Neuman, S.P., 1979. Perspective on 'Delayed Yield'. Water Resources Research, 15(4), 899-908.

Neuman, S.P., 1987. On Methods for Determining Specific Yield. Ground Water, 25(6), 679-684.

Nwankwor, G.I., 1984. A comparative study of specific yield in a shallow unconfined aquifer. M.Sc. Thesis, University of Waterloo, Waterloo, Ontario, Canada.

Nwankwor, G.I., J. A. Cherry, and R. W. Gillham, 1984. A comparative study of specific yield determination for a shallow sand aquifer, Ground Water, 22, 764-772.

Nwankwor, G.I., 1985. Delayed yield processes and specific yield in a shallow sand aquifer. Ph.D. Thesis, University of Waterloo, Waterloo, Ontario, Canada.

Nwankwor, G.I., Gillham, R. W., van der Kamp, G., and F.F. Akindunni, 1992. Unsaturated and saturated flow in response to pumping of an unconfined aquifer: Field evidence of delayed drainage. Ground Water, 30, 690-700.

O'Carroll, D.M., T.J. Phelan, and L. M. Abriola, 2005. Exploring dynamic effects in capillary pressure in multistep outflow experiments, Water Resources Research, 41, W 11419, 10.1029/2005WR004010.

Or, D., Jones, S.B., VanShaar, J.R., Humphries, and S.L. Koberstein, 2004. WinTDR soil analysis software: Users guide. Utah State University Soil Physics Group.

Parker, J.C., and R.J. Lenhard, 1987. A model for hysteretic constitutive relations governing multiphase flow, 1, Saturation-pressure relations. Water Resources Research, 23, 2187-2196.

Pinder, G.F., and M.A. Celia. 2006. Subsurface Hydrology. John Wiley & Sons, New Jersey.

Pruess, K., Oldenburg, C., and G. Moridis. 1999. TOUGH2 User's Guide Veriosn 2.0. Lawrence Berkeley National Laboratory, Report No. 43134.

Robin, M.J.L., Gutjahr, A.L., Sudicky, E.A., and J.L. Wilson, 1993. Cross-correlated random field generation with the direct Fourier transform method. Water Resources Research, 29, 2385-2397.

Ronen, D., Scher, H., Blunt, M. 1997. On the structure and flow processes in the capillary fringe of phreatic aquifers. Transport in Porous Media, 28, 159-180.

Ryan, M.C., MacQuarrie, K.T.B., Harman, T., and J. McLellan. 2000. Field and modeling evidence for a "stagnant flow" zone in the upper meter of sandy phreatic aquifers. Journal of Hydrology, 233, 223-240.

Sakaguchi, A., Nishimura, T., and M. Kato. 2005. The effect of entrapped air on the quasi-saturated soil hydraulic conductivity and comparison with the unsaturated hydraulic conductivity. Vadose Zone Journal, 4, 139-144.

Salandin, P., and Fiorotto, V., 1998. Solute Transport in Highly Heterogeneous Aquifers. Water Resources Research, 34, 949-961.

Sawangsuriya, A., Edil, T.B., and P.J. Bosscher, 2008. Modulus-suction-moisture relationship for compacted soils. Canadian Geotechnical Journal, 45, 973-983.

Silliman, S.E., Berkowitz, B., Šimůnek, J., and M.Th. van Genuchten, M. Th., 2002. Fluid flow and solute migration within the capillary fringe. Ground Water 40, 76–84.

Stephens, D.B., and S. Heermann, 1988. Dependence of Anisotropy on Saturation in a Stratified Sand. Water Resources Research, 24, 770-778.

Simpson, M.J., Clement, T.P., and T.A. Gallop. 2003. Laboratory and Numerical Investigation of Flow and Transport near a seepage face boundary. Ground Water, 41(5), 690-700.

Stretslova, T.D., 1973. Flow near a pumped well in an unconfined aquifer under nonsteady conditions. Water Resources Research, 9(1) 227-235.

Sudicky, E.A., 1986. A natural gradient experiment on solute transport in a sand aquifer: Spatial variability of hydraulic conductivity and its role in the dispersion process. Water Resources Research, 22, 2069-2082.

Tartakovsky, G. D., and S. P. Neuman. 2007. Three-dimensional saturated unsaturated flow with axial symmetry to a partially penetrating well in a compressible unconfined aquifer, Water Resources Research, 43, doi:10.1029/2006WR005153.

Theis, C.V., 1935. The relation between the lowering of the piezometric surface and the rate and duration of discharge of a well using groundwater storage. Trans. Amer. Geophys. Union 16, 519-524.

Therrien, G.D., and E.A. Sudicky, 2000. Well bore boundary conditions for variably-saturated flow modeling. Advances in Water Resources, 24, 195-201.

Therrien, R., McLaren, R. G., Sudicky, E.A., and S.M. Panday, 2006. HydroGeoSphere: A three-dimensional numerical model describing fully-integrated subsurface and surface flow and solute transport, Manual [Draft], Groundwater Simulations Group.

Trefry, M.G., Ruan, F.P., McLaughlin, D., 2003. Numerical Simulations of preasymptotic transport in heterogeneous porous media: Departures from the Gaussian limit. Water Resources Research, 39, 1063.

Ursino, N., Gimmi, T., and H. Flühler, 2001. Combined effects of heterogeneity, anisotropy and saturation on steady state flow and transport: A laboratory sand tank experiment, Water Resources Research, 37(2), 201-208.

van Genuchten, M.Th., 1980. A closed-form equation for predicting the hydraulic conductivity of unsaturated soils, Soil Science Society America Journal, 44, 892-898.

VanderKwaak, J.E., 1999. Numerical simulation of flow and chemical transport in integrated surface-subsurface hydrologic systems. Ph. D. Thesis, University of Waterloo, Waterloo, Ontario, Canada.

Ward, A. L., and Z. F. Zhang. 2007. Effective Hydraulic Properties determined from transient unsaturated flow in anisotropic soils. Vadose Zone Journal, 6(4), 913- 924.

Watermark Numerical Computing, 2004. PEST: Model Independent Parameter Estimation, User's Manual 5th Edition.

Wenzel, L.K., 1936. The Theim method for determining the permeability of water-bearing materials. Report Water Supply Paper, 679-A, United States Geological Survey, Washington, DC.

Wildenschild, P.J., and K.H. Jensen, 1999, Laboratory investigations of effective flow behavior in unsaturated heterogeneous sands. Water Resources Research, 35, 17-27.

Wildenschild, D., J. W. Hopmans, and J. Simunek, 2001. Flow Rate Dependence of Soil Hydraulic Characteristics, Soil Sci. Society of America Journal, 65, 35-48.

Woodbury, A.D., and Sudicky, E.A., 1991, the geostatistical characteristics of the Borden aquifer. Water Resources Research, 27, 533-546.

Wyckoff, R.D., H.G. Botset, and M. Muskat. 1932. Flow of liquids through porous media under the action of gravity. Physics, 3, 90–113.

Yeh, T. –C. J., Gelhar, L.W., and A.L. Gutjahr, 1985a, Stochastic Analysis of Unsaturated Flow in Heterogeneous Soils 1. Statistically Isotropic Media. Water Resources Research, 21, 447-456.

Yeh, T. –C. J., Gelhar, L.W., and A.L. Gutjahr, 1985b, Stochastic Analysis of Unsaturated Flow in Heterogeneous Soils 2. Statistically Anisotropic Media. Water Resources Research, 21, 457-464.

Yeh, T. –C. J., Gelhar, L.W., and A.L. Gutjahr, 1985c, Stochastic Analysis of Unsaturated Flow in Heterogeneous Soils 3. Observations and Applications. Water Resources Research, 21, 465-471.

Yeh, T. –C. J., and D.J. Harvey, 1990. Effective unsaturated hydraulic conductivity of layered sands. Water Resources Research, 26, 1271-1279.

Zhang, Z. F., Oostrom, M., and A. L. Ward. 2007. Saturation-dependent hydraulic conductivity anisotropy for multifluid systems in porous media. Vadose Zone Journal, 6(4), 925- 934.

Appendices

Appendix A

Observation, Analysis and Interpretation of Pumping Tests in Unconfined Aquifers

A.1 Landmark pumping tests in unconfined aquifer systems

Although pumping tests in unconfined aquifers are a very common tool, and data from millions of tests are available, there are several tests that stand out as definitive in the science. These tests are all research focused, and involve more time, expense, and people than the routine tests typically seen in practice. In defining "landmark" pumping tests Moench et al. (2001) required characteristics such as a mild degree of hydraulic conductivity heterogeneity on the scale of the test, uniform aquifer thickness, aquifer boundaries that are beyond the pumping induced drawdown cone, the inclusion of data from many appropriately located piezometers and no interference from outside sources. This section will focus on the tests documented by Wenzel (1936), Nwankwor et al. (1984) and Nwankwor et al. (1992), Moench et al. (2001), and Bevan et al. (2003) and Bevan et al. (2005). The development of the analytical solutions and numerical methods for pumping test analysis discussed in this chapter are based on the data collected during these tests. The tests are presented in chronological order, and pertinent observations from each are highlighted.

Wenzel (1936)

Two pumping tests were completed in the unconfined aquifer near Grand Island, Nebraska in 1931. Only those details pertinent to the first test will be discussed, and the second test was disrupted by pumping issues. The aquifer tested consisted of sand, gravel, and clay, with a wide range of grain sizes (Wenzel, 1936). The unit was underlain by bedrock at a depth of 34 m, and the water table position varied from 0.6 to 3.0 m below ground surface as a function of ground surface elevation. A preexisting irrigation well was used to pump the aquifer. The well was 0.61 m in diameter and fully screened to a depth of 12 m. A total of 80 monitoring wells were installed from approximately 1 to 366 m radial distance from the pumping well. These wells were monitored by hand. The well was pumped at an approximate rate of 2040 L/min. for a period of 48 hours. Recovery was monitored for a period of 24 hours. Following 6 hours of pumping the radius of the drawdown cone was approximately 245 m and after 12 hours drawdown could be detected at the most distant wells from the pumping well. The discussion of the pumping test noted that the rate of spreading and size of the drawdown cone appears to be a function of both specific yield and permeability, as a decrease in either appears to result in a larger cone (Wenzel, 1936). A volume balance method for the determination of specific yield was completed in this study, and it was found that the use of transient drawdown values resulted in an increase in specific yield as pumping progressed (Wenzel, 1936). This test was used in the development and testing of many of the analytical solutions used in the interpretation of unconfined pumping tests.

Nwankwor et al. (1984), Nwankwor et al. (1992)

Two pumping studies and a total of three pumping tests were conducted in the early 1990's at Canadian Forces Base (CFB) Borden, ON. The Borden aquifer consists of prograding foreshore deposits of glacial Lake Algonquian (Bohla, 1986). The texture of the aquifer varies locally from fine to coarse grained sand with hydraulic conductivities ranging within two orders of magnitude (Sudicky, 1986). While significant heterogeneity is present on the scale of a soil core, the aquifer is typically described as homogeneous at the pumping test scale (MacFarlane et al., 1983). The aquifer is 9 m thick and is underlain by a clayey aquitard. The pumping well used for all tests was 0.13 m in diameter and screened through the bottom 3.65 m of the aquifer (Nwankwor, 1992). Three groups of piezometers were installed at the site. The shallow group was installed 0.35 m below the static water table. Intermediate piezometers were installed 0.35 m below the shallow piezometers. Deep piezometers were installed at a depth equivalent to the centre of the well screen. The wells were installed at radial distances from the pumping well ranging from 1 to 100 m. In addition to the three main well groups, and bundle piezometer was installed at 3.5 m radial distance from the pumping well, with screens located every 1 m from 1 m below the water table to the aquitard (Nwankwor et al., 1984).

During the first experiment two pumping tests were conducted. The first test was run for a period of 4 hours, during which time the well was pumped at a rate of 36 ± 1 L/min.. The second test was run for a period of 65 hours at a pumping rate of 60 ± 1 L/min.. The results from both tests were used to compute a specific yield through volume balance methods using the transient drawdown cone. Results from the long test were also used to compute the specific yield through the type curve methods presented by Boulton (1963) and Neuman (1972). The specific yield estimated from the type curve methods was found to be approximately 1/3 of the laboratory derived value. The values obtained through the volume balance method were low early in the pumping test, but grew with pumping duration to a value slightly below that determined in the laboratory. Based on these results, it was concluded that type curve analytical methods must include both vertical flow as a result of a partially penetrating well, as well as a delay in the drainage of aquifer material, in response to the vertical gradients (Nwankowr et al., 1984).

The second experiment was conducted using the same site and instrumentation. Tensiometers, a gamma moisture probe and gravimetric sampling were added to the observation network to observe the response to pumping in the zone above the water table. This instrumentation was installed at 3, 5, and 15 m radial distance from the pumping well. The tensiometers were installed at 0.2 m intervals from below the static water table to above the top of the static capillary fringe. Gravimetric sample occurred at three times during the test, and samples were taken every 0.05 m over the same interval as the

tensiometers. Gamma moisture profiling was completed in 0.05 m intervals from 0.5 m below the water table to the top of the static capillary fringe. The well was pumped at a rate of 60 ± 1 L/min., and the test was terminated by a rain event that disrupted test results after 20 hours of pumping (Nwankwor et al., 1992).

The inclusion of observations above the water table provided some additional insight into the processes occurring during unconfined pumping tests. During early time, it was found that downward vertical gradients formed and increased in magnitude. During the period in which drawdown rates decreased, the vertical gradients were found to decrease to near negligible values, such that during late times in the pumping test flow is presumed to be horizontal throughout the aquifer. Based on this observation, the concept of delayed yield was introduced, in which downward vertical gradients cause a stretching of the moisture curve, resulting in excess storage which is slowly released as the vertical gradients decrease. Due to the delayed yield phenomenon, it was concluded that, for short duration data sets, it is more appropriate to use the volume balance method to determine the specific yield used for longer term predictions. Specific yield determined from type curve analysis will tend to over predict the long term drawdown (Nwankowr et al., 1992). The results from this experiment were used to further analytical developments, and to support the use of numerical simulations as the most appropriate method for unconfined pumping test analysis.

Moench et al. (2001)

In 1990 this test was run as a component of a larger study of a sand and gravel aquifer at Cape Cod, Massachusetts. A 0.2 m diameter pumping well was installed to a depth of 24 m with the bottom 14 m screened. Twenty observation piezometers were installed from 6 to 70 m radial distance from the pumping well, at depths from 10 to 37 m below ground surface. Prior to pumping, the static water table was 5.8 m below ground surface. The well was pumped at a rate of approximately 1211 L / min for a period of 72 hours. During pumping, drawdown was monitored by hand in 13 peizometers, while the remaining 7 piezometers were monitored using pressure tranducers. Data from this test has been widely used in the verification of a variety of analytical techniques due to the high data quality. This test promoted the development of an analytical solution which included well-bore storage, well skin effects, and complex drainage from the unsaturated zone. In the analysis of this test and the verification of the analytical solution, parameter estimation techniques were used on individual wells, groups of wells, and the entire data set. Based on these observations, it was concluded that for shallow wells, delayed yield and flow in the unsaturated zone are both important processes that must be accounted for in any analytical solution. As vertical flow through the zone above the water table is an important process, the drawdown in shallow wells of similar radial distances was found to be highly variable due to the effects of heterogeneity on the vertical flow component. It was proposed that if only deep wells are used and

the pumping duration is sufficiently long, accurate estimates of specific yield could be obtained without the inclusion of delayed drainage (Moench et al., 2001).

Bevan et al. (2003) and Bevan et al. (2005)

Tests were conducted in the Borden aquifer, at the same site as the Nwankowr et al. (1984) and Nwankwor et al. (1992) test, as a component of the thesis work of Michael Bevan (Bevan, 2001). The first test was designed to investigate the use of ground penetrating radar (GPR) as a method for monitoring the evolution of the drawdown cone during pumping. GPR generates a strong reflection where there is a large change in moisture content, such as the transition between fully and partially saturated conditions at the top of the capillary fringe (Bevan et al., 2001). Prior to the test in August 2000, the static water table was 1.95 m below ground surface. Pumping occurred for a period of 168 hours at a rate of 44 ± 1 L/min.. Recovery was monitored for a period of 120 hours. Of the 42 observations wells described by Nwankwor et al. (1984), 2 wells (the shallow locations at 3 and 5 m radial distance from the pumping well) were monitored by pressure transducer. The remaining wells were monitored by hand using an acoustic electric sounder. A total of 8 GPR lines were set, these were offset from the pumping well by 1 m and radiated outwards at various angles to capture the drawdown cone. At 1 m radial distance from the pumping well a neutron access tube was installed. This access tube was used during pumping to collect neutron profiles twice daily using a 0.1 m vertical spacing from 0.75 to 4 m below ground surface. Volume balance methods were used to determine the drained volume from both the GPR data and the piezometric data. Based on these calculations, it was found that the volumes based on GPR data significantly underestimated the volume drained based on hydraulic data. In analyzing the drawdowns of both the transition zone (neutron data and GPR) and the hydraulic head, it was concluded that the moisture profile was drawn down at a slower rate than the hydraulic head, resulting in excess storage that appeared to be contained within the capillary fringe. It was concluded that additional work was required to determine the cause of this differential drawdown (Bevan et al., 2003).

A second test was initiated at the same Borden site in 2001. Prior to pumping the static water table was 2.75 m below ground surface. During this tests the well was pumped at a rate of 40 ± 1 L/min. for a period of 168 hours, with recovery monitored for 120 hours. Neutron probe moisture content logging was performed in a series of six neutron access tubes using a 0.05 m vertical sampling interval from 1.25 to 3.5 m below ground surface. Neutron moisture profiles were completed at 18 times in all six access tubes during pumping. A total of 11 piezometers were continuously logged, these were grouped at 1.5, 3, 5, 10, 15 m radial distance from the pumping well. An additional 14 piezometers were measured periodically by hand (Bevan et al., 2005).

The monitored piezometers responded predictably for the majority of the test. Following a typical unconfined response curve, the hydraulic head-drawdown rates were high early in the test, slowed in the middle, and increased again towards the end of the test. By the fourth day of pumping, hydraulic head drawdown rates began to decrease, indicating a potential interaction with a recharge boundary condition; however, this did not impact on the main conclusions of the test. The neutron derived moisture profiles generated during pumping deviated significantly from the moisture profiles observed prior to the commencement of the test. Specifically, the moisture profiles showed a tension saturated zone (capillary fringe) that increased in thickness (i.e. extended) due to differential drawdown between the water table and the top of the capillary fringe (Bevan et al., 2005). The capillary fringe extension increased with pumping duration throughout the entire test. The extension was inversely dependent upon distance from the pumping well, with less significant extensions occurring at larger distances from the pumping well. Vertical gradients were calculated between the shallow and deep piezometer pairs. The peak magnitude was of similar order to those observed during the Nwankwor et al. (1992) test; however, in contrast to the Nwankowr et al. (1992) results the decrease in gradient magnitude was more gradual. It is noted however that the capillary fringe extension appears to be independent of the vertical gradients, as an extension was observed at 15 m radial distance from the pumping well, where gradients remained negligible for the duration of the test. It is the results of this tests that motivated the analytical study of Endres et al. (2007), and the numerical work of Moench (2008), as well as the research contained herein.

A.2 Analytical and Semi-Analytical Solution Techniques for Pumping Test Analysis

Although this thesis used numerical simulation techniques to analyze pumping test data, it is useful to provide an overview of the development of analytical solution techniques used for pumping test analysis, as they provide a basis for our conceptualization of the unconfined response to pumping. Although many of these solutions were developed long before the current availability of computing power, many are used today for their simplicity and ability to accurately estimate unsaturated parameters. Purely analytical solutions are divided into two main groups for unconfined response to pumping; those which include delayed yield and those which assume instantaneous drainage. Common solution methods for both assumption types will be discussed in detail. Modern developments have led to semi-analytical solutions which allow for more complex inclusion of unsaturated flow, while still offering a more rapid and less data intensive solution than full numerical simulations. The two main semi-analytical solution techniques available will also be discussed in this section.

A.2.1 Analytical Solutions

Analytical solutions can be divided into two main types; those that assume instantaneous drainage at the water table (e.g. Neuman (1972, 1974)) and those that account for delayed yield (e.g. Boulton (1954, 1963), and Moench (1996, 1997, 2003, 2004)). While there are many more available solutions, this section will provide an overview of these most prominent solutions. Although there are many possible points of discussion that may be touched on in terms of a comparison between solutions, in the interest of brevity, this section will focus on the differences in the water table boundary condition, and therefore this section will not include a discussion on well boundary types or the analytical methods used in the development of the solution.

Instantaneous Drainage Solutions

Although boundary conditions and solution methods can vary significantly between solution types, there are several assumptions that are common for all of the solution methods discussed herein. They are (Batu, 1998):

1. The well is pumped at a constant rate.
2. The aquifer is of infinite extent, and is underlain by a horizontal aquitard
3. The aquifer is homogeneous, anisotropic, and the principal hydraulic conductivities are aligned with the coordinate axis
4. Darcy's law for flow is valid at all times at all locations in the aquifer
5. The drawdown in the aquifer is significantly less than the saturated thickness

Assumptions regarding the nature of the pumping well, its penetration, and the effect of well-bore storage vary between each solution type, but will not be discussed explicitly in this section.

The instantaneous drainage solution proposed by Neuman (1972, 1974) implies that as the water table falls during pumping all water previously below the pre-pumping water table, but now above, will be instantly released from storage. Additional assumptions of the Neuman (1972, 1974) solution are as follows:

1. Water is released from compaction of the aquifer, expansion of water and gravity drainage at the free surface
2. Water is released instantly from the unsaturated zone. Capillarity effects are neglected

Neuman (1972) provides a solution for a fully penetrating well, while Neuman (1974) provides a solution for partially penetrating wells. In both cases, the well is treated as a line sink and the seepage face is neglected. These assumptions lead to the following governing equation:

$$K_r \frac{\partial^2 s}{\partial r^2} + \frac{K_r}{r}\frac{\partial s}{\partial r} + K_z \frac{\partial^2 s}{\partial z^2} = S_s \frac{\partial s}{\partial t} \qquad 0 < z < \xi \tag{A.1}$$

where S_s is the specific storage, and $s(r,t)$ is the drawdown at a given radial distance and time. The right hand side of the equation represents the rate of production of water from elastic storage. $K_{r/z}$ represents the conductivities in the direction of the coordinate axes, z represents the elevation from the bottom of the aquifer, and r represents the radial distance from the pumping well. The left hand side of the equation represents the rate of mass flux of water into and out of a unit area of the aquifer. This equation applies from the bottom of the aquifer ($z = 0$) to the water table ($z = \zeta(r,t)$). Although not explicitly stated in Neuman (1974) the water table is the atmospheric pressure isobar, not the top of the saturated zone.

As the governing equation is a function of both the position of the water table and drawdown, only iterative solutions would be possible; however, Neuman (1972, 1974) shifts the boundary condition to a constant plane ($z = b$), and then linearizes the problem based on Dagan (1967) such that a non-iterative approach may be used. This linearization is dependent upon the assumption that the drawdown is much less than the saturated thickness of the aquifer (this condition is not quantified (Neuman, 1972, 1974)). This simplification allows the above equations to be evaluated from 0 to b, or at b, which is now a constant. By assuming that recharge and horizontal flux at the water table are both negligible a two part type-curve solution can be achieved, whereby the transmissivity and specific yield can be derived from the late time data, and the storage coefficient and specific storage are derived from the early time curve (Batu, 1998). An implicit consequence of the assumptions used in the development of the analytical solution is that the delay in drainage which results in the inflection of the time-drawdown curve is due solely to elastic storage effects, and delayed water table drawdown (Neuman, 1979). This assumption results in a conceptual model in which the position of the top of the saturated zone remains at a fixed distance from the position of the water table.

Delayed Yield type solutions

Delayed yield type solutions imply that as the water table passes through a volume of soil, the water will be released from the pores as some function of time. It is known that this release of water is a complex function of the moisture content of this system, which is in turn a function of pressure head. This function cannot be incorporated into an analytical framework; therefore, simple empirical relationships have been developed to represent the drainage flux from above the water table. The first of this type of solution was presented by Boulton (1954, 1963), and included the following additional assumptions (Batu, 1998):

1. The specific yield (S_y) is a constant property of the aquifer material
2. Water released from compression of the porous matrix and compression of water may be neglected except at early times
3. Flow to the well is not at steady state
4. Water from the tension saturated zone of the aquifer is released with an exponential decay

To represent the effect of delayed yield Boulton (1954, 1963) generated an additional term in the governing equation to represent the contribution of an additional volume of water per unit horizontal area. This expression is given by (Batu, 1998):

$$\Delta s \alpha S_y e^{-\alpha(t-\tau)} \tag{A.2}$$

where Δs is the change in drawdown, S_y is the specific yield, and t-τ is the time interval over which the change in drawdown occurs. α is an empirical constant (units t^{-1}). This approach results in a governing equation of the form (Batu, 1998):

$$T\left(\frac{\partial^s s}{\partial r^2}+\frac{1}{r}\frac{\partial s}{\partial r}\right)=S\frac{\partial s}{\partial t}+\alpha S_y\int_0^t\frac{\partial s}{\partial t}e^{-\alpha(t-\tau)}dt \tag{A.3}$$

The physical cause leading to the need for a delay coefficient has never been stated explicitly. Boulton (1954) suggested two methods by which delayed yield may arise, both dependent upon the presence of fine grained compressible materials. Boulton (1963) hinted that delayed yield may arise in a homogeneous system due to effects of the unsaturated zone; however, the definition of the parameter remained vague. Further analysis of the parameter by Moench (1995) suggests that although we are unable to relate the empirical parameter to any physical parameter of the aquifer system, the fact that its inclusion improves the match of the model to field data should be sufficient to justify its use. It is noted that as α reaches large values, the solution begins to approximate an instantaneous drainage solution. The Boulton (1954, 1963) solution method is completed in two parts, with the early time data being fitted to a Theis (1935) type curve to derive the transmissivity and storage coefficients, while later time data is fitted to a second Theis (1935) type curve to determine specific yield.

The development of non-instantaneous yield solutions has been furthered by Moench (1995, 1997) and Moench et al. (2001). Moench (1995) presented a three-dimensional solution to the Neuman (1972, 1974) solution which incorporated the Boulton (1954, 1963) representation of delayed yield as a boundary condition for the water table, allowing for vertical components of flow from above the water table. Improved estimates of specific storage were obtained by Moench (1997) by accounting for well-bore storage in the analytical solution. As was noted by Narasimham and Zhu (1993), the single

exponential empirical parameter used in the drainage flux term was an overly simplified approximation of the actual flow process. Therefore, Moench et al. (2001) proposed a new solution with an infinite summation of empirical parameters that could be used to fit the solution to pumping test data. The governing equation for this solution is given by (Moench et al., 2001):

$$K_z \frac{\partial h}{\partial z}(r,b,t) = -S_y \int_0^t \frac{\partial h}{\partial t'}(r,b,t) \sum_{m=1}^{M} \frac{\alpha_m}{M} e^{-\alpha_m (t-t')} d\,t \tag{A.4}$$

where M represents the total number of exponential parameters used and α_m represents each of these parameters. As shown in Moench et al. (2001) this solution provides a much closer approximation to field data; however, no physical meaning behind the parameters has been presented.

Given the differences between the three solutions presented herein, they are typically compared by considering the value of specific yield obtained. The type curve methods of Neuman (1972, 1974), and Boulton (1954, 1963) both underestimate the laboratory derived value of specific yield. Endres et al. (2007) expanded this comparison to include the Moench (1995) single exponential solution, and the Moench et al. (2001) solution using three empirical coefficients in an analysis of the Bevan et al. (2005) pumping test. While both the Neuman (1974) and Moench (1995) solutions significantly underestimated the laboratory derived specific yield value of 0.3 for Borden sand determined by Nwankwor et al. (1984), the linear combination solution with 3α (Moench et al. 2001) generated a reasonable estimate of 0.284. However, none of the analytical solutions tested were able to accurately replicate the cumulative drainage flux across the water table or the persistence of undrained vadose zone storage inferred from neutron probe data collected by Bevan et al. (2005). Consequently, Endres et al. (2007) concluded that the implicit boundary conditions used to represent drainage in these analytical solutions do not accurately reflect the physical response of the vadose zone to pumping. Narasimhan (2007) has suggested that the physical processes leading to the results observed by Bevan et al. (2005) may be more realistically simulated by numerical codes.

A.2.2 Semi-Numerical Solutions

Although the preceding discussion suggests that unconfined aquifers are best addressed in a numerical framework, semi-analytical solutions provide an interesting alternative to account for unsaturated flow without the heavy computational and data requirements of a numerical simulation. In recent years, new developments have been made based on the framework presented by Kroszynski and Dagan (1975). This solution was largely ignored as it relied on an assumption of a rigid aquifer (ignoring the contribution of water from elastic storage). New solutions by Mathias and Butler (2006), and Tartakovksy and Neuman (2007) have overcome this issue. This section will provide a brief overview

of these two solutions, and discuss the application of this solution type to the Bevan et al. (2005) test by Moench (2008).

The assumptions of Mathias and Butler (2006) are similar to Neuman (1974); however, the pumping well must be fully penetrating. The boundary condition at the water table is replaced by a continuity assumption between flow in the saturated and unsaturated zones. It is assumed that horizontal flow in the unsaturated zone can be ignored. The initial head at the top of the saturated zone becomes ψ_s, which is the pressure head at which the aquifer beings to desaturate (bubbling pressure). The governing equation for flow in the unsaturated zone is (Mathias and Butler, 2006):

$$K_z \frac{\partial}{\partial z}\left(k(\psi)\frac{\partial \theta}{\partial z}\right) = S_y c(\psi)\frac{\partial \theta}{\partial t} \tag{A.5}$$

where θ is the hydraulic head in the unsaturated zone and ψ is the pressure head in the unsaturated zone. $k(\psi)$ and $c(\psi)$ are the exponential relative permeability and specific moisture capacity functions of Gardner (1958), as follows:

$$k(\psi) = e^{a_k(\psi-\psi_s)} \tag{A.6}$$

$$C(\psi) = \frac{dS_e}{d\psi} = a_c e^{a_c(\psi-\psi_s)} \tag{A.7}$$

where a_k is an empirical relative permeability exponent, and a_c is an empirical moisture retention exponent. Mathis and Butler (2006) speculate that these equations could be easily modified to include partially penetrating wells, finite wells and well bore storage following Moench (1997).

For the Tartakovsky and Neuman (2007) solution, the water table boundary condition is replaced by a continuity equation such that the drawdown in the unsaturated zone is equal to the drawdown in the saturated zone, and the total flux across the water table is continuous. The governing equation of flow in the unsaturated zone is (Tartakovsky and Neuman, 2007):

$$K\frac{1}{r_r}\frac{\partial}{\partial r}\left(k(\psi) r \frac{\partial \sigma}{\partial r}\right) + K_z \frac{\partial}{\partial z}\left(k(\psi)\frac{\partial \sigma}{\partial z}\right) = C(\psi)\frac{\partial \sigma}{\partial t} \tag{A.8}$$

where

$$C(\psi) = \frac{\partial \theta}{\partial \psi} = S_y \kappa e^{\kappa(b-z)}$$

(A.9)

σ is the drawdown in the unsaturated zone and θ is the moisture content. κ is the empirical exponential constant for both the relative permeability function and the moisture capacity function, following Gardner (1958) (note that this is the special case a_c=a_k for the solution of Mathias and Butler (2006)). It is worth noting that the governing equation used by Tartakovsky and Neuman (2007) allows for horizontal flow in the unsaturated zone.

The models of Tartakovsky and Neuman (2007) and Mathias and Butler (2006) were evaluated both theoretically and in comparison to published pumping tests. The theoretical work of Mathias and Butler (2006) found that if the unsaturated zone is assumed to be infinitely thick, their solution provides a good approximation of expected results. However, as the thickness is decreased the solution is not able to converge to the late time Theis curve, as would be expected. It was also found that as the permeability exponent was increased, the solution also deviated from the late time Theis curve, as water above the draining zone became immobilized. This effect is speculated to be one of the causes of an extended zone of tension saturation observed by Wildenschild et al. (2001). The theoretical work of Tartakovsky and Neuman (2007) as compared to the results of Neuman (1974) yielded ranges of the parameter κ_D for which unsaturated flow becomes important. If κ_D<1 (the aquifer has a high moisture retention capacity, or the saturated thickness is small) unsaturated flow is an important process, and the solution deviates from that of Neuman (1974). However, if κ_D>10, the effect is negligible and the solutions converge. It was also found that when horizontal permeability is high relative to vertical permeability, the effect of the unsaturated zone on drawdown is reduced, as the vertical flux component will be reduced (Tartakovsky and Neuman, 2007).

Moench (2008) used the Mathias and Butler (2006) solution to analyze the Bevan et al. (2005) pumping test. The analysis was completed using automated parameter estimation techniques to fit the solution to observed drawdown for two cases. In the first case $a_c \neq a_k$, while in the second case $a_c = a_k$, approximating the Tartakovsky and Neuman (2007) solution in the absence of horizontal flow above the water table. While both solutions yielded a good fit to the observed drawdown, the case for $a_c = a_k$ yielded an unrealistic soil moisture retention curve (Moench, 2008). Moench (2008) suggests that while the Tartakovsky and Neuman (2007) solution may be more physically realistic in its inclusion of horizontal flow above the water table, it should be altered to include separate parameters for relative hydraulic conductivity and soil moisture retention to generate realistic unsaturated parameter estimates. While semi-analytical solutions are a promising alternative to numerical simulation, they are still a more simplified approximation of the role of the vadose zone in the unsaturated response to pumping.

A.3 Numerical Simulation techniques

Although all of the analytical solutions discussed previously generate hydraulic head drawdown curves that are in agreement with the response observed in the field, they are simplified approximations that do not fully account for the impact of the unsaturated zone. It has been observed by Narasimham and Zhu (1993) that numerical simulations were able to produce more accurate approximations of the effects of the unsaturated zone and the well bore. It was strongly suggested by Narasimham (2007), and reiterated by Endres et al. (2007b) that numerical simulations may provide the most accurate representation of the unconfined response to pumping. Early numerical simulations of unconfined pumping tests include the work of Akindunni and Gillham (1992), who found that the numerical code SUNFLOW was able to accurately simulate the peak and subsequent decrease in vertical gradients observed by Nwankwor et al. (1992) during pumping. All numerical simulation techniques discuss herein are based on Richards' equation for conservation of mass in partially saturated conditions. Richards' equation, given in terms of pressure head for flow in the z-direction only, is as follows (Pinder and Celia, 2006):

$$\left[C(\psi_w) + S_w S_s{}^w\right]\frac{\partial \psi_w}{\partial t} - \frac{\partial}{\partial z}\left[K_{sat}^w k_{rw}\left(\frac{\partial \psi_w}{\partial z} + 1\right)\right] = 0 \qquad \text{(A.10)}$$

where ψ_w is the pressure head in the water phase, S_w is the degree of water saturation, $S_s{}^w$ is the storativity, and $K_{sat}{}^w$ is the saturated hydraulic conductivity of the water phase. The parameters $C(\psi_w)$, and k_{rw} are the specific moisture capacity and residual hydraulic conductivity, respectively; both are highly non-linear functions of pressure head. Specific moisture capacity represents the rate of change in moisture content per change in pressure head, its value is 0 at full saturation. Residual hydraulic conductivity is a function of moisture content and ranges from 1 at full saturation to 0 at residual saturation. Given these parameter values, Richards' equation collapses to the following at full saturation:

$$S_s{}^w \frac{\partial \psi_w}{\partial t} - \frac{\partial}{\partial z} K_{sat}^w \left(\frac{\partial \psi_w}{\partial z} + 1\right) = 0 \qquad \text{(A.11)}$$

It is noted that these equations are written in terms of the water phase, in one direction only. Similar equations can be written for an air and non-aqueous phase liquids, and equations are typically written for flow in the three principal directions. For anisotropic media, a different saturated hydraulic conductivity value is typically given for each principal direction, while the specific moisture capacity and relative hydraulic conductivity function tend to be considered independent of flow direction. For most flow simulations, the air phase is considered infinitely mobile and is not simulated; however, there are some cases in which air-phase flow may have an impact on water flow. This impact is discussed

later in this section.

While there are numerous methods used to solve Richards' equation, their discussion is outside of the scope of this work. The discussion herein will focus on the representation of the specific moisture capacity and unsaturated flow via the pressure-saturation (P-S) function and the residual hydraulic conductivity (RHC) function; these two functions are jointly referred to as the unsaturated flow constitutive relationships. The degree of saturation and relative permeability functions are both highly non-linear, and tend to be represented by empirical functions. This discussion will focus on the two main constitutive relationships used in the numerical simulation of partially saturated flow, the Brooks and Corey (1964) and van Genucthen (1980) relationships. Several additional relationships of note are discussed at the end of this section.

While early work in the development of constitutive relationships was based on simplified representations of pore structure and probability distributions of pore shapes, the developments that are used today in numerical simulations are predominately empirical relationships based on laboratory data. As it is extremely difficult to conduct experiments to generate RHC curves in the lab, the parameters generated from the P-S relationships are typically used in a related RHC function. It should also be noted that during the lab experiments it was observed that P-S curves are hysteretic, such that the saturation value at a given pressure head is also a function of the wetting-drying history of a system. When a soil is drained from full saturation (i.e., no entrapped air) to residual saturation the resulting curve is called the primary drainage curve. The subsequent rewetting follows a different curve called the primary imbibition curve, and will not reach full saturation due to the presence of entrapped air. Subsequent wetting and drainage curves will follow scanning curves between these two main curves. Figure A.1 shows a typical schematic for these curves, starting with drainage from fully saturated conditions. Although mathematical relationships have been generated to represent this hysteretic behavior, they are extremely complex and difficult to implement. Typically only those parameters representing the main drainage curve are used in numerical simulations. It is noted here that due to the non-unique relationship between pressure head and saturation, the RHC will be non-unique if written in terms of pressure head. Therefore, the RHC functions given herein are singular, as they are written in terms of saturation.

Brooks and Corey (1964) presented one of the first sets of paired constitutive relationships based on empirical data collected during oil and gas experiments in sandstone. These relationships were written in terms of capillary pressure (P_c), the difference in pressure between the wetting and non-wetting phases ($P_c=P_{nw}-P_w$). It also noted that the effective saturation (S_e) parameters used in the description is defined as follows:

$$S_e = \frac{S_w - S_{wr}}{1 - S_{wr}} \tag{A.12}$$

where S_w is the given wetting fluid saturation, and S_{wr} is the residual saturation of the wetting fluid in the porous media. Given that definition, the Brooks and Corey equation for effective saturation is given by:

$$S_e = \left(\frac{P_c}{P_d} \right)^{-\lambda} \quad \text{for} \quad P_c > P_d$$

$$S_e = 1 \quad \text{for} \quad P_c \leq P_d \tag{A.13}$$

P_d and λ are both empirical curve fitting parameters. P_d is displacement pressure (the capillary pressure at which soil pores begin to desaturate. Some examples of Brooks and Corey pressure saturation curves are given in Figure A.2(a-b). On the Brooks and Corey P-S curve, P_d is the point at which a sharp transition occurs between tension saturated and unsaturated conditions. This value is largely a function of the radius of the largest pores. As the largest pore size increases, the material will begin to drain at lower capillary pressures; for an example see Figure A.2(a). The parameter λ is a pore size distribution index that affects the shape of the soil moisture curve above the displacement pressure point. Smaller values of λ result in a more gradual transition from full to residual saturation, typical of materials with a large pore (or grain) size distribution. If λ is small there will be a small sub-set of pores which drain with each progressive increase in capillary pressure. If the pore size distribution is more uniform, λ will be large, and the transition from full to residual saturation will be abrupt, such that a large percentage of the pore may drain at a single capillary pressure value. For an example, see Figure A.2(b).

Brooks and Corey developed an equation for RHC based on their representation of the P-S curve and the hydraulic conductivity theory of Burdine (1953). The resulting hydraulic conductivity function is given as follows:

$$k_r = S_e^{\left(\frac{2+3\lambda}{\lambda} \right)} \tag{A.14}$$

It was noted by Brooks and Corey (1964) that this relationship is non-unique or hysteretic as effective saturation is a non-unique function of capillary pressure.

An alternative formulation for the P-S curve was presented by van Genuchten (1980) based on

air-water drainage experiments conducted on a range of agricultural soils. This function is written in terms of pressure head and, in contrast to the Brooks and Corey function, is continuous at the top of the saturated zone. The equations for effective saturation are written as follows:

$$S_e = \left(1 + \left|\alpha\psi\right|^n\right)^{-m} \qquad \text{for} \qquad \psi < 0$$

$$S_e = 1 \qquad \text{for} \qquad \psi \geq 0 \tag{A.15}$$

The term *n* is a pore size distribution. Higher values of *n* coincide with a narrower pore size distribution, resulting in a faster rate of change in saturation as capillary pressure changes. The parameter *m* is related to *n* by *m=1-1/n*. The van Genuchten soil moisture curve features a smooth transition between tension saturated and unsaturated conditions. As this transition is gradual, the van Genuchten formulation tends to be most suited to soils with wider pore size distributions. The capillary pressure at which this transition takes place is controlled by α. For soils with a narrow pore size distribution, α is the inverse of P_d (van Genuchten, 1980). Figure A.3 (a-b) shows a typical van Genucthen function, as well as the effect of variations in the two main parameters on the shape of the curve.

In the development of a RHC function van Genuchten (1980) made use of the Mualem (1976) representation of hydraulic conductivity as it proved to be more accurate than the Burdine (1953) representation. The resulting RHC takes the form:

$$k_{rw} = (S_e)^{1/2}\left\{1 - \left[1 - (S_e)^{1/m}\right]^m\right\}^2 \tag{A.16}$$

where m is taken from the fit of the pressure-saturation relationship. Figure A.4 shows both the van Genuchten and Brooks and Corey RCH for Borden sand. Note that the differences are quite subtle.

While this discussion has focused on the constitutive relationships of Brooks and Corey and van Genuchten, there are numerous others that could also be used (a detailed discussion can be found in Barbour (1998)). As mentioned earlier, Gardner (1958) presented a simple exponential decay function for both the P-S curve and the RHC. This form of simplified function is easily linearized, making it useful in semi-analytical solutions, such as those discussed previously, allowing for numerical simulations with reduced computational effort. However, the computational advantage offered in numerical simulations is not significant enough to outweigh the poor representation of actual pressure saturation curves, for which the Brooks and Corey, and van Genucthen curves provide closer matches to data collected for a wide range of soils. Moench (2008) made use of the Assouline (2001) RHC relationship in numerical simulations of the Bevan et al. (2005) data sets. This relationship is used in

conjunction with the Brooks and Corey P-S curve, using the pore size distribution (λ) parameter from the P-S curve, along with an additional parameter (η), which is not used to describe the soil moisture curve. Assouline (2001) states that η is a function of soil structure and texture. The parameter is determined through an empirical relationship with the coefficient of variation of the P-S curve for the soil, and parameter values range from 0.39 to 2.78 (Assouline, 2001). Although Moench (2008) found that the flexibility of an additional parameter in the Assouline (2001) model allowed for better fits to the data from the Bevan test, the value of η required to fit the data was well outside of the range given in the equation development. As the addition of the η parameter requires additional approximations and the empirical relationship is based on a limited number of data sets (8), the Assouline (2001) equation is less commonly used.

The preceding discussion has focused solely on the flow of water and has only given one set of equations representing the water phases. In any partially saturated media, air, a second phase, is always present. As the density and viscosity of air are much less than that of water, in most variably saturated modeling it is assumed that the air phase is infinitely mobile. An infinitely mobile air phase implies that no pressure gradients are supported by air, allowing for the assumption that air-phase pressure is equal to atmospheric pressure throughout the system. There are cases where this assumption does not hold and a multiphase flow model may provide a closer match to observations. Multiphase flow models work on the same principals as the single phase flow models discussed previously; however, a set of equations is required for each phase, be it gas or liquid. These additional sets of equations increase computational time significantly. Given the computational limitations these types of models are mostly reserved for multi-phase flow problems in which a third, non-aqueous phase liquid (NAPL) is present. As these liquids are far less mobile than the water phase, it is essential that their flow be accounted for. In the case of an air-water system, the flow of air is of most interest when air loses a connected pathway to the atmosphere, and becomes entrapped, allowing pressure to build. This condition can happen during progressive wetting and drying cycles. If the air phase becomes disconnected, it must dissolve into the aqueous phase before water can reoccupy the pore. This process has the potential to decrease both saturation and hydraulic conductivity for a given pressure head, and plays a role in hysteretic behavior. In unconfined aquifers in Ontario, Ryan et al. (2000) found that this phenomenon reduced hydraulic conductivity by 35 times in the zone of entrapped air. In a constructed heterogeneous system, Silliman et al. (2002) found that limited air phase flow can lead to the formation of air-entry barriers which prevent the drainage from coarse soils. This introduction serves as a reminder that even state-of-the-art numerical simulations techniques are still an approximation of the actual flow system.

A.4 Conceptual Understanding

While the previous sections have focused on methods used to simulate the shape of the time drawdown curve generated during unconfined pumping tests, none of these techniques have provided a solid conceptual explanation for the resulting shape. The debate over the processes which influence the shape of the curve began in the late 1970's, and continues to the present. While much more time in literature has been devoted to refinement of analytical solutions, the development of a proper conceptual understanding of the unconfined response to pumping is an important step in completing our general understanding of processes in unconfined aquifer, and will help to provide more accurate predictions of unconfined response to a variety of stressors. The following section will provide an overview of the development of the conceptual understanding of the unconfined response, from initial discussions to the most current publications.

The conceptual understanding of the unconfined response to pumping can be divided into two categories, those which posit that the variably saturated zone has significant impact and those that do not. Neuman (1975) supported the notion that unsaturated flow does not play a significant role in the unconfined response by attempting to relate the Boulton (1963) α parameter to known aquifer parameters such as hydraulic conductivity and storativity. It was found that α was also a function of radial distance from the well, suggesting that the parameter is not a constant of the aquifer material (Neuman, 1975). By adapting the α parameter for use in the Neuman (1972, 1974) solution, which neglects unsaturated flow, Neuman (1975) concludes that the Boulton (1963) α does not necessarily represent unsaturated flow contributions. Using the work of Stretslova (1973) and Krosynski and Dagan (1975) as support, Neuman (1979) again suggests that unsaturated flow has no impact on the second phase of the unconfined response curve. It is instead proposed that the initial high drawdown portion of the curve represents the flow contribution from elastic storage, while the second phase begins as the water table begins to fall and gravity drainage above the falling water table is initiated. The final portion of the curve represents the time at which elastic storage is exhausted, and the water is derived solely from gravity drainage as the water table continues to fall (Neuman, 1979). This theory forms the basis of the argument that unsaturated flow has an insignificant impact on the second phase of the unconfined aquifer response. The shape of the response curve is instead attributed to the transition from a contribution to flow from storage to a contribution to flow from gravity drainage.

Conceptual models which incorporate the influence of the unsaturated zone were initially related to aquifer material conditions, which were extremely specific and not easy to generalize. Boulton (1954) proposed two possible explanations for the shape of the unconfined response curve, both of which rely on the presence of finer grained compressible materials either overlying the aquifer, or interbedded within the aquifer material. Bouwer and Rice (1978) suggested the possibility that a fine layer overlying the aquifer material would limit air mobility, forming an air-entry barrier, and thus

preventing the aquifer from dewatering until the air entry pressure of the finer material was reached. Bouwer (1979) proposed that hysteresis could play a role in the delayed drainage phenomenon as the moisture profile transitions from a pre-pumping imbibition curve to a drainage curve. Of course, all of these situations would result in delayed drainage during pumping; however, the prevalence of the delayed drainage response in aquifers that do not fit in these specific situations suggests that a more general explanation is possible.

Support for the effect of delayed drainage in more general cases grew following the pumping test completed by Nwankwor et al. (1984). By using the volume of the drawdown cone and the volume of water pumped, Nwankwor et al. (1984) were able to estimate a specific yield much closer to that determined in the laboratory, and suggested that the significant underprediction of specific yield by the Neuman (1974) analytical solution was due to the assumption of instantaneous drainage, and exclusion of unsaturated flow. In response, Neuman (1987) suggested that the specific yield determined in the laboratory is not representative of that which is in effect during pumping due to the much shorter time scale. Neuman (1987) argues that the large specific yield values obtained using volume balance methods are erroneous as they place a finite boundary on a theoretically infinite domain. Neuman (1987) concluded delayed drainage does not need to be included in analytical solutions to produce accurate estimates of specific yield. The subsequent pumping test completed by Nwankwor et al. (1992) provided observations of vadose zone effects that support the delayed drainage phenomenon. By observing the downward vertical gradients that form above the water table early in pumping, they were able to document excess storage above the water table due to the pressure saturation relationship for the sand. The beginning of the second phase of the time drawdown curve was found to coincide with the reduction of the vertical gradient, and thus the dissipation of the excess storage. These observations support the notion of non-instantaneous drainage from above the water table during pumping, and suggest the importance of including vadose zone effects in the simulation of unconfined aquifers.

The pumping test observations of Bevan et al. (2005) again called for an improved conceptual model of the unconfined response to pumping, as the extension of the capillary fringe (or persistence of excess storage) appears to be independent of the occurrence of the second phase of the time drawdown curve. The potential causes of this phenomenon are discussed in detail in the main sections of this thesis. Numerical analysis of theoretical pumping tests by Mao et al. (In Press) has provided some additional insights into the second phase of the time drawdown curve. Using both a two-dimensional axial symmetric numerical model, and a one-dimensional model Mao et al. (In Press) investigated the change in storage in an aquifer at different locations and at different times during pumping simulations. The two-dimensional model results show that initially the change in water volume per unit area is concentrated near the pumping well, indicating that the contribution to the well is from elastic storage

below the water table. As time progresses, the greatest change in storage was found to occur near the water table, indicating the contribution of drainage from above the falling water table. The one-dimensional model shows that the three stage unconfined drawdown curve will occur both in the absence of horizontal flow, and in the absence of an unsaturated zone. Mao et al. (Press) conclude the paper by stating that the delayed yield term coined by Nwankwor et al. (1992) misrepresents the actual mechanism of transition between elastic storage and gravity drainage. Mao et al. (In Press) also note that the vertical gradients observed by Nwankwor et al. (1992) are solely a result of the partially penetrating well used for the test, and are not the cause of the so called delayed drainage portion of the time drawdown curve.

Given the history of the conceptual understanding of the unconfined response to pumping, it is clear that some controversy surrounds the cause of both the inflection point in the time drawdown curve and the factors which influence the shape of the curve through the second phase of the pumping response.

A.5 Figures

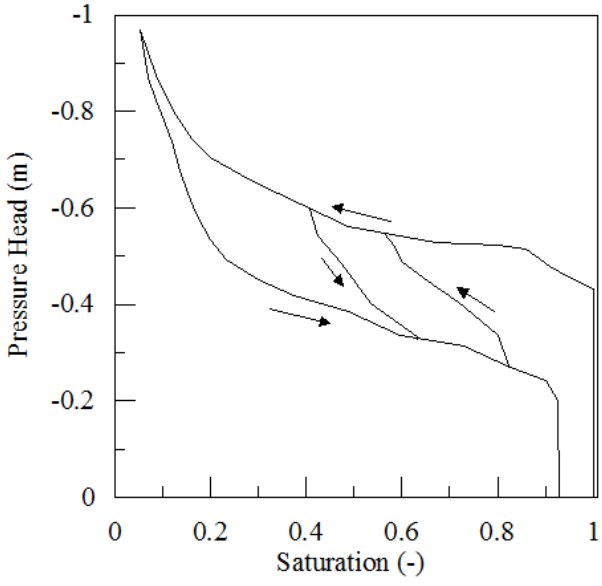

Figure A. 1. Example hysteretic pressure-saturation curves including a single scanning loop

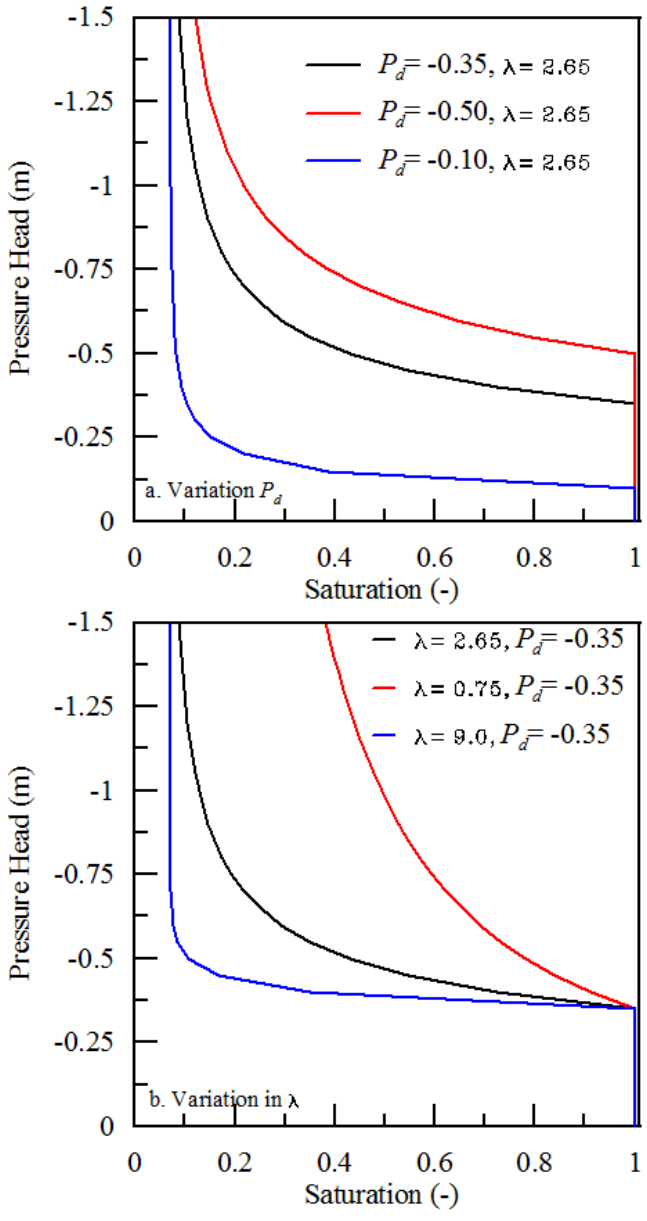

Figure A. 2 (a-b). Example Brooks and Corey pressure-saturation curves showing the effects of parameter variation (a. Variation in P_d, b. Variation in λ)

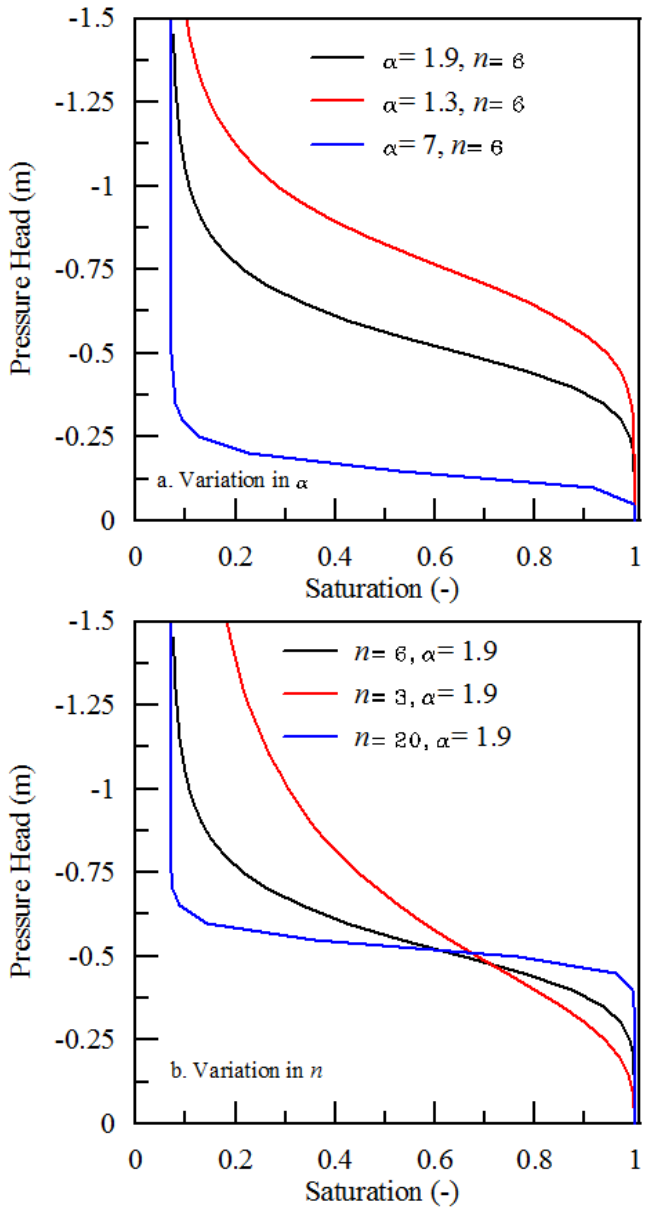

Figure A. 3(a-b). Example van Genuchten pressure-saturation curves showing the effects of parameter variation (a. Variation in α, b. Variation in n)

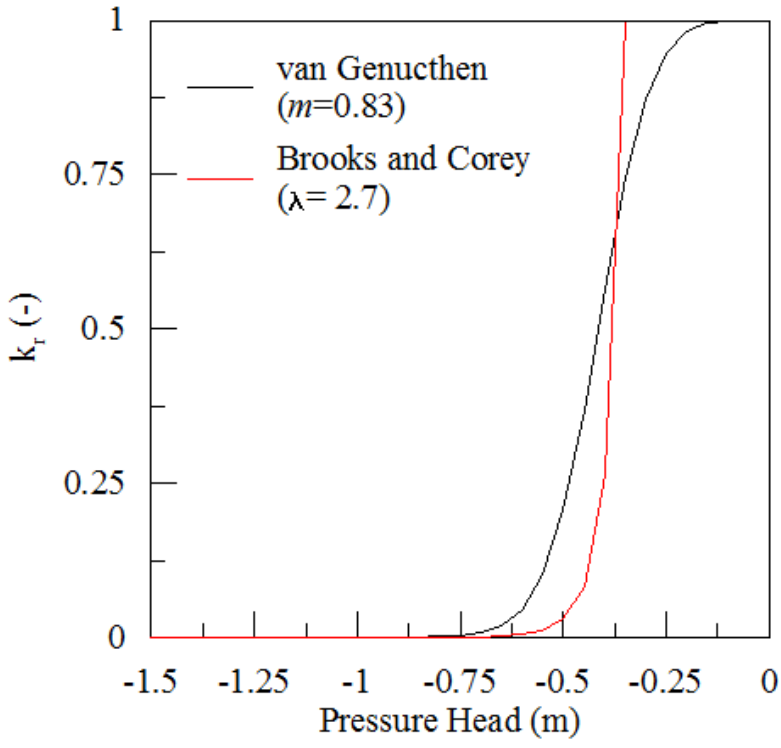

Figure A. 4. Example residual hydraulic conductivity functions for a Borden type sand.

Appendix B

A Comparison of Numerical Predictions and Observed Vadose Zone Response to Pumping in an Unconfined Aquifer

Prior to the initialization of the heterogeneous numerical experiments detailed in Chapter 3, three numerical codes of varying sophistication (VS2D, Integrated Hydrogeology Model and HydroGeoSphere) were used with a homogeneous conceptual model to analyze the heavily instrumented seven-day pumping test performed in the unconfined aquifer at Canadian Forces Base Borden, Ontario by Bevan et al. (2005). VS2D is a two-dimensional finite difference code, capable of simulating three-dimensional flow in an axial-symmetric system. InHM and HGS are both fully-integrated surface water/groundwater codes with rigorous subsurface flow and transport capabilities in three-dimensions. All three codes use Darcy's law and Richards' equation to describe variably saturated flow in the subsurface.

Numerical simulations of the pumping test were implemented in both InHM and HGS using the same 400 m x 400 m x 9 m finite element grid described in Chapter 3. The two-dimensional axial-symmetric grid used in VS2D consisted of 184 columns and 165 rows. Vertically, the grid was spaced at 0.05 m from the aquitard to 1 m BGS, and at 0.25 m from 1 m BGS to the ground surface. Horizontally, a minimum grid spacing of 0.01 m was implemented near observation points and the pumping well, while a maximum grid spacing of 5 m was implemented near the outer boundary. The VS2D finite difference grid was slightly coarser than the finite element mesh; however, this coarser grid spacing was necessitated by the prohibitively large computational times of finer meshes. As in Chapter 3, a no flow boundary condition was applied at the bottom of the domain for all three codes, simulating the clayey-silt aquitard of the Borden aquifer. The lateral boundaries of the finite element flow domains were located 200 m from the pumping well. Although both no flow and constant head boundary conditions were tested, lateral boundaries had little effect on simulation results; therefore, only those results using the no flow boundary conditions on the sides of the finite element domain are presented in this study. For consistency the outer boundary of the axial symmetric finite difference grid in VS2D was treated as a no flow boundary.

Table B.1 lists the hydrologic parameters used to populate all simulations. The values of these parameters are based on previous studies conducted at the Borden test site. No test specific calibration was performed due to the goodness of fit between the simulated and observed drawdown values.

Figures B.1(a-c) and B.2(a-c) show the numerical results and hydraulic head data at three radial distances (3, 5, and 15 m) from the pumping well for the shallow and deep piezometers, respectively, when the Brooks and Corey constitutive relationship is used. Figures B.3 (a-c) and B.4(a-c) give the

corresponding comparison between the numerical results and field observations when the van Genuchten (1980) constitutive relationship is used. It is clear that the hydraulic head drawdown results are relatively insensitive to the type of constitutive relationship used.

The results generated by the InHM and HGS simulations provide the closest match to hydraulic head data; the VS2D results tend to under predict hydraulic head drawdowns. The minor variations between HGS and InHM for specific piezometers can likely be attributed to differences in methods used to numerically implement the pumping wells in each code. Variations between VS2D and the two other codes are likely due in part to the coarser mesh.

In addition to piezometer data, model predictions and field estimates of the water table (i.e., the surface where pore pressure is equal to atmospheric pressure) drawdown were compared. Water table drawdown was inferred from the numerical codes by tracking the zero pressure isobar. For the field observations, water table drawdown was estimated for the piezometer pairs at 3, 5, and 15 m in the manner described by Bevan et al. (2005). Figures B.5 (a-c) and B.6 (a-c) show the field estimates and model predictions of the water table drawdown using the Brooks and Corey and van Genuchten relationships, respectively. For this comparison, the times shown correspond to the neutron profiling events. Again, the simulated results are insensitive to the choice of constitutive relationship. The InHM and HGS results provided a better approximation of the field estimates; the VS2D results tended to under predict water table drawdown. All simulations resulted in a slight under prediction of the water table drawdown at 15 m. These results may be due in part to small-scale stratigraphic variations in this aquifer.

In general, it can be seen that the numerical simulations produce reasonably accurate fits to both the hydraulic head and water table drawdown observed in the field. The hydraulic head drawdown results generated by InHM and HGS compare well with those obtained by Endres et al. (2007) using optimized analytical solutions. We attribute the small systematic misfits between field observations and simulations results primarily to small-scale stratigraphic variations in this aquifer.

Simulated soil moisture profiles (i.e., θ_w as a function of elevation above the water table) were compared to the soil moisture profile obtained from the neutron moisture probe data. Figure B.7(a-c) shows this comparison for the pre-pump (i.e., static) condition at time $t = 0$ for simulations using the Brooks and Corey constitutive relationship. The corresponding comparison for simulations using the van Genuchten relationship is given in Figure B.8(a-c). It can be seen that both constitutive relationships provide good fits to the profile derived from the neutron probe data. Due to its smoothly varying character, the van Genuchten relationship gives a somewhat better representation of the initial field conditions. These results clearly demonstrate that the constitutive relationships based on the

laboratory analysis of saturation pressure head measurements in Borden sand (Nwankor, 1982; Akindunni, 1987; Mickle, 2005) accurately describe the vertical soil moisture distribution in the unstressed aquifer.

The numerical simulations produced a predominately downward translating moisture profile during pumping, where the predicted moisture profile time-drawdown was nearly equal to the corresponding water table time-drawdown. This response differed significantly from the extension of the capillary fringe observed by Bevan et al. (2005). The contrast between the numerical predictions and the field observations is exemplified in the final set of measurements obtained prior to the termination of pumping (i.e., t = 633600 s). Figure B.9(a-c) shows this comparison for the late stage conditions at time t = 633600 s for simulations using the Brooks and Corey constitutive relationship. The corresponding comparison for simulations using the van Genuchten relationship is given in Figure B.10(a-c). These results clearly demonstrate that the numerical codes using either constitutive relationship do not replicate the differential drawdown between the moisture profile and the water table observed in the field data. Figures B.11(a-c) and B.12(a-c) show the observed and predicted capillary fringe extensions using the Brooks and Corey and van Genuchten relationships, respectively. The field data analysis resulted in a significant and persistent capillary fringe extension that increased with both time and proximity to the pumping well (i.e., 0.35 m at 3 m radial distance versus 0.05 m at 15 m radial distance). The numerical results for all simulations show no appreciable extension, and the predicted changes in capillary fringe thickness are on the scale of the grid discretization. These results suggest that while the numerical simulations are able to fully capture the pumping effects throughout the saturated zone, some aspect of the flow regime above the water table are not being captured, either by the conceptual model used for the simulations, or within the numerical codes themselves.

Table B. 1. Parameters used to populate the numerical simulations

Parameter	**Value**	**Source**
Horizontal conductivity (m/s)	6.36×10^{-5}	Endres et al. (2007)
Vertical conductivity (m/s)	3.29×10^{-5}	Endres et al. (2007)
Specific storage (m^{-1})	3.25×10^{-4}	Akindunni and Gillham(1992)
Porosity	0.37	Nwankwor (1984)
Residual moisture content	0.07	Nwankwor (1984)
Brooks and Corey (1964) λ	3.565	Mickle (2005)
Brooks and Corey (1964) P_d (m)	0.43207	Mickle (2005)
van Genuchten (1980) α	1.9	Akindunni (1987)
van Genuchten (1980) n	6	Akindunni (1987)

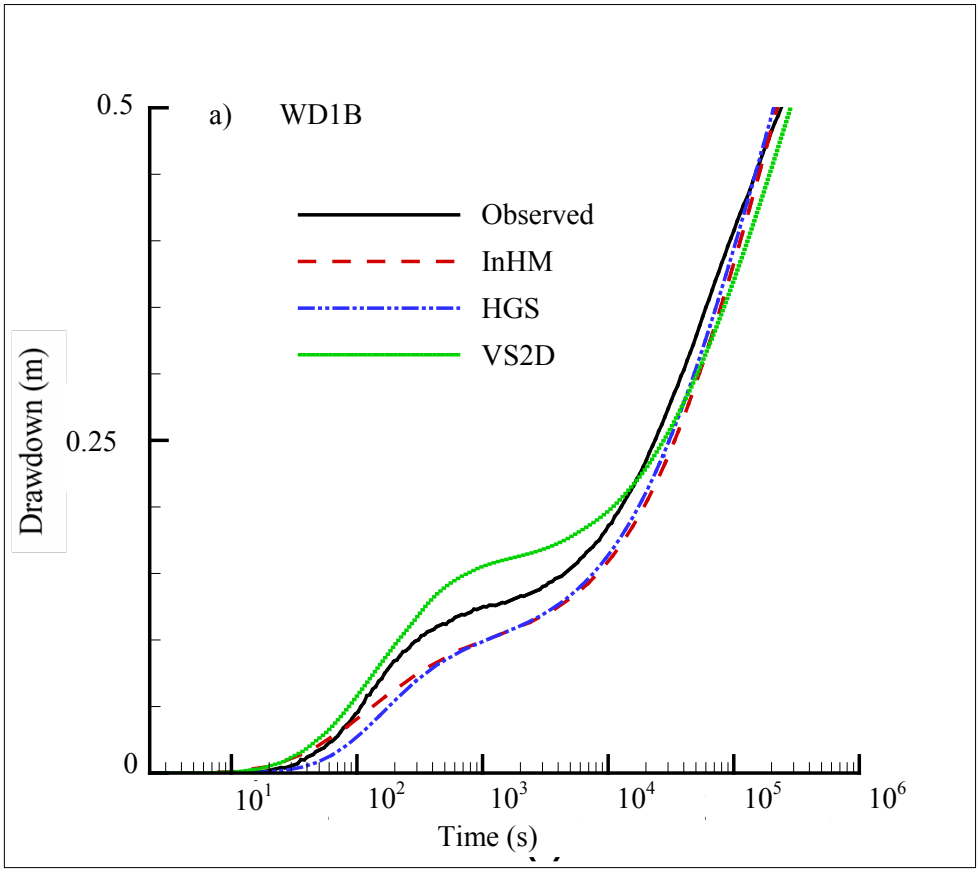
a) WD1B
Observed
InHM
HGS
VS2D
Drawdown (m)
0.5
0.25
0
10^1
10^2
10^3
10^4
10^5
10^6
Time (s)

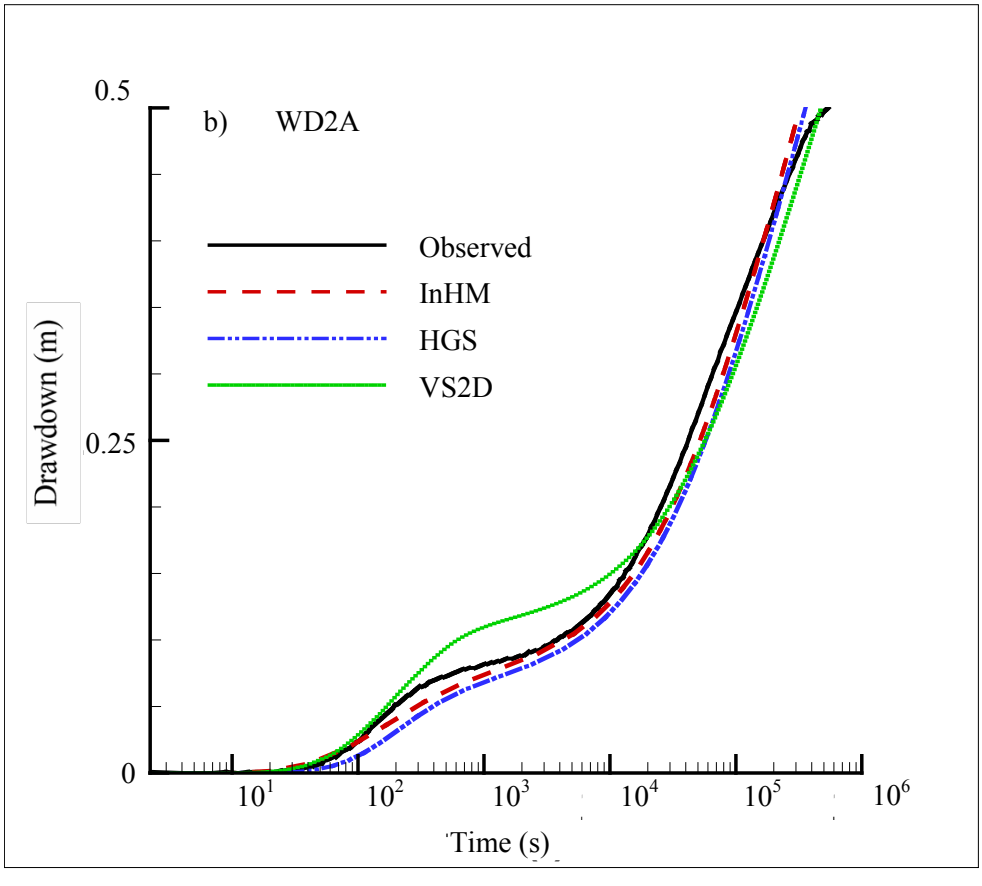
b) WD2A
Observed
InHM
HGS
VS2D
Drawdown (m)
0.5
0.25
0
10^1
10^2
10^3
10^4
10^5
10^6
Time (s)

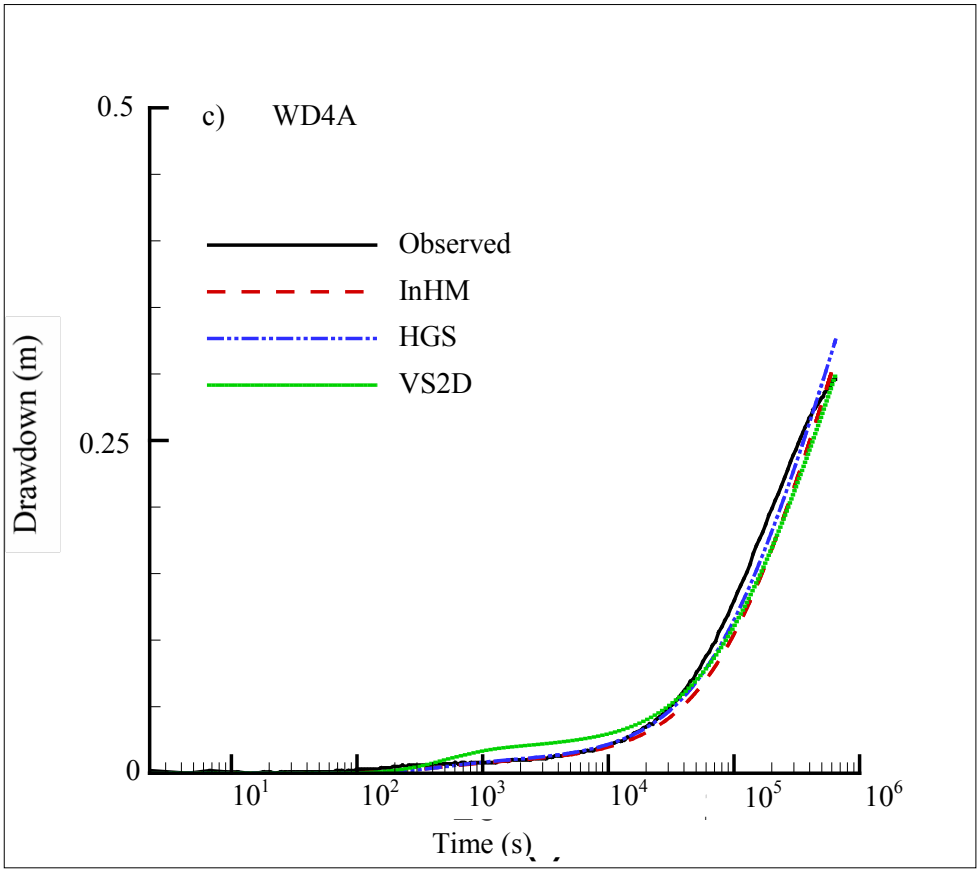

Figure B. 1 (a-c). A semi-log comparison between computed results and field observations of the hydraulic head drawdown in shallow observation wells using the Brooks and Corey constitutive relationship. (Radial distances: a. 3 meters; b. 5 meters; c. 15 meters)

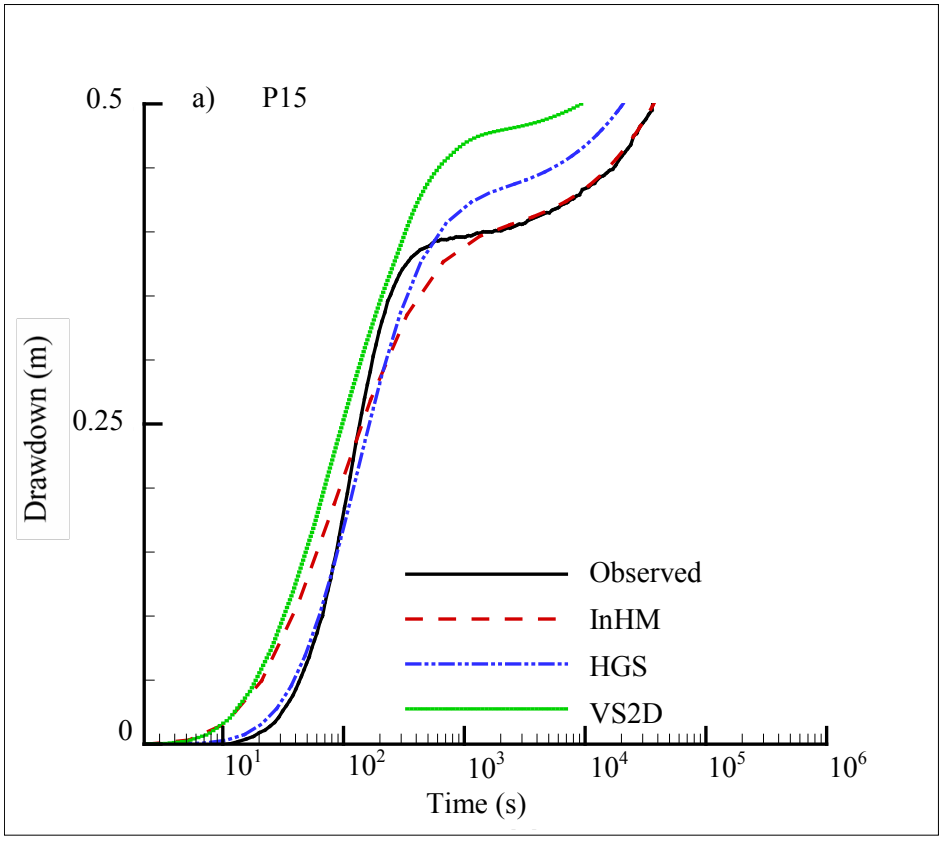
a) P15
0.5
0.25
0
Drawdown (m)
Observed
InHM
HGS
VS2D
10^1 10^2 10^3 10^4 10^5 10^6
Time (s)

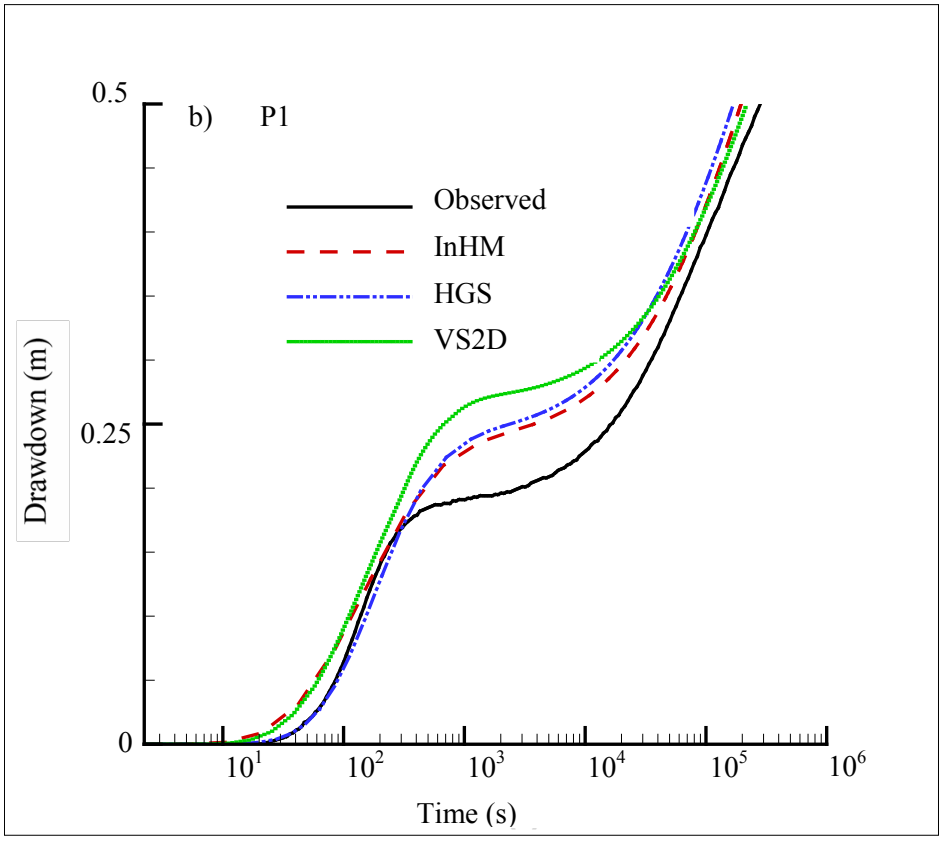
b) P1
0.5
0.25
0
Drawdown (m)
Observed
InHM
HGS
VS2D
10^1 10^2 10^3 10^4 10^5 10^6
Time (s)

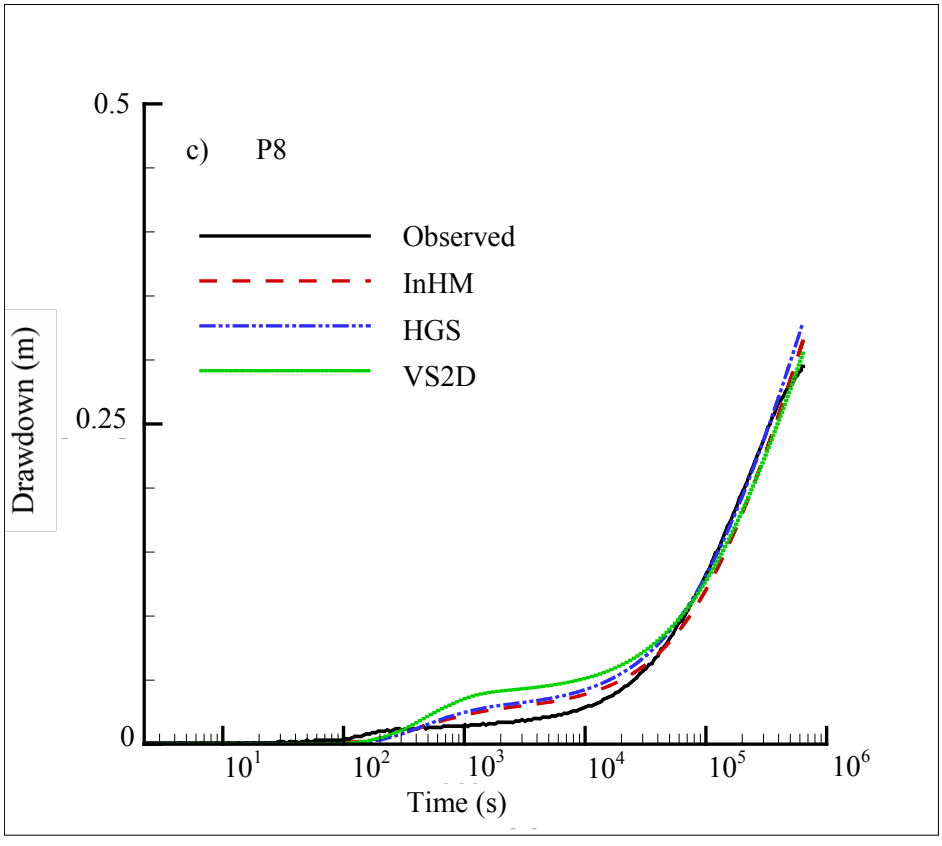

Figure B. 2(a-c). A semi-log comparison between computed results and field observations of the hydraulic head drawdown in deep observation wells using the Brooks and Corey constitutive relationship. (Radial distances: a. 3 meters; b. 5 meters; c. 15 meters)

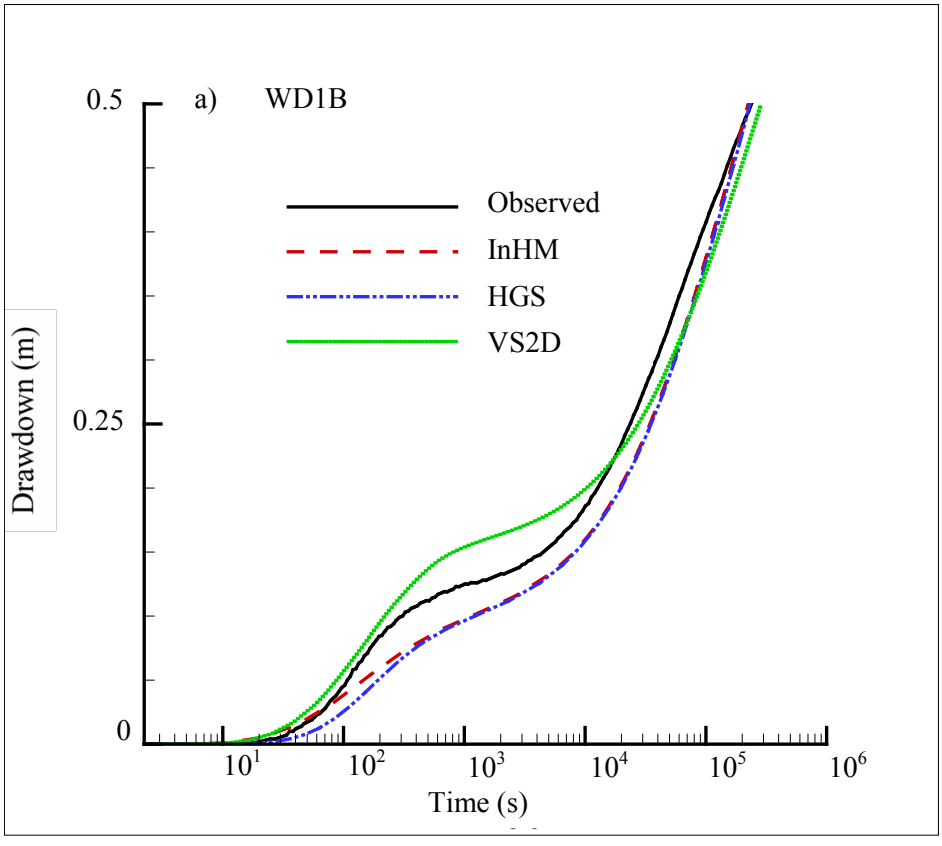
a) WD1B
0.5
0.25
0
Drawdown (m)
Observed
InHM
HGS
VS2D
10^1 10^2 10^3 10^4 10^5 10^6
Time (s)

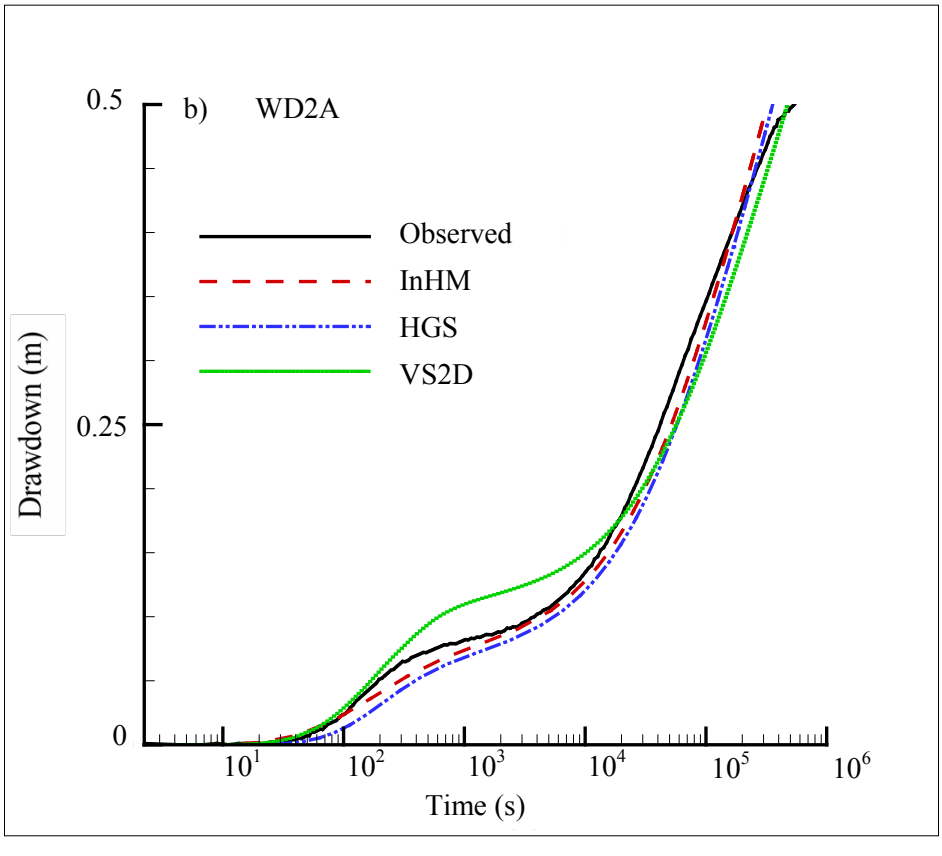
b) WD2A
0.5
0.25
0
Drawdown (m)
Observed
InHM
HGS
VS2D
10^1 10^2 10^3 10^4 10^5 10^6
Time (s)

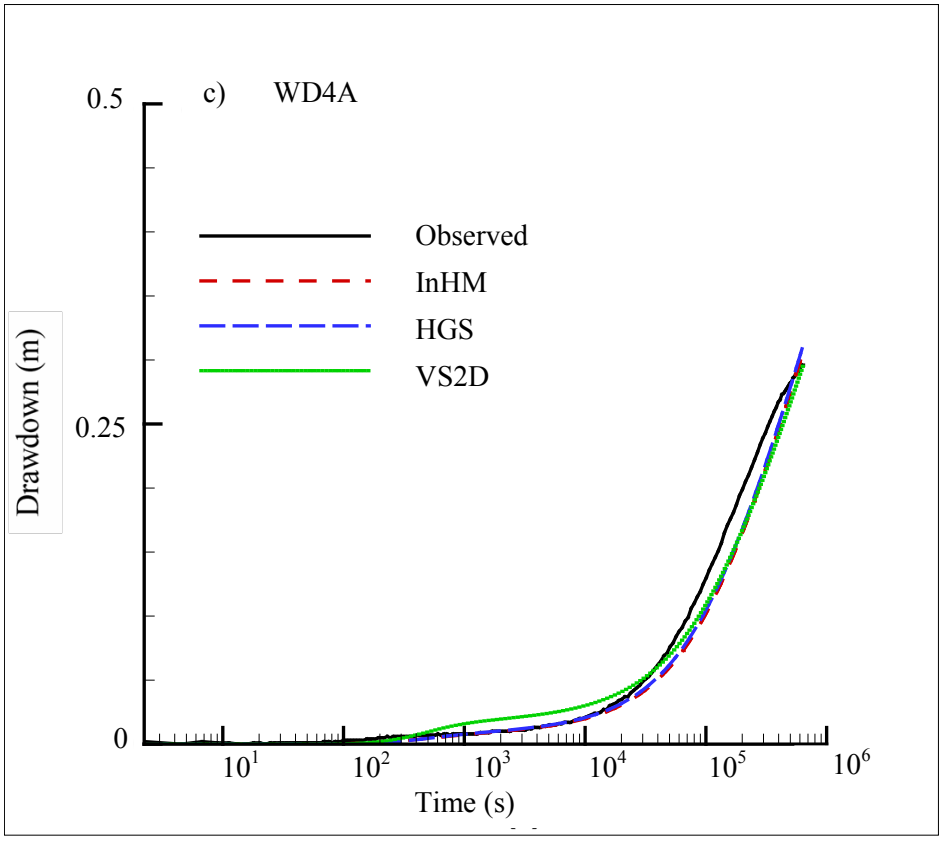

Figure B. 3 (a-c). A semi-log comparison between computed results and field observations of the hydraulic head drawdown in shallow observation wells using the van Genuchten constitutive relationship. (Radial distances: a. 3 meters; b. 5 meters; c. 15 meters)

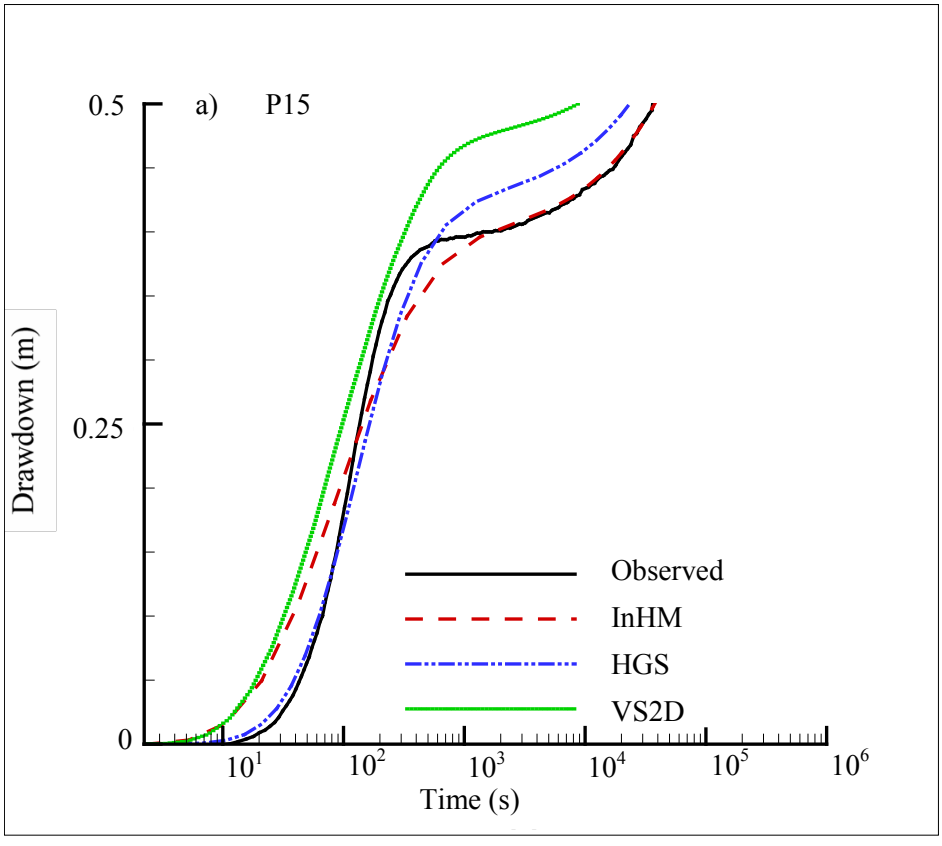
a) P15
0.5
0.25
0
Drawdown (m)
Observed
InHM
HGS
VS2D
10^1
10^2
10^3
10^4
10^5
10^6
Time (s)

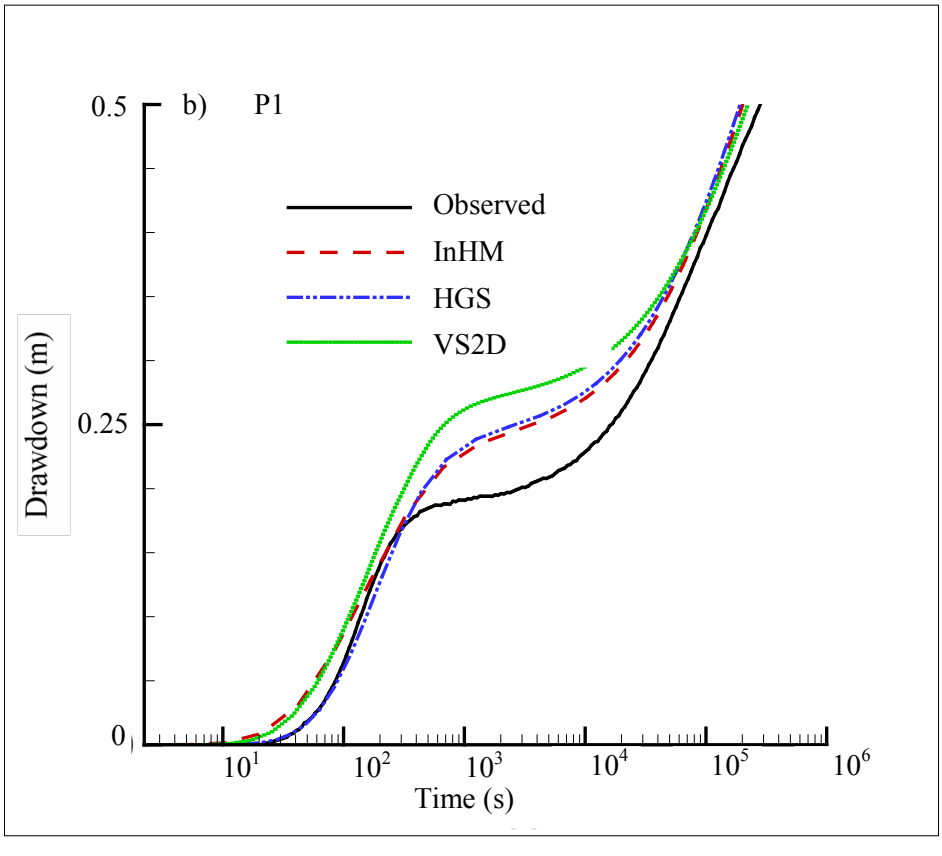
b) P1
0.5
0.25
0
Drawdown (m)
Observed
InHM
HGS
VS2D
10^1
10^2
10^3
10^4
10^5
10^6
Time (s)

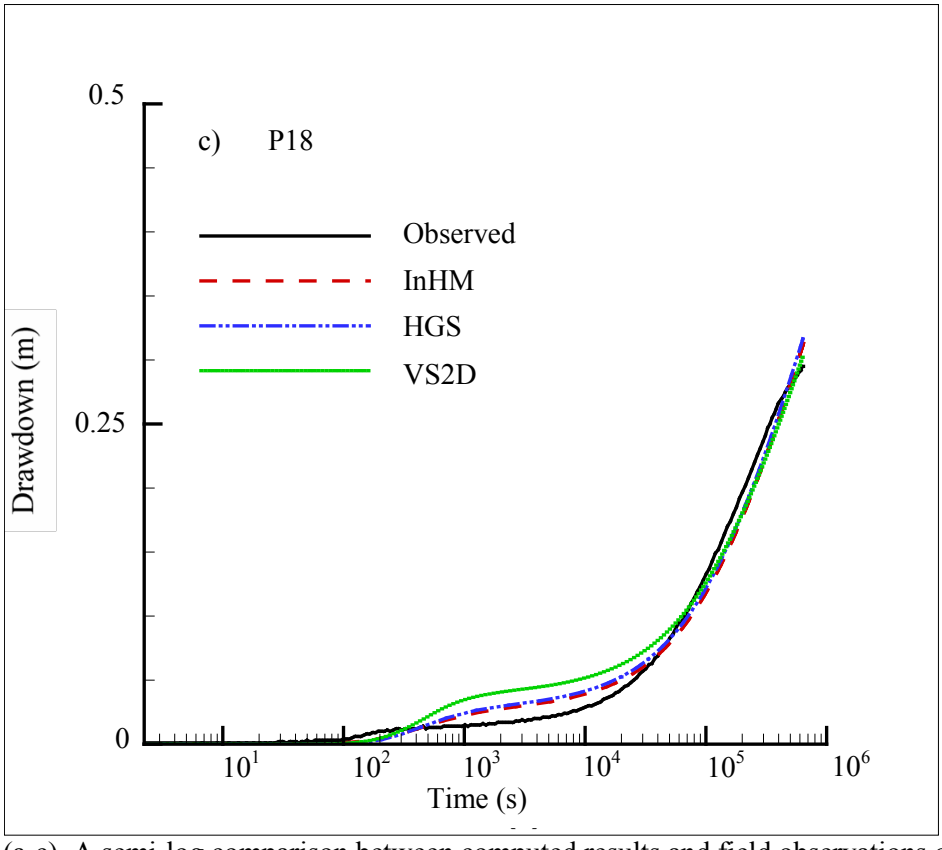

Figure B. 4(a-c). A semi-log comparison between computed results and field observations of the hydraulic head drawdown in deep observation wells using the van Genuchten constitutive relationship. (Radial distances: a. 3 meters; b. 5 meters; c. 15 meters)

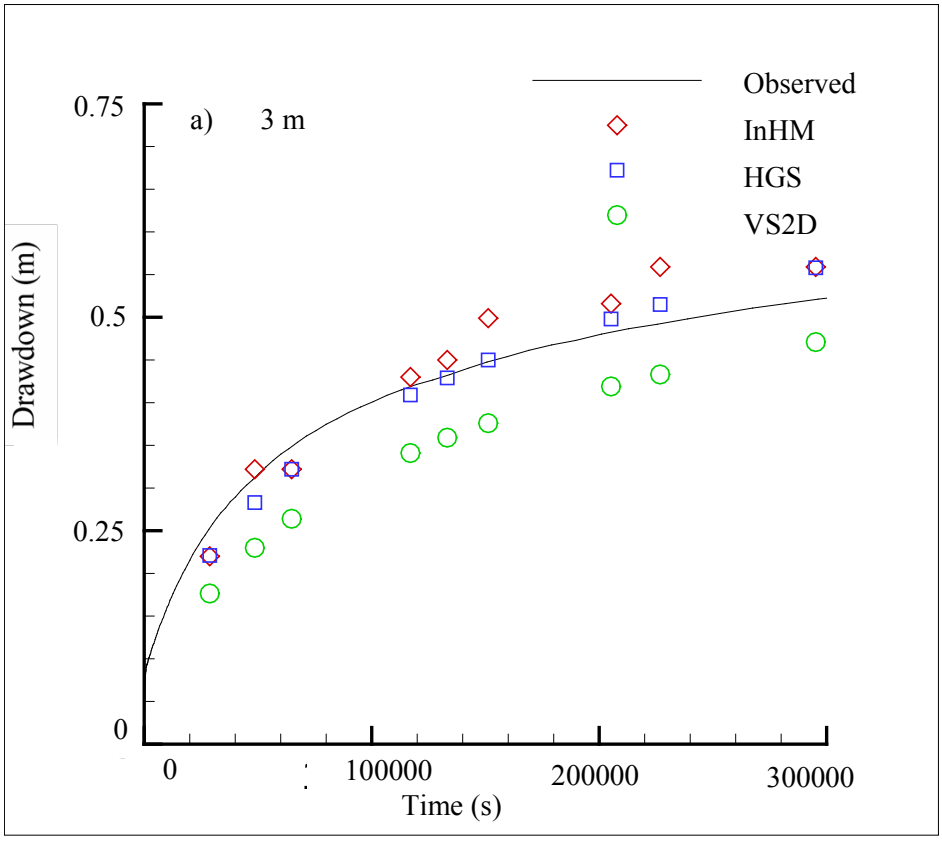
a) 3 m
Observed
InHM
HGS
VS2D
Drawdown (m)
0.75
0.5
0.25
0
0
100000
200000
300000
Time (s)

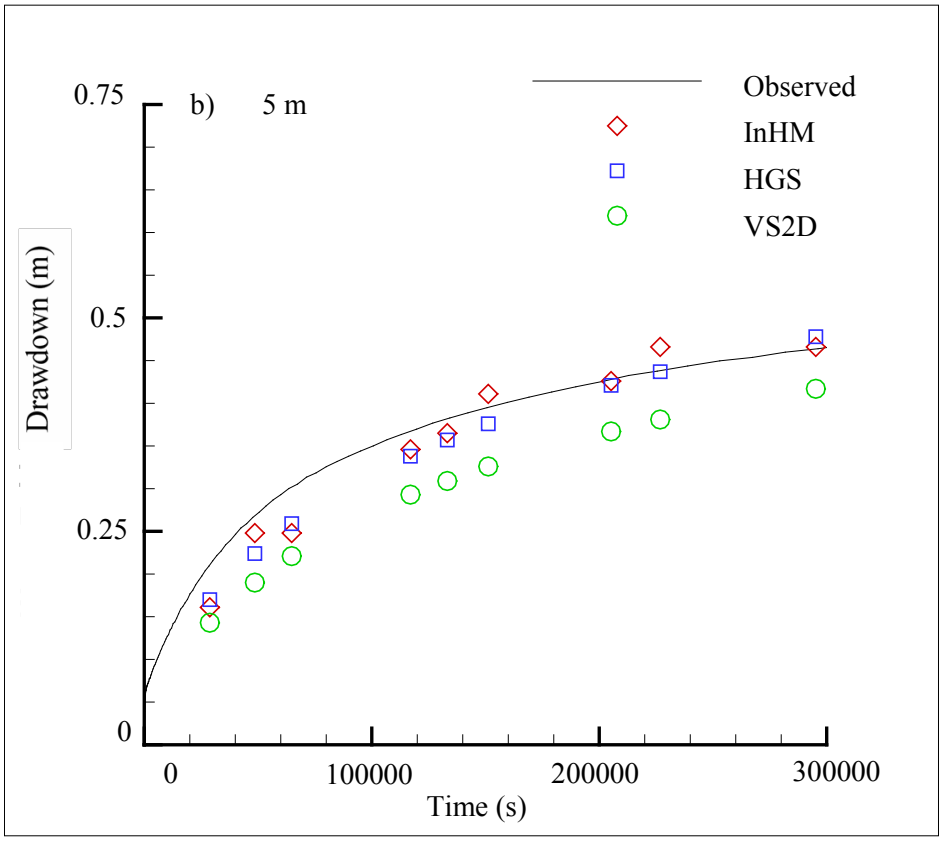
b) 5 m
Observed
InHM
HGS
VS2D
Drawdown (m)
0.75
0.5
0.25
0
0
100000
200000
300000
Time (s)

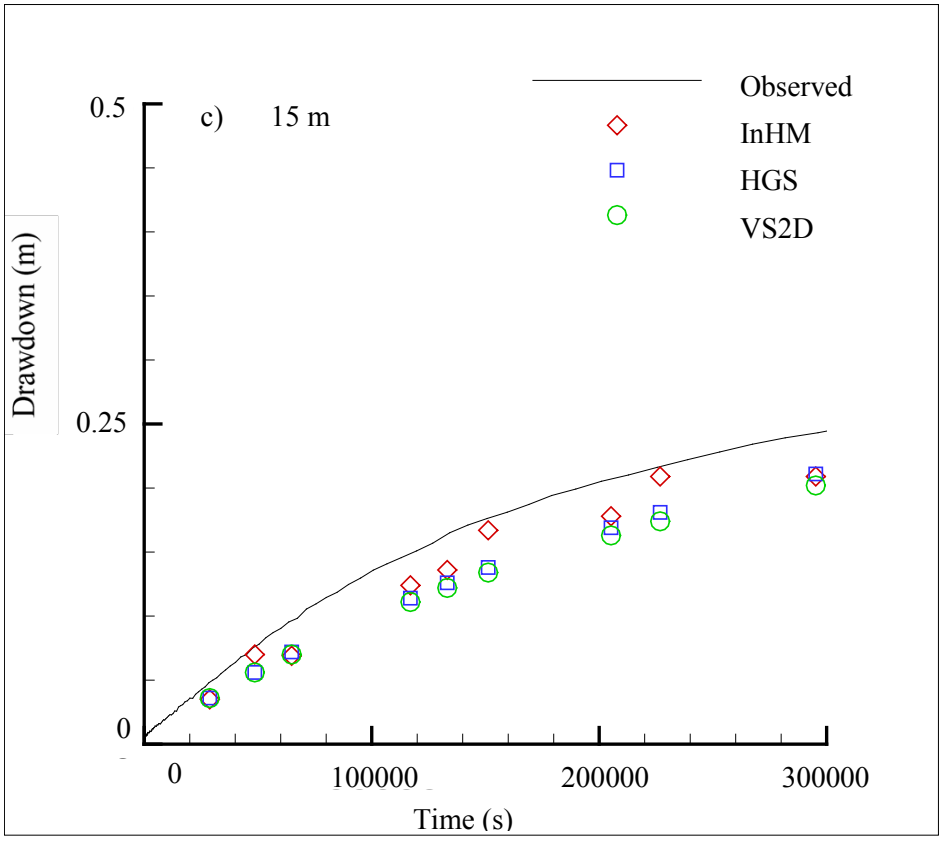

Figure B. 5 (a-c). A comparison between computed results and field estimate of the water table drawdown using the Brooks and Corey constitutive relationship. (Radial distances: a. 3 meters; b. 5 meters; c. 15 meters)

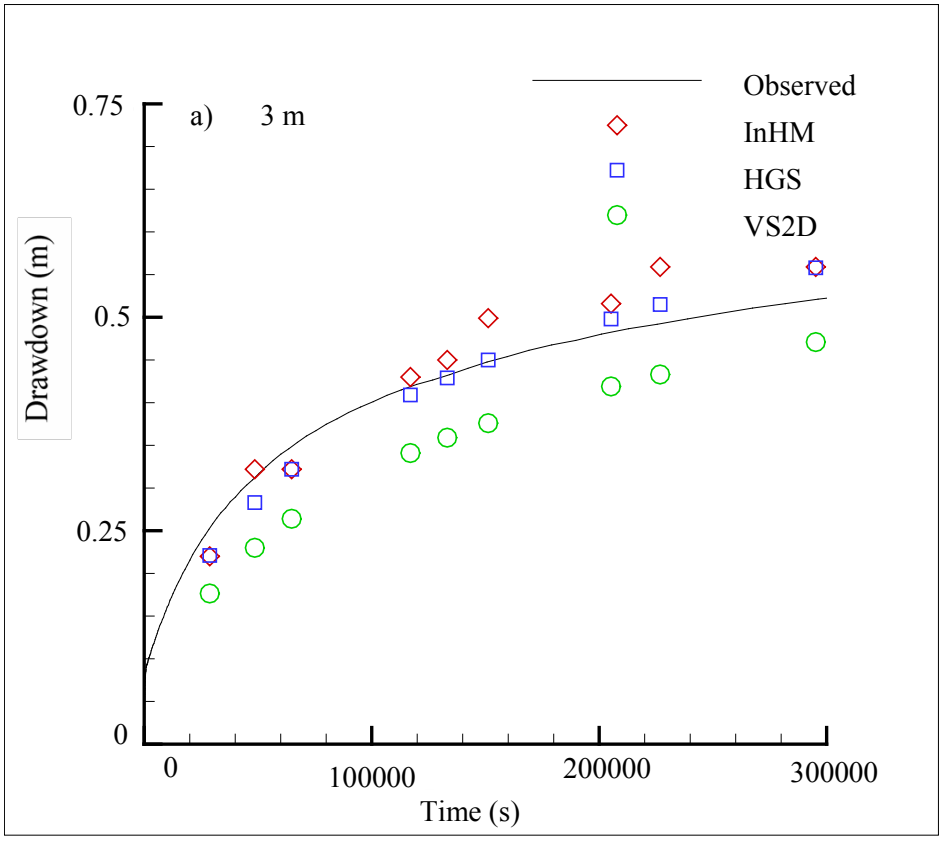
a) 3 m
Observed
InHM
HGS
VS2D
Drawdown (m)
0.75
0.5
0.25
0
0
100000
200000
300000
Time (s)

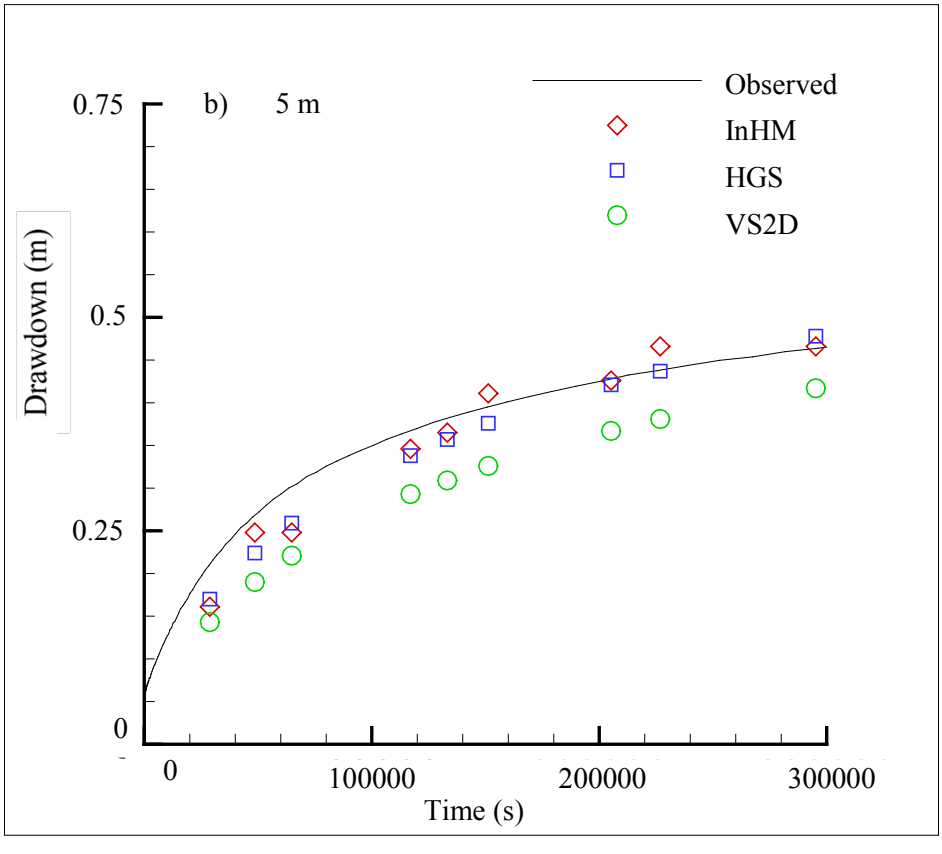
b) 5 m
Observed
InHM
HGS
VS2D
Drawdown (m)
0.75
0.5
0.25
0
0
100000
200000
300000
Time (s)

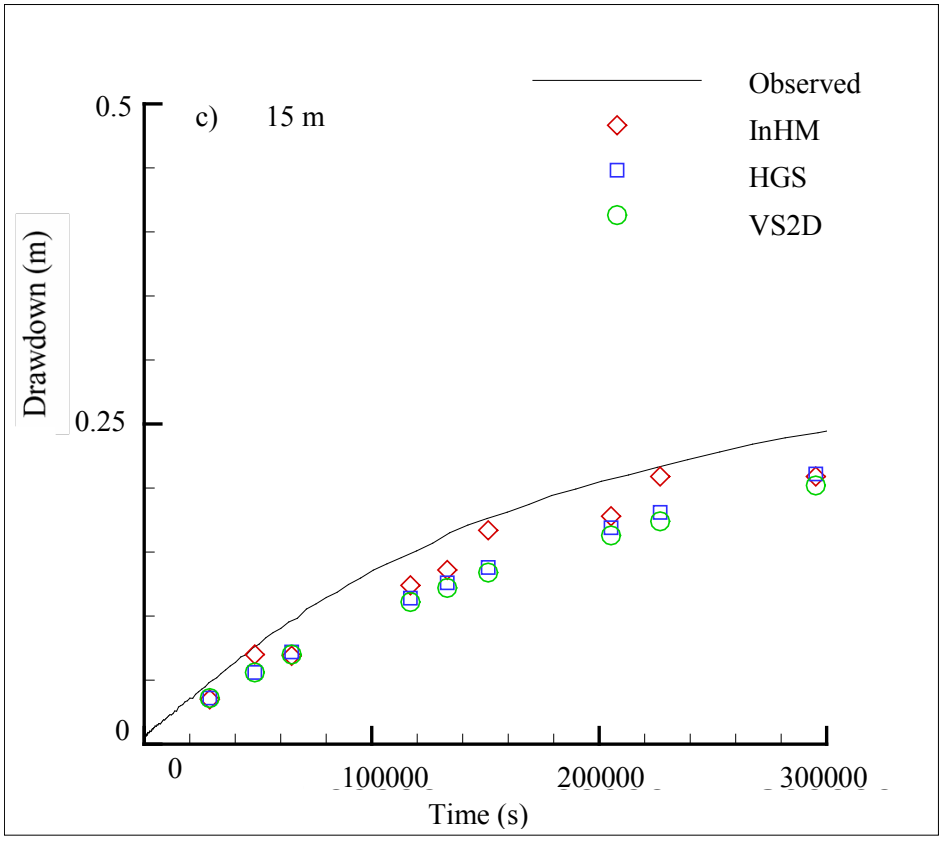

Figure B. 6 (a-c). A comparison between computed results and field estimates of the water table drawdown, using the van Genuchten constitutive relationship. (Radial distances: a. 3 meters; b. 5 24 meters; c. 15 meters)

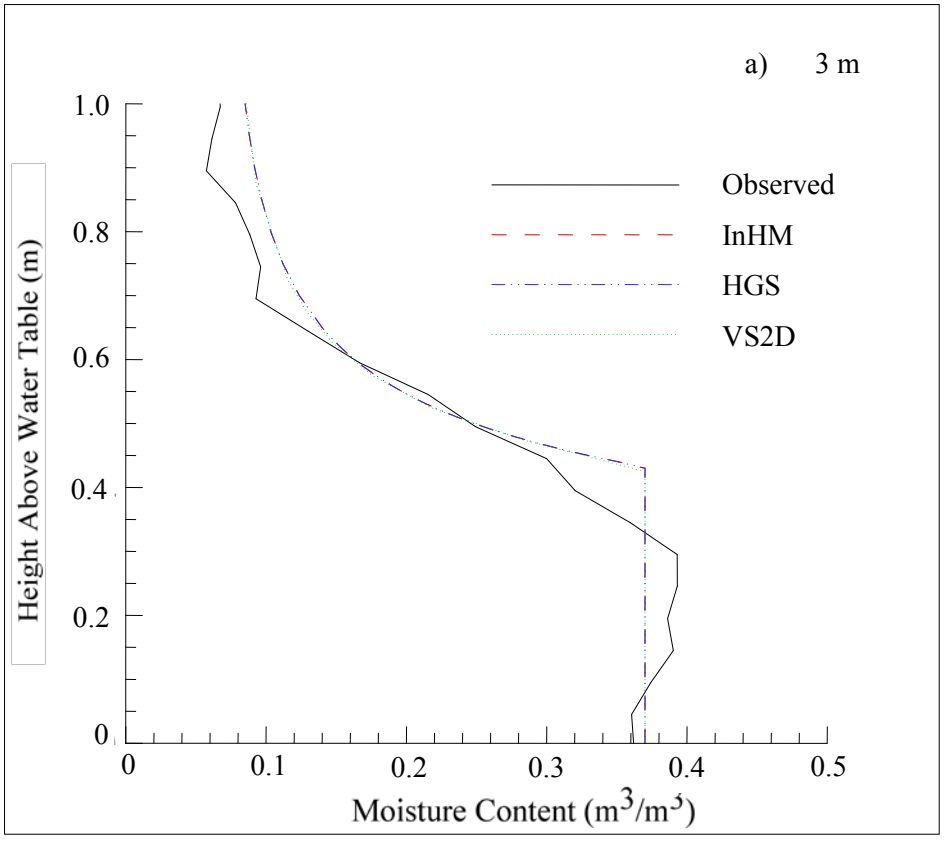
a) 3 m
Observed
InHM
HGS
VS2D
Height Above Water Table (m)
1.0
0.8
0.6
0.4
0.2
0
0
0.1
0.2
0.3
0.4
0.5
Moisture Content (m3/m3)

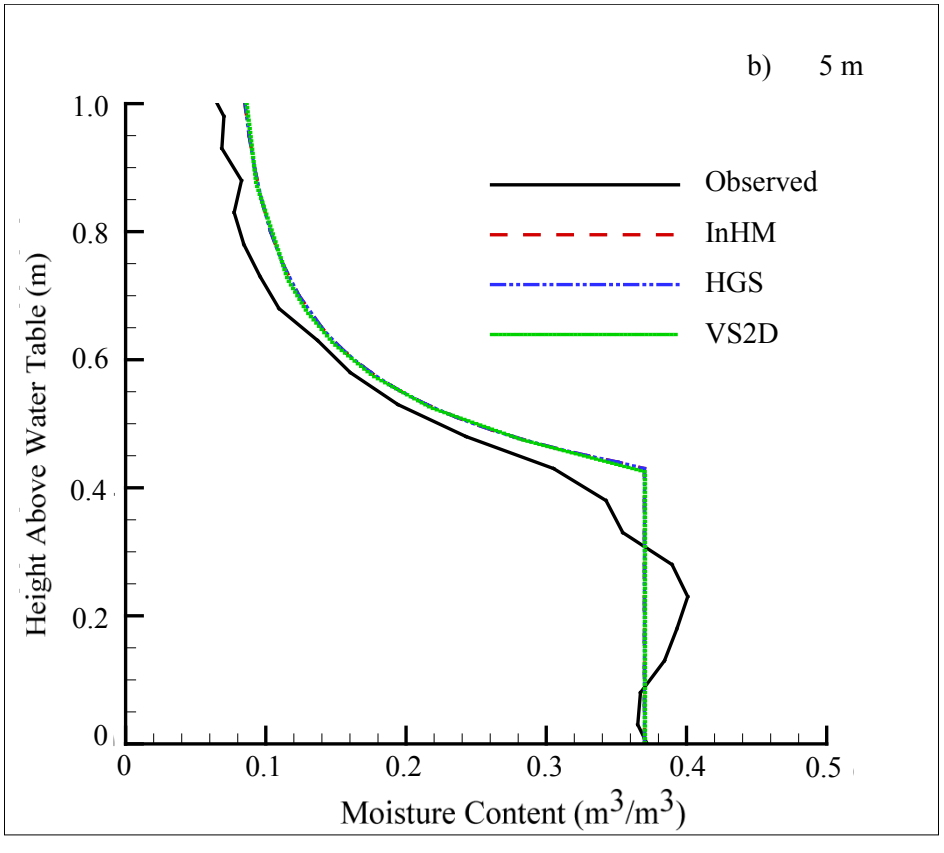
b) 5 m
Observed
InHM
HGS
VS2D
Height Above Water Table (m)
1.0
0.8
0.6
0.4
0.2
0
0
0.1
0.2
0.3
0.4
0.5
Moisture Content (m3/m3)

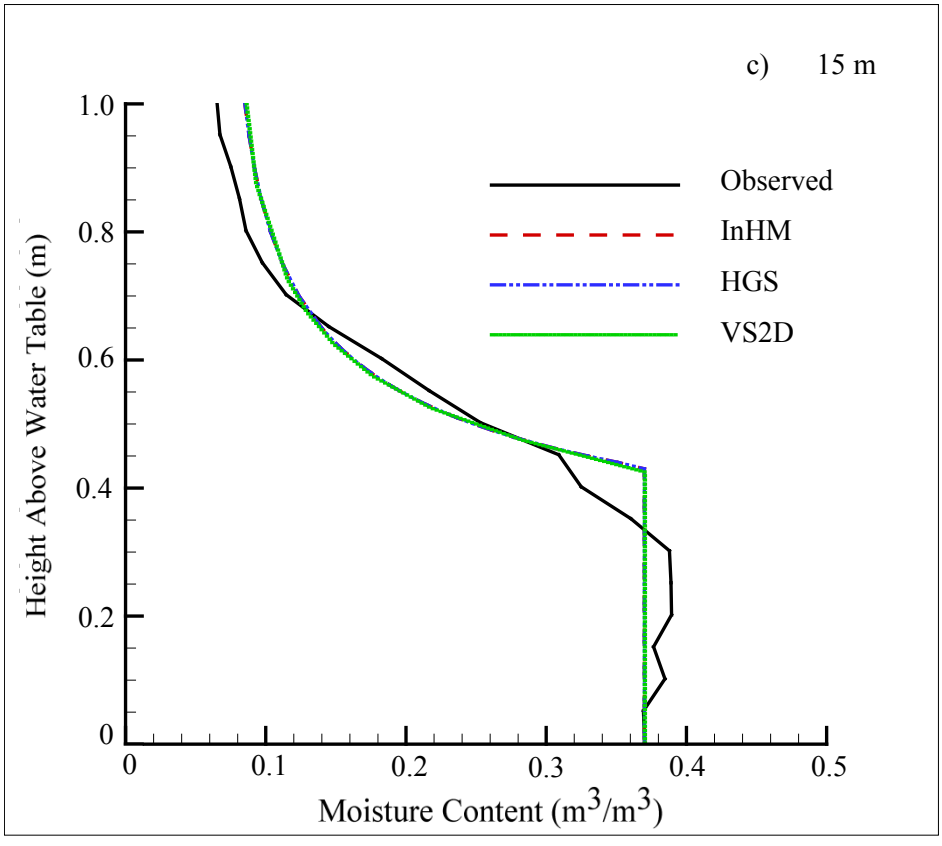

Figure B. 7 (a-c). Pre-pumping moisture content profiles observed and computed using the Brooks and Corey constitutive relationship. (Radial distances: a. 3 meters; b. 5 meters; c. 15 meters)

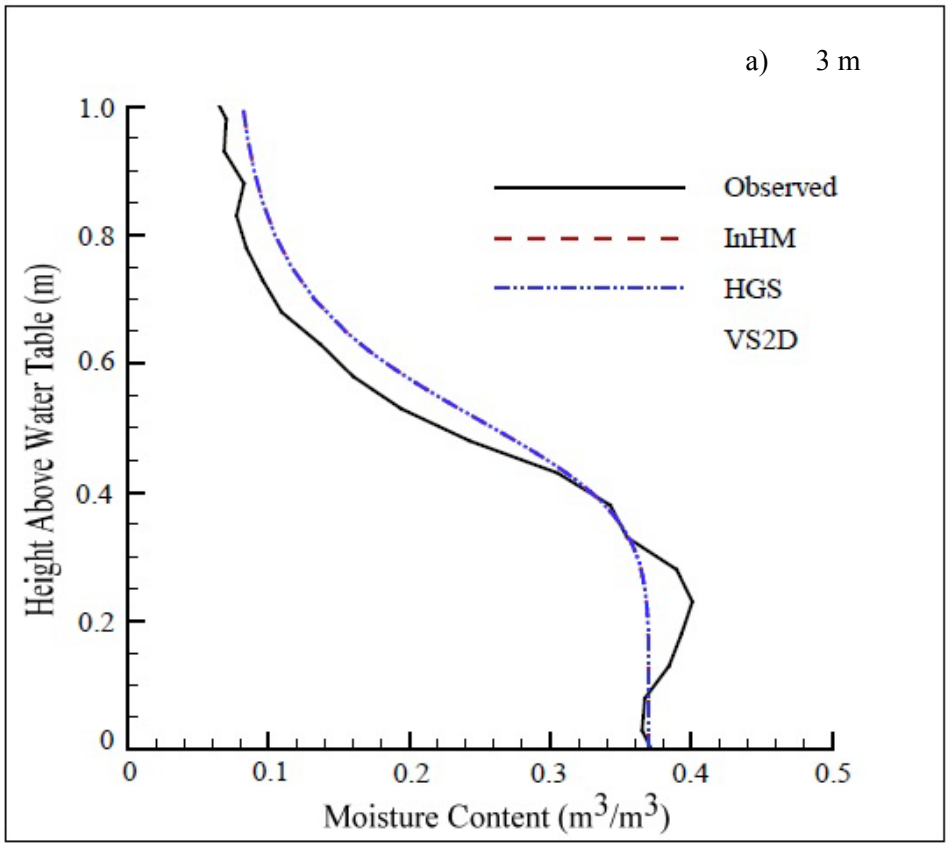
a) 3 m
Observed
InHM
HGS
VS2D
Height Above Water Table (m)
Moisture Content (m3/m3)
0
0.2
0.4
0.6
0.8
1.0
0.1
0.3
0.5

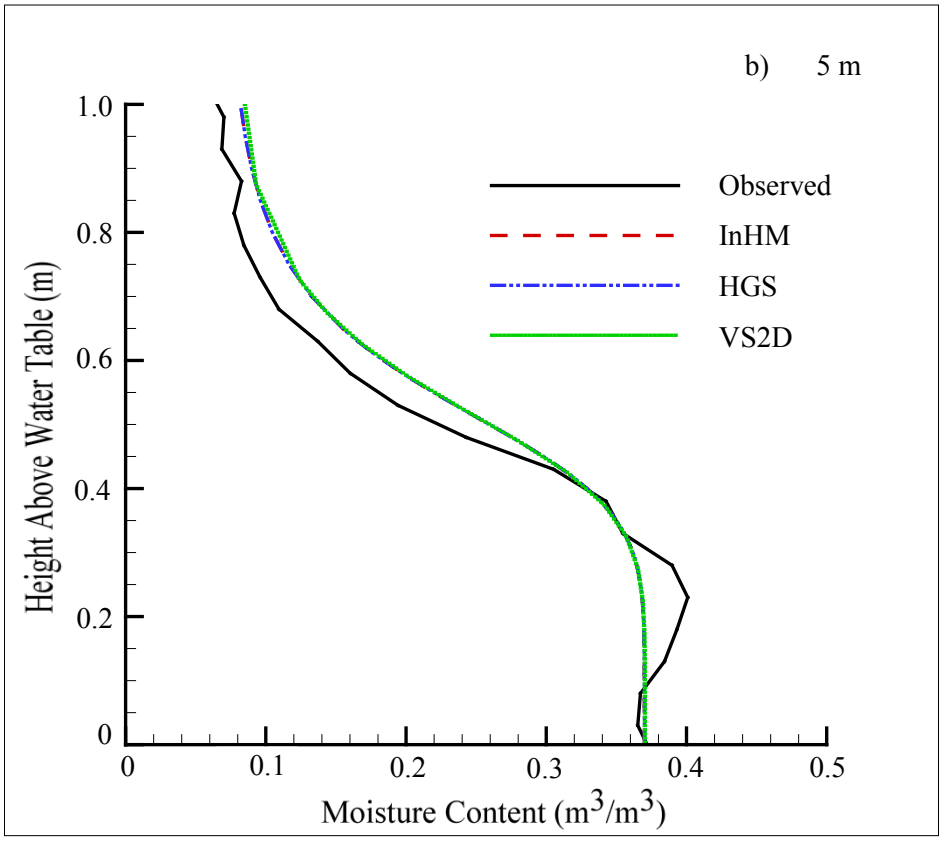
b) 5 m
Observed
InHM
HGS
VS2D
Height Above Water Table (m)
Moisture Content (m3/m3)
0
0.2
0.4
0.6
0.8
1.0
0.1
0.3
0.5

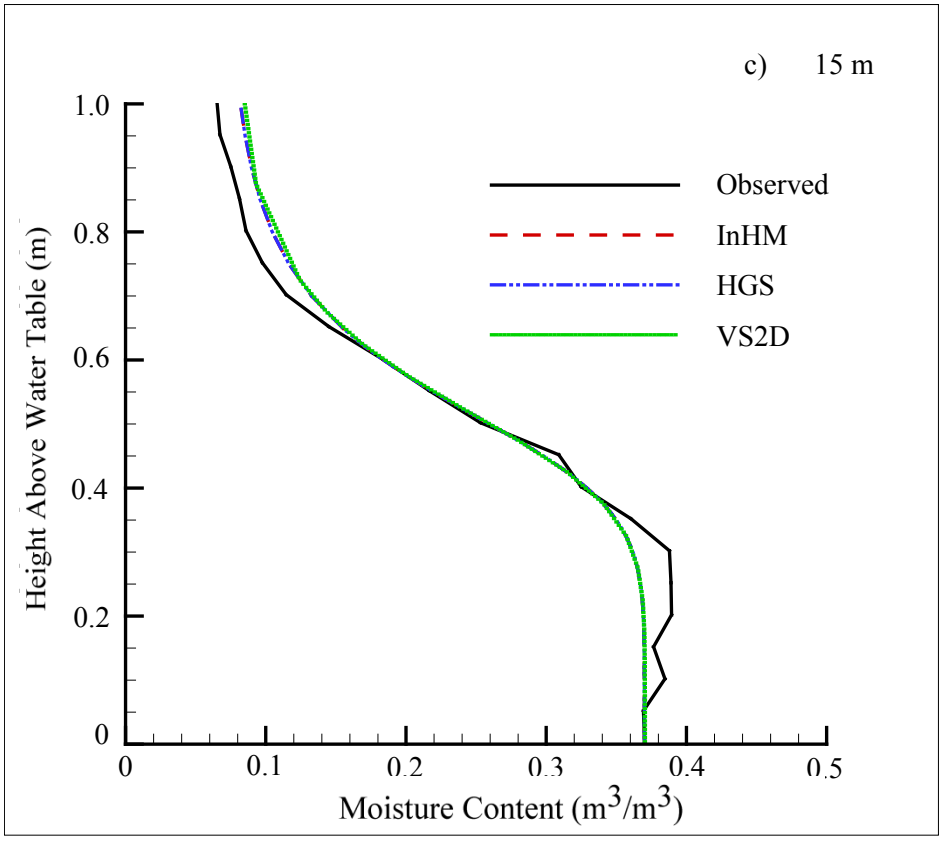

Figure B. 8 (a-c). Pre-pumping moisture content profiles observed and computed using the van Genuchten constitutive relationship. (Radial distances: a. 3 meters; b. 5 meters; c. 15 meters)

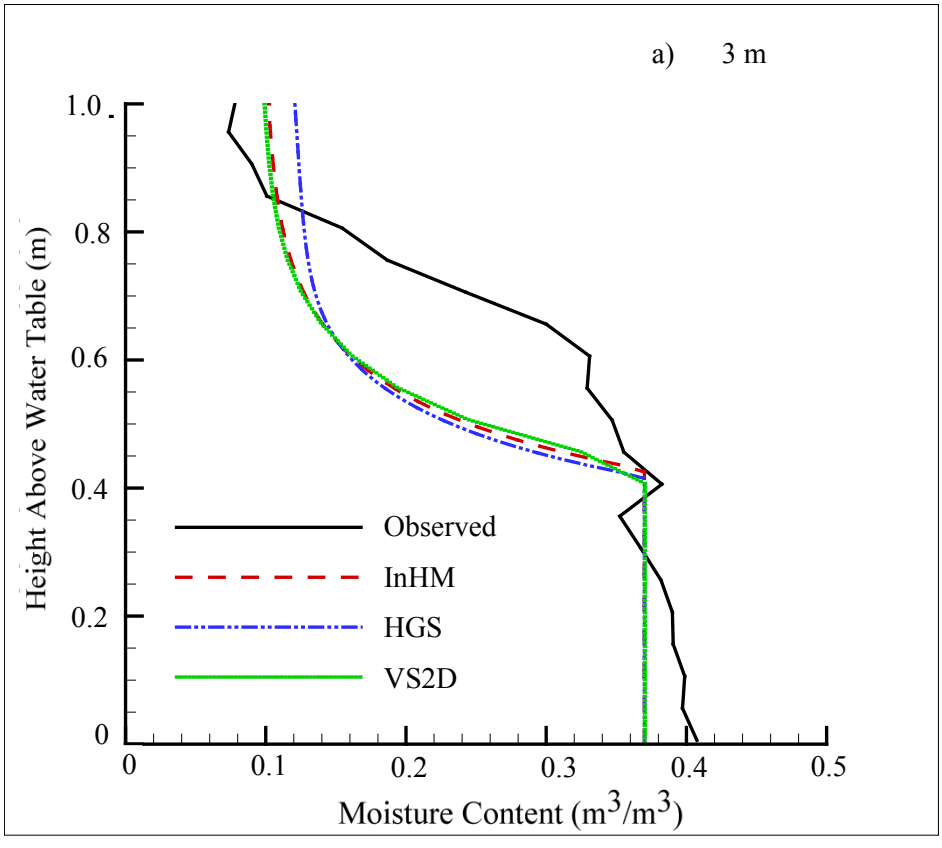
a) 3 m
Height Above Water Table (m)
1.0
0.8
0.6
0.4
0.2
0
0
0.1
0.2
0.3
0.4
0.5
Moisture Content (m3/m3)
Observed
InHM
HGS
VS2D

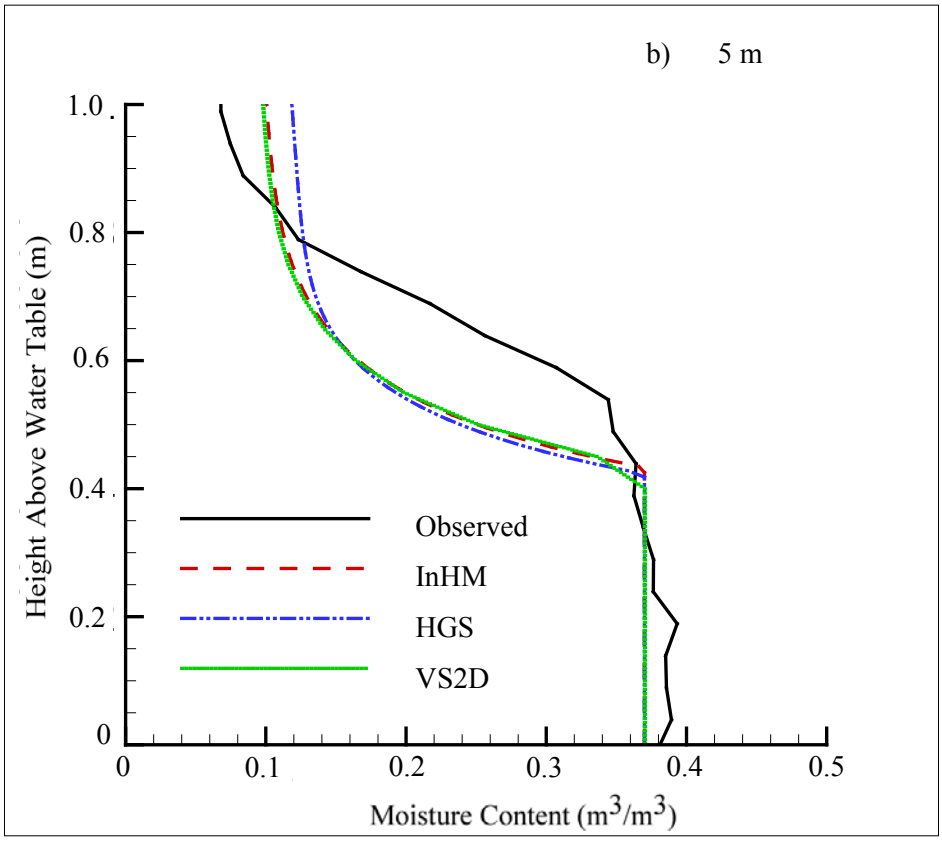
b) 5 m
Height Above Water Table (m)
1.0
0.8
0.6
0.4
0.2
0
0
0.1
0.2
0.3
0.4
0.5
Moisture Content (m3/m3)
Observed
InHM
HGS
VS2D

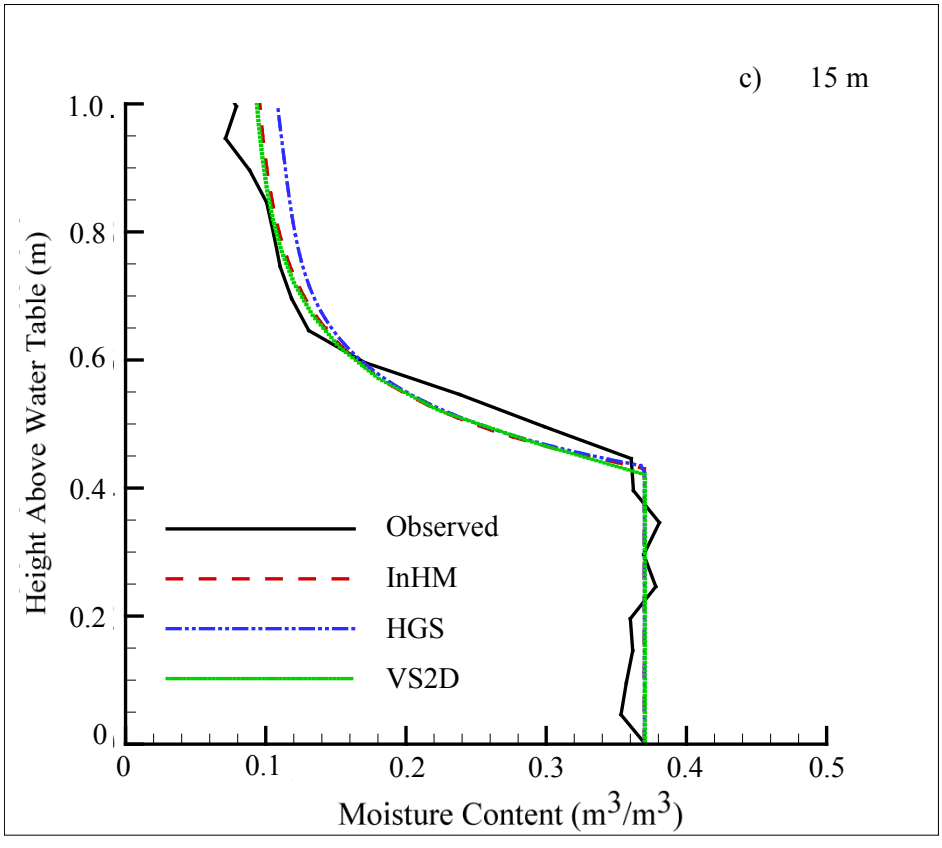

Figure B. 9(a-c). End of pumping moisture content profiles observed and computed using the Brooks and Corey (1964) constitutive relationship. (Radial distances: a. 3 meters; b. 5 meters; c. 15 meters)

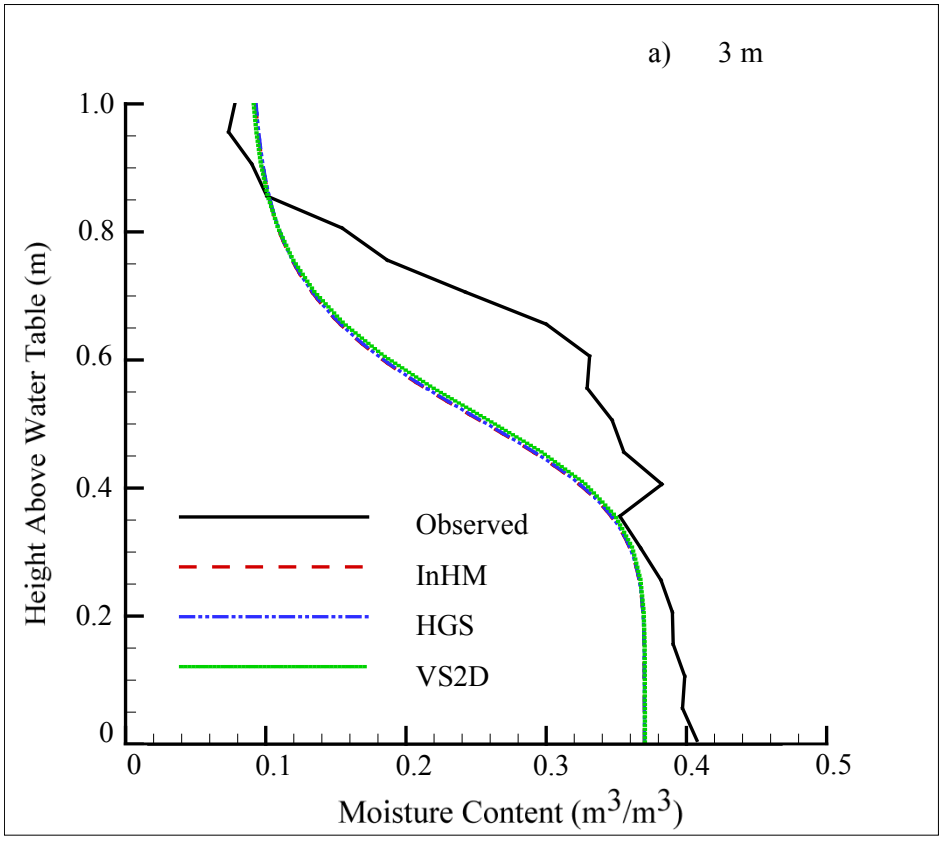
a) 3 m
Height Above Water Table (m)
1.0
0.8
0.6
0.4
0.2
0
0
0.1
0.2
0.3
0.4
0.5
Moisture Content (m3/m3)
Observed
InHM
HGS
VS2D

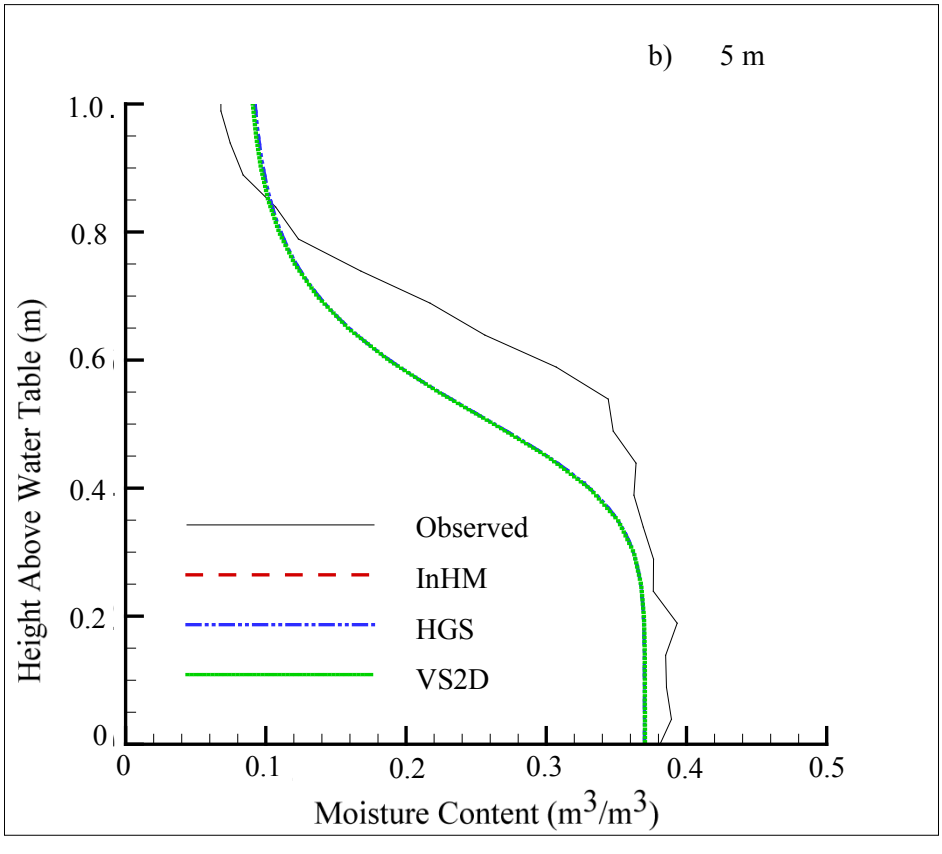
b) 5 m
Height Above Water Table (m)
1.0
0.8
0.6
0.4
0.2
0
0
0.1
0.2
0.3
0.4
0.5
Moisture Content (m3/m3)
Observed
InHM
HGS
VS2D

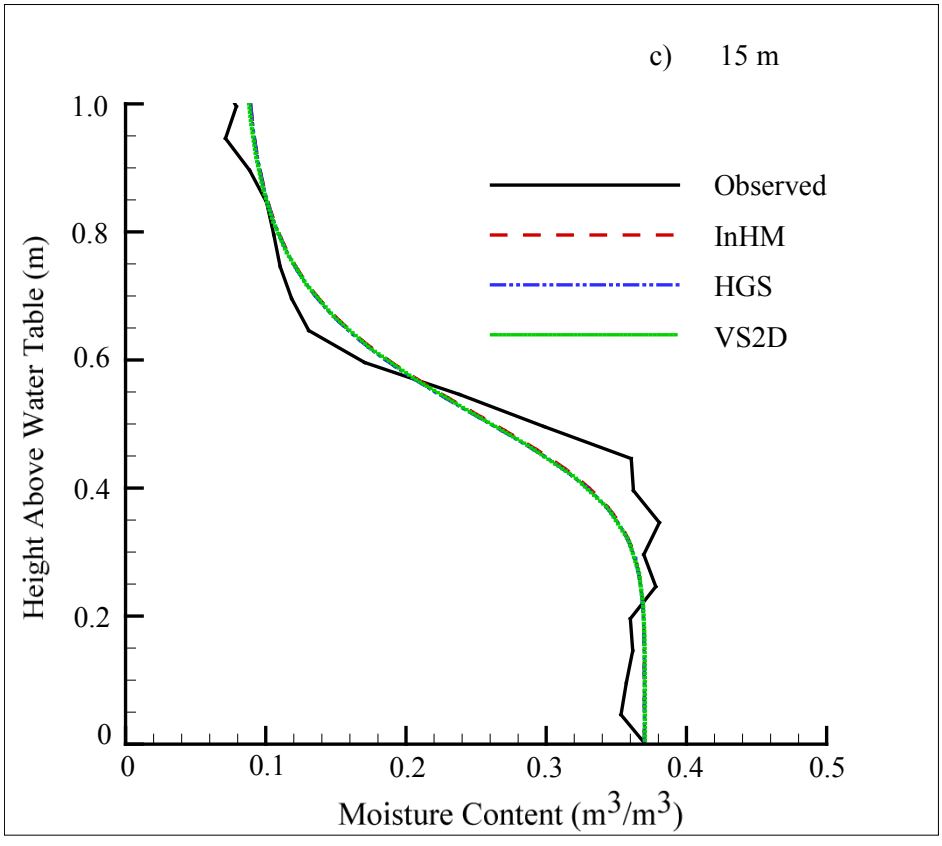

Figure B. 10(a-c). End of pumping moisture content profiles observed and computed using the van Genuchten constitutive relationship. (Radial distances: a. 3 meters; b. 5 meters; c. 15 meters)

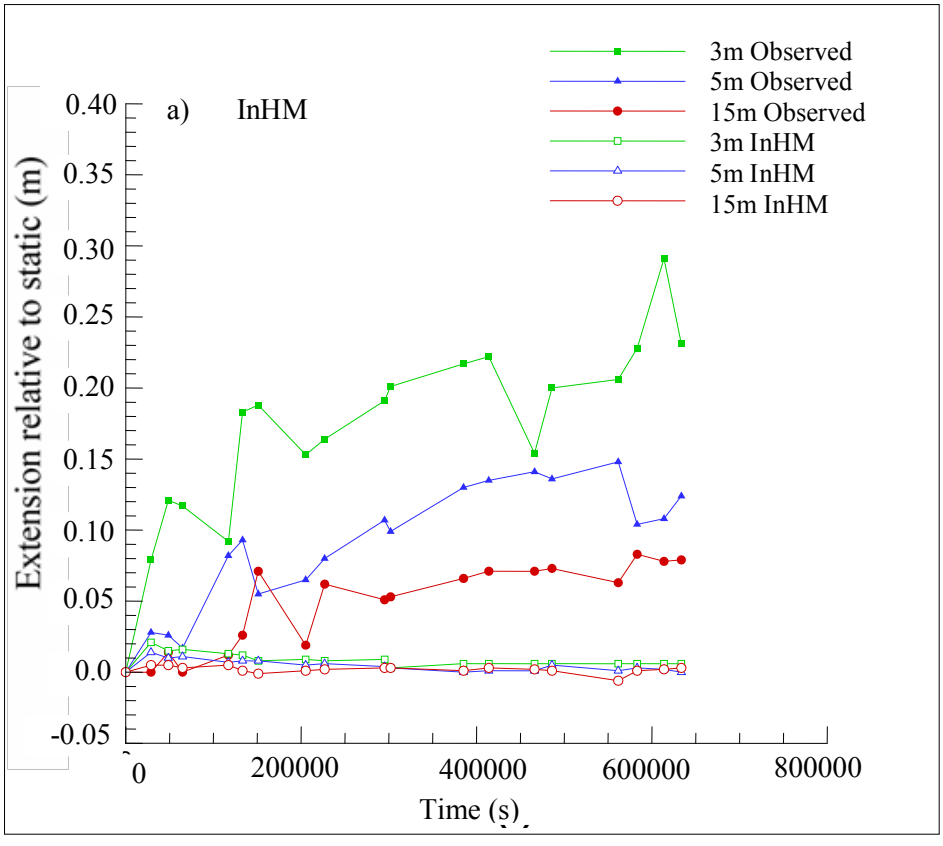
a) InHM
3m Observed
5m Observed
15m Observed
3m InHM
5m InHM
15m InHM
Extension relative to static (m)
0.40
0.35
0.30
0.25
0.20
0.15
0.10
0.05
0.0
-0.05
0
200000
400000
600000
800000
Time (s)

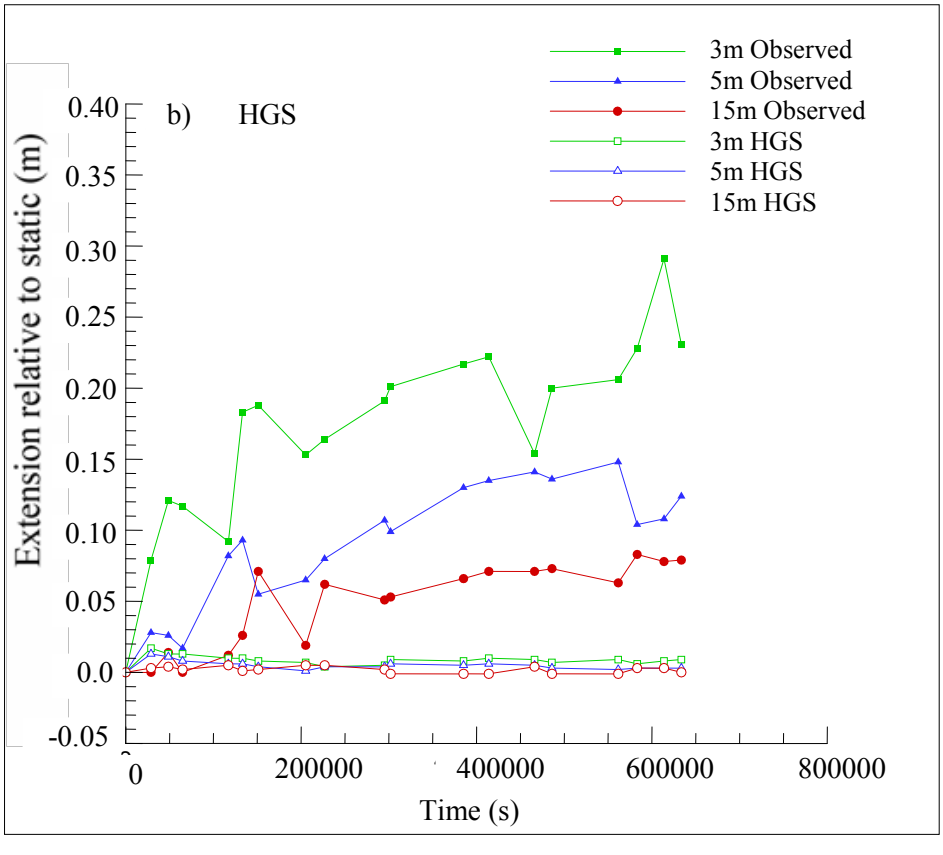
b) HGS
3m Observed
5m Observed
15m Observed
3m HGS
5m HGS
15m HGS
Extension relative to static (m)
0.40
0.35
0.30
0.25
0.20
0.15
0.10
0.05
0.0
-0.05
0
200000
400000
600000
800000
Time (s)

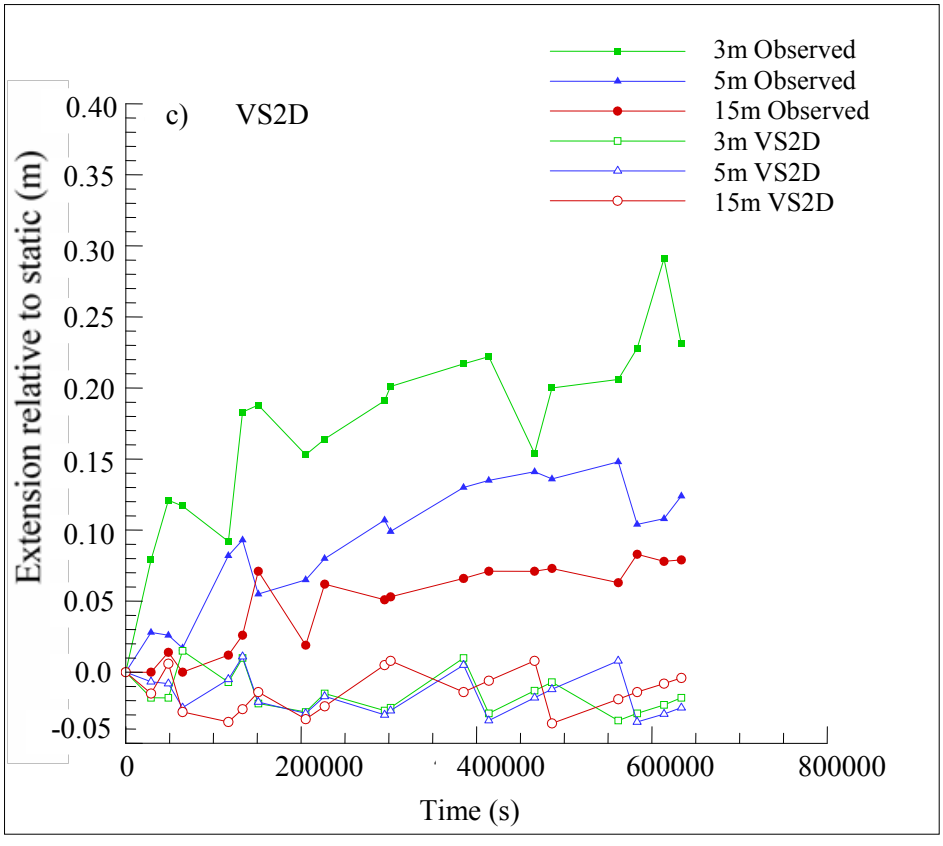

Figure B. 11(a-c). Capillary fringe extension inferred from field observations and computed using the Brooks and Corey relationship. (Numerical code: a. InHM; b. HGS; c. VS2D)

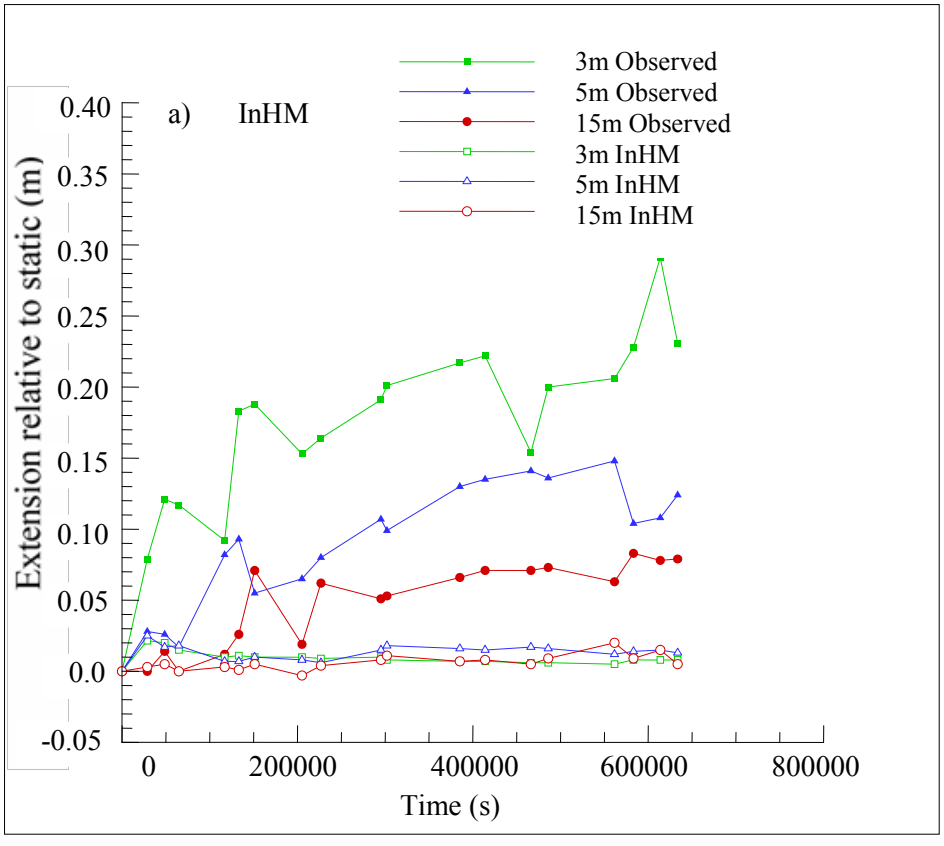
a) InHM
3m Observed
5m Observed
15m Observed
3m InHM
5m InHM
15m InHM
Extension relative to static (m)
0.40
0.35
0.30
0.25
0.20
0.15
0.10
0.05
0.0
-0.05
0
200000
400000
600000
800000
Time (s)

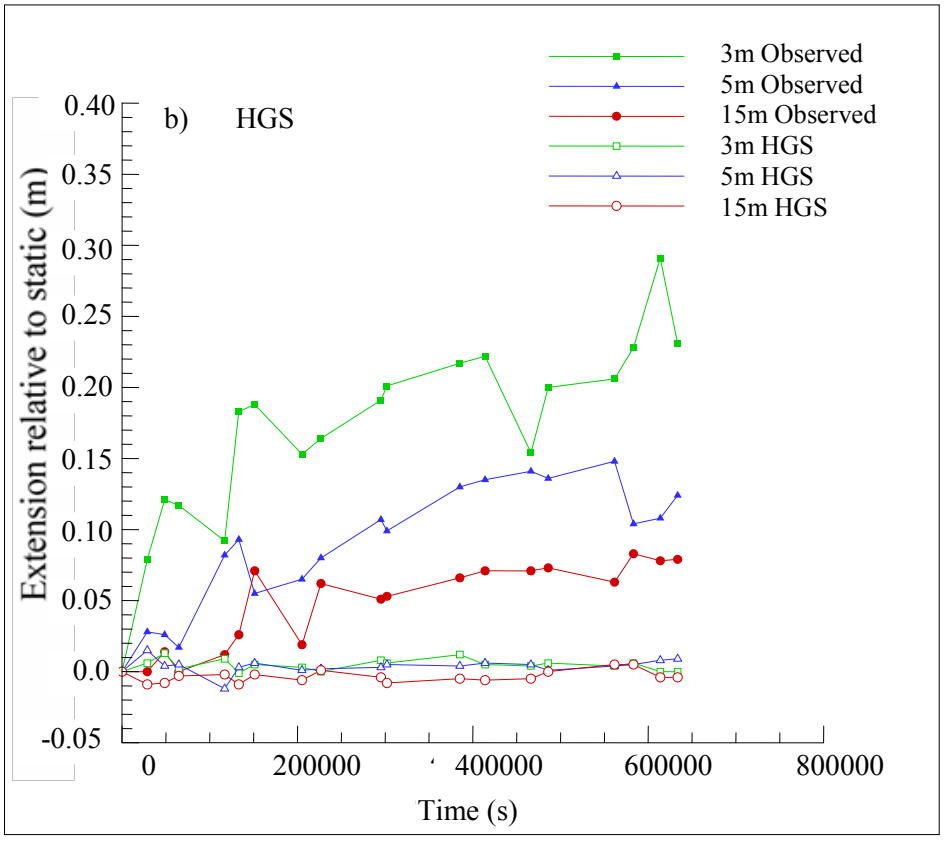
b) HGS
3m Observed
5m Observed
15m Observed
3m HGS
5m HGS
15m HGS
Extension relative to static (m)
0.40
0.35
0.30
0.25
0.20
0.15
0.10
0.05
0.0
-0.05
0
200000
400000
600000
800000
Time (s)

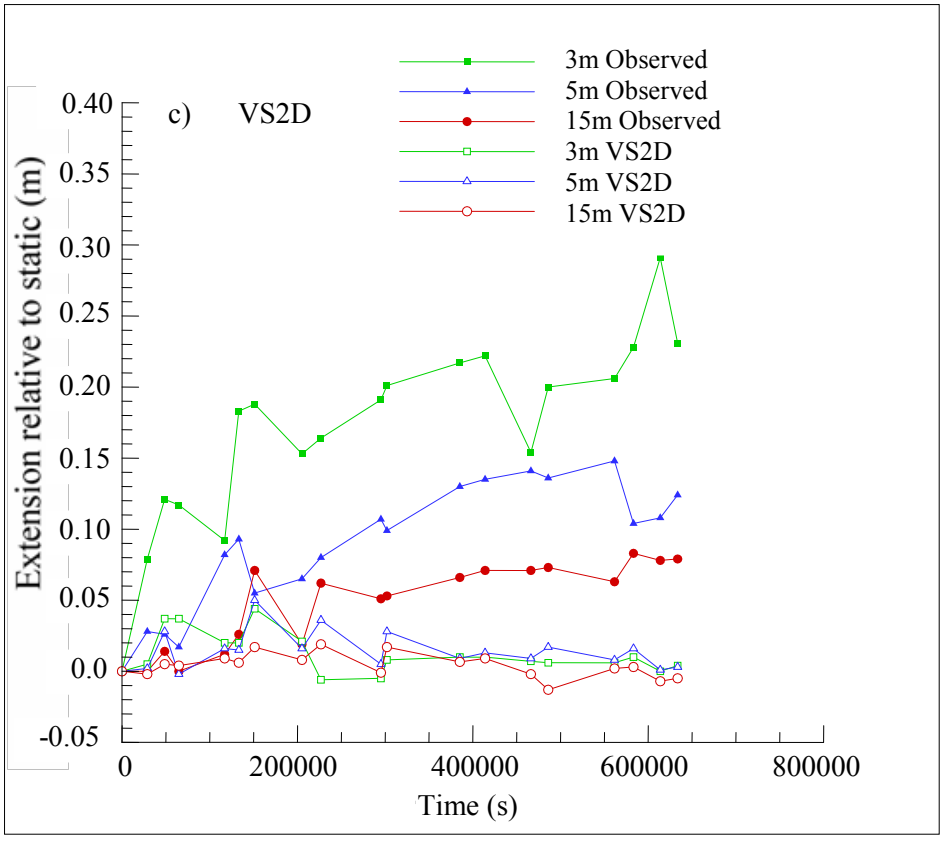

Figure B. 12 (a-c). Capillary fringe extension inferred from field observations and computed using the van Genuchten relationship. (Numerical code: a. InHM; b. HGS; c. VS2D)